Lim-only Domain Proteins in Developmental Haematopoiesis

Kapil Tuladhar

A thesis submitted to the University of Oxford in partial fulfilment of the requirement for the degree of Doctor of Philosophy

Wolfson College

Trinity 2012

For Dad

"Blut ist ein ganz besondrer Saft."

[Blood is a very special juice.]

- Johann Wolfgang von Goethe *Faust Part I* (1808) -

"Blood, toil, [and] sweat […] always were a good mixture"

- Max Perutz *Nobel Banquet Speech* (1962) -

Table of Contents

List of Figures and Tables

Abbreviations

AGM	aorta-gonad-mesonephros
ALM	anterior lateral plate mesoderm
AML	acute myeloid leukaemia
ASPP	apoptosis stimulating protein of p53
Bcor	BCL-6 corepressor
BLAST	basic local alignment search tool
BL-CFC	blast colony-forming cells
Bmp	bone morphogenic protein
CFU-S	colony-forming unit spleen
CHT	caudal haematopoietic tissue
CLP	common lymphoid progenitor
CML	chronic myelogenous leukaemia
CMP	common myeloid progenitor
DA	dorsal aorta
DAPM	3,5-difluorophenylacetyl-ala-phg-ome
DLAV	dorsolateral anastomotic vessel
DLP	dorsal lateral plate
DMSO	dimethyl sulfoxide
dpf	days post fertilisation
E	embryonic day
EB	embryoid body
EDTA	ethylenediaminetetraacetic acid
EHT	endothelial to haematopoietic transition
EMP	erythromyeloid progenitor
EMT	epithelial–mesenchymal transition
ES(C)	embryonic stem (cell)
FACS	fluorescent activated cell sorting
FGF	fibroblast growth factor
FL	foetal liver
FOG	friend of gata
GFP	green fluorescent protein
GMP	granulocyte/macrophage progenitor
Hdac	histone deacetylase
Hh	hedgehog
hpf	hours post fertilisation
HS(P)C	haematopoietic stem (and progenitor) cell
HSC (LT-/ST-)	haematopoietic stem cell (long-/short term-)
iASPP	inhibitory member of the ASPP family

ICM	intermediate cell mass
iPS	induced pluripotent stem cell
Irf2bp2	interferon regulatory factor-2 binding protein-2
ISV	intersegmental vessel
Ldb	LIM domain binding protein
LIM	*from* Lin11, Isl-1 and Mec-3
Lmo	LIM domain only
LMPP	lympho-myeloid primed progenitor
LSK	*from* Lin-/Sca+/c-Kit+
MBT	midblastula transition
MEL	mouse erythroleukaemic
MEP	myeloerythrooid progenitor
MO	morpholino
MPP	multipotent progenitor
myef2	myelin expression factor 2
NC	notochord
Ncor	nuclar co-repressor
PBI	proximal blood island
PBS(T)	phosphate buffered saline (tween)
PCV	posterior cardinal vein
PDGF	platelet derived growth factor
PFA	paraformaldehyde
PLM	posterior lateral plate mesoderm
PND	pronephric duct
P-Sp	para-aortic splanchnopleural mesoderm
SCID	severe combined immunodeficiency
Shh	sonic hedgehog
sib	siblings
ss	somite stage
SSC	saline sodium citrate
T-ALL	t-cell acute lymphoblastic leukaemia
TB	tail bud
TBS(T)	tris buffered saline (tween)
Tgf-β	transforming growth factor beta
UTR	untranslated region
VBI	ventral blood island
Vegf(r)	vascular endothelial growth factor (receptor)
WISH	whole mount *in situ* hybridisation
wt	wild type
YFP	yellow fluorescent protein
YSL	yolk syncytial layer

Abstract

The production of adult blood initiates from the haematopoietic stem cell (HSC). This clinically important cell has the capacity to maintain all blood lineages throughout the lifetime of an organism. HSCs emerge *de novo* from the haemogenic endothelium in the ventral wall of the embryonic dorsal aorta, from where they go on to seed adult sites of haematopoiesis. We have shown that Lmo4a is required for the emergence of HSCs in the zebrafish, and go on to demonstrate that Lmo4a regulates expression of the critical transcription factor, *gata2a*. Strikingly, both over- and under-expression of *gata2a* in the dorsal aorta severely diminishes HSC production. The LIM-only domain protein Lmo4 has previously been shown to interact with the known haematopoietic regulator, Ldb1. Together with our collaborators, we have identified novel binding partners of Lmo4 in mouse erythroleukaemic cells. Our functional analysis shows that many of these partners are also necessary for HSC emergence, thus revealing several new potential regulators of HSC formation. Given that these proteins were identified in an *in vitro* model of definitive erythropoiesis, it is remarkable that they also appear to act together *in vivo* at the level of HSC formation, and our data suggests that a transcriptional complex containing Lmo4 and these partners may directly repress *gata2a*. The related protein Lmo2 is also known to bind Ldb1. Together with Scl, Lmo2 is a master regulator of the haemangioblast programme. We have been utilising this activity, together with recent structural studies, to identify functionally important residues in the Lmo2 molecule. As a cell's transcriptional programme drives both normal and pathological development, and misexpression of both Lmo2 and Lmo4 is involved in a variety of oncogenic states, the work presented in this thesis is likely to inform efforts to develop therapeutically relevant reagents.

Acknowledgements

There are so many people who have helped me along the way the last four years. First and foremost, I would like to thank Roger for adopting me into the lab. Your wit and wisdom has in no small part contributed to me having a great time, and even learning a little bit too! And thanks to the MRC for funding me, and the department for taking care of things like money and core facilities.

I don't think I will ever have the privilege of working alongside such a fine group of people. Rui, you've been a great mentor, allowing me space to get on with things, while always making time for all my little questions. Philly, we don't appreciate you enough (even if we do have to endure the odd moan!). Filipa, Wenchao and Stuart – thanks for tolerating me encroaching into your bench/desk space. Arif, for the broad beans, and for playing devil's advocate in lab meetings. And to Janina and Rachel for providing excellent cake to get through the ordeal.

Jana, your German efficiency coupled with front bottom usage is quite formidable - almost as formidable as Jie's driving! And thanks Claire for help with the FACS. Aldo, I envy your knowledge of the literature and how you always seemed to have the crucial reagent – but I think we are all in debt to you for your syncopated renditions of the hits of Haydn, Boccherini and Aqua – "come on baby, let's go party!!"

For keeping the fish healthy, thanks to the BMS staff, especially Andy. To Paresh for hosting me when I first started, and Ibo for his unique approach to science and the English language. I am indebted to Catherine, Erika, Kamel and Sarah for the collaboration that lead to Chapter 3. Thanks to Karima for inviting me to Paris and teaching me how to use a microscope properly. And thanks to Charlotte and Terri for giving me a running start with Chapter 4 and 5.

Near and far, old and new, thanks to friends for providing a break from the lab, be it lunches, pints or singing – everything from Monteverdi to MacMillan. And to family for always encouraging me. Mum – I'm not sure how much of this you'll understand (although you're already half way there when you say it involves DNA!) but either way, the thesis will look good on the bookshelf!

Doug and Elaine, thanks for agreeing to examine me. I hope you enjoy reading and dissecting this *almost* as much as I enjoyed writing it!!

Finally, thank you Caroline for always being there. And for our little adventures; I look forward to all the adventures to come...

Research Declaration

The work presented in this thesis is my own work except where indicated. All text, figures, tables, data or results which are not my own work are indicated and the sources acknowledged.

Chapter III

- All X-ray crystallography and molecular modelling was carried out by Kamel El Omari and Erika Mancini at The Division of Structural Biology, Oxford, UK.

Chapter IV

- The biotinylation, streptavidin pull-down, and subsequent LCMS/MS identification of Lmo4 protein partners in MEL cells was carried out by Charlotte Andrieu-Soler, Eric Soler and Frank Grosveld at the Erasmus Medical Centre, Rotterdam, The Netherlands.

Chapter V

- ChIP-seq analysis of Lmo4 binding in MEL cells was carried out by Charlotte Andrieu-Soler and Frank Grosveld at the Erasmus Medical Centre, Rotterdam, The Netherlands.
- Sorting of dissociated cells was carried out by Kevin Clark at The Weatherall Institute of Molecular Medicine, Oxford, UK.

Work presented in Chapter III contributed to one publication and one manuscript in preparation (El Omari et al., 2011). Work presented in Chapter IV contributed to one publication (van Riel et al., 2012). Work presented in Chapters IV and V is currently under preparation for publication.

Chapter 1

Introduction

1.1 An overview of haematopoiesis

The study of blood has a distinguished history going back many centuries, during which the haematopoietic system has provided inspiration for the minds of scientists and artists alike. As a system, it is both homeostatic and dynamic, possessing the ability to meet as required, developmental, physiological, and immunological demands. Central to this role is the heterogeneous nature of blood: it is composed of several different specialised cell types. These various cells can last up to a lifetime, however most are quickly turned over and therefore need to be replenished. Haematopoiesis is the process by which all blood lineages of a particular organism are generated and maintained across its lifetime.

The elegance of developmental processes often conceals the coordination required, and the complexity involved. The construction of an embryo from a single cell is an outstanding case in point. The ability to exchange waste with oxygen and nutrients quickly becomes essential for embryogenesis; it is therefore unsurprising that blood is one of the first tissues to develop (Baron, 2003; Dzierzak and Speck, 2008). In vertebrate embryos, development of blood occurs from mesodermal derivatives, an observation first made over a century ago (His, 1900). It proceeds in a roughly hierarchical manner, and in distinct waves. A primitive wave generates transient erythrocytes and myeloid cells, to respectively oxygenate tissues, and to facilitate basic immune responses. This is replaced by the definitive wave that initiates from the HSC and generates all adult blood lineages. Many of the current and historical challenges, and controversies in the field, arise from the multiple sites of haematopoiesis coupled with the inherent mobility of blood cells.

1.1.1 The haemangioblast

At multiple stages of development, endothelium and blood are closely linked. The seminal observation of anatomical proximity, and simultaneous emergence of blood and endothelium in the chick yolk sac, led to the idea that there exists a population bipotent for both blood and endothelium (Sabin, 1917; Sabin, 1920). This conclusion was independently reached by Murray who termed this

bipotent population the haemangioblast (Murray, 1932). Consistent with this concept is the observation that many genes expressed in mature blood and endothelium are co-expressed earlier in development (Eichmann et al., 1993; Godin and Cumano, 2002; Huber et al., 2004; Walmsley et al., 2002). Furthermore, inactivation of many of these genes results in both blood and endothelial defects, for example in the *flk1* null mouse (Shalaby et al., 1997) and zebrafish *cloche* mutants (Stainier et al., 1995). A strict definition of the haemangioblast could therefore be a mesodermal cell that can generate endothelial and blood cells and, importantly, no other cell type.

Identification and detailed characterisation of the haemangioblast in whole embryos has proved challenging owing to rapid development, relative inaccessibility and low numbers of cells. Therefore, the strongest evidence for the existence of the haemangioblast has come from the ability of ES (or iPS) cells in culture to be driven towards various cell fates, including blood progenitors (Orkin and Zon, 2008), allowing easy access to a large quantity of cells. In semi-solid culture, ES cells can be induced to form embryoid bodies (EBs), cystic aggregates of pluripotent stem cells that mimic early embryonic development, and that can form all three primary germ layers, the ectoderm, mesoderm and endoderm. Re-plating of the blast colony forming cell (BL-CFC) present in day 2.5 - 3.5 EBs into liquid culture results in blast colonies. By exposure to Vegf, cells in these colonies, expressing the Vegf receptor Flk1, can clonally give rise to both blood and endothelium, and therefore probably represents an *in vitro* approximation of the haemangioblast (Choi et al., 1998; Nishikawa et al., 1998). Smooth muscle cells can also be derived from blast colonies (Ema et al., 2003; Huber et al., 2004; Pearson et al., 2008), leading some authors to suggest redefining the potential of the haemangioblast (Orkin and Zon, 2008). However, the lack of anatomical restriction, and a set of markers exclusively defining the haemangioblast population in culture, may account for this additional potentiality.

Around E6.5, gastrulation initiates in the developing mouse. The epiblast, a single epithelial layer, resolves into the three germ layers, and the basic body plan is laid down (Baron et al., 2012). Ectodermal cells migrate to the extra-embryonic yolk sac where they form a mesodermal layer adjacent to the visceral endoderm (Baron, 2005). Embryoid bodies derived from *gata4*-null ES cells and lacking visceral endoderm, show reduced primitive erythropoiesis (Belaoussoff et al., 1998). Explants from

mouse suggested that the diffusible factors Indian hedgehog and Vegf from visceral endoderm are required for *bmp4* expression and subsequent blood and vascular development in the adjacent mesoderm around the time of gastrulation (Artus et al., 2012; Baron, 2001; Dyer et al., 2001). Using the mesodermal marker Brachyury, which is also expressed in blast colonies, along with Flk1, rare BL-CFC have been identified in the mouse and shown to be restricted to the mid-streak stage of gastrulation and neural plate stage in the mouse, around E7.5 (Figure 1.1), rather than the yolk sac (Huber et al., 2004; Rhee and Iannaccone, 2012). In mouse tetrachimeras, the extra-embryonic yolk sac blood islands, the first site of haematopoiesis, were derived from multiple clonal populations of differentially labelled ES cells (Ueno and Weissman, 2006). Taken together, this suggests that rare haemangioblasts in the primitive streak may generate a more restricted progenitor that seeds the yolk sac. A cell resembling the haemangioblast has now also been identified in human ES cells (Zambidis et al., 2008) and drosophila embryos (Mandal et al., 2004). In the zebrafish, single cell fate mapping supports the notion of a bipotent haemangioblast located around the ventral margin of the gastrula (Vogeli et al., 2006). However, only a subset of these cells gave rise to both blood and endothelium. Other cells were already committed to one or other fate (Vogeli et al., 2006). Recently, it was shown that cross antagonism between Gata1 and HoxB4, respectively stabilises blood and endothelial outcomes of the haemangioblast, possibly by altering nuclear organisation (Rhee and Iannaccone, 2012). Precisely when loss of bi-potentiality occurs still needs to be demonstrated.

Although the concept of the haemangioblast is most commonly associated with embryonic haematopoiesis, there is evidence that an analogous cell exists in adult life. In a subset of CML patients, the BCR-ABL translocation has been detected in cells of the bone marrow and endothelium, suggesting that this translocation event took place in a common progenitor (Gunsilius et al., 2000). Furthermore rare CD34+/Kdr positive human bone marrow and cord blood cells can clonally generate colonies of both blood and endothelial cells (Pelosi et al., 2002). Additionally, in the mouse, HSC enriched populations could be driven to an endothelial fate *in vivo* (Bailey et al., 2004; Grant et al., 2002; Jiang et al., 2008). The identification of haemangioblast-like cells in the adult mouse uterus added significant weight to the adult haemangioblast hypothesis (Sun et al., 2010). Whether the presumptive

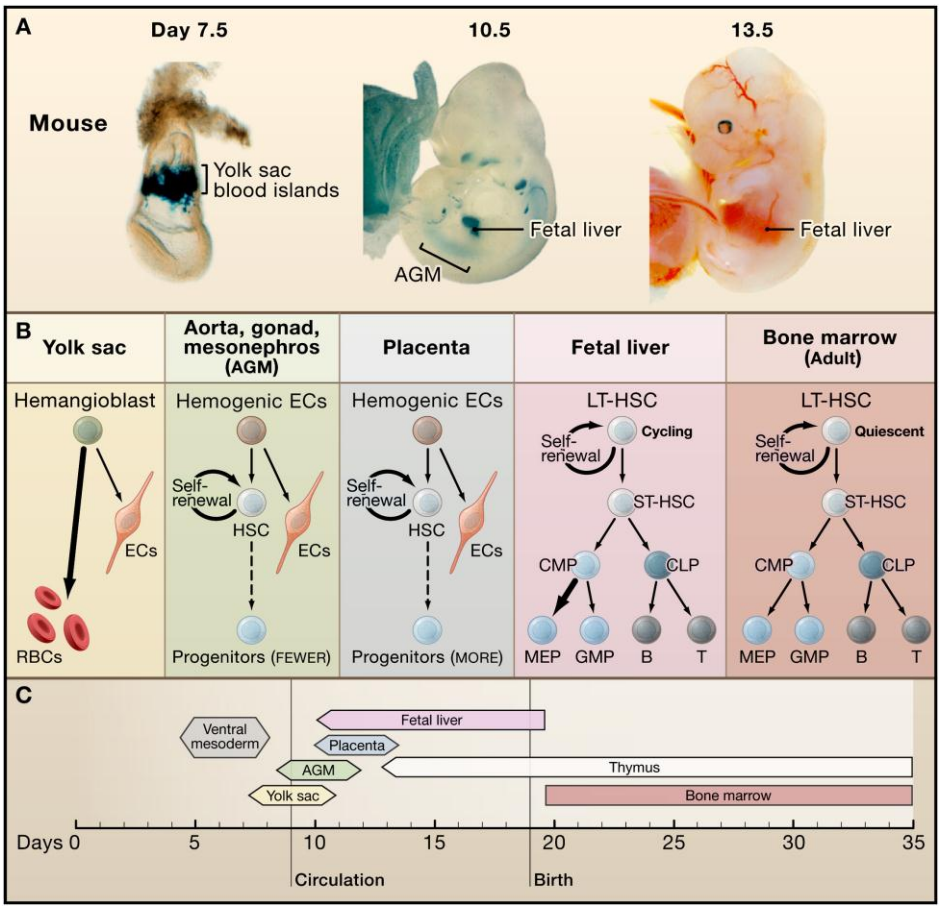

Figure 1.1 Overview of murine developmental haematopoiesis

(A) Haematopoiesis initiates in the yolk sac blood islands, followed by the definitive wave in the AGM, placenta and foetal liver. (B) Varying sites of haematopoiesis give rise to specific lineages. (C) Following the timing of haematopoiesis from the specification of ventral mesoderm in the embryo to the adult sites of haematopoiesis. AGM, aorta-gonad-mesonephros; RBC, red blood cell; EC, endothelial cell; LT-HSC, long term HSC; ST-HSC, short term HSC; CMP, common myeloid progenitor; CLP, common lymphoid progenitor; MEP, megakaryocyte-erythroid progenitor; GMP, granulocyte-macrophage progenitor; B, B-cell; T, T-cell. Reproduced from (Orkin and Zon, 2008).

adult haemangioblast is due to a persistence of the classical embryonic haemangioblast, and whether they are equivalent is still not clear.

1.1.2 Primitive and pre-definitive blood

In developing avian and mammalian embryos, the first morphological evidence of haematopoiesis is the appearance of immature erythroid cells in the presumptive blood islands in the extra-embryonic visceral yolk sac. This has been observed in the chick and quail (Dieterlen-Lievre, 1975), the gerbil (Smith and Glomski, 1977), mouse (Silver and Palis, 1997), cat (Tiedemann, 1977) and human (Takashina, 1987). More recently, it had been proposed that Flk-1 positive haemangioblasts transition through a haemogenic endothelial stage prior to emergence of primitive blood (Altschul et al., 1990; Eilken et al., 2009; Lancrin et al., 2009), however, in light of very recent data (Iacovino et al., 2011) it is still not clear whether this is entirely the case. The lower vertebrates *Xenopus* and zebrafish do not possess any extra-embryonic structures, however the ventral blood island (VBI) (Ciau-Uitz et al., 2000) and intermediate cell mass (ICM) (Willett et al., 1999) can be considered analogous to the blood islands, in that they generate a primitive haematopoietic output.

Within the yolk sac mesoderm of the chick, mouse and human, discrete blood islands emerge from homogeneous cellular aggregates (Figure 1.1). The clusters are arranged such that angioblasts surround erythroblasts (Cumano and Godin, 2007). These endothelial and erythroid progenitors rapidly differentiate to form respectively the yolk sac vasculature and primitive erythrocytes, the first circulating cells in the embryo (Lensch and Daley, 2004). Unlike mature red blood cells, these erythrocytes are large in size and nucleated (Wong et al., 1986), much like erythroid progenitors found in adult bone marrow or mature cells in *Xenopus* and zebrafish. They also differ at a molecular level, expressing embryonic, rather than adult, globins (Palis et al., 2010). In addition to the erythrocytes that dominate primitive blood, a limited number of transient megakaryocytes and macrophages are also produced, presumably for immunity, blood clotting, and to aid tissue remodelling. Like primitive red blood, these cells differ from their adult counterparts in their size and enzymatic complement (Naito et al., 1996; Xu et al., 2001).

Primitive blood production occurs in a narrow window of time, and in concert with vascular development. In the mouse, erythroid progenitors are first detected around E7.5, before circulation initiates (Palis et al., 1999). The initiation and termination of primitive blood is therefore subject to tight regulation. Loss of primitive blood results in embryonic lethality in mice where the transcription factors Gata1, Gata2, Lmo2 or Scl have been inactivated (Orkin and Zon, 2008). Recently, it was shown that microRNAs may be involved in turning off primitive erythropoiesis in cultured cells, the so called primitive to definitive switch (Sturgeon et al., 2012). It has become clear with time that, at least in the mouse, the switch from primitive to definitive haematopoiesis is more subtle, with transient waves of haematopoiesis occurring after emergence of primitive blood but before adult-definitive HSCs are generated. While prior to E10.0-10.5 the murine yolk sac is the principal haematopoietic site, several other haematopoietic sites have been identified.

The generation of erythroid and myeloid precursors has been documented in E7.5-8.0 allantois (Corbel et al., 2007; Zeigler et al., 2006), E8.25-9.5 yolk sacs (Altschul et al., 1990; Lux et al., 2008; Palis et al., 1999; Rampon and Huber, 2003), and in E9.0 placentas (Alvarez-Silva et al., 2003). In the zebrafish, analogous progenitors, distinct from primitive blood, and restricted to erythroid and myeloid outputs, are also observed (Bertrand et al., 2007). Explant pre-cultures demonstrated that the E7.5-8.0 para-aortic splanchnopleural mesoderm (P-Sp) could generate a more complex pre-definitive cell, with erythroid, myeloid and lymphoid potential (Cumano et al., 1996; Cumano et al., 2001). As with all explant experiments, this may reflect a potential that is not realised *in vivo* owing to the difficulty in recreating all the extrinsic influences that make up the haematopoietic niche, where the niche is the three-dimensional stromal network that supports haematopoietic development (Hsu and Fuchs, 2012; Schofield, 1978). It was recently shown that the murine yolk sacs and P-Sp independently generate precursors of the first B lymphocytes at E9.0 (Yoshimoto et al., 2011). Subsequently, a HSC with potent neonatal, but not adult, engraftment potential was isolated from the yolk sacs and AGMs of E9.0 mice (Yoder et al., 1997).

1.1.3 Adult-definitive haematopoiesis

The identification of the yolk sac as the first site of blood generation led to the idea that yolk sac-derived cells seed the embryo proper and give rise to all adult blood (Moore and Metcalf, 1970). Classical experiments using chimeric avian embryos challenged this idea (Dieterlen-Lievre, 1975). Developing quail embryos were grafted onto chick yolk sacs stripped of embryonic tissue. It was demonstrated that primitive blood was derived from the chick and the definitive blood from the quail, therefore demonstrating an embryonic site of blood generation. Further use of this avian grafting approach demonstrated that the development of the HSC was independent of the yolk sac and that the ventral aspect of the dorsal aorta was the likely source of HSCs (Dieterlen-Lievre and Martin, 1981). A dual origin of blood was also revealed by grafting experiments in *Xenopus* embryos: primitive blood originates in the ventral blood island (VBI) whereas definitive blood has its origin in the dorsal lateral plate (DLP) (Altschul et al., 1990; Maeno et al., 1985; Turpen et al., 1981). Single cell lineage tracing in regularly cleaving frog embryos supported this result, and demonstrated that separation of these two lineages of blood has already occurred by the 32-cell stage (Ciau-Uitz et al., 2000).

The precise location and timing of definitive haematopoiesis has been the focus of intense recent study. This has led to the identification of the AGM as the major initiating site of definitive haematopoiesis, including in the human (Ivanovs et al., 2011). The E9 aortic region was shown to contain B-lymphoid potential when transplanted into irradiated mice. This activity was not detected in E9 yolk sacs (Cumano et al., 1993; Godin et al., 1993), although recent data suggests that the E9 yolk sac may contribute to a subset of B-lymphoid cells (Yoshimoto et al., 2011). Around the same time, CFU-S activity was identified in E9 AGMs at a higher frequency than in yolk sacs, and this preceded detectable CFU-S activity in the foetal liver (Medvinsky et al., 1993). Subsequently, it was shown that transplanted E10.5 AGMs had long term reconstituting activity, and were therefore an intra-embryonic site of HSC generation (Medvinsky and Dzierzak, 1996; Muller et al., 1994). By analysis of phenotypic and molecular makeup, and transplantation into mouse models, it was shown that the human AGMs also contain cells that initiate definitive haematopoiesis (Tavian et al., 1996; Tavian et al., 1999; Tavian et al., 2001).

Histological analysis of vertebrate embryos revealed clusters of cells, often associated with the floor of the embryonic dorsal aorta. These were first observed in pig (Emmel, 1916), and have now been identified in various vertebrate organisms including the human (Tavian and Peault, 2005), mouse (Robert-Moreno et al., 2008), chick (Dieterlen-Lievre et al., 2006), quail (Jaffredo et al., 1998) and *Xenopus* (Ciau-Uitz et al., 2000). Additionally, haematopoietic activity is observed in the floor of the zebrafish dorsal aorta (Gering and Patient, 2005). In avian embryos, it was shown that multipotent haematopoietic progenitors are present around the time of cluster emergence (Cormier and Dieterlenlievre, 1988). Further, functional and phenotypic studies have shown that HSC activity is contained within these clusters and that their size and number peak with the HSC activity in the AGM. It was therefore accepted that at least some of the cells in these clusters represented *de novo* HSCs (Altschul et al., 1990; de Bruijn et al., 2002; Godin et al., 1999; North et al., 1999; North et al., 2002; Taoudi and Medvinsky, 2007). The origin of these clusters has however proved controversial. Some authors believed that these cells were generated in the mesenchyme underlying the dorsal aorta and migrated into the vessels. Others supported the idea that cells in the cluster emerged directly from a subset of endothelial cells termed haemogenic endothelium.

Experiments where avian aortic endothelial cells labelled with vital dyes could be detected in the clusters demonstrated for the first time the potential existence of haemogenic endothelium (Jaffredo et al., 1998). Orthotypic grafting demonstrated that the floor of the dorsal aorta is initially generated from splanchnopleural mesoderm, however when numbers of clusters diminish, the floor of the dorsal aorta becomes replaced with somite derived endothelial cells, suggesting that haemogenic endothelium is a transient structure derived from the splanchnopleura (Pouget et al., 2006). It was subsequently shown by live imaging that a subset of cultured endothelial cells could directly transition to blood (Eilken et al., 2009). In the mouse, it was shown that almost the entire pool of adult-HSCs is derived from a cell that previously expressed the vascular marker VE-cadherin and that the transcription factor Runx1 is required for the transition of endothelium to blood (Chen et al., 2009; Zovein et al., 2008). In embryos haploinsufficient for *runx1*, but not wild type mice, HSCs were also found in the mesenchyme underlying the dorsal aorta at E10.5, around the time HSCs are first generated (North et al., 2002) although the analysis may have been confounded by the premature

generation of HSCs in *runx1* haploinsufficient embryos (Cai et al., 2000). In a separate study, cells under the dorsal aorta, so called sub-aortic clusters, were shown to generate multipotent haematopoietic colonies *in vitro* and had limited multilineage repopulating activity *in vivo* (Bertrand et al., 2005), although these cells may have originated from the dorsal aorta, as was seen in DiI and retrovirally labelled cells in avian models (Jaffredo et al., 2005; Jaffredo et al., 1998). Nevertheless, this data supported an alternative model for HSC generation, whereby HSCs are generated in the sub-aortic mesenchyme, possibly from haemangiobasts, and migrate to form the intra-aortic clusters.

Live imaging in the zebrafish and mouse has refined our understanding of the site and mechanism of HSC generation in the AGM. Taking advantage of transgenic animals where fluorescent reporter expression in the vasculature is driven by the the *kdrl* and *cmyb* promoter, two groups directly visualised the transition of endothelial cells to blood (Bertrand et al., 2010a; Kissa and Herbomel, 2010). It was shown that *kdrl*-GFP positive cells (Kissa and Herbomel, 2010), or those genetically marked by *kdrl*-Cre activity (Bertrand et al., 2010a), migrate to the thymus and kidney marrow, the secondary haematopoietic organs in the zebrafish. These cells leave the floor of the dorsal aorta over a period of several hours, whereby they bend towards the abluminal surface allowing their lateral neighbours to join, hence maintaining vascular integrity, before releasing their remaining cellular contacts. This novel process was termed the endothelial to haematopoietic transition (EHT), as the blood cell was not generated by an asymmetric division of the endothelial cell. Supporting this direct transition, it was observed that the diameter of the dorsal aorta decreased in 40-52 hpf embryos, which corresponded to the time of highest EHT frequency (Kissa and Herbomel, 2010)

Complementary studies in thick sections of cultured E10.5 *ly6a*-GFP transgenic mouse trunks allowed the observation of a similar budding process, although here the cells budded into the lumen of the vessel. Analysis of CD41 and c-kit verified the haematopoietic nature of these cells (Boisset et al., 2010). In contrast to the intact zebrafish where 3 events were observed per hour, in mouse sections only 0.11 events per culture, per hour were observed. This may reflect reduced expansion of the HSC pool in the zebrafish, or the absence of haemodynamic force in explanted tissue, given that blood flow has been shown to enhance *Runx1* expression and blood generation (Adamo et al., 2009; North et al.,

2009; Wang et al., 2011). Our current understanding is that adult-HSCs generated in the AGM region most likely emerge *de novo* from the floor of the dorsal aorta, although the complement of signals necessary to restrict EHT in space and time has not been fully described. For example it is not known why, in contrast to the mouse, HSCs in the zebrafish bud away from the vessel lumen. Furthermore, a recent study suggests the full picture may be more complicated, with HSC primed cells arising from both the floor of the aorta and the underlying mesenchyme, but then maturing exclusively in the endothelial lining of the dorsal aorta (Rybtsov et al., 2011), a process which would require the disruption of aortic tight junctions (Marshall et al., 2000). Additionally, it has been proposed that distinct haemogenic endothelial populations, restricted in space and time, generate HSCs and erythroid/myeloid progenitors (Chen et al., 2011).

In the developing mammalian embryo, the dorsal aorta is linked to the placenta and yolk sac by the umbilical and vielline arteries respectively (Costa et al., 2012). Haematopoietic cells were identified in these vessels raising the possibility that these sites independently generated HSCs (Garcia-Porrero et al., 1995). This was later confirmed by the detection of cells with HSC potential at E10.5, at the same time HSCs are emerging from the AGM (Alvarez-Silva et al., 2003; Gekas et al., 2005). The placenta itself results from a fusion of the chorionic-plate with the allantois and connects the maternal and embryonic circulations. Cells isolated from E10.5-11.0 placentas were shown to be able to reconstitute irradiated mice (Gekas et al., 2005; Ottersbach and Dzierzak, 2005). Taking advantage of mice with defective circulation, it was shown that the placenta could generate multilineage precursors (Rhodes et al., 2008). Additionally, using a non-invasive lineage tracing strategy in a tamoxifen-inducible *runx1*-Cre mouse, it was claimed that *runx1* expressing cells of E7.5 yolk sac precursors could also contribute to adult-HSCs (Samokhvalov et al., 2007). These results remain controversial as relatively few labelled cells were found in the adult and the *in utero* induction used is prone to staging error. Thus, while attempts have been made to quantitate the contribution of various tissues to the final HSC pool, the precise involvement of each tissue is still open to debate, and comparatively little is known about the signals that define the niche of non-AGM sources of HSCs.

By limiting dilution experiments, it has been estimated that there are three HSCs in an intact E11 mouse. By E12, 70 HSCs are present, with the majority residing in the foetal liver (Kumaravelu et al., 2002). It was concluded that due to the length of the cell cycle, this expansion could not be explained by cell division alone, and probably represented maturation of newly produced HSCs. Like all blood cells, HSCs do not remain at their site of production but enter circulation, where they are able to seed various secondary sites supporting haematopoiesis, and can expand and differentiate by symmetrical and asymmetrical cell divisions. From about E9.0, cells begin to migrate, homing to the foetal liver, a transient haematopoietic organ, where they expand to form a pool of cells that colonise the bone marrow from about E15 – 16 (Cumano and Godin, 2007) (Figure 1.1). From E11, the thymus becomes a lymphopoietic organ and is constantly seeded, first from the foetal liver and then from the bone marrow (Fontaineperus et al., 1981; Luc et al., 2012). Towards the end of gestation, *de novo* HSC generation ceases and the haematopoietic output of the foetal liver regresses (Figure 1.1). HSCs reside in the spleen and bone marrow throughout adult life, and although functionally similar, have different cycling behaviours in the two tissues, likely reflecting the different micro-environments (Morita et al., 2011).

1.2 The haematopoietic stem cell

The HSC is a remarkable and rare cell type, endowed with the ability to self-renew and clonally generate all the adult blood lineages throughout life; unlike other waves of multi- and oligo-potent blood production, it is not restricted to limited haematopoietic outputs. It has therefore aroused both basic and clinical interest and is one of the best studied tissue stem cells, setting up many of the paradigms in stem cell biology.

1.2.1 Current understanding of the HSC

The concept of the HSC began over fifty years ago with the demonstration that intravenous injection of bone marrow into lethally irradiated mice resulted in splenic colonies of cells containing

erythrocytes and myeloid cells (Till and McCulloch, 1961). Nodules on the spleen, termed splenic colonies, were also observed, and shown to be proportional to the number of marrow cells injected. Therefore, splenic colonies were thought to be clonal and at least oligopotent. This was confirmed by tracking injected marrow cells with an abnormal karyotype, and the colonies were termed colony forming units-spleen (CFU-S) (Becker et al., 1963). The identification of rare CFU-S cells within splenic colonies suggested that these cells could self-generate and may represent the HSC (Curry and Trentin, 1967; Siminovitch et al., 1963; Wu et al., 1967). It was however later shown that splenic colonies from embryos younger than E12 were not multipotent and could not self-renew, and represent a transient amplifying population (Hodgson and Bradley, 1979; Magli et al., 1982). Therefore it was suggested that HSCs produce CFU-S cells via a pre-CFU-S that, like the HSC, resides in the bone marrow (Hodgson and Bradley, 1979). The HSC was formally shown to exist when retrovirally labelled foetal liver cells were shown to reconstitute the entire haematopoietic system in lethally irradiated mice (Jordan and Lemischka, 1990; Jordan et al., 1990; Keller and Snodgrass, 1990), leading to the most rigorous description of an HSC as a cell capable of self-renewal and long term reconstitution of all blood lineages following serial transplantation into lethally irradiated mice . This definition incorporates the ability to home to a given niche, together with the long-term self-renewal and multipotency of an HSC (Lemischka, 1991; Matsuzaki et al., 2004; Osawa et al., 1996).

Due to the availability of experimental tools, HSC development has been best characterised in the mouse. They can be prospectively isolated based on their cell surface phenotype, for example, by FACS (Baum et al., 1992; Doulatov et al., 2012; Greaves et al., 1981; Spangrude et al., 1988). Functional HSCs can be isolated based on the absence of cell surface marker Lineage (Lin) present on mature blood cells and expression of Sca-1 and c-Kit, the so called $Lin^-/Sca\text{-}1^+/c\text{-}kit^+$ (LSK) population (Okada et al., 1992; Spangrude et al., 1988). They can be further separated, based on their functional output and marker profile, into LT- and ST-HSCs, with respectively extensive and limited self-renewal and repopulation capacity when serially transplanted (Adolfsson et al., 2001; Adolfsson et al., 2005; Doulatov et al., 2012; Morrison and Weissman, 1994) (Figure 1.2). Consistent with this and other tissue stem cells, is the emerging idea is that the HSC compartment does not represent a homogenous population, and has led some authors to suggest redefining the HSC as a group of cells

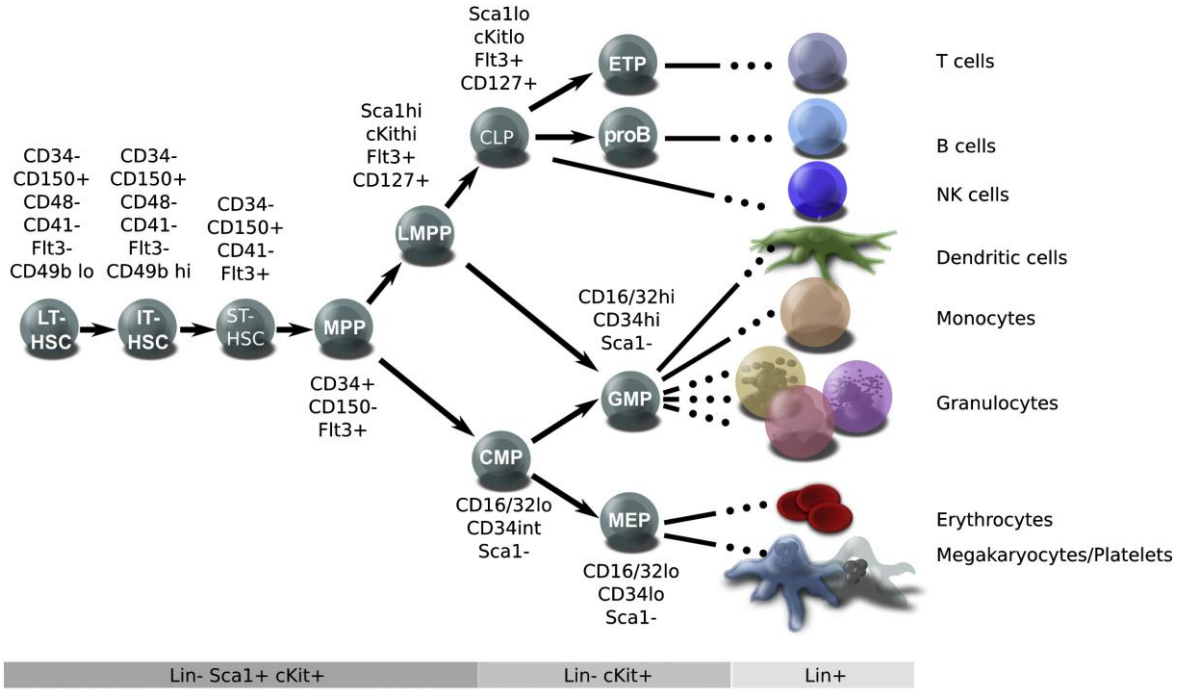

Figure 1.2 Current model of the haematopoietic tree in the mouse

Various committed and transiently stable cell populations can be prospectively isolated on their cell surface phenotype, as indicated. HSCs lie at the top of the tree and can be split into long term- (LT-) intermediate term- (IT-) or short term- (ST-) HSCs based on their repopulating potential. Inferred lineage relationships are indicated by arrows. Analogous trees can be drawn for different model systems, however, lineage commitment has been most widely studied in the mouse. MPP, multi-potent progenitor; LMPP, lymphoid primed MPP; CLP, common lymphoid progenitor; CMP, common myeloid progenitor; ETP, early thymocyte progenitor; GMP, granulocyte macrophage progenitor; MEP, megakaryocyte erythroid progenitor; NK, natural killer; Adapted from (Doulatov et al., 2012).

with varying developmental potentials based on intrinsic networks set up by transcription factors and extrinsic inputs from the niche (Orkin and Zon, 2008). Recent data tracking virally barcoded HSCs suggested that a seemingly homogenous population of HSCs show differential repopulating activity in lethally irradiated mice (Lu et al., 2011). This result adds an additional layer of complexity to the interpretation of transplantation assays, where human or mouse HSCs are introduced into lethally irradiated mice (Doulatov et al., 2012).

1.2.2 Generating the haematopoietic tree

An often overlooked property of the HSC, and of stem cells in general, is its ability to resist differentiation, but when required, to commit to a more differentiated state. Commitment can be considered roughly synonymous with lineage restriction, and therefore represents a combined loss *and* gain of activity. A classical view of lineage commitment envisages a series of bifurcations generating a hierarchy, with the HSC at the top, mature differentiated cells at the bottom, and multi- and oligo-potent progenitors in the middle (Doulatov et al., 2012; Orkin and Zon, 2008) (Figure 1.2). This concept can be visualised in schematic form as a sequence of binary fate decisions on Waddington's eponymous and elegant landscape (Waddington, 1957) (Figure 1.3). During development, cells can follow pathways that have already been set up, or etch new ones, much like water flowing down a mountain. Although attractive, this idea represents an oversimplification and may even be deceptive. It was originally thought that multipotent progenitors segregated into myeloid or lymphoid lineages (Akashi et al., 2000; Kondo et al., 1997), however there is increasing evidence for heterogeneity in transiently stable precursor populations, for example in the HSC (Lu et al., 2011). In the LSK MPP population, a cell was identified with B- and T-lymphoid, and granulocyte/macrophage potential, termed the LMPP (Adolfsson et al., 2001; Adolfsson et al., 2005; Yang et al., 2005) (Figure 1.2). This suggests that the binary segregation of the HSC to the CLP and CMP does not reflect the first commitment step, although it is not clear if an analogous population exists in humans (Doulatov et al., 2012). Transcription factors, and their network of interactions, play a key role in maintaining and driving various states. Population-based studies have suggested that lineage choice is governed by

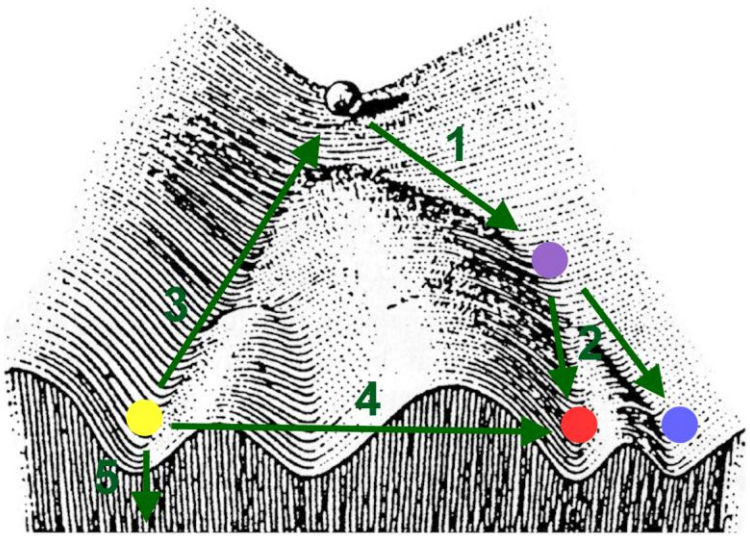

Figure 1.3 Lineage commitment and reprogramming

A pluripotent cell, such as the HSC, is maintained at the top of a metaphorical topological genetic landscape. Through a combination of induction and stochastic variation in regulatory factors, it may 'roll' down a route of minimum energy. Alternatively, a new valley may be carved into the landscape. This leads to the generation of variously committed multipotent progenitors (1), and fully differentiated mature cells (2). A committed cell can be driven to a stem like state to generate iPS cells that may be differentiated along another route (3). More recent work has shown that a commited cell may be forced to adopt a new fate without transiting through an earlier developmental state (4). Finally, a cell at any point may enter a quiescent, senescent or apoptotic state (5). Adapted from (Waddington, 1957).

global transcriptional noise, whereby multipotent cells sample various lineage-affiliated programs prior to commitment, leading to reversible lineage bias (Chang et al., 2008a). This idea has recently been challenged by analysis at the single cell level, which found the transition from self-renewal to commitment is not plastic, but rather dependent on stochastic, independent variation of master regulators, leading to discrete and uncoordinated transitions that resolve to the observed lineage commitment seen at a population level (Pina et al., 2012). Although much progress has been made describing the cellular journey taken by HSC to mature cells, technical limitations such as the relative inaccessibility of cells in the process of commitment, means the progression is not yet fully understood.

1.2.3 Current and future clinical applications

Much of the interest in studying the haematopoietic stem cell comes from its proven and potential clinical uses. The HSC represents the prototypical tissue stem cell, and, partly due to its accessibility, is the most studied stem cell. It is also the only stem cell-based therapy in routine clinical use, for both malignant and non-malignant diseases (Staal et al., 2011). While in some cases, autologous transplantation is possible, this is not always so. In the case of allogeneic transplantation, there is a risk of developing graft-versus-host disease, in which immune cells in the transplanted tissue attack the tissue of the patient. While there are ways of reducing the risk of such complications, this can result in reduced efficacy of the transplant (Hale and Waldmann, 1994; Le Blanc et al., 2008). Furthermore, not all cells transplanted engraft, as the numbers of functional HSCs is limiting. For example, in the case of cord blood transplants, tissue isolated from one umbilical cord results in a 90 % engraftment in a paediatric transplants, but only 60 % in adults. While two umbilical cords can be used in adults to reach 90 % engraftment, this results in the introduction of two exogenous immune systems into a patient, which compete, with one eventually predominating (Leonard Zon, *personal communication*). Therefore, there is an unmet clinical need to expand the HSPC pool prior to transplantation, or to HSCs in culture from a patient's own tissue, negating the need for immunologically matched donors.

Building on isolation of mouse and human ES cells, it was demonstrated that by the introduction of a defined set of transcription factors, somatic cells, including blood, could be reprogrammed to a stem-like fate – so called iPS cells (Seki et al., 2010; Staerk et al., 2010; Takahashi et al., 2007; Takahashi and Yamanaka, 2006; Yu et al., 2007) (Figure 1.3). This raised the potential for novel cell transplantation therapies and models of genetic disease. It has not yet been possible to expand the LT-HSC, or generate it by means of reprogramming strategies. However, cells resembling those found in the mature haematopoietic system have been generated, either by re-differentiation of iPS cells, or directly by trans-differentiation of fibroblasts (Szabo et al., 2010) (Figure 1.3). The first iPS cells were generated by viral introduction of reprogramming factors, however this led to concerns about insertional mutagenesis and mis-expression of oncogenes or tumour suppressor genes. More recent reprogramming strategies have involved using integration-free vectors, synthetic mRNA, direct protein delivery and small molecule approaches (Stadtfeld and Hochedlinger, 2010). This will be important in the quest to generate clinical grade HSPCs.

1.3 Programming blood

There has been an intense focus on the developmental signals involved in programming the first blood cells, with the ultimate hope that the set of knowledge gained will inform efforts to produce clinical grade HSCs *ex vivo*, to help understand disease, and to advance our biological understanding. Haematopoietic cells are specified by a combination of intrinsic factors, such as transcription factors, and extrinsic factors, such as morphogen gradients.

1.3.1 Growth factor signalling

In the chick, it has been demonstrated that blood islands only develop when endodermal and prospective haematopoietic explants are co-cultured (Miura and Wilt, 1969; Pardanaud and Dieterlen-Lievre, 1993; Wilt, 1965). Somatopleural mesoderm, which contributes to the roof of the dorsal aorta, was shown to contribute to the floor of the dorsal aorta and associated haematopoietic clusters upon

transient exposure to endoderm (Pardanaud and Dieterlen-Lievre, 1999). Alternatively, exposure to Vegf, bFgf and Tgf-β prior to grafting gave the same result, suggesting that these are endodermal signals involved in specification of adult blood (Pardanaud and Dieterlen-Lievre, 1999). In the zebrafish AGM equivalent, it has been shown that a cascade of Hh, Vegf and Notch signalling acts instructively to specify endothelial cells and blood (Burns et al., 2005; Gering and Patient, 2005). Notch1 is important for AGM but not yolk sac haematopoiesis. In the zebrafish, reduced notch signalling results in reduced *runx1* expression and fewer HSC (Burns et al., 2005; Gering and Patient, 2005). Notch1 null mice show grossly normal primitive blood development but die at E10 due to an absence of AGM haematopoiesis and HSCs (Kumano et al., 2003). Notch1 and 4, along with their ligands Dll4, Jag1 and Jag2 are expressed in the dorsal aorta, and overexpression of *runx1* in mice or zebrafish with impaired notch signalling rescues AGM haematopoiesis, suggesting that Runx1 acts downstream of Notch (Burns et al., 2005; Nakagawa et al., 2006).

Data predominantly utilising *in vitro* and *in vivo* murine models has suggested that haematopoietic signals can be split into two broad categories: Vegf, bFgf, Tgf-β and Bmp4, which are considered ventralising factors early in development, mostly promoting blood (Adamo et al., 2009; Faloon et al., 2000; Shalaby et al., 1997; Winnier et al., 1995); EGF and TGF-α which are dorsalising, inhibit haematopoietic development (Dzierzak and Speck, 2008; Pardanaud and Dieterlen-Lievre, 1999). Mice lacking *bmp4* die mostly during gastrulation, or show severe reductions in mesoderm specification and primitive erythrocyte production (Winnier et al., 1995). Overexpression of *bmp4* during ES cell differentiation or presumptive anterior head-fold explants can induce blood (Johansson and Wiles, 1995; Kanatsu and Nishikawa, 1996). In the human, mouse and zebrafish, *bmp4* is expressed in the mesenchyme underlying the dorsal aorta and in haematopoietic clusters (Durand et al., 2007; Marshall et al., 2000; Wilkinson et al., 2009). In AGM explants, overexpression of *bmp4* increases numbers of HSCs (Durand et al., 2007) whereas depletion of *bmp4* in the zebrafish reduces HSC output (Wilkinson et al., 2009) demonstrating a critical role for Bmp4 in programming the first HSCs.

1.3.2 Scl/Tal1

Scl/Tal1 (from here on Scl) is a basic helix-loop-helix transcription factor involved in human chromosomal translocations that drive some T-cell leukaemias (Lecuyer and Hoang, 2004). In the mouse, it is expressed at E7.5 in the blood islands, then subsequently mostly in haematopoietic and vascular cells (Elefanty et al., 1999; Kallianpur et al., 1994). Mice where *scl* has been knocked out lack yolk sac haematopoiesis and die at E9.5 (Robb et al., 1995; Shivdasani et al., 1995). In culture, Scl is not required for commitment of mesoderm to Flk1 positive haemangioblast, however there is a subsequent requirement for further haematopoietic commitment (D'Souza et al., 2005; Endoh et al., 2002). Conditional depletion of *scl* in *tie2* expressing blood tissue resulted in quantitatively and qualitatively normal HSCs, suggesting that Scl is necessary for specification of haemogenic endothelium before *tie2*-Cre mediated gene ablation becomes effective, but is subsequently not required for maintenance of the HSCs, even though it continues to be expressed in this population of cells (Schlaeger et al., 2005). It has been shown that HSC specific enhancers of Scl are regulated by Gata and Ets factors (Gottgens et al., 2002).

1.3.3 Lmo2

Similarly to Scl, the LIM domain only protein, Lmo2 is an essential transcriptional regulator of normal haematopoietic development. Lmo2 was first cloned from a T-ALL patient bearing a chromosomal translocation (Boehm et al., 1991; Royer-Pokora et al., 1991). Ectopic activation of Lmo2 is thought to drive T-ALL by reactivating the HSC programme in preleukemic thymocytes (McCormack et al., 2010). Furthermore, in a cohort of patients undergoing retroviral mediated gene therapy for SCID-X1, a proportion developed T-ALL. In these patients, it was shown that *lmo2* was insertionally activated, resulting in clonal proliferation of thymocytes (Hacein-Bey-Abina et al., 2003). During development, Lmo2 is expressed in haematopoietic progenitors, erythroid cells, megakaryocytes and endothelial cells (Warren et al., 1994; Yamada et al., 2000). Mice lacking *lmo2* die around E9.5 due to severe anaemia (Warren et al., 1994) and null ES cells could not contribute to adult haematopoietic lineages in chimeric mice (Yamada et al., 1998), demonstrating a role in primitive and

adult blood. A role for Lmo2 in remodelling the primitive network of capillaries into the mature vasculature has also been described in chimeric mice (Yamada et al., 2000).

Lmo2 is a member of a subset of the zinc finger family of transcription factors, the Lmo proteins. These are small proteins containing two LIM domains, each made up of two zinc fingers (Kadrmas and Beckerle, 2004). Rather than directly binding DNA, Lmo proteins are thought to act as molecular scaffolds; Lmo2 has been shown to interact with Scl and its heterodimerisation partner E2A (E47/E12) (Begley and Green, 1999; Larson et al., 1996; Patterson et al., 2007; Porcher et al., 1996; Shivdasani et al., 1995; Valgearcher et al., 1994), the haematopoietic transcription factors Gata1/2, AF6 (whose fusion to MLL can drive leukaemia) (Osada et al., 1997), and Ldb1, a widely expressed nuclear adapter protein (Agulnick et al., 1996; Jurata et al., 1996). These higher order complexes are able to bridge multiple DNA sites, for example between E-boxes (CANNTG) and GATA (WGATAR) sites, and drive distinct cell fates (Bach, 2000). Additionally, the synergy between Scl and Lmo2 is required for haematopoietic development in the zebrafish and in cultured cells (Patterson et al., 2007; Schlaeger et al., 2004).

1.3.4 Gata2

Several roles for the zinc finger transcription factor Gata2 in programming HSPCs have been described (Rodrigues et al., 2012). Mice lacking the transcription factor Gata2 have severe anaemia due to defects in primitive blood, and die around E10.5 (Tsai et al., 1994). As Gata2 is expressed in the arotic endothelium (Minegishi et al., 1999), and from experiments in cultured cells (Tsai et al., 1994), it was suggested that Gata2 may also play a role in programming the HSC in the AGM. This was shown to be the case in Gata2 haploinsufficient mice. While yolk sac haematopoiesis was largely normal, AGM HSCs were severely depleted (Ling et al., 2004). Gata2 also has a role in adult HSCs, where a two-fold increase in expression resulted in a 40 fold decrease in numbers of HSCs and reduced differentiation potential upon transplantation (Heyworth et al., 1999; Pearson et al., 2008). It was also found that upregulation of Gata2 in cord blood blocked its repopulating activity and increased G_0 residency (Tipping et al., 2009). It has recently been shown that increased expression of Gata2 in AML

patients leads to a poor prognosis (Vicente et al., 2012). This may be due in part to resistance of the non-cycling G_0 population to cytotoxic agents.

1.3.5 Runx1

Runx1 is a Runt domain-containing transcription factor expressed in haematopoietic cells and the endothelium that contacts nascent blood cells, both in extra-embryonic tissue and in the embryo proper (North et al., 1999; North et al., 2002). Like Scl and Lmo2, it has been shown to regulate haematopoiesis (Speck and Gilliland, 2002). Knockout embryos die around E12.5 due to haemorrhaging. While primitive blood is largely normal, intra-aortic clusters do not form (North et al., 1999), and there is no definitive output (Lacaud et al., 2002; Okuda et al., 1996; Wang et al., 1996). Runx1 is not required for endothelial development, however it is required for transition of endothelium to blood (Kissa and Herbomel, 2010; Lancrin et al., 2009; Yokomizo et al., 2001). Conditional depletion of Runx1 in VE-cad positive endothelial cells, including cells of the dorsal aorta, results in fewer HSCs, whereas HSC production is unaffected when Runx1 is deleted later on in cells expressing the haematopoietic nucleotide exchange factor Vav1, suggesting that like Scl, Runx1 is dispensable after the haemogenic endothelial stage (Chen et al., 2009). It has been suggested that Runx1 mediated down regulation of the endothelial programme is required for the EHT (Lancrin et al., 2009; North et al., 2002). Consistent with this, only Runx1 could reverse the endothelial signature established by Hoxa3 in haemogenic endothelium (Iacovino et al., 2011). In mice haploinsufficient for Runx1, transplantation into irradiated recipients demonstrates an increase in AGM HSCs. However, if cultured prior to transplant, fewer AGM, but increased yolk sac and placental HSCs are observed. This may reflect differential mechanisms in play at the various sites (North et al., 2002; Robin et al., 2006). Additionally, it has been shown that a complex containing Scl, Ets factors and Gata factors regulates the HSC activity of Runx1 (Landry et al., 2008; Nottingham et al., 2007; Patterson et al., 2005) and the Ets family TF Pu.1, which is required for definitive haematopoiesis, is a downstream target of Runx1 (Huang et al., 2008; McKercher et al., 1996; Okada et al., 1998). It has since been shown that in ES cells undergoing haematopoietic commitment, Runx1 only transiently interacts with *pu.1* regulatory

elements to contribute to an open chromatin state around the haemangioblast stage (Hoogenkamp et al., 2009).

1.4 Vascular development

Together with blood, the vasculature is one of the first organ systems to develop, reflecting how the demands for oxygen in a growing embryo quickly exceed what can be provided by diffusion alone. The mature vasculature is set up by three mechanisms: vasculogenesis, angiogenesis and arteriogenesis. By these cellular processes, a circulatory system is laid down to meet the demands of tissue oxygenation, nutrient delivery, waste removal, immune response, and in mammals and birds, temperature regulation. During development, the initial vascular network is established *de novo* by vasculogenesis. Angiogenic events remodel this primary network, allowing extensive growth of blood vessels. Additionally, endothelial cells adopt an arterial or venous fate. In response to increased blood flow and mechanical stress, the diameter of arterial vessel increases through the process of arteriogenesis (Patel-Hett and D'Amore, 2011). Additionally, aberrant vessel development is important in a number of disease states, for example cancer, psoriasis, rheumatoid arthritis, ulcers, cardiovascular disease, stroke and age-related vision loss. Therefore, therapies that either promote or inhibit vascular development are important in a clinical setting (Folkman, 1971; Patel-Hett and D'Amore, 2011).

1.4.1 Vasculogenesis

The first blood vessels in mammals form in intra- and extra-embryonic tissues, a process first observed almost 100 years ago (Reagan, 1915; Sabin, 1920). The term vasculogenesis was coined a quarter century ago to describe this *de novo* generation of vasculature (Risau and Lemmon, 1988; Risau et al., 1988). Vasculogenesis initiates shortly after gastrulation at E8.5 in the embryonic mesoderm along with the periphery of yolk sac blood islands. The allantois and placenta have also been identified as vasculogenic sites (Caprioli et al., 2001). The axial vessels within the embryo and primitive vascular plexuses are generated by vasculogenesis. Highly motile cells termed angioblasts, first detected in the

periphery of the blood islands and later in the embryo proper generate a primitive vascular network by a combination of proliferation, coalescence, migration and differentiation to endothelial cells. Neo-vascularisation of organs, including the liver, spleen and lungs, also occurs through vasculogenesis (Pardanaud and Dieterlen-Lievre, 1993; Ribatti et al., 2009). Additionally, a role for vasculogenesis has been described in post-ischemic injury (Asahara et al., 1997; Tongers et al., 2010).

Fgf and endodermal Hh signalling is required for the induction of angioblasts (Cox and Poole, 2000; Vokes and Krieg, 2002; Vokes et al., 2004). Soon after endothelial specification, the Vegf receptors Flk1 (Vegfr2) and Flt1 (Vegfr1) are expressed (Millauer et al., 1993; Yamaguchi et al., 1993) and it has been shown that activity of the Vegf gene family plays an instructive role in forming the angioblasts (Coultas et al., 2005; Rossant and Howard, 2002). The angioblast precursors express the major VegfA receptor Flk1 and arise from a subset of Brachyury-positive cells in the primitive streak (Millauer et al., 1993; Wise et al., 1999; Yamaguchi et al., 1993). Flk1 null embryos die at E9 due to failure of both haematopoietic and endothelial development (Shalaby et al., 1997; Shalaby et al., 1995). Flt1 null embryos also die during development, but have excessive endothelial progenitors. Therefore Flt1 may act negatively to modulate VegfA signalling (Fong et al., 1999). Furthermore, embryos lacking a single allele of VegfA die during mid-gestation due to reduced numbers of blood vessels (Carmeliet et al., 1996; Ferrara et al., 1996). In Xenopus, angioblasts migrate from the lateral mesoderm towards the *vegfa*-expressing hypochord, a transient midline structure. Implanting Vegf-soaked beads caused aberrant angioblast migration towards the beads, demonstrating a role for Vegf in this process (Cleaver and Krieg, 1998). In zebrafish, the knockdown of *vegf* results in fewer angioblasts, but normal migration, suggesting that Vegf is not required for migration, or that there is some level of redundancy (Jin et al., 2005). Although not as well studied, roles for neuropilins and Tgf-β signalling in vasculogenesis have also been proposed (Patel-Hett and D'Amore, 2011). Additionally, recent data in the zebrafish has suggested a potential role for Gata2 in the formation of the dorsal aorta (Zhu et al., 2011b).

1.4.2 Angiogenesis

Following vasculogenesis, angiogenic remodelling takes place. More endothelial cells are generated, and the processes of sprouting, elongation, division and anastomosis generates the mature vascular tree (Risau, 1997). Many molecular cues have been implicated in the process, including Notch signalling, Semaphorins, Ephrins, Netrins, Slits, Sprouty, Angiopoietin/Tie and Tgf-β signalling (Larrivee et al., 2009; Patel-Hett and D'Amore, 2011; Rossant and Howard, 2002). In the embryo, angiogenesis commences around E9.5 to eventually form the majority of blood vessels. In addition, this process is also responsible for the vascularisation of organs derived from ectoderm and mesoderm, such as the brain and kidney (Patel-Hett and D'Amore, 2011). To effectively oxygenate a tissue, an even distribution of vessels is necessary, and this may be achieved by pruning an existing vascular plexus or by sprouting angiogenesis. Of interest, some of these signals are shared with those described as cues for development of the axonal network, a structure topologically similar to the vasculature (Eichmann et al., 2005; Larrivee et al., 2009; Mukouyama et al., 2002).

Sprouting angiogenesis is a highly coordinated process that has been extensively studied. It initiates with the local disruption of the vesicular basement membrane. Specialised endothelial cells termed tip cells are primed to respond to angiogenic stimuli and migrate toward the source of signalling, taking with them connected endothelial stalk cells to generate a branch (Figure 1.4). Further proliferation and alignment occurs, followed by lumenisation of the new vessel (Gerhardt et al., 2003; Karamysheva, 2008; Patan, 2000). The vessel is stabilised by the association of pericytes, smooth muscle and basement membrane deposition. Pdgf, Angiopoietins and Tie receptor have been shown to be important in this process. Vessels may also connect to neighbouring vessels to create a perfused vascular circuit (Patel-Hett and D'Amore, 2011).

In the zebrafish, the first, and best characterised, angiogenic events are those that contribute to the formation of the intersegmental vessels (ISVs). ISV formation involves two angiogenic waves (Isogai et al., 2003) (Figure 1.4). At around 22 hpf, endothelial tip cells in the roof of the dorsal aorta, sprout and migrate dorsally, following the somite boundary towards the horizontal myoseptum. From here, they continue dorsally towards the roof of the neural tube, taking with them stalk cells to form

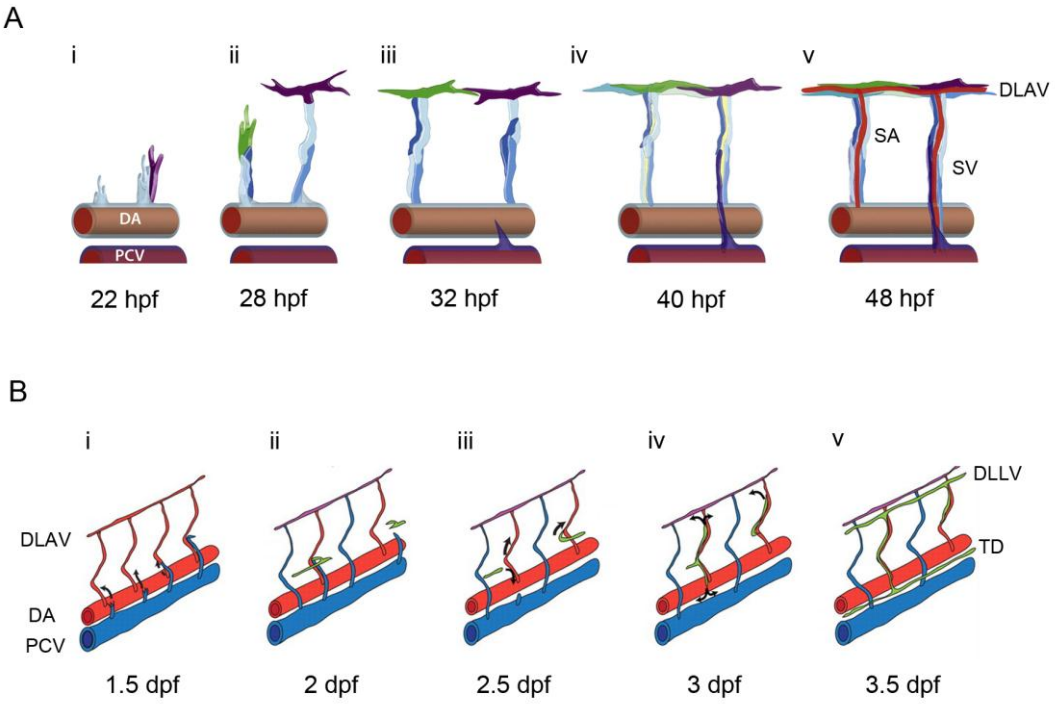

Figure 1.4 Lymph-angiogenesis in the zebrafish trunk

(A) Two neighbouring sprouts are depicted, with tip cells indicated in green and purple. Around 22 hpf, tip cells from the dorsal aorta sprout and migrate dorsally, taking with them stalk cells to form primary ISVs (i). At this stage, sprouts consist of 2 to 4 cells (ii). Tip cells generate anterior and posterior extensions and connect to their neighbours to create the future DLAV, and secondary ISVs begin to sprout from the PCV (iii). Secondary ISVs either connect to existing primary ISVs, converting them to a venous identity, or contribute to the lymphatic vasculature, and the newly formed vessels begin to generate a lumen (iv). The newly established vasculature loop becomes perfused with blood (v). (B) Secondary sprouts from the PCV that do not connect to primary sprouts migrate to the horizontal myoseptum to generate a pool of parachordal lymphangioblasts, green cells (i – ii). These cells proceed to migrate ventrally or dorsally, using the segmental artery as a scaffold, to form the DLLV and TD (iii – v). Anterior to the left, posterior to the right. PCV, posterior cardinal vein; DA, dorsal aorta; DLAV, dorsal longitudinal anastomotic vessel; SA, segmental artery, SV, segmental vein; DLLV, dorsal longitudinal lateral lymphatic vessel; TD, thoracic duct. Adapted from (Bussmann et al., 2010; Ellertsdottir et al., 2010).

the primary ISVs. They branch and connect dorsally with their anterior and posterior neighbours to form the future dorsal longitudinal anastomotic vessel (DLAV). From around 32 hpf, a second angiogenic wave initiates from the roof of the cardinal vein (Yaniv et al., 2006). These sprouts either connect to the primary ISVs, converting them to veins, or contribute to the lymphatic vasculature (Hogan et al., 2009; Isogai et al., 2003) (Figure 1.4). The molecular mechanisms controlling angiogenic sprouting in the fish are similar to those in the mouse (Ellertsdottir et al., 2010). Tip cells exhibit low Notch signalling, are highly migratory and extend numerous filopodia, thus displaying the strongest angiogenic behaviour. In contrast, stalk cells exhibit high Notch signalling and have reduced migratory behaviour which is important in maintaining the sprout integrity (Siekmann et al., 2008).

The lumens of the ISVs and DLAV become patent soon after they have connected. Endothelial cells pinocytose solutes from the extracellular space to form vacuoles (Ellertsdottir et al., 2010). By following labelled circulating blood, it was observed that the lumen opens up in a step-wise fashion to form the axial vessels. This is consistent with a mechanism where successive intracellular vacuoles fuse to form a lumen within an endothelial cell, and eventually between neighbouring endothelial cells (Kamei et al., 2006). Hence a unicellular tube devoid of cell junctions across the transverse axis of the vessel is formed. However analysis of cell junctions in ISVs suggests extensive overlapping, more consistent with a process of cord hollowing, when a continuous apical surface bounded by at least two endothelial cells is formed. Vacuoles are then exocytosed into this space to form a lumen (Blum et al., 2008). These two processes may however not be mutually exclusive.

1.4.3 Arterial versus venous identity

A classical view of vascular identity was based on the direction and pressure of blood flow. Circulatory dynamics was thought to be both necessary and sufficient to set up the structural and functional differences between arteries and veins (Lawson and Weinstein, 2002). This paradigm was challenged 15 years ago with the discovery of Ephrin-B2 and EphB4 as specific markers of arteries and veins, suggesting that vascular fates were set up prior to the onset of circulation (Wang et al., 1998).

Subsequent studies have confirmed a molecular function in vascular fate (Gore et al., 2012; Lin et al., 2007).

Deletion of Notch1 and Notch2, its receptor Dll4, or its target genes Hey1 and Hey2, has shown that Notch signalling plays an important role in setting up an arterial fate (Lin et al., 2007; Villa et al., 2001). In zebrafish mindbomb mutants containing mutations of the *mib* gene, which encodes a RING E3 ligase required for Notch activation via ubiquitylation and internalization of Notch ligands, arterial formation is defective and expression of *ephrin-b2a* and *notch3/5* is reduced. Overexpression of Notch3/5 results in decreased expression of the venous marker *flt4* (Lawson et al., 2001). The zebrafish mutant gridlock (*grl*), which encodes a *hey2* orthologue, lacks circulation due to failure of dorsal aorta maturation (Zhong et al., 2000). Depletion of *grl* results in reduced arterial gene expression, whereas overexpression causes ectopic arterial gene expression and a reduction in venous *flt4* expression (Zhong et al., 2001). Hh and Vegf signalling act upstream of Notch signalling to specify arterial fate (Gering and Patient, 2005; Lawson et al., 2002). Zebrafish lacking the midline patterner Shh, which is expressed in the notochord, do not develop circulation due to failure of dorsal aorta specification (Krauss et al., 1993; Lawson et al., 2002). Knockdown of *shh* results in a loss of *vegfa* in the somites and knockdown or overexpression of *vegfa* results in a respective loss or gain of arterial markers (Lawson et al., 2002). Furthermore, introduction of *vegfa* can rescue the *shh* mutants (Lawson et al., 2001). Recently, it was shown that Hh signalling can act instructively in inducing an arterial identity indepent of Vegf signalling via the calcitonin receptor-like receptor (Wilkinson et al., 2012).

It had been proposed that the venous programme was the default state of a nascent endothelial cell, or was programmed by low or absent Hh signalling (Thurston and Yancopoulos, 2001). However, it has now been shown that venous identity is actively established, and arterial identity repressed (You et al., 2005). Expression of the orphan nuclear receptor chicken ovalbumin upstream promoter transcription factor II (*coup-tfII*) is restricted to veins and mediates the balance between the arterial and venous fates. Its ablation results in an aberrant arterial identity, whereas overexpression causes fusion of arteries and veins (Huppert et al., 2000; Kawasaki et al., 1999; You et al., 2005). In the zebrafish, PI3K signalling plays a role in maintaining venous identity, acting downstream of Vegf to

inhibit MAPK signalling. MAPK signalling promotes an arterial fate by signalling through Erk. In the zebrafish, Erk is one of the earliest markers of future arterial fate in angioblasts that have recently migrated to the midline (Hong et al., 2006).

1.5 The zebrafish as a model system

Over the past quarter century, the zebrafish has become a popular model to study various aspects of embryonic development, complementing studies in more established systems (Dahm and Geisler, 2006). More recently, is has been used to model human disease and in drug discovery (Jing and Zon, 2011). The zebrafish has proved particularly powerful in the study of haematopoietic and vascular development (Chen and Zon, 2009), facilitated by numerous mutants generated from forward genetic screens exhibiting haematopoietic and vascular defects (Ransom et al., 1996; Stainier et al., 1995; Weinstein et al., 1996).

The zebrafish has several practical and experimental advantages. They are relatively easy to maintain and breed. They generate a large number of non-adherent and externally fertilised embryos, which are easy to harvest. Their generation time is relatively fast and early development is very quick; within 24 hours, the main body plan has been established, and by 5 dpf, organogenesis is complete (Kimmel et al., 1995). Large scale forward genetic screens are feasible, and embryos are robust and therefore amenable to microinjection. Owing to a high quality annotation of the genome, it is quick to clone a gene (http://www.sanger.ac.uk/Projects/D_rerio/). Genes can be easily knocked down with antisense morpholinos, or overexpressed with exogenous RNA or DNA (Summerton and Weller, 1997; Summerton, 2007). The chorion surrounding the embryo, and at early stages of development the embryo itself, is translucent, greatly facilitating the observation and imaging of developmental processes. Finally, and most importantly, it has become increasingly clear that genetic regulation and developmental processes are overwhelmingly conserved between the teleosts and higher vertebrates.

1.5.1 Zebrafish embryonic development

Soon after fertilisation, cytoplasmic streaming occurs to generate a large blastodisc on top of the yolk. Over the following three hours, cleavage occurs. This process is characterised by synchronous divisions without cell growth every 20 minutes, thus generating a mass of approximately 1000 small cells on the yolk cell (Kimmel et al., 1995). At the 512-cell stage, a critical ratio between DNA and cytoplasm is reached, triggering the midblastula transition (MBT). The cell cycle lengthens and zygotic gene expression initiates (Kane and Kimmel, 1993). At the beginning of MBT, cells in the blastoderm margin subside onto the yolk cell to form a thin multi-nucleated layer of cells termed the yolk syncytial layer (YSL) (Kimmel and Law, 1985). At around 4 hpf, gross cellular rearrangements begin to pattern the blastoderm into the vertebrate body plan. The process of epiboly initiates: the blastoderm cells migrate over the yolk, thinning in the process. At 50 % epiboly, gastrulation begins, generating the three germ layers. Cells on the dorsal blastoderm margin involute, a process which continues, expanding to include cells all around the margin, until the tailbud-stage when the mass of cells has fully enveloped the yolk (Figure 1.5 A-B). The process of convergence and extension begins at 60 % epiboly and continues to the tailbud stage, remodelling the gastrulating cells into the vertebrate body plan (Figure 1.5 C).

At 50 % epiboly, it becomes technically possible to generate a fate map for the zebrafish embryo (Kimmel et al., 1990; Schier and Talbot, 2005) (Figure 1.5 D-E). Cells at the margin of the blastoderm contribute to mesodermal structures, and those further away to ectodermal structures. Cells on the dorsal axis have a tendency to contribute to axial and anterior structures, whereas ventral cells contribute to posterior structures. Blood and endothelial cells form from ventral mesodermal cells (Stern, 2004) (Figure 1.5 D-E). Between the tailbud stage (10 hpf) and 24 hpf, somitogenesis occurs, characterised by regular segmentation of the paraxial mesoderm occuring in an anterior to posterior direction to generate blocks of somites. Additionally, a yolk extension develops posteriorly, under the trunk of the embryo. The heart begins to beat at 24 hpf and circulation initiates just after 26 hpf (Schier and Talbot, 2005).

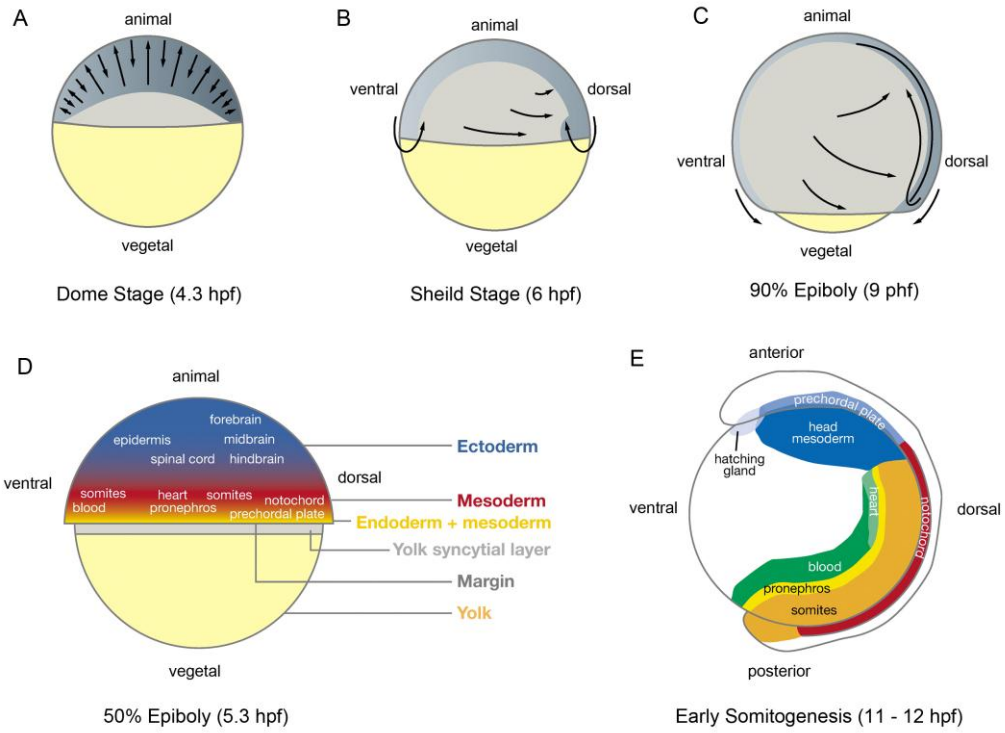

Figure 1.5 Zebrafish gastrulation and fate maps

(A) At the dome stage, cells undergo radial intercalation, contributing to epibolic movements. (B) From shield stage, cells internalise and migrate towards the animal pole, defining the three embryonic germ layers in the process. (C) At 90 % epiboly, the process of convergence and extension remodels the mass of cells enveloping the yolk. (D) A zebrafish fate map at 50 % epiboly, with germ layers arranged along the animal-vegetal axis, and mesodermal and ectodermal fates along the dorsal-ventral axis. At this stage, fate boundaries are not sharply defined. (E) Inferred fate map of mesoderm during early somitogenesis, from expression of known lineage restricted genes. The posterior tailbud region will continue to extend to form mesodermal and ectodermal structures of the trunk and tail. Adapted from (Schier and Talbot, 2005).

1.5.2 The origin of blood and endothelium in zebrafish

In contrast to the mouse and chick, in the zebrafish, all blood and endothelial development, including the formation of primitive blood, occurs within the embryo proper. Lineage tracing experiments have demonstrated that blood is derived from ventral mesoderm, whose patterning is due to signalling through the Tgf-β family, Wnt and Fgf (Mathieu et al., 2004; Schier and Talbot, 2005; Walmsley et al., 2008). A gradient of Bmp, a Tgf-β family member, is key in dorsal ventral patterning (Ben-Zvi et al., 2008). High Bmp patterns ventral mesoderm, and an environment of low Bmp set up by Bmp antagonists, patterns dorsal ectoderm (Harland and Gerhart, 1997). Furthermore, within the mesoderm, a dorsal-ventral gradient of Bmp specifies various fates. Low Bmp specifies axial mesoderm dorsally, and paraxial mesoderm more ventrally. High Bmp ventrally specifies lateral plates, from which blood and endothelium arises (Neave et al., 1997). Bmp within the lateral plate further restricts fate, with the PLM, heart and ALM being specified by a respective high to low gradient of Bmp signalling (Lieschke et al., 2002).

Gross cellular rearrangements and morphological movements during gastrulation result in the formation of the lateral plate mesoderm. This tissue is characterised by bilateral stripes adjacent to the more medial paraxial mesoderm (Gering and Patient, 2005). Within the PLM, the more lateral tissue forms the pronephric duct, whereas the more medial tissue contains derivatives of the haemangioblast. These cells have been shown to initiate gene expression in a hierarchical manner, and resolve to express both blood and endothelial genes at the population level until the 10 ss, after which blood and endothelial progenitors diverge and migrate under the somites towards the midline (Brown et al., 2000; Patterson et al., 2005). Initiation of migration occurs in an anterior to posterior fashion, beginning at 12 ss in the anterior most PLM. The first cells to migrate are Flk1 positive angioblasts that go on to form the dorsal aorta, reaching the midline at the 15 ss. This is followed by migration of the primitive erythroid progenitors, and angioblasts destined to become the axial vein (Gering and Patient, 2005) (Figure 1.6). These reach the midline at 18 ss and form a mass of cells at the midline termed the ICM, whose haematopoietic output is analogous to that of the yolk sac blood islands in mice (Detrich et al., 1995). Around 22 hpf, the dorsal aorta lumenises and from 23 hpf polarises, such that cells in the roof are transcriptionally and functionally distinct from the floor (Wilkinson et al., 2009). The axial vein

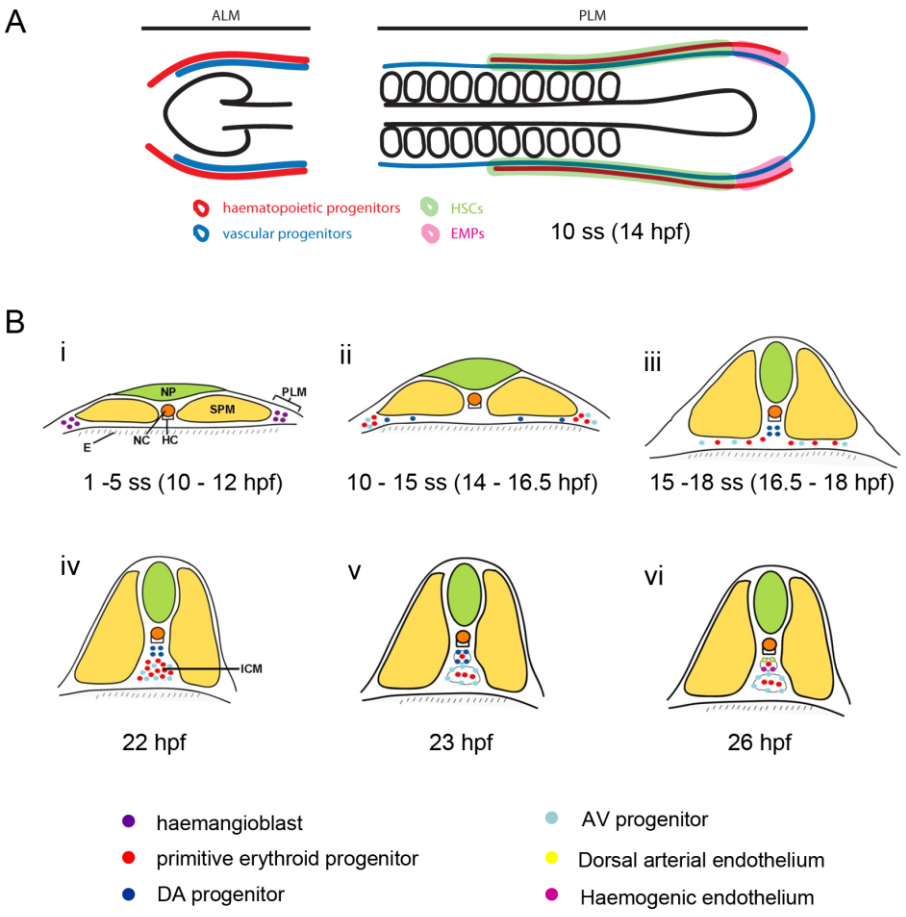

Figure 1.6 Early zebrafish blood and endothelial development

(A) Fate map of the ALM and PLM. Schematic representation of a flat mounted embryo with the anterior to the left and posterior to the right, viewed from the dorsal aspect. (B) Transverse projection of the developing trunk, following migration of cell populations to the midline. ALM, anterior lateral plate mesoderm; PLM, posterior lateral plate mesoderm; EMP, erythromyeloid progenitor; SPM, somitic paraxial mesoderm; NC, notochord; HC, hypochord; NP, neural plate; ICM, intermediate cell mass; E, endoderm. Adapted from (Gering and Patient, 2005; Monteiro et al., 2011).

lumenises at 25 hpf, just prior to the initiation of circulation (Figure 1.6 and Figure 1.7). Primitive erythrocytes remain intermingled with, and attached to, cells of the axial vein, before being synchronously released into the circulation. This release has been shown to be dependent on the activity of the metalloprotease, Adam8 (Iida et al., 2010).

The ALM and PLM have distinct endothelial and haematopoietic outputs, reflecting their distinct genetic programming. The ALM expresses the myeloid marker *pu.1* but not the erythroid marker *gata1* and contributes to the head vasculature and primitive myeloid cells (Detrich et al., 1995; Lieschke et al., 2002). Some of these leukocytes enter circulation. Others migrate through the tissue and differentiate into macrophages, and later on into neutrophils (Herbomel et al., 1999; Herbomel et al., 2001; Le Guyader et al., 2008; Lieschke et al., 2002). In contrast, the PLM expresses erythroid genes and mostly generates the trunk and tail vasculature, together with primitive red blood (Detrich et al., 1995; Herbomel et al., 1999). Tissue from the posterior most *lmo2* positive PLM forms the posterior blood island (PBI) (Figure 1.7). Erythromyeloid progenitors (EMPs) arise between 24 and 30 hpf from this tissue, independently of HSC generation (Bertrand et al., 2007) (Figure 1.7). These cells are analogous to the second wave of yolk sac haematopoiesis in the mouse, and represent a transient population with limited potential. More recently it has been shown that, in contrast to the development of HSCs, Notch signalling is not required for EMP development (Bertrand et al., 2010b).

In the zebrafish, definitive haematopoiesis initiates with the generation of HSCs from *runx1* positive cells arising from the floor of the dorsal aorta (Kalev-Zylinska et al., 2002; Zhang and Rodaway, 2007). Expression of *runx1* in the dorsal aorta is dependent on Notch and Hh signalling. Although a direct role for Notch in setting up the HSC programme has been demonstrated, it is not clear if it is required within HSCs themselves (Burns et al., 2005; Gering and Patient, 2005; Kalev-Zylinska et al., 2002; Thompson et al., 1998). Recently, taking advantage of zebrafish mutants lacking circulation, it has been shown that a haemodynamic force is required to maintain the HSC programme and for maturation of the dorsal aorta, and that this effect is at least in part mediated by a *klf2a*-Nitric Oxide cascade (Adamo et al., 2009; North et al., 2009; Wang et al., 2011). Additionally, it has been shown that non-canonical Wnt16 signalling is required to turn on the somitic expression of the Notch

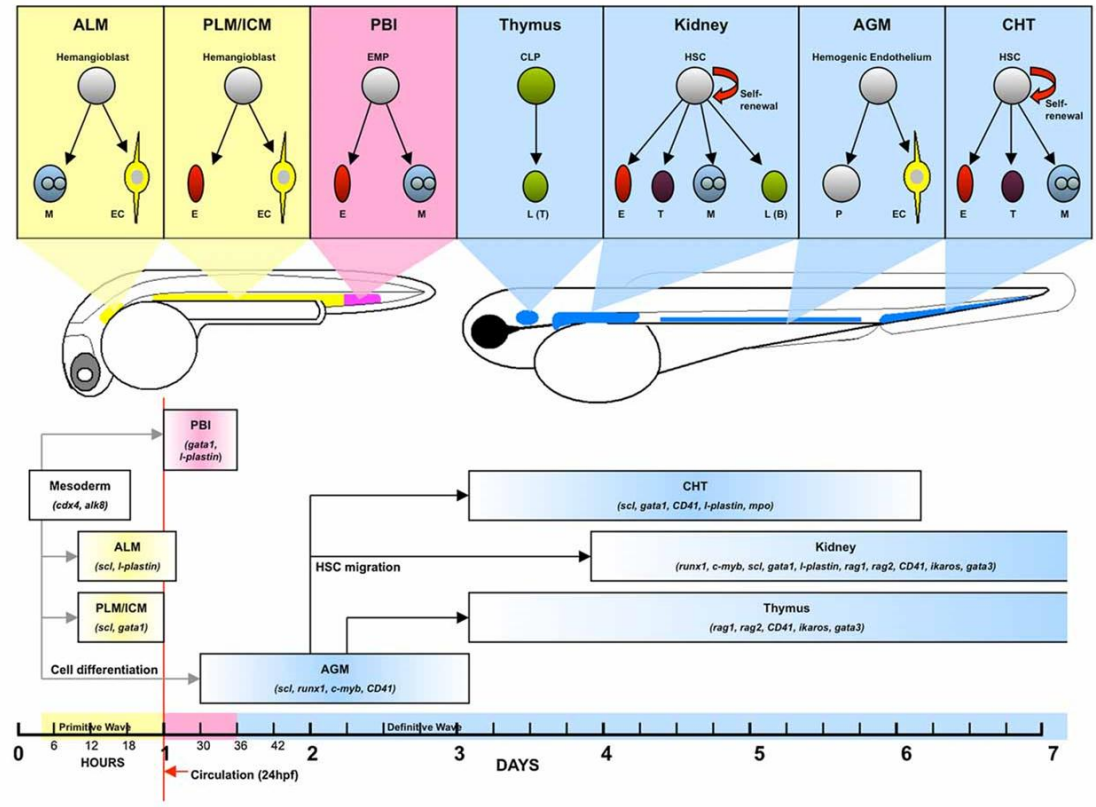

Figure 1.7 Spatial and temporal restriction of zebrafish haematopoiesis

Top panel depicts the various sites and outputs of haematopoiesis in the zebrafish. Yellow indicates primitive haematopoiesis from the presumptive haemangioblast. Pink indicates the first haematopoietic progenitors with multilineage potential. Definitive haematopoiesis is shown in blue. The bottom panel shows the timing of the various waves of haematopoiesis and migration of the HSC to secondary and adult sites of haematopoiesis, along with genes typically used to mark these tissues. ALM, anterior lateral mesoderm; PLM, posterior lateral mesoderm; ICM, intermediate cell mass; PBI, posterior blood island; AGM, aorta-gonad-mesonephros equivalent; CHT, caudal hematopoietic tissue; HSC, hematopoietic stem cell; M, myeloid; EC, endothelial cell; E, erythroid; EMP, erythromyeloid progenitor; CLP, common lymphoid progenitor; L(T), lymphoid T cell; L(B), lymphoid B cell; T, thromboid; P, hematopoietic progenitor cell; hpf, hours post-fertilization. Reproduced from (Chen and Zon, 2009).

ligands *deltaC* and *deltaD*, which in turn are necessary for HSC development (Clements et al., 2011). This data supports the view that, in addition to cell autonomous cues, signals from the somites are also able to modulate haemogenic endothelium (Ciau-Uitz et al., 2010).

Consistent with observations in the mouse, lineage tracing in the zebrafish demonstrated that from the AGM, HSCs homing to secondary haematopoietic niches, before colonising the adult haematopoietic sites. After entering circulation, HSCs seed the caudal haematopoietic tissue (CHT), a vascular plexus analogous to the foetal liver. Here they expand and undergo limited lineage commitment (Kissa et al., 2008; Murayama et al., 2006) (Figure 1.7). Subsequently, HSCs and progenitors seed the thymus from 3.5 dpf, where they mature into T-cells, and subsequently the kidney marrow, where they reside in the adult fish (Kissa et al., 2008; Murayama et al., 2006; Willett et al., 1999) (Figure 1.7). Recently, it was shown that cMyb transcription factor is required to allow HSPC migration away from the AGM to secondary haematopoietic tissues by modulating Sdf1a signalling (Zhang et al., 2011).

1.6 Objectives

Transcriptional control is central to the development of blood and endothelial populations; several key transcription factors and transcriptional complexes have previously been reported. Understanding the interplay between these factors with respect to their transcriptional output is therefore important, and it is reasonable to predict that this will lead to new biological insights. Moreover, many transcription (co-)factors have been linked with various human disease states, therefore a more sophisticated understanding of their biology is likely to result in novel therapies.

A complex containing the transcription factors Scl and Lmo2 has previously been linked with erythroid development. It has now been shown that the combined activity of these two proteins is reused in earlier developmental contexts. This thesis will utilise these observations, together with a set of recently solved crystal structures, to identify functionally important residues within the Lmo2 molecule. This will include investigating interactions with other transcription factors. A complex

containing the related transcription factor Lmo4, has been identified in erythroid cells. This thesis investigates whether Lmo4 and its partners, like Lmo2, have an earlier haematopoietic input into both primitive and definitive blood. The epistatic relationships between Lmo4 and known haematopoietic regulators will also be studied. Given that pathways are often reused during development (Patterson et al., 2007), this will often necessitate conditional strategies to overcome earlier functions. Finally, as HSC emergence and arterial specification are intimately linked, potential roles for novel haematopoietic genes in vasculogenesis and angiogenesis will be investigated.

In short, through gain-of-function and loss-of-function experiments, the main goals of this thesis are: (1) to extend the understanding of transcription factors that play a role in developmental haematopoiesis; (2) to identify novel molecules that regulate the blood and endothelial programmes; and (3) to investigate genetic mechanisms of, and relationships between these novel players, within the four dimensions of development.

Chapter 2

Materials and Methods

2.1 Maintenance and manipulation of zebrafish embryos

2.1.1 Maintenance of fish

Zebrafish (*Danio rerio*) were maintained in flowing system water at 28.5 °C, a conductance in the range 450-550 μS, and pH 7.1-7.2. Fish were cycled between 14 hours of light, and 10 hours of darkness. Fish were fed on a mixed diet of flake food, high protein pellets and enriched brine shrimp three times a day (BMS Staff, University of Oxford). All zebrafish work was approved by the University of Oxford research ethics committee.

2.1.2 Obtaining and staging zebrafish embryos

Marbles boxes were placed in tanks about 15 hours before the lights came on. Eggs were collected from natural spawning and washed in system water. Embryos were grown between 22 °C and 32 °C in system water or E3 medium. Methylene blue was added to inhibit fungal growth and embryos were staged under a dissecting microscope according to (Kimmel et al., 1995).

2.1.3 Zebrafish lines

Zebrafish lines employed in this thesis were wt^{kcl}, $Tg(fli1:EGFP)^{y1}$ (Lawson and Weinstein, 2002), $Tg(kdrl:EGFP)^{s843}$ (Jin et al., 2005), $Tg(flt1:YFP)^{hu4624}$ (Hogan et al., 2009), $Tg(gata1:dsRed)^{sd2}$ (Traver et al., 2003) crossed with $Tg(kdrl:EGFP)^{s843}$ and $Tg(hsp70l:dnBmpr\text{-}GFP)^{w30}$ (Pyati et al., 2005).

2.1.4 Microinjection of embryos

Embryos were aligned against a glass slide in a petri dish and injected with 1 nl of DNA, mRNA or morpholino as required. DNA, mRNA and morpholino were diluted in water containing 10% phenol red (Sigma) to aid visualisation during injection. DNA was injected into the cell of 1-cell

stage embryos. mRNA was injected into the streaming yolk of 1- to 2-cell stage embryos. Morpholinos were injected into the yolk of 1- to 4- cell embryos.

2.1.5 Pharmacological treatment of embryos

The small molecules used in this thesis were diluted in E3 media and added to embryos at the desired stage until collection. Embryos were incubated in the dark post-treatment. DAPM and DMH-1 (Sigma-Aldrich) (Hao et al., 2010) were dissolved in DMSO to a stock concentration of 10 mM. K-11706 (Nakano et al., 2004) was solvated in DMSO to a stock concentration of 1 mM. All stock compounds were stored at -20 °C. Dexamethasone was dissolved in ethanol to a stock concentration of 10 mM. DAPM was used at a final concentration of 100 μM, DMH-1 and K-11706 were used at 0.08 – 10 μM as indicated, and dexamethasone was used at 10 μM. Control embryos were exposed to the appropriate concentration of DMSO or ethanol.

2.1.6 Dechorionation and fixation of embryos

To prevent a curvature of the anterior-posterior axis, embryos fixed or imaged after 18-somites, but before hatching, were manually dechorionated with INOX number 5 forceps. Embryos fixed at 4 and 5 dpf were allowed to hatch naturally. Embryos were fixed in 4% paraformaldehyde for at least 3 hours at room temperature, then moved through 25 %, 50 % and 75 % ethanol washes to 100 % ethanol and, stored at -20 °C. Embryos younger than the 18-somite stage were fixed in their chorions, washed with PBST, and dechorionated and stored as above.

2.1.7 Dissection of trunks and tails

Dechorionated embryos were anesthetised with MS222 and placed in dishes lined with 5 % agarose. Trunks and tails were separated from the head and yolk regions under a dissecting microscope with a microscalpel.

2.2 Solutions, morpholinos and primers

2.2.1 Solutions

Solutions were made up with Milli-Q water and autoclaved as required. Solutions were stored at room temperature, 4 °C (*) or -20 °C (†).

Name	Composition
AP Buffer	100 mM Tris-HCl pH 9.5, 100 mM NaCl, 50 mM $MgCl_2$, 0.1 % Tween (freshly made)
Bleaching solution	10 % hydrogen peroxide, 5 % formamide, 0.5 % SSC (made up fresh)
Deyolking buffer	55 mM NaCl, 1.8 mM KCl, 1.25 mM $NaHCO_3$
E3 (*) 60 x	1.75 % NaCl, 0.08 % KCl, 0.3 % $CaCl_2 \cdot 2H_2O$, 0.5 % $MgCl_2 \cdot 6H_2O$, pH 7.2
Hybe -/- (*)	50% Formamide, 5x SSC, 9.2 mM Citric Acid, 0.1% Tween
Hybe +/+ (*)	50% Formamide, 5x SSC, 9.2 mM Citric Acid, 0.1% Tween, 0.05 % tRNA, 0.005 % Heparin
Laemmli 2 x	126 mM Tris-Cl, 20% Glycerol, 4 % SDS, 0.02 % Bromphenolblue, pH 6.8, 10 mM fresh DTT
LB (Agar(*))	1 % Bactotryptone, 0.5 % Bactoyeast, 1 % NaCl, pH 7.0 (1.5 % Bactoagar)
Lysis Buffer	10 mM Tris pH 7.5, 2% Triton, 1 % β-glycerophosphate, 10 mM EDTA, 3 mM fresh DTT
MAB Block (†)	0.1 M maleic Acid, 0.15 M NaCl, pH 7.5, 2 % Boehringers Blocking Reagent
MABT (*)	0.1 M maleic Acid, 0.15 M NaCl, 0.1 % Tween, pH 7.5
MS222 (*)	0.4% Ethyl-3-amino benzoate methanesulfonate salt, pH 7.0
o-dianisidine	0.06 % o-dianisidine, 50 µmol sodium acetate, 0.65 % hydrogen peroxide
PBS(T)	0.8 % NaCl, 0.02 % KCl, 0.15 % Na_2HPO_4, 0.025 % KH_2PO_4, pH 7.2 (0.1 % tween)
PTU (†) 50 x	0.15 % 1-phenyl-2-thiurea
QLE buffer	10 mM Tris-Cl, 0.1 mM EDTA, pH 8.5 (*from* Qiagen)
SOC (†)	2 % Bactotryptone, 0.5 % Bactoyeast, 2
SSC (*) 20 x	3 M NaCl, 0.3 M Sodium Citrate
TAE 50 x	2 M Tris-acetate, 50 mM EDTA
TBS(T)	0.9 % NaCl, 0.02 % KCl, 0.3 % Tris base, pH 7.4 (0.1 % tween)
TE buffer	10 mM Tris, 0.1 mM EDTA, pH 7.6

Table 2.1 List of solutions used in this thesis

2.2.2 Morpholinos

All morpholinos were obtained from Gene Tools, Oregon, USA. Morpholinos were designed to bind to the 5'UTR or initiating ATG on mRNA. Alternatively, they were designed to bind over a splice junction to cause aberrant splicing. All sequences were checked for nonspecific genomic binding

(Altschul et al., 1990). A stock solution of 50 or 25 μM was prepared. Morpholinos were injected into embryos in the range of 1 ng to 20 ng and the highest concentration that resulted in largely morphologically normal embryos at 30 hpf was used for further experiments. Morpholinos were diluted in water and stored at -20 °C. Just before use, they were heated to 65 °C for 5 minutes and kept at 4 °C.

Morpholino	Ensembl id	Target	Sequence (5' – 3')	ng	Reference
bcor MO	ENSDARG00000017798	E8I8	GCATGTGTTTACCTGGTGCCGTCCT	1.8	(Ng et al., 2004)
bmp4 MO	ENSDARG00000019995	E1I1	GGTGTTTGATTGTCTGACCTTCATG	0.8	(Chocron et al., 2007)
ep400 MO1	ENSDARG00000074040	E7I7	ACCAAACGAAACACCTCTCACCTTC	4.0	This thesis
ep400 MO2	ENSDARG00000074040	E16I16	TGTCTTGTTCTGCTTCATACCGATC	2.0	This thesis
gata2a MO1	ENSDARG00000059327	E3I3	CATCTACTCACCAGTCTGCGCTTTG	8.0	(Galloway et al., 2005)
gata2a MO2	ENSDARG00000059327	ATG	GCCGCAACCTCCATCTCAAGTGTCC	2.0	This thesis
hdac7 MO1	ENSDARG00000093701	E12I12	TGGACAGTAGTGGCAGTACCTCACA	2.0	This thesis
hdac7 MO2	ENSDARG00000093701	I15E16	GCCATTCTGAAAGATGGAAAGCAAC	9.0	This thesis
irf2bp2b MO	ENSDARG00000006275	I1E2	CGTGAAGCGTGACCCGTACCTGTTT	15.0	This thesis
lmo4a MO2	ENSDARG00000013853	5'UTR	GTCAAAGGGTGCTGGAATCACTTCA	2.0	This thesis
lmo4a MO3	ENSDARG00000013853	E2I2	CCAACTGCCTGTTTCTTTTAGTACC	15.0	This thesis
lmo4b MO1	ENSDARG00000054749	ATG	CACTTCCTCCAGGGTTCACCATTGT	5.0	This thesis
lmo4b MO2	ENSDARG00000054749	I1E2	CTGCAGAAACATAAAGAGACAGGGA	2.0	This thesis
myef2 MO1	ENSDARG00000059398	E2I2	GTGCTCTCTGTGTGCGTTACCTTTC	1.0	This thesis
myef2 MO2	ENSDARG00000059398	I2E3	CTCACCAACTACATGAGACATACAA	6.5	This thesis
ncor MO1	ENSDARG00000035285	E11I11	TTAAAACGTTGGTTTACCTCCTGCT	10.0	This thesis
ncor MO2	ENSDARG00000035285	E12I12	CATGAGCTGCATTTACTCACTTCTC	16.0	This thesis

Table 2.2 List of morpholinos used in this thesis

Morpholinos were designed to specifically bind the target indicated, where E is exon number, I is intron number, and ATG is the initiating codon. The indicated amount of morpholino was microinjected per embryo.

2.2.3 Primers

RP1 purified primers were obtained from Sigma, resuspended to a stock concentration 100 μM and stored at -20 °C. Typically, 10 pmol of primer was used per reaction.

Primer	Sequence (5' – 3')
aspp1 f	CATGGAGGTGACACTGATGG
aspp1 r	TAGGAGGCAGGAGTGGCTTA
aspp2a f	GCCTATGTTCCTGACGGTGT
aspp2a r	CATGTTAGCCACCTCCTGGT
aspp2b f	TTCCACCTCGATCTCCAATC
aspp2b r	CCACCACCACTCTGTTTCCT
bcor f2	CAGGAGTGTCCCGAGCTAAG
bcor r3	TCAGGAGCGAGGTCTGGAAG
dll4 check r	CTCCGGCCAAGCTAAGCGTCC
dll4 sh f1	GGGAACAAAAGCTGGAGCTCCAC
dll4 sh f2	CGCTTAGCTTGGCCGGAGCTG
dll4 sh f3	CCCTCTGGCCTGTGCTTACTTG
dll4 sh f4	CTAGTAGTGAAGCCACAGATGTAC
dll4 sh f5	CTGACCTACGGCGTGCAGTGC
dll4 sh f6	GCATGGACGAGCTGTACAAGTAAAG
-EcoRI f	CTGTATTTTACACCTTTTGCAAATTCCGCTCCTTTGGAAAG
-EcoRI r	CTTTCCAAAGGAGCGGAATTTGCAAAAGGTGTAAAATACAG
-EcoRI seq f	GGCTGCAAATAGCAGGAAACGTG
-EcoRI seq r	CTCAAAGTGAGGCTGAGACGCG
ef1α f	CACCCTGGGAGTGAAACAG
ef1α r	ACTTGCAGGCGATGTGAGC
ep400 (1) f	CACAAACAGTCCAGATTGGTG
ep400 (1) r	TGTCGTAGATCTCAAAATGATGC
ep400 (2) f	CATGAACACCCCATTGGA
ep400 (2) r	AGAGTATTTTGTAGAGGAGTGTTGATTAG
f to EOS	TGTCTCATCATTTTGGCAAAGAAT
flt1 f	ATGTTCGATATATTATTTGTGATGATATTTG
flt1 r	TTAGAAACTGGGGTAAAGAAGATCG
gata1 mut f	GACTGTACCATAAGATGAACGGCCAGAACGGAAGCAGCGGCAGCCCAAAAAAGAGGCTGATTGTCAGCAAACG
gata1 mut r	CGTTTGCTGACAATCAGCCTCTTTTTTGGGCTGCCGCTGCTTCCGTTCTGGCCGTTCATCTTATGGTACAGTC
gata2 mut f	GCCAGAACAGACCCCTTATCAGGCCAAAGCGCA
gata2 mut r	TGCGCTTTGGCCTGATAAGGGGTCTGTTCTGGC
gata2a I1	CCAGCGCCGCTTATCCGTGCAG
gata2a I2	GTGAACTGTGGAGCCACCTCCAC
gata2a zon f	CTAAATGTAAAAGCAAGACGCG
gata2a zon r	GTTGTGGAGTTTGTAGTAGAGCC
gata2b f	ATGGATGCCCCAGCGGAACCC
gata2b r	TCAGCCTATAGCAGTGACTAAGCTGC
glmo2 f	GGGGACAAGTTTGTACAAAAAAGCAGGCTTCGCCACCATGGAAGGGAGCGCGGTGA

Primer	Sequence (5' – 3')
glmo2 f2	GGGGACAAGTTTGTACAAAAAAGCAGGCTTCGCCACCATGTCCTCGGCCATCGAAAGG
glmo2 r	GGGGACCACTTTGTACAAGAAAGCTGGGTCGATGATCCCATTGATCTTGGTCCAC
glmo4 f	GGGGACAAGTTTGTACAAAAAAGCAGGCTTCGCCACCATGGTGAACAGTCGTGTGGAAAGCT
glmo4 r	GGGGACCACTTTGTACAAGAAGGACCACTTTGTACAAGAAAGCTGGGCAGCAGCAGG
gM13 f	GTAAAACGACGGCCAG
gM13 r	CAGGAAACAGCTATGAC
HA fwd	TACCCATACGATGTTCCAGATT
HA lmo4 f	TAGGATCCACCATGTACCCATACGATGTTCCAGATTACGCTGTGAACAGTCGTGTGGAAA
HA lmo4 f3	TAGGATCCATGTACCCATACGATGTTCCAGATTACGCTGTGAACAGTCGTGTGGAAA
HA lmo4 r	TAAGGCCTGAATTCTCAGCACACCTTTTGGTC
HA rev	AGCGTAATCTGGAACATCGTA
iaspp f	ATCTTCCTCTGCCCCAAGAT
iaspp r	CATGGCTGTCTGGAGCACTA
iflt1 f	TGATAACGGGAGCATCGC
iflt1 r	ACTGCCAGTTTGGCAACCT
irf2bp2 f1	ATGTCGTCTGCGGCGGTCGC
irf2bp2 f2	GGCGATGATCTGGGATTTTA
irf2bp2 r1	TCAAGGGTCCCGCTCCTTTT
irf2bp2 r2	AGACGGCATCTTGAGCACTT
lmo4 f1	TTGACGGTTGTGGTAAAGCA
lmo4 f4	TAGGATCCATGGTGAACAGTCGTGTGG
lmo4 HA f	TAGGATCCACCATGGTGAACAGTCGTGTGG
lmo4 HA r	TAAGGCCTGAATTCTCAAGCGTAATCTGGAACATCGTATGGGTAGCACACCTTTTGGTCGGG
lmo4 mo2 site	AGGACGATTCTGAAGTTTCTG
lmo4 mo3 site	TGTCCCGCAGGCAGGCAATG
lmo4 r1	GCCCTCATCACCATCTCACT
lmo4 r3	TAGAATTCTCAGCACACCTTTTGGTC
lmo4b f	ATGGTGAACCCTGGAGGAAG
lmo4b f	CAGCGAGAAGTGTTCATCCA
lmo4b r	CTAACACACTTTCTGGTCAGG
lmo4b r	GAGCTCAAGCCTGAGATTGG
lmo4HA r4	TAGAATTCTCAAGCGTAATCTGGAACATCGTATGGGTAGCACACCTTTTGGTCGGG
mflt1 f	CTCGGCGCATGTACCAAATCAGG
mflt1 r	CATCCGAGTGCCGTGCTTCAGTC
mlmo2 f	ATGTCCTCGGCCATCGAA
mlmo2 r	GATGATCCCATTGATCTTGGTC
mscl f	ATGACGGAGCGGCCGCCG
mscl r	CATCAGCGGCAGGCAGCAGGG
myef2 f1	AGTAATGGCGGACACAGAGC

Primer	Sequence (5' – 3')
myef2 f2	CAGAACCAAGACGACACGAA
myef2 r1	TGCTCTCCATCTGGATCCTC
myef2 r2	CGATGGATGGAGGAATGTTT
ncor f	GAGCAGAAAATTTGTCAGCG
ncor r	CTGATTCCGTCGCCTTC
qbactin 2 f	GGACCTGTATGCCAACACTGTA
qbactin 2 r	ATGTGATCTCCTTCTGCATCCT
qef1α f	GAGAAGTTCGAGAAGGAAGC
qef1α r	CGTAGTATTTGCTGGTCTCG
qfli1a f	GAGAAGTTCGAGAAGGAAGC
qfli1a r	CGTAGTATTTGCTGGTCTCG
qgfp 3' f	GACCATCTTCTTCAAGGACGAC
qgfp 3' r	ATTCCCTTAAGCTCGATCCTGT
qgfp 5' f	CACTGGAGTTGTCCCAATTC
qgfp 5' r	CCGTATGTTGCATCACCTTC
qlmo2gfp f	AAGAATTGGGACAACTCCAGTG
qlmo2gfp r	TCTACGAGTGGACCAAGATCAA
qpu1 f	AAGTCCACTGGATGAATGTG
qpu1 r	AGAGAGGGTAACCTGGACTG
qrfp f	AGGACGTCATCAAGGAGTTCAT
qrfp r	CTTGGTCACCTTCAGCTTGG
qrunx1 f	CGGTGAACGGTTAATATGAC
qrunx1 r	CTTTTCATCACGGTTTATGC
qsmad5 f1	CACAGACAAGATGTGACAAGCA
qsmad5 f2	AAACTCACCCTACCCTCCATCT
qsmad5 r1	ACAGAAGAGATGGGGTTCAGAG
qsmad5 r2	TAGGCAGGAGGAGGAGTATCAG
r to EOS	AACTCATCAATGTATCTTA
scl f	ATGATGGAAAAACTGAAATCCG
scl r	TCACCGCTGGGCATTTC
sflt1 f	CTTCCCAGCAGCGTGATT
sflt1 r	GAGACCCGTAGAGTAGAAACAAAC
Sp6	ATTTAGGTGACACTATAGAA
T7	TAATACGACTCACTATAGGG

Table 2.3 Sequences of primers used in this thesis

A "q" prefix denotes primers designed for qRT-PCR and a "g" prefix, primers designed for gateway cloning.

2.3 Isolation and analysis of proteins

2.3.1 Deyolking of zebrafish embryos

Zebrafish embryos younger than 24 hpf contain a high proportion of yolk proteins that can confound proteomic analysis, therefore embryonic tissue was separated from the underlying yolk (Link et al., 2006). Up to 100 dechorionated embryos were transferred into 500 µl of deyolking buffer and the yolk sac disrupted by pipetting through a 200 µl tip and shaken at 1100 rpm for 5 minutes at room temperature (Thermomixer, Eppendorf). The embryonic tissue was harvested by centrifugation at 300 g for 30 s and supernatant containing yolk proteins discarded. The pellet was stored at -80 °C until required.

2.3.2 Polyacrylamide gel electrophoresis and western blotting

To isolate total protein, the embryo pellet was typically lysed at 4 °C in 25 µl of 2x Laemmli buffer. Where the concentration of genomic DNA precluded efficient pipetting, the sample was sonicated as required to sheer genomic DNA. Embryo equivalents were heated to 90 °C for 5 minutes and placed immediately at 4 °C before loading, along with a Rainbow marker (Amersham), into 10 % Bis-Tris polyacrylamide gels placed in MOPS SDS running buffer (Invitrogen). The set-up was run at 100 V then ramped to 200 V when the samples had entered the gel. Resolved protein was transferred to a nitrocellulose membrane (Amersham) by wet blotting in NuPage transfer buffer (Invitrogen), supplemented with 10% methanol, at 200 mA for 2 hours. Post transfer, residual protein on the gel was visualised by exposure to Coomassie Bradford reagent (Thermo Scientific) for 30 minutes, followed by extensive washing with water as required.

Specific proteins on the membrane were revealed by hybridisation of primary, and where required secondary, antibodies. The membrane was briefly rinsed in TBST before being allowed to sit against the walls of a 50 ml falcon tube. Potential non-specific interactions with antibody were blocked by exposure for 1 hour at room temperature to 2 % non-fat milk (Marvel) in TBST. Primary antibodies

were incubated in blocking solution at 4 °C overnight and washed with 3 x 10 min TBST washes. HRP-conjugated secondary antibodies were incubated in blocking solution for 1 hour at room temperature before being washed off with 3 x 10 min TBST washes. All antibody incubations were carried with gentle rotation and rocking. To develop the horse radish peroxidase signal, hybridised membranes were laid on a flat surface and covered with enhanced chemiluminescence developing reagent (GE Healthcare) at room temperature for 5 minutes. Developing reagent was drained off and membranes wrapped in saran wrap before exposure to photographic film (Kodak) in the dark for an appropriate amount of time. The film was developed (*WIMM developing facility*) and the image digitised at 300 dpi. Membranes were stored at 4 °C in TBS. If required, they were stripped with Restore Stripping buffer (Pierce) for 20 min shaking at room temperature, before re-blocking and probing. Antibodies used were mouse anti-HA-peroxidase at 1:1000 (Roche 11 667 475 001), rabbit anti-β tubulin at 1:500 (Santa Cruz H-235), and donkey anti-rabbit-peroxidase at 1:1000 (GE Healthcare NA9340).

2.3.3 Isolation of single cells and fluorescence-activated cell sorting

Up to 200 dissected trunks and tails were collected in 1.5 ml eppendorf tubes and dissociated with 1 ml of fresh dissociation buffer at 29 °C (0.28 unit/ml liberase blenzyme (Roche), 1 mM EDTA in Hank's buffer (Sigma)). Embryos were pipetted every 10 min until fully dissociated, typically taking 20 min. All further steps were carried out at 4 °C, unless otherwise indicated. The cells were pelleted by spinning at 300 g for 5 min, the supernatant removed and pellet washed twice with fresh PBS-serum (0.9 % PBS, 5 % heat inactivated serum) and re-suspended in PBS-serum. Single cells were obtained by filtration through a 30 µm filter (Cell Trics, Partec) into 5 ml FACS tubes (Falcon 352063) or 1.5 ml tubes, pelleted at 300 g and re-suspended in 1 ml FACS solution (PBS-serum with 1 µg/ml Hoecht 33258 pentahydrate (Invitrogen)) and kept in the dark (Bertrand et al., 2007).

Cells were immediately sorted at room temperature on a MoFlo cell sorter (Kevin Clark, *WIMM FACS facility*). Live cells were gated by excluding cells that fell outside the side-scatter, forward-scatter double positive cloud and which were Hoechst negative. GFP and Hoechst auto

fluorescent cells were excluded by comparing the $GFP^+/Hoescht^+$ sample respectively with a $GFP^-/Hoescht^+$ and $GFP^+/Hoescht^-$ samples. From the resultant fraction, GFP positive cells were collected in PBS-serum, RNA immediately isolated with the RNeasy Micro kit (Qiagen), and resultant RNA stored at -20 °C.

2.3.4 Whole mount o-dianisidine histochemical staining

To stain haemoglobin, non-fixed, dechorionated embryos were incubated in the dark at room temperature in o-dianisidine (Iuchi and Yamamoto, 1983). The reaction was stopped with 3 x water washes. After staining, embryos were fixed in 4 % PFA for 1 h and stored at -20 °C in ethanol. To visualise staining, embryos were cleared in a 2:1 volumetric mix of benzyl benzoate:benzyl alcohol. The staining process resulted in pooling of circulating cells in the yolk.

2.3.5 Whole mount immunohistochemistry

Fixed embryos in ethanol were rehydrated to PBST through 75 %, 50 % and 25 % ethanol and washed 3 x 5 min in PBST. Embryo post 24 hpf were further permiabilised with proteinase K (10 μg/ml in PBST) for 3 minutes for 24 hpf embryos, to 20 min for 3 dpf embryos. Embryos were washed 2 x in PBST and refixed in 4 % paraformaldehyde for 20 min at room temperature followed by 4 x PBST washes. Potential non-specific interactions were blocked with 0.5 % bovine serum albumin in PBST for 2 hours at room temperature and embryos incubated with primary antibody in block (rabbit anti-activated caspase-3 at 1:250, Pharmingen 559565) (Kratz et al., 2006). Embryos were washed 5 x in PBST before incubation in the dark at room temperature with secondary antibody for 1 hour (goat anti-rabbit-alexa 555 at 1:500, Molecular Probes A-21428) and 5 x washes in PBST. Embryos were transferred to 90 % glycerol for storage and photography.

2.3.6 Analysis of luciferase reporter activity

The CMVe-Id1-BRE2-EGFP (Monteiro et al., 2008) or SBE-luc (Jonk et al., 1998) DNA reporter constructs were injected with pTK-LacZ DNA (Monteiro et al., 2008) at the one-cell stage; 25 pg of each construct was used. Gastrula stage embryos were washed with PBS and up to 20 embryos lysed in 200 µl lysis buffer by aspirating through a 23 G syringe. Cell debris we removed by centrifugation and the supernatant stored at -80 °C. Isolation of total protein was carried out at 4 °C.

To measure luciferase activity, 50 µl/well of supernatant or lysis buffer control was plated along with 100 µl per well of luciferase substrate (Roche) into white flat bottomed plates (Nunc) in triplicate. To measure β-galactosidase activity, 100 µl per well of substrate reagent was added and incubated in the dark for 30 min followed by 50 µl/well of enhancer solution (Roche). Luminescence was read immediately after addition of luciferase reagent or enhancer on a FLUOstar OPTIMA plate reader. The integrated signal over 5 sec/well was recorded and the luciferase reading divided by the β-galactosidase reading to normalise for injection efficiency.

2.4 Preparation, manipulation and analysis of DNA

2.4.1 Bacterial culture

Bacteria were cultured at 37 °C for 9–18 h as required either in shaking liquid culture (LB) or solid culture (streaking on LB agar). As required, cultures were supplemented with 50 µg/ml of ampicillin or kanamycin, and stored at 4 °C.

2.4.2 Transformation of chemically competent *E.coli*

Approximately 20 µl of DH5α competent cells (NEB) were thawed per transformation, and incubated with DNA at 4 °C for 30 min. Cells were heat shocked for 30 s at 42 °C and allowed to recover for 30 min at 37 °C in 200 µl SOC, before plating onto selective LB agar.

2.4.3 Isolation and sequencing of plasmid DNA

Bacterial cells from liquid culture were pelleted and plasmid DNA isolated by the principle of alkaline lysis on an immobilised column with either the Quicklyse mini- or HiSpeed midi-kit (Qiagen) according to the manufacturer's instructions. DNA was eluted in QLE elution buffer and stored at -20 °C. Plasmids were sequenced by semi-automated Sanger sequencing (*WIMM sequencing service*) with the appropriate primers. Sequences files (.abi) were aligned with SeqMan II (DNAStar).

2.4.4 Determining the concentration of nucleic acid

Nucleic acid concentration was determined by its A_{260} with an ND-1000 spectrophotometer. An extinction coefficient of 50 or 40 was used respectively for dsDNA and RNA. Purity was determined by the profile of the sample on an agarose gel and/or the $A_{230:260:280}$, with an idealised ratio of 1:2:1 for DNA and 1:1.8:1 for RNA.

2.4.5 Agarose gel electrophoresis

Nucleic acid and 1 kB DNA ladder (NEB) was mixed 1:1 with loading buffer (Ambion), and resolved on a 1 % agarose gel made up with 0.5 % TAE and supplemented with 0.01 % gel red. Typically, the gel was run at 22.5 V/cm in 0.5 % TAE for the required amount of time. Nucleic acid was visualised with trans-UV light and photographed at 300 dpi.

2.4.6 Restriction endonuclease digestion and DNA ligation

DNA was digested at 37 °C for 1-12 h with restriction enzymes (NEB) in the provided buffers, and according to the manufacturer's instructions. The cut and uncut fragments were analysed on an agarose gel. Typically, 2 units of enzyme was used per 1 μg of DNA. DNA fragments were ligated as required with 3:1 molar ratio of fragment to vector using T4 DNA ligase (Promega). Reactions were typically left for 6 hours at room temperature before being used to transform bacteria.

2.4.7 Purification and gel extraction of DNA

As required, DNA was purified by selective binding to a silica membrane using the PCR purification kit (Qiagen). Resolved DNA bands were visualised through an orange filter under 470 nm transillumination (Safe Imager, Invitrogen). The bands were excised as required and agarose melted at 50 °C. DNA was adsorbed onto silica particles, washed and eluted (Qiaex II, Qiagen).

2.4.8 Polymerase chain reaction and colony PCR

For a typical PCR reaction, 10 pmol of forward and reverse primer was used along with the JumpStart taq (Sigma). PCR reactions were heated to 95 °C for 5 min then cycled between 95 °C for 30s, T_m -5 °C for 30 s and 72 °C for 1 min/kB plasmid length followed by a 5 min final extension step on a thermocycler with a heated lid (DNA engine). Reactions were analysed on agarose gels; JumpStart reaction mix could be directly run on a gel as it contained loading buffer.

To screen bacterial colonies, individual colonies were picked and placed in 20 µl water. PCR was carried out as above with 5 µl of the colony suspension. The remaining 15 µl from positive colonies was used to inoculate liquid culture as appropriate.

2.4.9 Site directed mutagenesis

Forward and reverse mutagenic primers to introduce the desired mutation were designed with the QuikChange primer design software (Agilent). Primers were designed to minimise the mis-match and site directed mutagenesis carried out with the QuikChange lightning kit (Stratagene) according to the manufacturer's guidelines. Typically 10-100 ng of plasmid template was used along with 125 ng of each mutagenic primer per reaction. Cycling conditions were identical to above, with the exception that each reaction was cycled 18 times between 95 °C for 20s, 60 °C for 10 s and 68 °C for 30 s/kB plasmid length. Parental and hemimethylated DNA was digested with DpnI before the mixture was

used to transform bacteria. Resultant colonies were sequenced to check for specific introduction of the desired mutation.

2.5 Preparation, manipulation and analysis of RNA

2.5.1 Isolation of total RNA

Total RNA was isolated from staged zebrafish using 500 µl TRIzol (Invitrogen). Embryos were homogenised by aspiration through a 23 G syringe. A further 500 µl TRIzol was added and the sample vortexed and cell debris removed by centrifugation. Nucleic acid was isolated by the addition of 200 µl chloroform, mixing and isolation of the aqueous phase. Nucleic acids were precipitated with 500 µl isopropanol, pelleted and resuspended. DNA was digested with 1 µl DNase I (Ambion). For RT-PCR, resultant RNA was precipitated with 3.75 x volume of ethanol, pelleted and resuspended in 20 µl water. For qRT-PCR, RNA was isolated by selective binding to a silica membrane (RNeasy micro kit, Qiagen) according to the instructions provided. For sorted cells, total RNA was isolated immediately post-sorting using the RNA micro kit (Qiagen), using carrier DNA to increase yield, and an on-column DNaseI treatment. RNA quality was always assessed on an agarose gel and by UV spectroscopy. Isolated RNA was stored at -20 °C.

2.5.2 Reverse transcription of RNA

RNA was reverse transcribed to cDNA using the SuperScript III enzyme (Invitrogen), according to the manufacturer's instructions, in a total volume of 20 µl. For RT-PCR, 1 µg of RNA and oligo dT primers were used, and for qRT-PCR, 250 ng of RNA and random primers used. RNA was made up to 10.5 µl and heated to 65 °C for 3 min, then placed at 4 °C just prior to assembling the reaction. The reaction was heated to 25 °C for 5 min, 50 °C for 60 min and 70 °C for 15 min. The resultant cDNA was stored at -20 °C. For RT-PCR, 30 µl of water was added to the cDNA and 1 µl used per reaction. For qRT-PCR, the cDNA was diluted 1:30 in water and 5 µl used per reaction well.

2.5.3 Real time-PCR

Quantitative real-time PCR was carried out using SYBR green chemistry on an Applied Biosystem 7500 real-time cycler according to the manufacturer's instructions. Reactions were carried out in triplicate. Each reaction was made up to a volume of 20 µl with water and cycled 40 times prior to melting curve analysis. Reactions with more than one peak on a melting curve were discarded and thresholds automatically determined by 7500 fast system software (Applied Biosystems). Data was analysed by the ΔΔCt method (Dussault and Pouliot, 2006). The arithmetic mean of Ct values from replicates was determined, resulting in a mean Ct value for the gene of interest (GOI). A combined value for the two housekeeping genes (HkG) was determined from the geometric mean of the two arithmetic means of the individual genes. The genes *ef1a* and *βactin2* were selected at housekeepers due to their stable expression during the developmental time-points analysed. The ΔΔCt value between the control and test sample was calculated using equation 1 and the fold increase approximated by equation 2.

$$\Delta\Delta Ct = [(Ct_{GOI\text{-}control} - Ct_{HkG\text{-}control}) - (Ct_{GOI\text{-}test} - Ct_{HkG\text{-}test})] \quad (1)$$

$$\text{Fold increase} = 2\exp(\Delta\Delta Ct) \quad (2)$$

Results from at least three biological replicates were combined. Error bars were representative of the standard error about the mean, and significance assessed by a two-tailed Student's t-test.

2.5.4 *In vitro* synthesis of mRNA

Capped mRNA in appropriate expression vectors were *in vitro* transcribed from 1 µg purified linearised DNA plasmid template using the Sp6, T3 or T7 mMessage mMachine kit (Ambion) according to the manufacturer's instructions. Reactions containing 0.5 mM Cap analogue were incubated at 37 °C for 1 – 3 hours. DNA was digested with the Turbo Dnase provided (Ambion) and RNA cleaned and purified on RNeasy micro columns (Qiagen). Purity and concentration of the mRNA was determined by agarose gel electrophoresis and UV spectroscopy. Synthesised mRNA was aliquoted and stored at - 80 °C.

mRNA	Restriction site	Enzyme	Reference
gata1a	EcoRI	T3	(Gering et al., 2003)
gata1a - linker mutant	EcoRI	T3	This thesis
gata2a	EcoRI	T3	(Gering et al., 2003)
gata2a – K310R	EcoRI	T3	This thesis
h2b-dsred	NotI	Sp6	(Megason and Fraser, 2003)
mlmo2-gfp	NotI	Sp6	This thesis
mlmo2-gfp F88A	NotI	Sp6	This thesis
mlmo2-gfp F88D	NotI	Sp6	This thesis
mlmo2-gfp L59G	NotI	Sp6	This thesis
mlmo2-gfp R100/102A	NotI	Sp6	This thesis
mlmo2-gfp R77A	NotI	Sp6	This thesis
mlmo2-gfp R86A	NotI	Sp6	This thesis
mlmo2-gfp V67A	NotI	Sp6	This thesis
mlmo2-myc	EcoRI	T3	(Gering et al., 2003)
mlmo2-myc F88A	EcoRI	T3	Sarah Hoosdally, *unpublished*
mlmo2-myc F88D	EcoRI	T3	Sarah Hoosdally, *unpublished*
mlmo2-myc L59G	EcoRI	T3	Sarah Hoosdally, *unpublished*
mlmo2-myc R100/102A	EcoRI	T3	Sarah Hoosdally, *unpublished*
mlmo2-myc R77A	EcoRI	T3	Sarah Hoosdally, *unpublished*
mlmo2-myc R86A	EcoRI	T3	Sarah Hoosdally, *unpublished*
mlmo2-myc V67A	EcoRI	T3	Sarah Hoosdally, *unpublished*
mlmo4	EcoRI	T3	(Gering et al., 2003)
mscl-HA	EcoRI	T3	(Gering et al., 2003)
mscl-HA Y235A	EcoRI	T3	Sarah Hoosdally, *unpublished*
pCS2HA-lmo4a	NotI	Sp6	This thesis
pCS2lmo4a	NotI	Sp6	This thesis
pCS2-lmo4a-gfp	NotI	Sp6	This thesis
pCS2lmo4a-HA	NotI	Sp6	This thesis
pβut3-lmo4a-HA	SfiI	T3	This thesis
tol2 transposase	NotI	Sp6	(Kawakami et al., 2004)
xgata2-GR-HA	SalI	Sp6	Aldo Ciau-Uitz, *unpublished*

Table 2.4 List of plasmids used to make mRNA

All constructs contained the zebrafish sequence for the indicated gene, unless prefixed, where 'm' corresponds to the mouse sequence and 'x' to the *Xenopus laevis* sequence. The id number refers to the Patient lab plasmid database. Plasmids were linearised with the indicated restriction enzyme and transcribed with the indicated RNA polymerase to generate sense mRNA.

2.5.5 *In vitro* synthesis of antisense probes

Antisense riboprobes were synthesised from 1 µg purified linearised DNA plasmid template using the Sp6, T3 or T7 mMessage mMachine kit (Ambion). A 20 µl reaction mix contained 2 ul DIG-dUTP NTP mix (Roche)and 0.5 µl RNaseOUT (Invitrogen). Reactions were incubated for 2 – 6 hours at 37 °C and the DNA template digested with the DnaseI provided (Ambion). A volume of 80 µl water was added and the probes precipitated with 1/3 volume 10 M ammonium acetate and 2.5 volumes ethanol. Probe was pelleted and washed with 70 % ethanol and resuspended in water and analysed on an agarose gel to estimate purity and concentration. Typically, probe was diluted at 1:100 – 1:200 in hybe +/+ for use in WISH. Probes were reused up to ten times and stored at -20 °C.

Probe	Restriction site	Enzyme	Reference
alas2	BamHI	T7	RZPD clone ID: LLKMp964E092
aspp1	SpeI	T7	This thesis
aspp2a	SpeI	T7	This thesis
aspp2b	SacII	Sp6	This thesis
bcor	SpeI	T7	Rui Monteiro, *unpublished*
bmp4	EcoRI	T3	(Kishimoto et al., 1997)
cmyb	EcoRI	T7	(Thompson et al., 1998)
dab2	SalI	T7	Rui Monteiro, *unpublished*
deltaC	XbaI	T7	(Lawson et al., 2001)
dll4	SpeI	T7	Martin Gering, *unpublished*
ep400	SacII	Sp6	This thesis
ephrinB2a	XhoI	T3	(Lawson et al., 2001)
eto2	EcoRI	T7	IMAGE: 4144043
fli1	XbaI	T3	(Brown et al., 2000)
flk1	EcoRI	T7	(Fouquet et al., 1997)
flt1	NcoI	Sp6	(Bussmann et al., 2007)
flt4	EcoRI	T7	(Thompson et al., 1998)
foxn1	SalI	T7	(Wilkinson et al., 2009)
gata1	XbaI	T7	(Detrich et al., 1995)
gata2a	EcoRI	T7	(Detrich et al., 1995)
gata2b	SacI	T7	This thesis
hdac7	SacII	Sp6	This thesis
iaspp	SacII	Sp6	This thesis
ikaros	SalI	T3	(Willett et al., 2001)
lmo4a	ApaI	SP6	Rui Monteiro, *unpublished*

Probe	Restriction site	Enzyme	Reference
lmo4b	SacII	Sp6	This thesis
mrc1	SacII	Sp6	Rui Monteiro, *unpublished*
msr	EcoRI	T7	IMAGE: 6795347
ncor	PstI	T7	This thesis
nkx2.5	EcoRI	T7	(Chen and Fishman, 1996)
notch1b	HindIII	T7	IMAGE: 3725324
notch3/5	PstI	T7	(Lawson et al., 2001)
pax2.1	BamHI	T7	(Pfeffer et al., 1998)
pu1	EcoRI	T7	(Lieschke et al., 2002)
rag1	HindIII	T7	(Wilkinson et al., 2009)
runx1	HindIII	T7	(Kalev-Zylinska et al., 2002)
scl	EcoRI	T7	(Gering et al., 1998)
smad5	HindII	T3	Patrick Blader, *unpublished*
tal2	EcoRV	T3	(Pinheiro et al., 2004)
tbx20	BamHI	T7	(Griffin et al., 2000)
tie-2	XhoI	T3	(Lyons et al., 1998)
vegfA	XbaI	T7	(Gering and Patient, 2005)
βE globin	XhoI	T3	(Quinkertz and Campos-Ortega, 1999)

Table 2.5 List of antisense riboprobes used in this thesis

All probes were designed against the zebrafish sequence for the indicated gene. The id number refers to the Patient lab plasmid database. Plasmids were linearised with the indicated restriction enzyme and transcribed with the indicated RNA polymerase to generate antisense RNA.

2.5.6 Whole mount *in situ* hybridisation

Fixed embryos were stored in 100 % ethanol and rehydrated to PBST through 75, 50 and 25 % ethanol washes and 4 x PBST washes at room temperature. Embryos older than 24 hpf but less than 4 dpf were treated with 10 µg/ml proteinase K (Sigma) for 3 – 20 minutes are required. Embryos older than 4 dpf were treated with 20 µg/ml proteinase K for 20-25 minutes. Proteinase K treated embryos were washed with 2 x PBST, re-fixed with 4 % PFA for 20 min and washed 5 x with PBST. Embryos were transferred to 50 % hybe+/+ for 5 min then 100 % hybe+/+ for at least 2 hours at 65 °C. The hybe was replaced with diluted antisense riboprobes and embryos incubated overnight at 65 °C.

Probes were removed and embryos transferred to a Biolane HT-1 *in situ* machine (Intavis). All further steps were with gentle rocking. Embryos were washed at 65 °C through 100 % hybe -/-, 75 % hybe-/- 25 % 2 x SSC, 50 % hybe-/- 50 % 2 x SSC, 25 % hybe-/- 75 % 2 x SSC and 2 x SSC (10 min for each wash) then 4 x 15 min in 0.2 x SSC. At room temperature, embryos were washed through 75 % 0.2 x SSC 25 % MABT, 50 % 0.2 x SSC 50 % MABT, 25 % 0.2 x SSC 75 % MABT and 100 % MABT (5 min for each wash). Non-specific sites were blocked with MAB block for 1 hour at room temperature and incubated for 10 hours with anti-DIG antibody (Roche) at 1:5000 at 4 °C before washing 8 x 15 min in MABT. Embryos were washed in 3 x 5 min in AP buffer and the *in situ* signal developed at 4 - 37 °C with BM Purple (Roche) mixed 1:1 with AP buffer. Staining was stopped as appropriate by fixation in 4 % PFA for at least 20 min followed by 3 x 5' PBST rinses.

Embryos older than 26 hpf were placed in bleaching solution on a light box to remove pigment and aid visualisation of the *in situ* signal. Embryos were bleached for 10 – 35 min as required then washed 3 x PBST. Bleached embryos, along with younger unbleached embryos, were transferred to 90 % glycerol for storage and imaging.

2.6 Plasmids and their construction

2.6.1 Novel antisense probe constructs

PCRs using gene specific primers (see table 2.3), and 26 amplification cycles were used to isolate the required sequence from 26 hpf whole zebrafish embryo cDNA. Accession numbers for genes were as follows: *iaspp1*, NM_001014320; *aspp1*, NM_001044824; *aspp2a*, NM_214814; *aspp2b*, NM_001045153; *ncor*, ENSDARG00000035285; *ep400*, ENSDARG00000074040; *hdac7*, ENSDARG00000093701; *lmo4b*, ENSDARG00000054749; and *gata2b*, ENSDARG00000009094. PCR fragments were cloned into pGEM-T Easy (Promega). Resultant colonies were grown and sequenced with T7 and Sp6 primers to confirm sequence identity and directionality. Probes were synthesised as in table 2.5.

2.6.2 lmo4-HA and lmo4-gfp

The glmo4f and glmo4r primers with gateway compatible arms were used to isolate the *lmo4a* sequence from 26 hpf cDNA. The fragment was gateway cloned into pDONR221 (Invitrogen). Colonies were selected on kanamycin resistance plates and the gM13f and gM13r primers used to check the insert. The pDONR221-lmo4a construct was used to generate pCS2-lmo4a-gfp and pβut3-lmo4-HA by an LR reaction with pCS2-gfp (id 504) and pβut3-HA (id 505) respectively. The pCS2-lmo4a-gfp and pβut3-lmo4-HA were respectively sequenced with gfp (cs2) and mrg129 primers and grown with ampicillin selection.

2.6.3 (HA)-lmo4-(HA)

HA-lmo4 (HAlmo4f3 and lmo4r3), lmo4 (lmo4f4 and lmo4r3) and lmo4-HA (lmo4f4 and lmo4HAr4) fragments were isolated from 26 hpf cDNA with the primer pairs indicated in parentheses. Fragments were cloned into pGEM-T Easy (Promega) and sequenced with T7 and Sp6 primers. A fragment was excised with BamHI and EcoRI. Excised and purified fragments were cloned into pCS2+ (id 1482) also cut with the same restriction enzymes.

2.6.4 Tol2 flanked lmo4

The Tol2-Ef1α-EOS construct (id 1295) (Kawakami et al., 2004) was cut with ClaI, purified, blunted with T4 DNA polymerase (Fermentas), purified and cut with BamHI to remove the EOS sequence. The (HA)-lmo4a-(HA) fragments in pGEM-T Easy isolated in the previous section were cut with BamHI and StuI, purified and cloned into the cut Tol2-Ef1α plasmid and sequenced with the primers f-to-eos and r-to-eos. Resultant plasmids were Tol2-Ef1α-HA-lmo4a, Tol2-Ef1α-lmo4a and Tol2-Ef1α-lmo4a-HA. The Tol2-Ef1α-GFP construct (id 1294) was used to estimate the efficiency of integration.

2.6.5 lmo2-GFP constructs

The various mouse lmo2 wt and mutant constructs (Gering et al., 2003) and (Sarah Hoosdally, *unpublished*), were used as a template and the *lmo2* sequence isolated by PCR with the primers glmo2-f2 and glmo2-r which were gateway cloned into pDONR221 (Invitrogen). Colonies were grown with kanamycin selection. Plasmid DNA was isolated and used for an LR reaction with the gateway compatible vector pCS2-gfp (Patterson et al., 2005) (id 504). The sequence was checked by sequencing with the gfp (cs2) reverse primer.

2.7 Imaging zebrafish embryos

2.7.1 Still digital photography

The number of embryos showing a particular phenotype was scored and images captured with a Nikon DXM1200 camera attached to a Nikon SMZ-U 1500 dissecting microscope and the Nikon Act-1 software. Exposure and white balance was set automatically and embryos were illuminated from the top and bottom on a glass depression slide, or from the top on a white depression tile as appropriate. Figures were prepared with Adobe Photoshop CS5.

2.7.2 Wide field fluorescence imaging

Live embryos were imaged in E3 medium, or mounted in 3 % methylcellulose, and imaged on a SteREO Lumar.V12 microscope (Zeiss). Exposure time was manually fixed for each experiment. Both image acquisition and analysis was carried out with the Zeiss AxioVision software.

2.7.3 Live confocal imaging

Embryos were grown in E3 medium supplemented with PTU to prevent pigment cell formation. For imaging, embryos were anaesthetised with 160 µg/ml tricane and orientated and

immobilised at the bottom of 35 mm glass bottomed dishes (Iwaki) in 1 % low melt agarose (Renaud et al., 2011). Embryos were covered with E3 media containing MS222 and PTU and a three somite segment of the GFP positive dorsal aorta imaged on an inverted LSM 510 confocal (Zeiss) at 28.5 °C from 30 hpf t 70 hpf using a x40 oil immersion objective. Images were acquired every five minutes with confocal stacks of 2 μm. Maximal projections and movies were generated with the LSM image browser software (Zeiss).

2.8 Bioinformatics tools

2.8.1 Ensembl and EditSeq

The human (build GRCh37), mouse (build NCBIM37) and zebrafish genomes (build Zv8 and Zv9) were interrogated with the Ensemble genome browser (Flicek et al., 2012). Nucleic acid sequences were manipulated *in silico* with EditSeq (DNAStar).

2.8.2 Sequence alignment

Nucleic acid sequences were aligned with SeqMan II (DNAStar). Graphs were generated with mVista (Frazer et al., 2004). FASTA formatted protein sequences were aligned with the T-COFFEE multiple alignment server (Notredame et al., 2000).

2.8.3 Homology model builder

The human LMO4 sequence (ENSG00000143013) and zebrafish Lmo4a sequence (ENSDARG00000013853) were aligned with T-COFFEE. Based on the structure of human LMO4 (PDB code 1RUT) (Deane et al., 2004), the alignment was used to provide a model for the structure of zebrafish Lmo4 using the SWISS-MODEL workspace (Arnold et al., 2006). All structures were manipulated and annotated with PyMol (DeLano Scientific).

2.8.4 Analysis of synteny and identity

The synteny of genomic loci was assessed using the Cinteny server (Sinha and Meller, 2007) or manually using the Ensembl genome browser. Identity and homology between protein sequences was determined using the Lalign server (William Pearson) and ClustalW2 (EBI) respectively.

Chapter 3

Structure-Function Analysis of Lmo2

3.1 Introduction

The dynamic assembly of proteins onto chromatin fibres, to form transcriptional complexes, is central to the rapid transcriptional response of a cell to signals from various intracellular and extracellular compartments. Lmo proteins are an evolutionarily conserved family of scaffold proteins which, through their four zinc fingers, can nucleate such complexes, and hence play a central role in control of gene expression (Bach, 2000). To date, four Lmo proteins (Lmo1-4) have been identified, and drive diverse cellular fates (Aoyama et al., 2005; Fisch et al., 1992; Visvader et al., 2001). Lmo2 is a key transcriptional regulator of haematopoiesis, and its ectopic expression in T-cell precursors is observed in up to 60% of childhood T-ALL cases, and may drive a leukaemic state through reactivation of HSC-specific genes. Alternatively, it may displace Lmo4 from its normal binding partners, given that Lmo4 is expressed in the T-cell lineage (Ferrando et al., 2004; Ferrando et al., 2002; Grutz et al., 1998; McCormack et al., 2010).

Lmo2 has been shown to interact with Ldb1, bHLH and Gata cofactors (El Omari et al., 2011; Wadman et al., 1997). Ldb1 is a widely expressed protein, which also acts as a nuclear scaffold protein and can bind Lmo2 through its C-terminal LID domain (El Omari et al., 2011). Its N-terminal domain is involved in multimerisation, and is thought to be involved in various competitive binding events, which result in distinct pools of complexes that can drive specific fates (Bach, 2000). Like Lmo proteins, bHLH family members are evolutionarily conserved and can be divided into two classes. Class I bHLHs are ubiquitously expressed whereas class II proteins are tissue restricted. Class II proteins can drive distinct developmental fates by forming heterodimers through their HLH domains with class I proteins, which go on to bind their cognate DNA E-box recognition sequences through their basic regions (Porcher et al., 1996; Tapscott, 2005). Scl, a class II bHLH, forms obligate heterodimers with E-proteins, which are class I bHLH proteins (Porcher et al., 1999). During normal blood development, Lmo2:Ldb1 dimers can mediate interactions with E2A:Scl heterodimers, and Gata1 or Gata2, to form the so-called pentameric complex, which bridges a bipartite Gata-E-box motif DNA motif in erythroid cells (Kassouf et al., 2010; Wadman et al., 1997).

Given the key role of Lmo2 and its partners in the pentameric complex during haematopoiesis, an understanding of complex assembly and function at the molecular level is of great interest. Despite numerous studies, the lack of structural information has hampered efforts to this effect. In this chapter, recently solved crystal structures of Lmo2:Ldb1-LID and E47(bHLH):Scl(bHLH):Lmo2:Ldb1(LID):DNA(E-box) are presented. Taking advantage of the well-characterised role of Lmo2 and Scl in early haematopoietic development in zebrafish, we carry out a structure-guided mutational analysis of the Lmo2 molecule, identifying residues that are necessary for its structure and function. Additionally, we begin to investigate the interaction of Lmo2 with Gata1 and Gata2.

3.2 Conformational flexibility of Lmo2 is required for its activity

As previously reported for Lmo4, full-length recombinant Lmo2 either did not exist as stable single molecules or was insoluble, and was therefore unsuitable for crystallization (Deane et al., 2001; El Omari et al., 2011). Consistent with this, it has previously been shown that binding of Lmo2 to other proteins is required for it to maintain a stable fold and prevent degradation by the proteasome (Lecuyer et al., 2007). To get around this, most of the full-length human Lmo2 was fused to the LID domain of human Ldb1, separated by a flexible linker sequence (Figure 3.1A). A similar strategy had been successfully employed for Lmo2 (Deane et al., 2004; Deane et al., 2001). Additionally, it was shown that folding of this artificial fusion was not disrupted (El Omari et al., 2011). The fusion allowed the generation of diffraction-grade crystals, and hence structure determination. Similar to the structure of Lmo4, Lmo2 forms an elongated bar of ~80 Å, and is comprised of two tandem LIM domains, each containing two zinc fingers (Figure 3.1B). As secondary structure is relatively low, Lmo2 relies heavily on coordination of four zinc atoms, one in each zinc finger, for stability. This region is highly conserved between members of the Lmo family. Additionally, the LID domain of Ldb1 binds across one surface of the Lmo2 molecule. This interaction is stabilised by non-specific

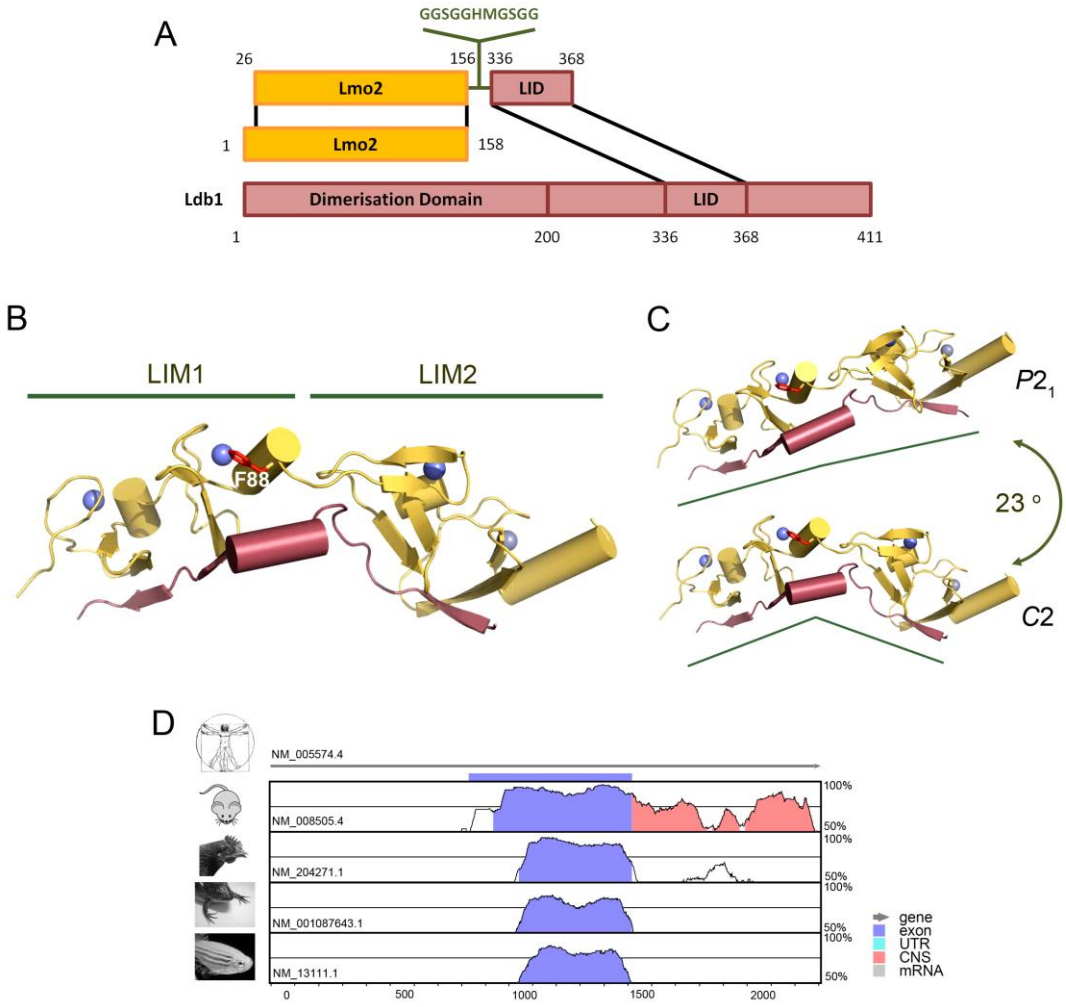

Figure 3.1 The structure of Lmo2 reveals its conformational flexibility

(A) Schematic representation of the Lmo2:Ldb1(LID) fusion expressed for crystallisation. The LID domain from Ldb1 was fused to Lmo2 and separated by a flexible linker (depicted in green). (B) The structure of human Lmo2:Ldb1(LID) was solved to a resolution of 2.4 Å. The LID domain (maroon) folds back over one surface of Lmo2 (yellow), leaving four zinc fingers exposed on the opposite surface. Each zinc finger coordinates a zinc ion (blue spheres). The two LIM domains are indicated, along with the residue Phe88. (C) A second crystal form was obtained in the $P2_1$ space group. Superimposing the LIM1 domain of the two structures revealed a 23 ° rotation of LIM2 about Phe88. Adapted from (El Omari et al., 2011) and PDB 2XJY and 2XJZ. (D) VISTA alignment of human, mouse, chicken, *Xenopus tropicalis*, and zebrafish *lmo2* sequences. All sequences aligned to the human reference sequence (blue bar), and identity between 50 and 100% is shown.

backbone:backbone hydrogen bonding, electrostatic interactions and hydrophobic contacts. Indeed, the interface between Lmo2 and Ldb1-LID results in the exclusion of an extensive surface from bulk solvent; with each protein respectively burying 16% and 40% of their total surface area (El Omari et al., 2011). Of note, this overall arrangement leaves the face of Lmo2, from which the zinc fingers protrude, free to interact with other proteins (Figure 3.1B).

Superimposition of the LIM1 domain from two independent structures of Lmo2, derived from independent space groups, revealed that while the LIM domains are structurally very similar, a rotation of 23° exists between the LIM2 domains of each structure (Figure 3.1C). A similar motion is also observed when 5 non-crystallographically related copies of Lmo2:Ldb1-LID in the same space group, or the Lmo2:Ldb1-LID and Lmo4:Ldb1-LID, are superimposed (El Omari et al., 2011). Together, this suggests that each LIM domain behaves as a rigid bar, which are separated by a flexible hinge region. Using the HingeProt algorithm, which utilises elastic network modelling to predict protein hinges from a structure (Emekli et al., 2008), it was shown that the hinging motion occurs about two residues: F88 in Lmo2 and E349 in Ldb1-LID, matching the region where rotational freedom is experimentally observed (El Omari et al., 2011). Additionally, F88 and the surrounding residues are conserved between Lmo family members, suggesting that the predicted hinging is functionally important. Furthermore, it is likely that conformational flexibility facilitates the role of Lmo2 as protein nucleator, for example by allowing the 2 LIM domains to independently bind different cofactors, such as Scl and Gata1.

To test the requirement of conformational flexibility within Lmo2, we generated two point mutations at the hinge residue in Lmo2; F88A and F88D. Given the high degree of conservation of Lmo2 between species (Figure 3.1D) and the availability of reagents, we used the mouse Lmo2 orthologue. We reasoned that the two mutations would allow us to uncouple the role of an aromatic side chain from conformational flexibility, as the mutation to alanine results in a loss of the aromatic side chain, while preserving the hydrophobic characteristic of phenylalanine and remaining sterically conducive to a hinging motion. In contrast, the mutation to aspartic acid was predicted to create intramolecular salt bridges with R77 and K74, effectively creating a totally rigid molecule. To test the

functionality of these mutations, we took advantage of an overexpression strategy in the zebrafish whereby co-overexpression of *scl* and *lmo2* mRNA, but not single overexpression, causes an expansion of *fli1* into the anterior and cardiogenic regions which usually do not express *fli1* (Gering et al., 2003). Introduction of wild type *scl* along with either of the *lmo2* point mutants failed to exhibit this expansion (Figure 3.2A). We quantitated this effect by qRT-PCR on whole embryos, demonstrating a 2-fold increase in *fli1* expression when wild type *lmo2* was introduced with wild type *scl*. However, we observed reduced enhancement upon introduction of the F88A mutant and loss upon introduction of the F88D mutant (Figure 3.2D). This presumably reflects the reduced ability of the Lmo2 mutants to interact with Scl. Consistent with this, an analogous observation was made using a mammalian 2-hybrid luciferase reporter system in HEK293 cells, where Lmo2 was fused to the Gal4 DNA binding domain and Scl to the VP16 activation domain (El Omari et al., 2011).

Importantly for our analysis, levels of Scl and the various Lmo2 mutants were unaffected, suggesting that the mutations did not affect protein availability. In the case of Scl, this was demonstrated by western blotting for the HA tag corresponding to the *scl-HA* fusion (Figure 3.2B). Although we were unable to directly detect Lmo2 by western blotting, we could detect the fluorescence signal and mRNA from the *lmo2-GFP* fusion construct that was employed, and from a *h2b-RPF* tracer that remained constant across all experimental conditions (Figure 3.2 C-D). Taken together, we show that while the aromatic side chain of the hinge residue may increase the binding affinity of Lmo2 for Scl, conformation flexibility is absolutely required, at least for Lmo2 to function with Scl.

3.3 Identifying functional residues on the surface of Lmo2

In addition to the Lmo2:Ldb1-LID crystal structure, the structure of human Lmo2:Ldb1-LID in complex with the human $(Scl:E47)_{bHLH}$ heterodimer bound to an 11 bp blunt-ended DNA fragment was solved to a resolution of 2.8 Å (Figure 3.3A). As crystals could not be obtained with the CAGCTG E-box preferred by Scl, the CATCTG E-box motif successfully employed in previous

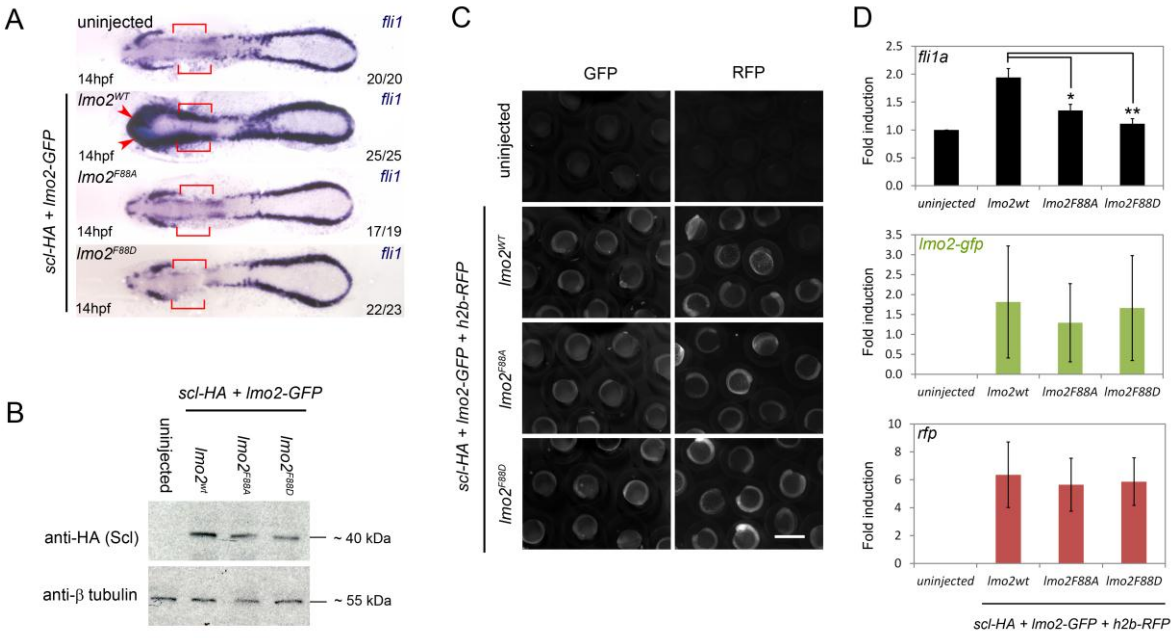

Figure 3.2 The conformational flexibility of Lmo2 is required for its activity

(A) Co-overexpression of *lmo2* and *scl* results in an expansion of lateral mesoderm, marked by *fli1*. This effect is lost when point mutations predicted to reduce flexibility of Lmo2 are introduced. (B) Western blots for HA demonstrate that Scl is stable in each case. (C) Fluorescence microscopy at approximately 10 ss. Lmo2 tagged with GFP is detected, demonstrating all Lmo constructs are stable. An RFP construct, which remains constant throughout the experiment, is also detected. Scale bar is 1 mm. (D) qRT-PCR quantitation of total *fli1*, in pooled 10 ss embryos. Wild type *lmo2* results in a two-fold induction of *fli1* , which is reduced or lost in *lmo2* point mutants. * $p < 0.05$, ** $p < 0.01$, compared to wild type induction. Primers against the controls *lmo2-gfp* and *rfp* revealed no significant change in levels. Error bars are representative of the SEM from four independent experiments.

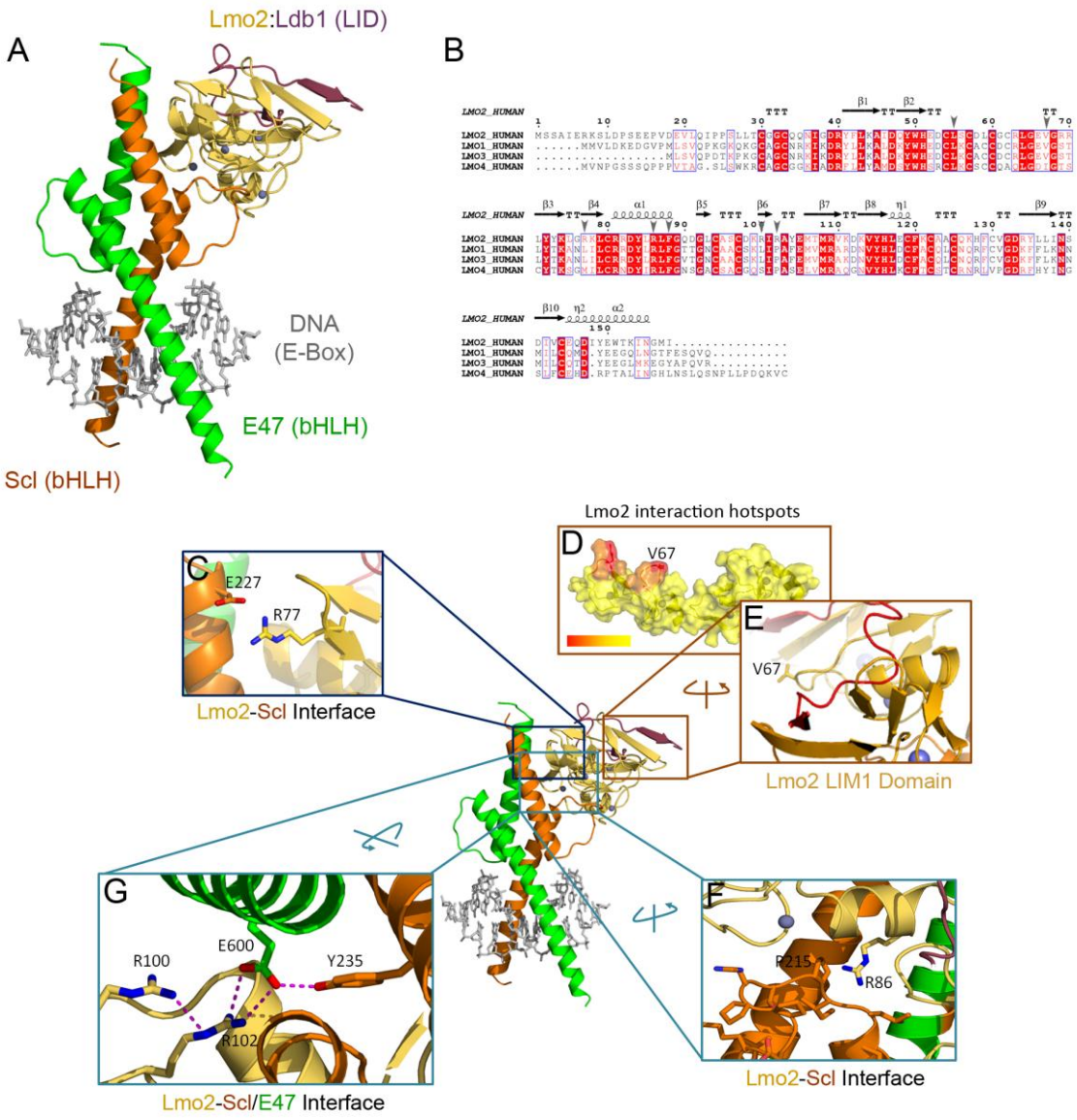

Figure 3.3 Crystal structure of E47(bHLH):Scl(bHLH):Lmo2:Ldb1(LID) bound to DNA

(A) The structure of a complex containing the bHLH domains of human E47 and Scl bound to their cognate DNA sequence, along with Lmo2:Ldb1(LID), was solved to a resolution of 2.8 Å. (B) Protein alignment of human Lmo proteins. Residues mutated in this study are indicated by a grey arrowhead. α-helicies and β-sheets from the structural work are mapped onto the alignment. (C) Arg77 on Lmo2 contacts Scl. (D) The WHISCY algorithm was used to predict protein binding hotspots on the Lmo2 molecule (red shades). (E) Val67 on the Lmo2 surface does not interact with other members of the complex. (F) Lmo2 interacts with Scl through R86. (G) Arg100 and Arg102 interact with Scl via E47. Structures and alignment adapted from (El Omari, *unpublished*).

studies was used (Longo et al., 2008). The basic domains of the $(Scl:E47)_{bHLH}$ heterodimer are topologically identical to previously reported bHLH structures, and contact the major groove of the DNA fragment, with E47 binding the CAT half-site and Scl the CTG half-site (Kamel El Omari, *unpublished data*). Consistent with the hypothesis that conformational flexibility is required for full activity of Lmo2, the Lim domains of Lmo2 must rotate relative to each other in order to bind $(Scl:E47)_{bHLH}$ (Kamel El Omari, *unpublished data*). Lmo2 binds to the $(Scl:E47)_{bHLH}$ heterodimer through interactions mainly occurring in the first LIM domain. However two residues in LIM2, R100 and R102, also contact $(Scl:E47)_{bHLH}$. Work *in vitro* has shown that E47 and Scl homodimers are able to form, although $(Scl:E47)_{bHLH}$ heterodimers are thermodynamically favoured, in part due to instability of Scl homodimers (Longo et al., 2008; Ryan et al., 2008). Additionally, binding of Lmo2 to $(Scl:E47)_{bHLH}$ induces the formation of new hydrogen bonds and salt bridges at the $(Scl:E47)_{bHLH}$ interface, likely increasing the likelihood of heterodimers over homodimers. In contrast, due to altered conformation, binding of Lmo2 is predicted to destabilise the $(Scl:E47)_{bHLH}$:DNA interface (Kamel El Omari, *unpublished data*), providing a structural explanation for this previously observed change in DNA binding affinity (Ryan et al., 2008).

Analysis of the structure has also allowed the Scl:Lmo2 interface to be defined for the first time. Interactions occur mainly through the LIM1 domain of Lmo2 with the Helix 2 and loop regions of Scl (Figure 3.3 C, E, F and G). The residues L59 and F88 on Lmo2 are among the main stabilisers of this interface, while a hydrogen bond between Lmo2 R86 and Scl L213, and a salt bridge between Lmo2 R77 and Scl D245 may provide specificity (Figure 3.3 C and F) (Kamel El Omari, *unpublished data*). Additionally, a salt bridge is formed between R102 in Lmo2 and E600 in E47, which goes on to form a hydrogen bond with Y235 in Scl. Furthermore, there is another arginine, R100, within a distance of 4.5 Å from R102, and together these two residues provide a charged groove that would facilitate E47 E600 binding (Figure 3.3G). Given that these two arginines are involved directly or indirectly in binding both E47 and Scl, it is possible that they may allow Lmo2 to distinguish between bHLH homodimers and heterodimers to form a functional complex. As the reported association constant between Scl and Lmo2 is relatively high, and only a relatively small surface area is buried from bulk solvent at the interface, it is likely that residues involved at this interface are crucial in maintaining

the integrity of the complex (Ryan et al., 2008) (Kamel El Omari, *unpublished data*). Finally, taking advantage of the WHISCY server (de Vries et al., 2006), surface binding hotspots on the Lmo2 molecule can be predicted. The strongest candidate hotspots are concentrated in the LIM1 region, and specifically V67, which does not contact any proteins in the complex (Figure 3.3 D-E). This residue may therefore contact other as yet unknown proteins.

In order to investigate the biological functionality of the Lmo2 residues described, we generated a series of point mutations and took advantage of the increase in *fli1* expression associated with co-overexpression of *lmo2* and *scl* used previously (Section 3.2) (Gering et al., 2003). As before, the effect on *fli1* expression was quantitated by qRT-PCR. When expressed with wild type *scl*, *lmo2* R100A/R102A and L59G mutants were as efficient as wild type *lmo2* in driving *fli1* overexpression. However R86A, V67A and R77A mutants led to significant reduction in the degree of *fli1* overexpression (Figure 3.4A). As with our analysis of F88, expression of *lmo2* and *scl* were unchanged across the various conditions (Figure 3.4 D-E). A mammalian two-hybrid assay measuring the ability of the same Lmo2 mutations to bind to Scl gave similar results to our *in vivo* system (Kamel El Omari, *unpublished data*). Data for Lmo2 R86A and R77A mutants, which result in reduced activity, were in excellent agreement between the two systems. However, in contrast to their activities in our system, the biochemical interaction between the R100A/R102A and L59G mutants was increased in the two-hybrid assay. This may reflect saturation of the up-regulation of *fli1* seen in the zebrafish with wild type Lmo2, which would prevent detection of increased activity. Alternatively, the increased strength of binding may not have a functional consequence *in vivo*. Of note, Lmo2 V67A did not show altered binding to Scl in the two-hybrid system, whereas it resulted in a significant reduction in *fli1* expression in the zebrafish. This effect will be investigated further in the following section.

3.4 Lmo2 may interact with the linker region of Gata1

Previous mutational studies and immunoprecipitation experiments have demonstrated that the LIM2 domain of Lmo2, but not LIM1, is required for binding to Gata proteins and therefore for intact

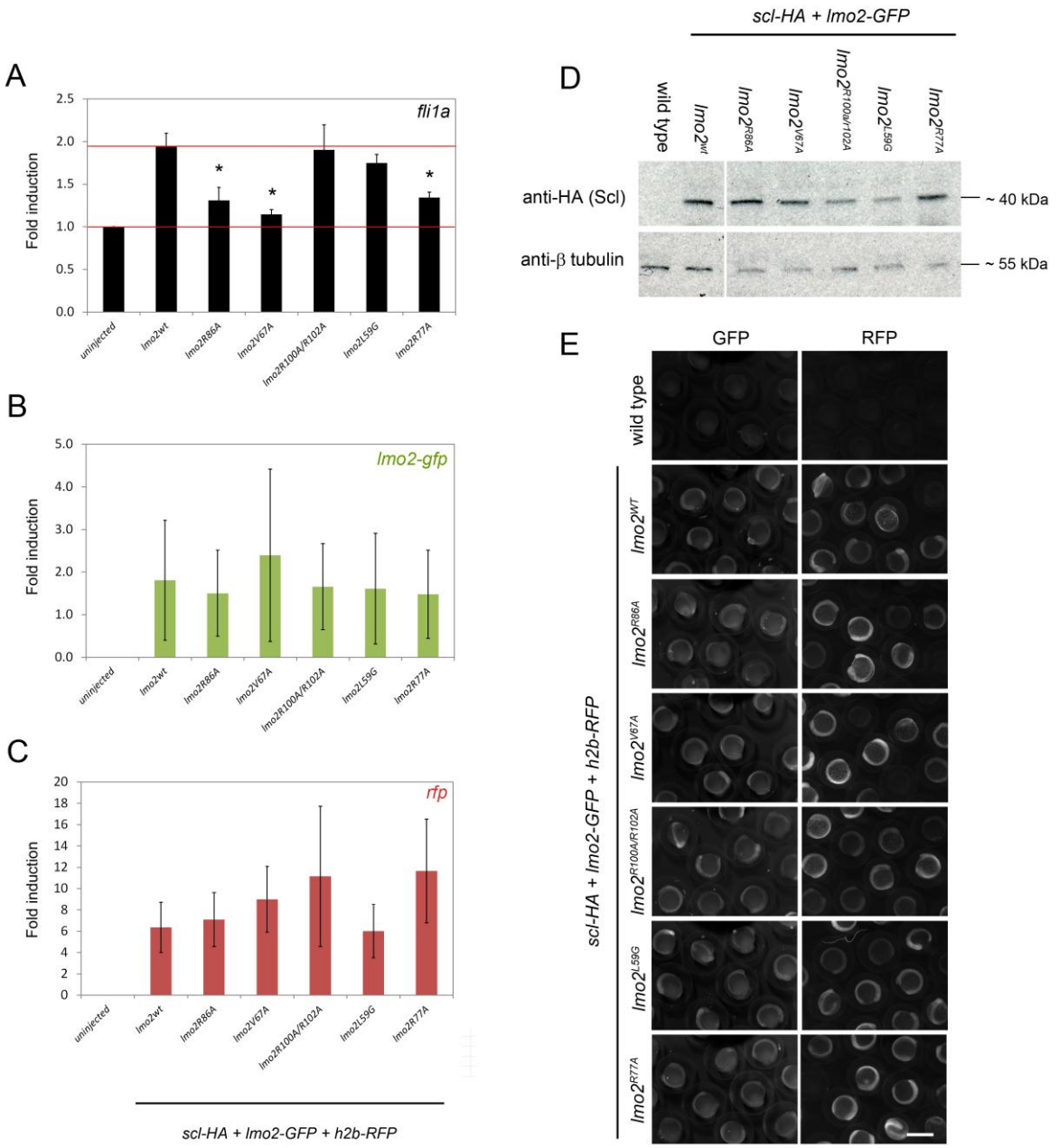

Figure 3.4 Identifying functionally important residues on the surface of Lmo2

(A) Co-overexpression of *lmo2* and *scl* causes a twofold increase in *fli1a* expression as measured by qRT-PCR. Various *lmo2* point mutants result in unchanged or reduced induction of *fli1a*. The range of the assay is indicated by red lines. * $p < 0.05$ compared to wild type induction. (B – C) Primers against the controls *lmo2-gfp* and *rfp* revealed no significant change in levels. Error bars are representative of the SEM from four independent experiments. (D) Western blots for HA demonstrate that Scl variants are stable. (E) Fluorescence microscopy at approximately 10 ss. Lmo2 tagged with GFP is detected, demonstrating all Lmo constructs are stable. An RFP construct, which remains constant throughout the experiment, is also detected. Scale bar is 1 mm.

haematopoiesis (Teranoa et al., 2005). The Gata1 protein contains 2 zinc fingers. The C-finger is sufficient to confer specific DNA binding activity, whereas the N-finger is involved in the modulation of DNA binding activity and interactions with cofactors, including Lmo2 (Osada et al., 1995). An NMR structure of the Gata1 N-finger bound to the first of nine zinc fingers in Friend of Gata (FOG) was used as a guide to dock the N-finger of Gata1 onto LIM2 of Lmo2, as the structures of the first FOG zinc finger and Lmo2 LIM2 are homologous (El Omari et al., 2011; Liew et al., 2005). Together with an NMR solution structure of the Gata1 C-finger bound to its cognate DNA sequence (Omichinski et al., 1993), a model was generated for Gata1 docked to Lmo2:Ldb1(LID), which does not exclude the simultaneous binding of Gata and bHLH proteins, or require major deformation of the DNA fibre (Figure 3.5A) (Kamel El Omari, *unpublished*). The N- and C-fingers of Gata1 are separated by a 30 amino acid flexible linker region for which no structural data is available. However, molecular dynamic simulations were used to predict minimal energy conformations for this flexible region. In 3 out of 4 simulations, within 50 ns, a five residue run comprising R421, P422, L423, I424 and R425 came to lie near V67 in Lmo2 (Kamel El Omari, *unpublished*). It is possible that a similar arrangement of the flexible linker region exists in the canonical erythroid complex (Figure 3.5B) (Wadman et al., 1997).

In our model, Gata1 is anchored to the DNA and to Lmo2-LIM2, therefore Lmo2 V67 in LIM1 is unlikely to be necessary for Gata1 binding to Lmo2. However, we were interested in whether the interaction with Lmo2 V67 was required to set up an active conformation. To test this hypothesis, we extended the co-overexpression of mouse *lmo2* and *scl* used previously to include overexpression of zebrafish *gata1a*, in which the five residue run is identical to the run in human *gata1* (Figure 3.5D). This triple co-overexpression has been shown to cause an expansion of the erythroid marker *alas2* expression, which is usually restricted by the endogenous expression domains of *lmo2, scl* and *gata1* (Gering et al., 2003; Mead et al., 2001). Overexpression of wild type *lmo2*, but not the *lmo2* V67A mutant, with *scl* resulted in an expansion of *alas2* expression within the ICM, reflecting the earlier increase in endothelial and blood development in the PLM (Figure 3.5 E-G). Overexpression of *lmo2, scl* and *gata1a* resulted in an even more dramatic expansion of *alas2* expression, most notably into the head region which normally never expresses *alas2* (Figure 3.5H). This expansion is lost when *lmo2* is

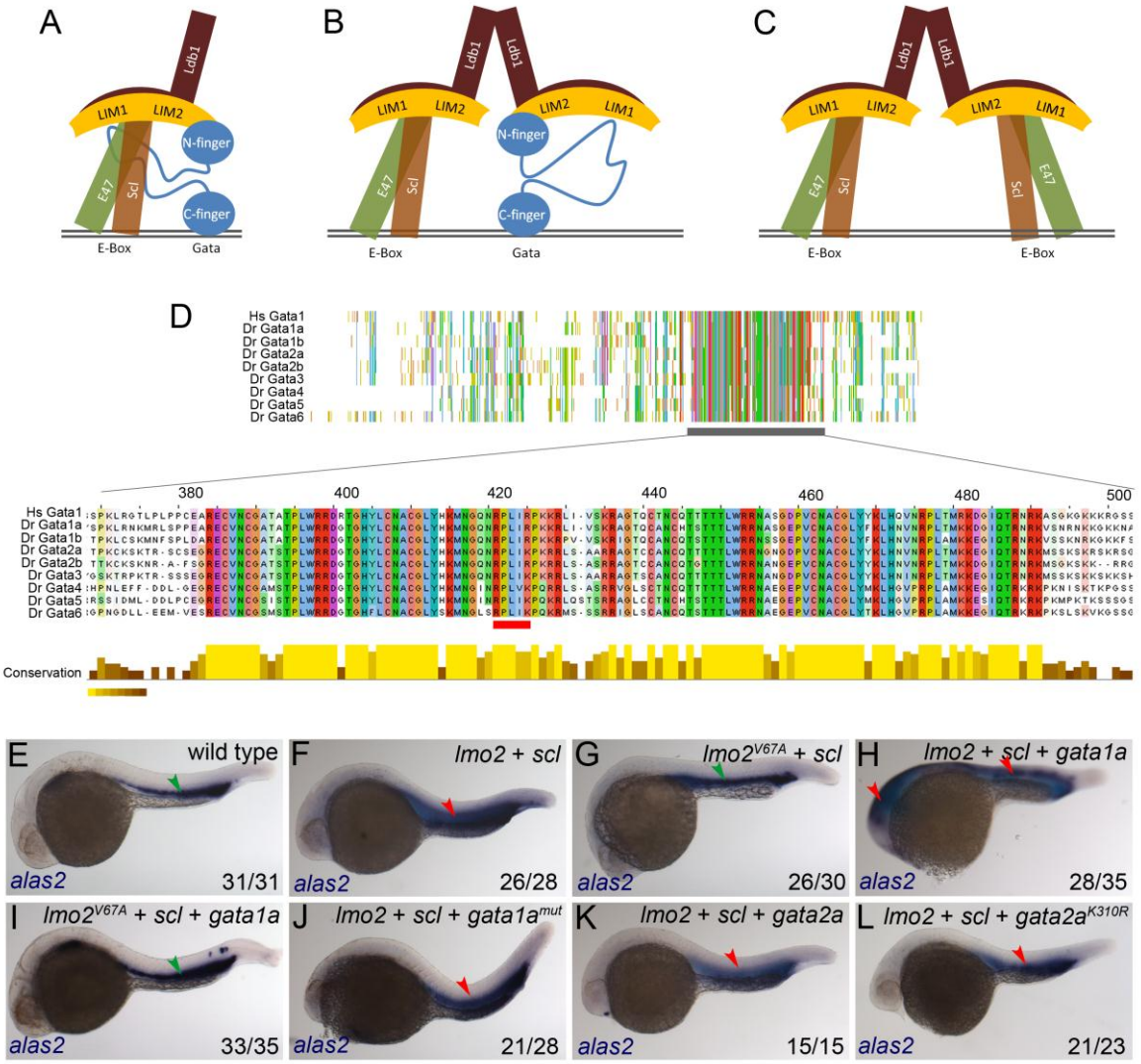

Figure 3.5 Five adjacent residues in the Gata1 linker region may interact with Lmo2-LIM1

(A) Gata1 (blue) was modelled onto the E47(bHLH):Scl(bHLH):Lmo2:Ldb1(LID) crystal structure. Molecular dynamic simulations of the flexible linker region revealed a five residue stretch that came to lie next to V67 in Lmo2 (yellow). (B) The canonical erythroid complex. (C) An alternative complex identified in leukaemic T-cells isolated from an *lmo2* transgenic murine model. (D) Alignment of human Gata1 and all zebrafish Gata proteins. Top panel, an overview of the entire gene; middle panel, enlarged view of the indicated region with the five amino acid run indicated by the red bar; lower panel, degree of conservation. (E – H) Co-overexpression of *lmo2*, *scl*, and *gata1a* results in ectopic expression of the erytrhoid marker, *alas2*, in the head of zebrafish embryos. (I – J) The expansion of *alas2* expression is lost when *lmo2* and *gata1a* are respectively replaced with an $lmo2^{V67A}$ mutant, or a version of *gata1a* where the five amino acid run has been mutated. (K – L) Replacement of *gata1a* with *gata2a* or $gata2a^{K310R}$ does not result in an expansion of *alas2*. Green arrowheads indicate wild type levels of *alas2*, and red arrowheads ectopic expression in the trunk and head.

replaced with the *lmo2* V67A mutant, or *gata1a* is replaced with a *gata1a* mutant in which the 5 residue run in the flexible linker was replaced with the sequence GSSGS (Figure 3.5 I-J). As the amino acid sequence GSSGS is predicted to maintain flexibility of the region but not specific protein interactions (Erika Mancini, *personal communication*), this mutation allows us to uncouple these two activities.

Expansion of *alas2* outside of the ICM does not occur when Gata1 is replaced with Gata2 in the triple overexpression setting (Gering et al., 2003). The region in Gata2a corresponding to the mutated five adjacent residues in Gata1a is identical, with the exception of the final arginine, which is replaced by a lysine in Gata2a (Figure 3.5D). Although these two residues have similar physical properties, we were interested in whether this small change could account for the differential functional output of Gata1a and Gata2a. We therefore generated a *gata2a* mutant, in which K310, the final residue in this 5 amino acid run, was mutated to arginine. Co-overexpression of wild type *gata2a* or the *gata2a* K310R mutant, together with wild type *lmo2* and *scl* did not expand *alas2* outside the ICM (Figure 3.5 K-L). Thus, taken together, our data suggests that some or all of the amino acids within the 5 residue run in Gata1 interact with V67 in Lmo2 to confer biological function, at least in erythroid development. Furthermore, the difference in a single amino acid at the end of this 5 residue run in Gata2a, when compared to Gata1a, cannot on its own account for their differential functions. However, we have not investigated whether Gata1b or Gata2b, in which the 5 residue run is absolutely conserved (Figure 3.5D) are also involved. Additionally, as we cannot differentiate between exogenous and endogenous *gata* protein, we cannot as yet exclude the possibility that mutations in Gata factors affect the viability of the proteins.

3.5 Discussion

3.5.1 Overview

Modular protein units assemble in a dynamic fashion on DNA to form molecular machines that control its expression. A key complex driving erythroid development consists of the scaffold proteins Lmo2 and Ldb1, bridging the bHLH dimers and Gata factors (Wadman et al., 1997).

Although much work has been carried out defining the network of interactions, the molecular basis of how this complex assembles to control gene expression is poorly understood. In this chapter, we take advantage of crystal structures and structural modelling of components of this complex to identify and detail the functional relevance of some of the key protein:protein interactions which allow Lmo2 to communicate with other members of the complex.

3.5.2 Lmo2 is a versatile adapter protein

Consistent with the known role of Lmo2 as a nucleator of protein complexes, we observe a hinging motion between the two rigid LIM domains. This is dependent on the hinge residue F88, and demonstrates that the resulting conformational flexibility is required for the full activity of Lmo2. This likely reflects the increase in potential interactions that can be accommodated and would therefore facilitate the formation of a variety of context-dependent complexes. Through pull-down experiments in MEL cells, the hinge movement has also been shown to be required for Lmo2's interaction with the cofactors Scl:E47, pCaf, eto2 and p300, but not with ldb1, gata1, mSin3a or Lsd1 (Sarah Hoosdally, *unpublished*), demonstrating that the hinging motion is not required for all binding events. The conformational flexibility in Lmo2 may additionally allow for its activation and deactivation, and hence dynamic regulation of gene expression.

Binding of Lmo2 to the $(Scl:E47)_{bHLH}$ heterodimer may also regulate gene expression, along with complex formation, as Lmo2 stabilises heterodimerisation between Scl and E47, but alters the dimerisation angle, weakening the affinity for specific DNA binding. Thus, ectopic expression of Lmo2 in T-cell precursors is likely to result in the displacement of Scl:E47 heterodimers from DNA, allowing them to associate with additional DNA-binding proteins at alternative genomic loci. This is likely to disrupt the balance between E47:E47 and Scl:E47 mediated gene expression, and may explain why Lmo2 overexpression can drive a leukaemic state (Palii et al., 2011) (Kamel El Omari, *unpublished*). Stabilisation of Scl:E47 heterodimers upon Lmo2 binding may also prevent aberrant formation of other bHLH dimers during the specification of blood from mesoderm. Although the precise complex driving this transformation has not been defined, it has been shown that in the absence of Scl, ectopic

cardiac development occurs (Adamo et al., 2009; Simoes et al., 2011; Van Handel et al., 2012), possibly reflecting a shift to the use of other bHLH dimers.

Within the PLM, it has been demonstrated that expression of *fli1* is dependent on the interaction between Lmo2 and Scl, but not on Scl DNA binding activity, and that overexpression of *lmo2* and *scl* causes an expansion of *fli1* expression (Gering et al., 2003; Patterson et al., 2007). To specifically investigate the Lmo2:Scl interaction, we introduced a series of Lmo2 point mutants into the zebrafish, in the context of *scl* overexpression. Murine constructs were used in this analysis, and gave the same phenotype as zebrafish constructs, demonstrating functional conservation between these two species in this developmental context. Additionally, although there was a high degree of variability in our RNA injections between experiments, this did not result in large error bars in *fli1* expression. This may reflect a thresholding effect.

We had hypothesised that the residues L59, R100 and R102, which are unique to the Lmo2 molecule, were directly or indirectly involved in interfacing with Scl and E47. Furthermore, L59 was shown to contact F238 in Scl, which has been shown to be sufficient in conferring haematopoietic activity on class II bHLH proteins (Schlaeger et al., 2004). Our data however suggests that L59 on its own, and R100 and R102 in combination, are not necessary for Lmo2 binding to Scl. We however cannot exclude the possibility that these residues are required for functional complex conformation or stability in other developmental contexts. Additionally, we identified three residues on the Lmo2 surface which when mutated, disrupt its functional output. It was unsurprising that R86, which is conserved between Lmo family members, and R77, which is unique to Lmo2, were necessary for binding to Scl, given that they respectively form a salt bridge and hydrogen bonds with residues in Scl. We were however surprised that V67, which is conserved between Lmo1-3, was required for the activity associated with overexpression of Lmo2 and Scl, given that it does not contact Scl. Indeed, direct binding between Lmo2 and Scl in the mammalian two-hybrid system did not require this residue (Kamel El Omari, *unpublished*). However, we show that V67 in Lmo2 is likely required to set up a functional interaction with Gata1, at least in the PLM. Consistent with this, *fli1* was only ever expanded into tissues that expressed a Gata factor, and could be further expanded throughout the embryo upon

ectopic expression of *gata1*. It is therefore possible that a similar complex to that driving erythroid development, comprising of bHLH dimers, Lmo2:Ldb1 dimers and Gata factors (Wadman et al., 1997), is functioning in the PLM. As well as bridging neighbouring DNA binding sites, such a complex may also be involved in mediating interactions between distant regulatory elements.

3.5.3 Future therapeutic directions

Due to the small area of the Scl:Lmo2 interface, along with its defined secondary structure, this interaction is amenable to disruption, for example by use of small molecules or biological strategies (Bourgeas et al., 2010). An aptamer peptide has previously been shown to bind Lmo2 LIM2, and disrupt its interaction with binding partners in a murine T-cell tumour transplantation assay (Appert et al., 2009). Our mutational analyses, together with future work identifying interaction surfaces with other Lmo2 partners, will provide direction for the rational design and optimisation of libraries containing moieties that alter the stability of this interaction, by directly identifying residues that are involved at the relevant interface. Lmo2 plays a role in the angiogenic process, remodelling immature capillary networks to mature vasculature (Yamada et al., 2000), and is associated with a variety of solid tumours of the thymus, lung and prostate (Ma et al., 2007; Yamada et al., 2002). In addition, 44% of T-ALL samples ectopically co-express Scl and Lmo2 (Ferrando et al., 2004; Ferrando et al., 2002). Therefore, the ability to modulate the transcriptional output of Lmo2, for example by affecting the affinity for its partners, is likely to have relevance to a variety of disease states.

Chapter 4

Lmo4 and its Protein Partners Programme Nascent HSCs

4.1 Introduction

In the previous chapter, it was shown that the LIM Domain Only protein Lmo2 binds the LID domain of Ldb1. This interaction occurs through the Lmo2 surface opposed to the face projecting four zinc fingers. Ldb1 has also been shown to bind the related Lmo protein Lmo4, and it was through this interaction that Lmo4 was first identified (de la Calle-Mustienes et al., 2003; Deane et al., 2004; Grutz et al., 1998; Tran et al., 2006). Through liquid chromatography–mass spectrometry (LCMS) analysis of complexes pulled-down with biotinylated Ldb1 in MEL cells, it was shown that Ldb1 binds Lmo4 in differentiated, but not undifferentiated, MEL cells (Meier et al., 2006). Morpholino-mediated depletion of *lmo4a* in the zebrafish has been shown to result in loss of expression of the master HSC regulator *runx1* in the dorsal aorta (Meier et al., 2006). Additionally, in the mouse, *lmo4* expression has been seen in the somites, lateral mesoderm, and the caudal AGM at E9, just before HSC emergence (Kenny et al., 1998). *lmo4* knockout mice die prenatally, due to anterior-posterior patterning defects, and failure of neural tube closure (Hahm et al., 2004; Lee et al., 2005; Tse et al., 2004). Although no defects in blood development were reported in newborn mice, half of the *lmo4* null mice died during gestation at around E9, conceivably of a haematopoietic phenotype with reduced penetrance. In contrast to the developing mouse, failure of blood development in the zebrafish is not embryonically lethal (Patterson et al., 2007). Thus, together with the advantages previously described (section 1.5), the zebrafish is ideally placed to investigate components required for the development of the first blood cells. We were therefore interested in further investigating the potential role for *lmo4a* in the development of blood.

Extending the biotin tagging, pull-down and LCMS strategy in MEL cells to Lmo4, has led to the identification of a putative erythroid transcriptional complex (C Andrieu-Soler, *unpublished data*). As described in the previous chapter, Lmo2 and Scl, are members of a canonical erythroid complex. They have been shown to act together at an earlier point in development to specify the precursors of vasculature and blood (Patterson et al., 2007; Patterson et al., 2005). This chapter will therefore investigate if, like Lmo2 and Scl, the partners of Lmo4 identified in MEL cells required in a context distinct from erythroid development, for example during HSC development.

Soon after the dorsal aorta is laid down, it becomes transiently polarised, with the floor and roof exhibiting distinct gene expression profiles; *tbx20* is expressed in the roof of the vessel and *bmp4* and *runx1* in or around the floor (Gering and Patient, 2005; Wilkinson et al., 2009). The emergence of HSCs and primary ISVs also occurs in a polarised fashion, respectively forming from the floor and the roof of the vessel. These two processes both begin with the bending of endothelial cells (Bertrand et al., 2010a; Boisset et al., 2010; Isogai et al., 2003; Kissa and Herbomel, 2010). We will therefore briefly explore the possibility that initiation of these two processes is controlled by the same genetic signals.

In this chapter, we have taken advantage of morpholino-mediated knockdown to identify several novel regulators of HSC development. We confirm a role for *lmo4a* in the early HSC compartment and go on to image the emergence of the first HSCs. Furthermore, we show that *lmo4a* is not transcriptionally up or downstream of various known players in HSC development. Significantly, we show that it is likely that components of the novel erythroid complex are reused during development. Although no mechanistic data is presented in this chapter, an understanding of the factors involved in setting up the HSC state is a first step in the efforts to manipulate this important cell type.

4.2 Identification of an Lmo4 complex and relationships between Lmo4 orthologues

The cellular functions of proteins are often modulated or dependent on higher order interactions with distinct polypeptide molecules, and these functional units can provide forward momentum for developmental processes (Nooren and Thornton, 2003). Much previous work has focused on dissecting protein complexes involved in haematopoiesis, allowing the construction of graphs representing the topology of protein interactions (Anguita et al., 2004; El Omari et al., 2011; Meier et al., 2006; Orkin and Zon, 2008). Partners of the key erythroid transcription factor Gata1 were identified using an *in vivo* biotinylation strategy in MEL cells. Gata1 was expressed with a tag, where the tag was recognised by its cognate BirA biotin ligase, which was itself stably expressed in MEL cells.

Coupled with streptavidin purification and LCMS, this allowed the identification of factors bound to Gata1 under the specific culture conditions used (de Boer et al., 2003; Grosveld et al., 2005; Rodriguez et al., 2005). This strategy was extended to the LIM domain binding protein Ldb1, which is important in haematopoiesis (Mukhopadhyay et al., 2003). In MEL cells where differentiation has been induced, the scaffold protein Lmo4 was identified as an Ldb1 partner. In naïve MEL cells, the cyclin dependent kinase Cdk9 was identified as an Ldb1 partner. In both induced and uninduced states, the repressor Eto2 was shown to interact with Ldb1 (Meier et al., 2006). Recent work tagging the transcription factor Lmo4 has led to the identification of a putative transcriptional complex in MEL cells, and highlighted a possible role for Lmo4 in definitive haematopoiesis (Figure 4.1A), (C Andrieu-Soler, *unpublished*) (Meier et al., 2006).

Alignment of vertebrate orthologues of *lmo4* revealed a high degree of conservation (Figure 4.1B). In the zebrafish, two versions of the *lmo4* gene exist, *lmo4a* and *lmo4b*. This likely represents an ancient gene duplication event that occurred in the telosts (Taylor et al., 2003). The *lmo4b* cDNA sequence displays a higher degree of conservation to its vertebrate counterparts than the *lmo4a* sequence (Figure 4.1B). Comparative analysis of the two zebrafish orthologues at the protein level reveals a 74.9% identity and 93.4% homology between Lmo4a and Lmo4b. The Human Lmo4 sequence shares a 96.4% and 76.0% identity between zebrafish Lmo4b and Lmo4a respectively, with a 99.9% and 92.2% homology between zebrafish Lmo4b and Lmo4a. Within the two LIM domains, Lmo4b and human Lmo4 are 100% homologous. Analysis of synteny between the human *lmo4* locus on chromosome 1 and the zebrafish *lmo4b* locus on chromosome 6 revealed multiple rearrangements. The *lmo4a* locus on chromosome 5 did not align to its human orthologue (Figure 4.1C). Thus, of the two *lmo4* genes present in the zebrafish, *lmo4b* is closer to its vertebrate orthologues, and *lmo4a* is more divergent.

The expression profile of a transcription factor can provide insights into its activity, and is necessary for the interpretation of phenotypes associated with manipulation of its level. We were therefore interested in the expression of *lmo4a* and *lmo4b* in the zebrafish, along with how it relates to the expression of its orthologues in higher vertebrates. *lmo4a* is present as maternally deposited RNA at

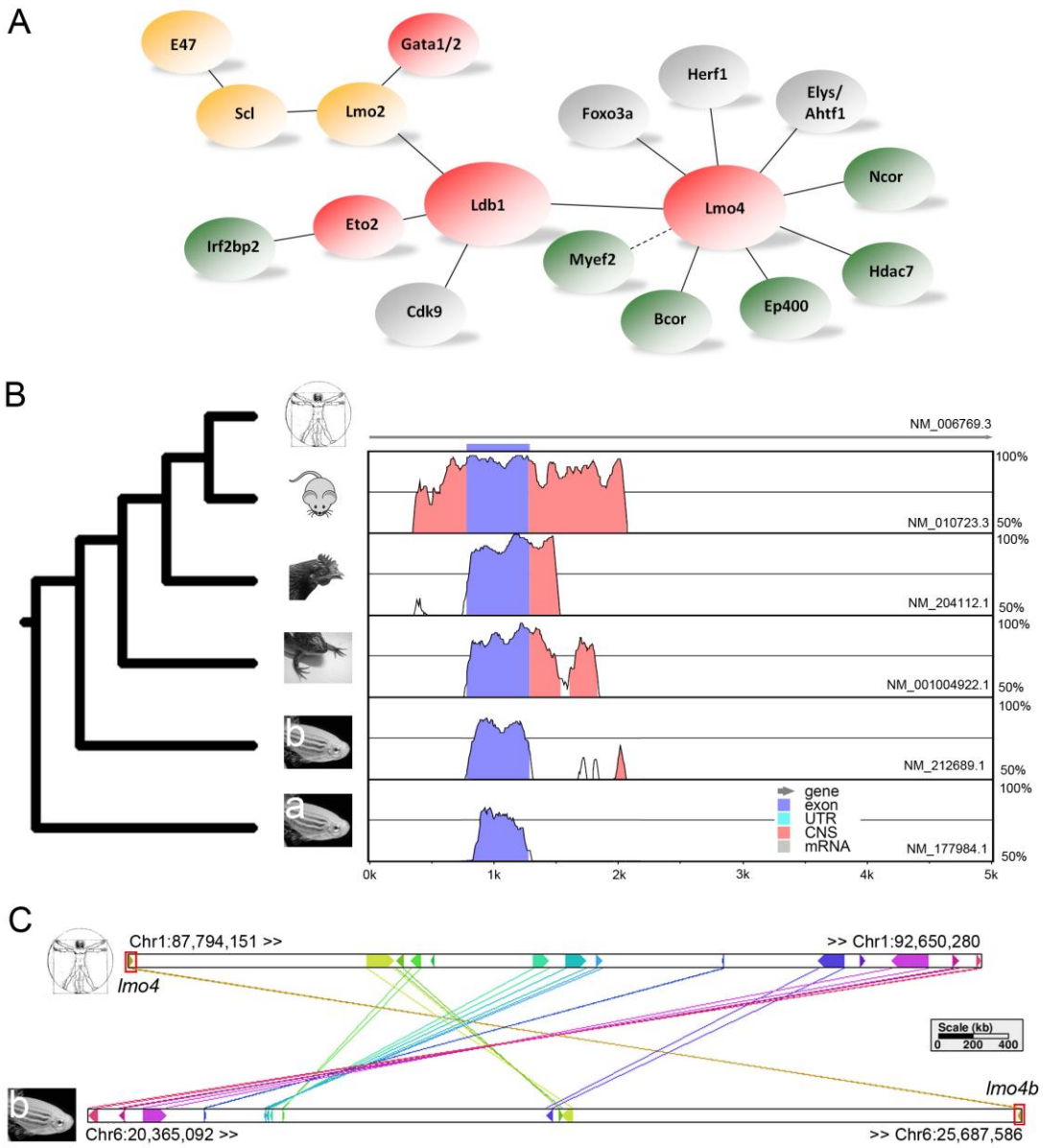

Figure 4.1 Lmo4 is found in an erythroid complex and has been conserved throughout evolution

(A) A topological network describing some of the known and novel interactions in mouse erythroleukaemic cells. In this study, *lmo4* and protein partners shown in green have been knocked down. Proteins that have been *in vivo* biotin-tagged are shown in red. The interaction between proteins shown in yellow was investigated in Chapter 3. Solid lines represent confirmed interactions; dotted lines represent possible interactions. (B) VISTA alignment and phylogenetic analysis of *lmo4* cDNA sequences between the human, mouse, chicken, *Xenopus tropicalis* and zebrafish. Identity between 50 and 100% is shown, and the human sequence used as the reference. In the zebrafish, two versions of *lmo4* are present; *lmo4b* is closer to its vertebrate orthologues and *lmo4a* is more divergent. UTR, untranslated region; CNS, conserved non-coding sequence. (C) Analysis of synteny between the human *lmo4* and zebrafish *lmo4b* locus. *lmo4a* did not align to human *lmo4*.

the 2-cell stage. Zygotic expression commences ubiquitously between 30% epiboly and the tailbud stage (Figure 4.2 A-D). By the 10ss, expression has become restricted to the head region, somites and posterior lateral plate mesoderm, and by 24 hpf, is expressed in the dorsal aorta, pronephric duct and posterior blood island (Figure 4.2 E-F'). Within the dorsal aorta, *lmo4a* is expressed in both the floor and roof (Figure 4.2 F'). *lmo4b* is weakly expressed from maternal RNA, with zygotic expression starting between tailbud and the 10ss, where it is expressed in the somites, but not the posterior lateral plate. At 24 hpf, *lmo4b* is still expressed in the somites and also in the posterior pronephric duct, becoming restricted to the lateral line by 48 hpf (Figure 4.2 G – M'). Expression of *lmo4a* in the PLM and throughout the dorsal aorta, tissues important in the development of the blood and vasculature, suggests that it could act cell autonomously to control these fates. In contrast, lack of *lmo4b* expression in these tissues excludes a cell autonomous role for *lmo4b* in programming blood and endothelium. However, the somites have previously been shown to contribute important signals to the development of blood and vasculature (Ciau-Uitz et al., 2010; Gering and Patient, 2005), and therefore *lmo4b* may influence the development of these tissues in a cell nonautonomous fashion.

In the developing mouse, *lmo4* is expressed in the mid- to hind-brain region, somites, lateral mesoderm, and the caudal AGM around E9 (Hahm et al., 2004; Kenny et al., 1998). In *Xenopus laevis*, *lmo4* is expressed in the presomitic mesoderm, posterior somites and haemangioblast progenitors from stage 14 (16.25 hpf), neural crest cells and the posterior lateral plate at stage 17 (18.75 hpf), and pronephric cilium and heart at stage 22 (24 hpf). However, it is never expressed in the VBI or DLP, precursor states of primitive and definitive blood respectively (de la Calle-Mustienes et al., 2003; Ochoa et al., 2012) (A Ciau-Uitz, *unpublished data*). Thus, expression of zebrafish *lmo4a* and *lmo4b* in the somites, pronephric duct and mid- to hind-brain regions generally overlaps with *lmo4* expression in the mouse and frog. An important exception is zebrafish *lmo4a*, which is also uniquely expressed throughout the dorsal aorta, from where the HSC emerges.

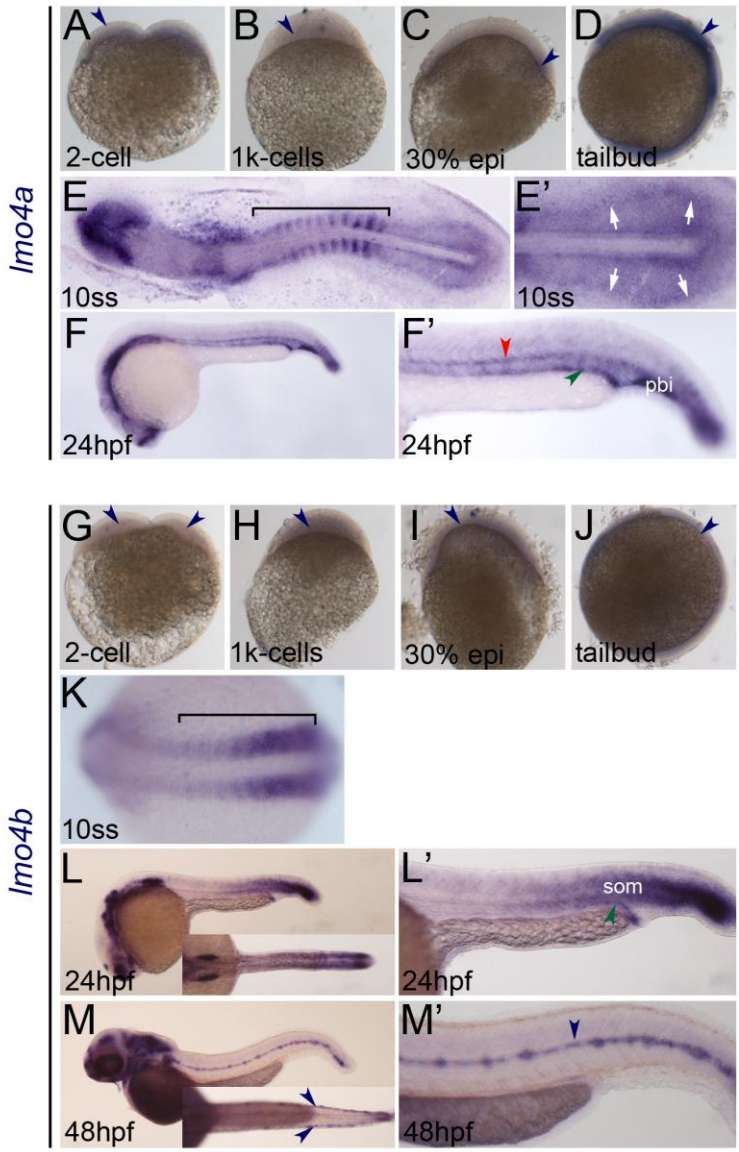

Figure 4.2 Expression of *lmo4* in the zebrafish

(A – F') Expression of *lmo4a*. (A – D) *lmo4a* is weakly maternally expressed, and expressed ubiquitously at the tailbud stage (blue arrowheads). (E –E') At the 10 somite stage (ss), *lmo4a* is expressed in the somites (black bar) and weakly in the posterior lateral plate (white arrows). Embryos flat mounted and viewed from the dorsal aspect. (F – F') At 24 hpf, *lmo4a* is expressed in the dorsal aorta (red arrowhead), pronephric duct (green arrowhead) and posterior blood island (pbi). (G – M') Expresison of *lmo4b*. (G – J) *lmo4b* is weakly expressed from maternal stores and at the tailbud stage (blue arrowheads). (K) Later, *lmo4b* is expressed in the developing somites (black bar), but not the lateral plate. Embryo viewed from the dorsal aspect. (L – M') At 24 hpf, *lmo4b* is expressed in the somites and posterior pronephric duct (green arrowhead), and at 48 hpf in the lateral line (blue arrowheads). Insert is viewed from the dorsal aspect. All embryos viewed laterally unless stated otherwise.

4.3 Knockdown of *lmo4a* causes a specific loss of the HSC

Having shown that *lmo4a* is expressed in the dorsal aorta, we were interested in whether it was required for HSC production from the floor of the aorta. Previous work has suggested that this is the case, as *runx1* is reduced in the AGM region of the zebrafish injected with a translation blocking morpholino targeting *lmo4a* (Meier et al., 2006). However, this result was not investigated further. Neither was it shown to be specific; only one morpholino was used and potential off target effects were not controlled for (Eisen and Smith, 2008). We designed two additional morpholinos, one targeting the 5'UTR region, and one targeting a splice junction. These were predicted to respectively inhibit translation or correct splicing of mRNA. Analysis of cDNA from zebrafish injected with the splice morpholino revealed a five amino acid deletion at the end of exon 2 and beginning of exon 3. This deletion was mapped onto a homology model of zebrafish Lmo4, based on the structure of human Lmo4, predicting partial loss of the most N-terminal alpha helix (Figure 4.3 A-C'). The predicted disruption of this structural element is likely to result in an unstable protein that is targeted for degradation (Kamel El-Omari, *personal communication*). As there were no specific antibodies against zebrafish Lmo4, and available antibodies against the mouse orthologue did not cross react with the zebrafish (*data not shown*), we were unable to formally demonstrate that the *lmo4a* 5'UTR morpholino successfully targeted *lmo4a*. Nevertheless, the two morpholinos gave the same phenotype with respect to the HSC.

Knockdown of *lmo4a* resulted in a reduction in expression of the master HSC regulator *runx1* in the AGM region at 30 hpf (Figure 4.3 D-F), just before HSCs emerge from the floor of the dorsal aorta (Kissa and Herbomel, 2010). However, as this does not represent a functional readout of the HSC, we investigated if HSC derived blood populations were also reduced (Figure 4.3 G-O). The CHT represents a transient vascular plexus, and is a site of HSC expansion and limited haematopoiesis, to which HSCs migrate from the dorsal aorta (Murayama et al., 2006). In *lmo4a* morphants, *cmyb* is only expressed in a few cells in this tissue, in contrast to wild type embryos where it is expressed through the CHT (Figure 4.3 G-I). The CHT forms normally in *lmo4a* splice morphants, but not in *lmo4a* 5'UTR morphants (Figure 4.23 L-N), therefore at least in *lmo4a* splice morphants, loss of *cmyb* is

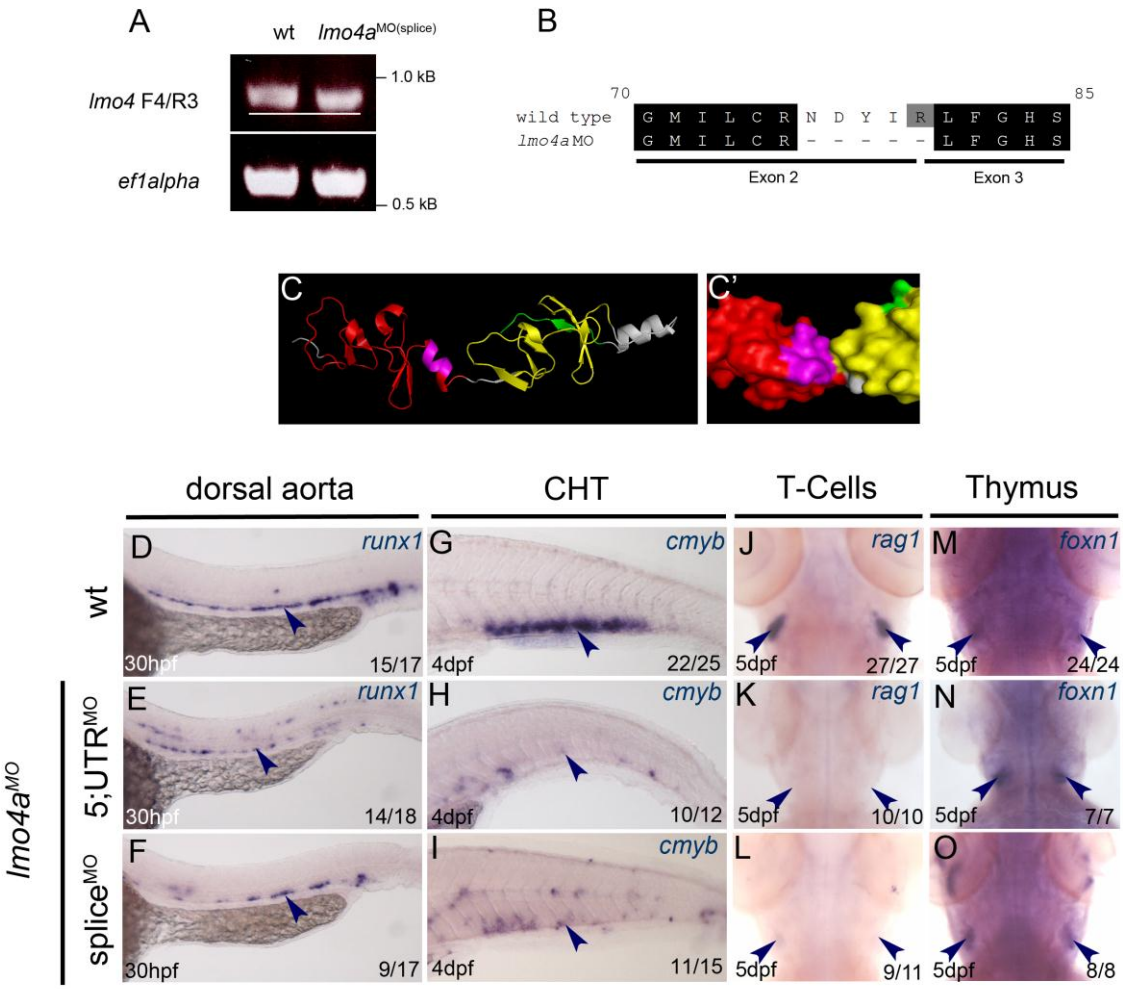

Figure 4.3 Lmo4a is required for production of the haematopoietic stem cell

Zebrafish *lmo4a* was knocked down with a morpholino targeting the 5'UTR of the gene and a splice morpholino targeting the exon 2-intron 2 boundary. (A) PCR on cDNA from wild type and *lmo4a* splice morphants. The band corresponding to the morphants has an increased mobility. (B) Cloning of the PCR products revealed a five amino acid deletion (T Cornforth, *unpublished data*). Exons as indicated; grey residue is coded for by two exons. (C – C') Mapping the five lost amino acids onto a ribbon and surface representation of a homology model of zebrafish Lmo4. Red, LIM1; magenta, lost residues; yellow, LIM2. (D – F) Expression of the HSC marker *runx1* in the dorsal aorta is reduced in *lmo4a* morphants. (G – I) Expression of *cmyb* in the caudal haematopoietic tissue (CHT) marks HSCs and their derivatives, and is reduced in *lmo4a* morphants. (J – O) Expression of *rag1* positive T-cells in the thymus is lost in *lmo4* morphants; thymic epithelium marked by *foxn1* is unaffected. (D – I) Embryo trunks and tails viewed laterally; (J – O) embryo heads viewed dorsally.

reflective of fewer HSCs. Additionally, expression of *rag1* in HSC derived T-cells developing in the bilateral thymus, are absent in both *lmo4a* morphants. It has been reported that *lmo4* null mice have hypoplastic thymuses (Michell et al., 2010), however development of the thymic epithelium in the zebrafish, marked with *foxn1*, still takes place. *lmo4a* 5'UTR morphants also have craniofacial defects as their heads are smaller, however this may represent a non-specific effect of the morpholino as it is not reproducible with the splice morpholino (Figure 4.3 J-O).

As the HSC is derived from cells of the PLM, and later the dorsal aorta (Gering and Patient, 2005; Patterson et al., 2007), and *lmo4a* is expressed in both of these tissues (Figure 4.2 A-F'), we looked at markers of these populations to rule out the possibility that the failure in HSC programming was a direct result of an earlier developmental defect. Markers of cells in the PLM that give rise to the trunk vasculature, primitive blood, and eventually the HSC, were unaffected in *lmo4a* morphants, however they were expanded into the posterior most region (Figure 4.4 A-E' and discussed in Section 4.8). Expression of *nkx2.5*, marking the cardiac mesoderm in the anterior lateral plate, was unaffected (Figure 4.4. F-F'). Cells in the PLM migrate and meet at the midline to form the axial vessels. Expression of the endothelial marker *flk1* was unchanged in the axial vessels of *lmo4a* morphants, but intersomitic vessels were absent (Figure 4.4. H-H' and Section 4.10). Nascent endothelial cells quickly adopt an arterial or venous identity (Gore et al., 2012). Arterial markers are not reduced in *lmo4a* morphants (Figure 4.4 I-L'). This includes expression of *ldb2a* and *tgfb1a* which are also required for HSC development (Rui Monteiro and Wenchao Gu, *unpublished data*). However, the expression of venous markers are reduced, most notably in *lmo4a* splice morphants (Figure 4.4. M-N'), although as *lmo4a* expression is not detected in the vein, this may represent an effect on cells in the PLM fated to contribute to the vein. As *lmo4a* is also expressed in the pronephric duct, we were interested in whether this tissue also required *lmo4a*. However, expression of the pronephric duct marker *pax2.1* was unaffected in *lmo4a* morphants (Figure 4.4. O-O'). Paracrine signalling from the somites to the dorsal aorta plays an important role in specifying the HSC (Ciau-Uitz et al., 2010; Gering and Patient, 2005). Therefore, we looked at genes expressed in the somites, including *vegfa, eto2* and *smad5* (Figure 4.4. P-R'). The expression of *vegfa* was not affected, while *eto2* and *smad5* may be increased. Consistent with

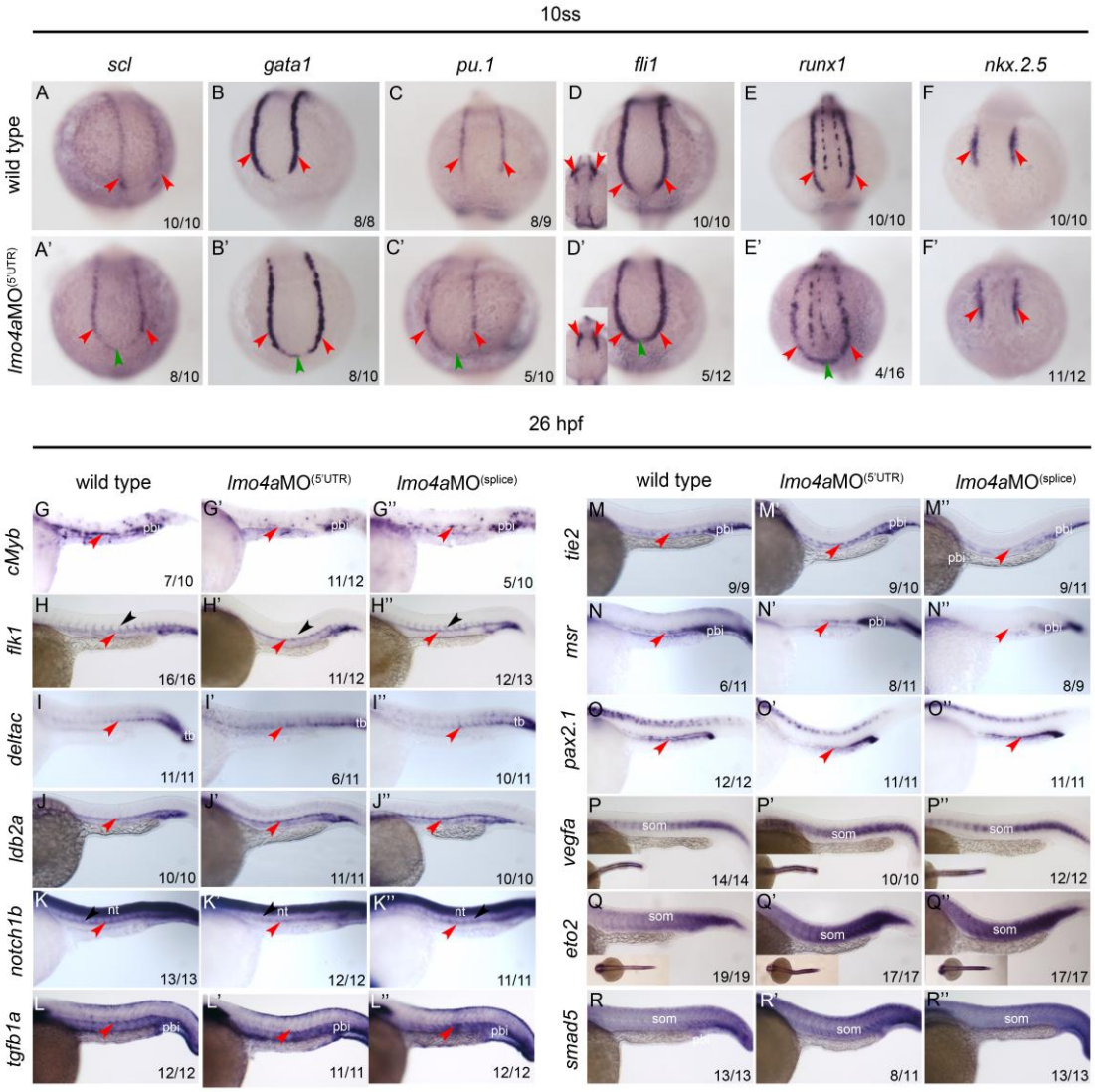

Figure 4.4 Precursor states of the haematopoietic stem cell are unaffected in *lmo4a* morphants

(A – E') Markers of cells in the posterior lateral plate are largely unaffected (red arrowheads), however are expanded to the posterior most region (green arrowheads). Insert in (D – D') shows anterior *fli1* expression. (F – F') Expression of *nkx2.5*, marking the cardiac mesoderm, is unaffected in *lmo4a* morphants. (G – G") The expression of the HSC marker *cmyb* is reduced in *lmo4a* morphants, however expression of markers of the endothelium (H – H") and arterial fates (I – L") in the axial vessels are unaffected. (M – N") Markers of the venous fate are reduced in *lmo4a* morphants, but the pronephric duct (O – O") and molecules in the somites are unaffected (P – R"). (A – F') Embryos viewed dorsally. (G – R") embryos viewed laterally with inserts showing the dorsal view; nt, neural tube; pbi, posterior blood island; som, somites. Red arrowhead, dorsal aorta; black arrowheads, intersegmental vessels.

this observation, Lmo4 has been shown to bind the promoter of *smad5* in MEL cells (C Andrieu-Soler, *unpublished*).

4.4 *lmo4b* is required to specify multiple tissues

Having confirmed that *lmo4a* is required for production of the HSC, we were interested if there was also a requirement for *lmo4b*, for example by paracrine signalling to the dorsal aorta from the somites. Through knockdown and overexpression experiments in the zebrafish, *lmo4b* has previously been shown to restrict the size of the forebrain and eyes through negative regulation of homeodomain proteins known to be important in this process (McCollum et al., 2007), although the molecular analysis of the *lmo4b* morphant phenotype did not extend beyond the 10ss, or to the analysis of blood and vasculature. We designed novel morpholinos targeting the initiating codon and targeting a splice junction. Analysis of cDNA from embryos injected with the splice morpholino revealed the dose-dependent emergence of an mRNA lacking the sequence corresponding to exon 2 and additionally resulting in a frame shift (Figure 4.5 A-B). Even at the highest dose of morpholino used, the wild type *lmo4b* predominated, therefore this morpholino would be predicted to generate a hypomorph.

Analysis of markers of cells in the ALM and PLM at the 10ss revealed no major defects in *lmo4b* morphants (Figure 4.5 C-Q), although expression of *pax2.1* and *gata1* in the PLM was slightly reduced in *lmo4b* ATG morphants (Figure 4.5 L-Q). Strikingly, all the markers tested at 26 hpf showed reduced expression in both *lmo4b* morphants, most notably in the trunk and tail regions (Figure 4.6). This included mesodermal derivatives, such as blood, somites, pronephric duct and vasculature, along with neural populations derived from the ectoderm. Remarkably, the embryos looked morphologically normal and developed a perfused circulatory system. However, increasing the concentration of morpholino used resulted in non-viable embryos (*data not shown*). It is therefore possible that the remaining weak expression in the trunk represents the minimum expression compatible with life.

Consistent with the loss of *notch3* in the neural tube of *lmo4b* morphants (Figure 4.6 N-N'), the mouse *lmo4* knockouts die due to failure in neural tube closure (Hahm et al., 2004; Tse et al., 2004).

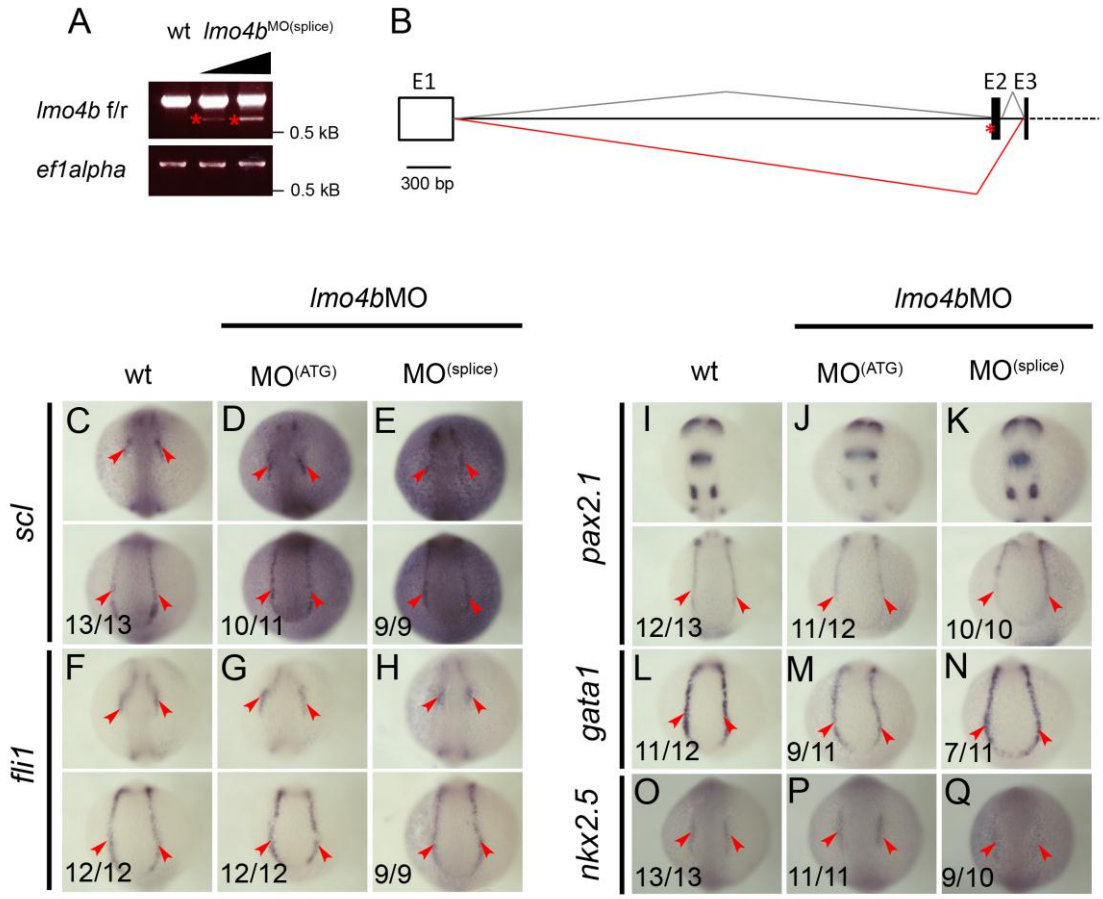

Figure 4.5 Knockdown of *lmo4b* does not affect lateral plate mesoderm

An ATG and splice morpholino were designed to target *lmo4b*. (A) PCR on cDNA from *lmo4b* splice morphants resulted in a band with increased electrophoretic mobility (red stars). (B) Cloning of the PCR fragments revealed that exon 2 was skipped in *lmo4b* splice morphants. Red star indicates binding site of the morpholino. (C – K) Markers of cells in the lateral plate are unaffected in *lmo4b* morphants. Top panels, anterior; bottom panels, posterior. (L – N) Expression of *gata1* in the posterior lateral plate is reduced in *lmo4b* ATG morphants. (O – N) The marker of cardiac mesoderm, *nkx2.5*, is reduced in *lmo4b* splice morphants. All embryos imaged dorsally.

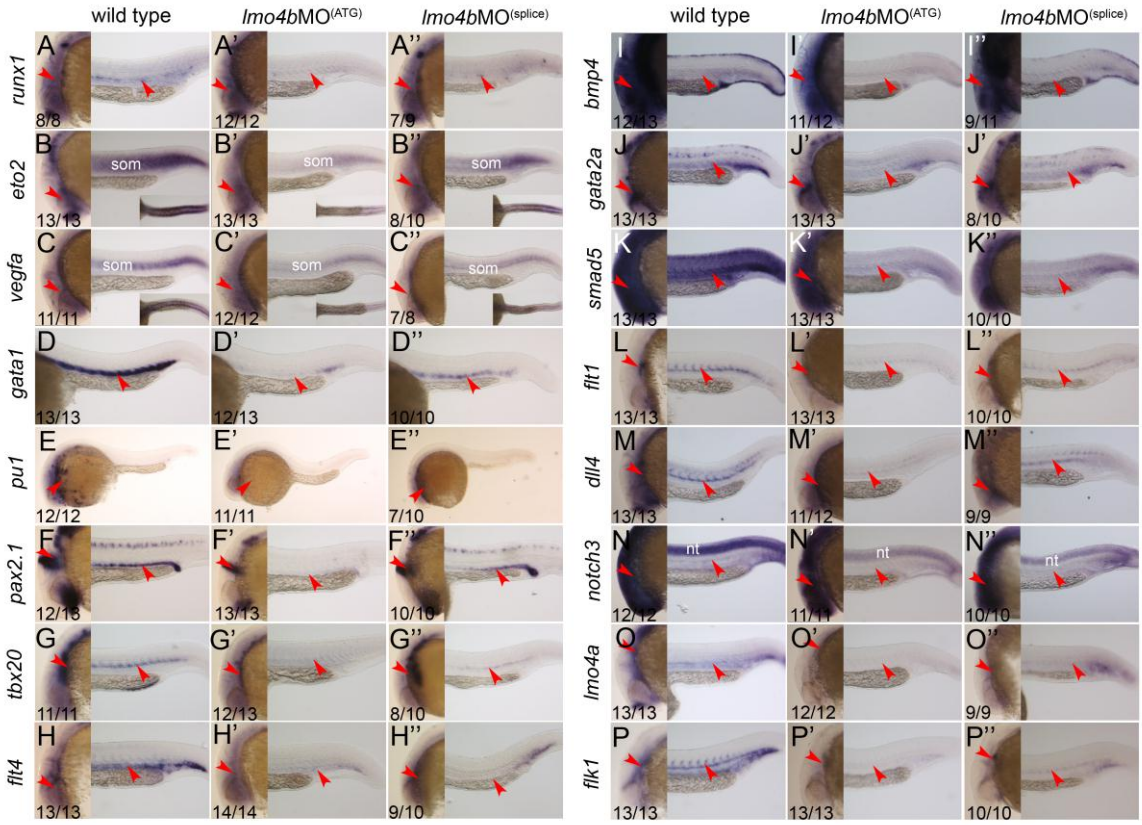

Figure 4.6 Ectodermal and mesodermal derivatives are lost at 26 hpf in *lmo4b* morphants

Markers of the HSC (A – A"), the somites (B – C", K – K"), primitive erythrocytes (D – D"), primitive myeloid cells (E – E"), pronephric duct (F – F"), arterial cells (G – G", J – J", L – O"), venous cells (H – H"), subaortic mesenchyme (I – I") and vascular endothelium (P – P") are reduced in the head, trunk and tail of *lmo4b* morphants. Main panels viewed laterally; inserts viewed dorsally; som, somites; nt, neural tube.

Although this correlation was not investigated further, it should be noted that unlike in higher vertebrates where primary neural folds bend to form a tube, in the zebrafish, primary neural precursors condense to form a solid rod that lumenises. (Lowery and Sive, 2004). This process is loosely analogous to the formation of the ICM that gives rise to primitive erythrocytes and the trunk and tail vasculature.

In summary, although we have not looked at any tissues derived from endoderm, such as gut, we conclude that *lmo4b* is required for the specification and/or maintenance of multiple tissues between the 10ss and 26 hpf in the zebrafish. However, in the absence of a conditional knockdown, we cannot formally exclude the possibility that as with *lmo4a*, there is a specific requirement for *lmo4b* in HSC development. We therefore chose to focus predominantly on the role of *lmo4a*, whose earliest blood related phenotype is the specific absence of HSCs, and whose phenotype would therefore likely be easier to interpret.

4.5 Lmo4 partners are required to programme the HSC

4.5.1 Expression of Lmo4 partners in the zebrafish

It has previously been shown that in both differentiated and undifferentiated MEL cells, Lmo4 can bind to Bcor, Ep400 and Hdac7. Ncor also bound Lmo4 in differentiated cells and Myef2 may also bind Lmo4 (Figure 4.1A and C Andrieu-Soler, *unpublished*). We were therefore interested in whether individually knocking down their expression would result in a similar phenotype as in *lmo4a* or *lmo4b* morphants. As a first step, we looked at the expression of mRNA transcribed from the various genes (Figure 4.7). *bcor* was expressed in the PLM at the 10 ss and ubiquitously throughout the trunk and tail at 24 hpf, with stronger expression forming a dorsal and ventral stripe in the trunk (Figure 4.7 A-B). The dorsal stripe corresponds with expression in the neural tube, and is also seen in the mouse (Wamstad and Bardwell, 2007). Transcripts for *ncor* were deposited from the mother, and expression was ubiquitous up to the 10 ss. At 24 hpf, *myef2* is expressed throughout the trunk and tail, most notably in the posterior region and throughout the neural tube, however by 30 hpf, expression in the

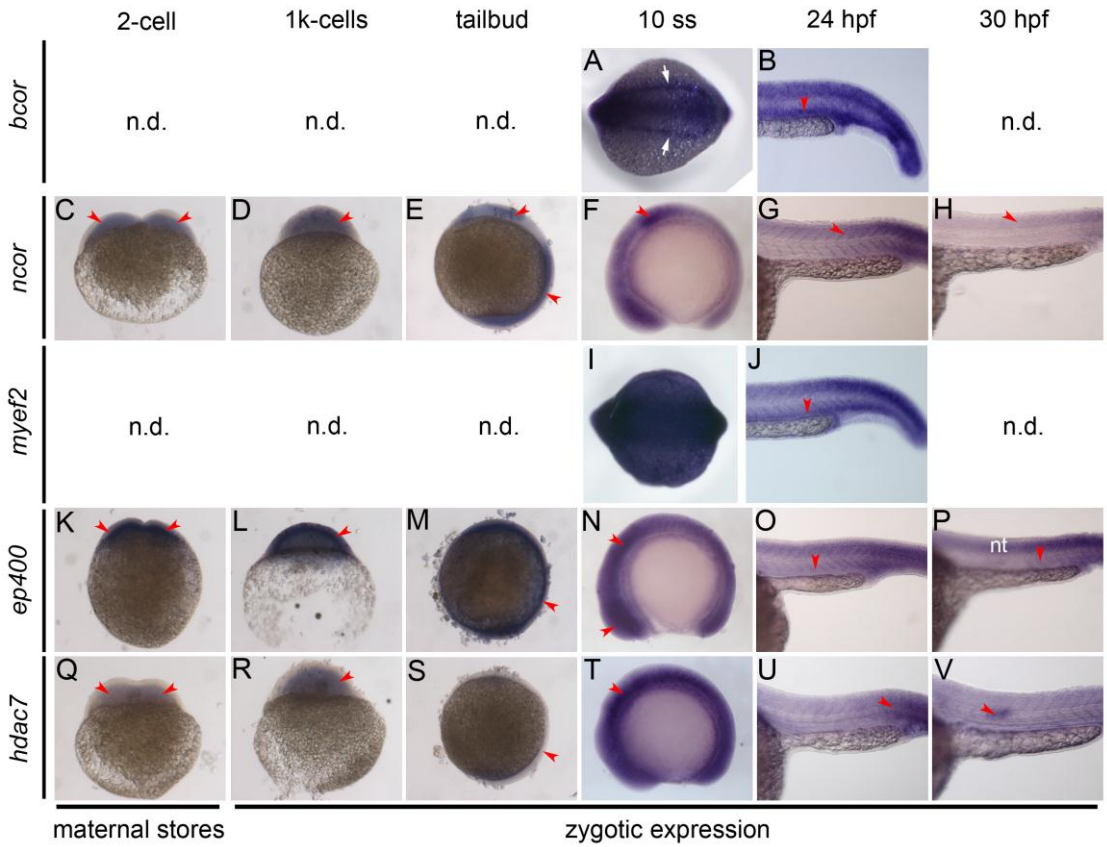

Figure 4.7 Expression of Lmo4 protein partners

(A – B) *bcor* is expressed in the posterior lateral plate and around the dorsal aorta (R Monteiro, *unpublished data*). (C – H) *ncor* is expressed maternally and then ubiquitously in the trunk and tail. (I – J) *myef2* is expressed ubiquitously (R Monteiro, *unpublished data*). (K – P) *ep400* is expressed maternally and then ubiquitously in the trunk and tail, becoming more restricted to the neural tube (nt). (Q – V) *hdac7* is expressed maternally and then weakly throughout the trunk and tail of the embryo. All embryos viewed laterally; n.d., not done.

trunk is reduced and becomes restricted mostly to the neural tube (Figure 4.7 C-H). The neural expression of *ncor* is consistent with the failure of neural differentiation seen in the mouse knockout (Jepsen et al., 2000). *myef2* is expressed throughout the embryo at the 10 ss and 24 hpf, with stronger expression forming a dorsal and ventral stripe, similar to the expression of *bcor* (Figure 4.7 I-J). Expression of *ep400* is similar to that of *ncor*. It is expressed maternally and ubiquitously up to the 10 ss. At 24 hpf, *ep400* is expressed throughout the posterior trunk and in the neural tube. By 30 hpf, it is expressed weakly throughout the trunk with stronger expression remaining in the neural tube (Figure 4.7 K-P). *hdac7* is deposited maternally. Strong, ubiquitous expression, is observed at the 10 ss. At 24 hpf, it is expressed weakly throughout the trunk and strongly in the tail. By 30 hpf, *hdac7* is expressed weakly throughout the trunk, with stronger expression in an unknown tissue within the trunk (Figure 4.7 Q-V). Thus, although none of the genes corresponding to MEL cell partners of Lmo4 are specifically expressed in the dorsal aorta, they were expressed in and around the tissue during specification of the HSC. We therefore proceeded to systematically knockdown expression of each gene.

4.5.2 Knockdown of *bcor* results in a loss of HSCs

The Bcl-6 corepressor (Bcor) was originally identified through its interaction with the POZ domain of the transcriptional repressor Bcl-6 (Ghetu et al., 2008; Huynh et al., 2000). Somatic mutations and translocations of the gene have been implicated in various human diseases, including mixed lineage leukaemias (Srinivasan et al., 2003), myeloid leukaemias (Grossmann et al., 2011; Yamamoto et al., 2010), bone sarcomas (Pierron et al., 2012), medulloblastomas (Pugh et al., 2012), and oculofaciocardiodental syndrome (Ng et al., 2004), a condition resulting in ocular, skeletal and cardiac defects. Bcor has been shown to regulate gene expression, in part through epigenetic mechanisms, for example in mesenchymal stem cells (Fan et al., 2009). Furthermore it has been shown to form complexes with Polycomb group proteins, Skp-Cullin-F-box sub-components, ubiquitin ligase components, and histone demethylases, including those containing Jumonji C domains (Gearhart et al., 2006; Sanchez et al., 2007; Wamstad et al., 2008).

Although *bcor* has been knocked down in *Xenopus tropicalis* (Hilton et al., 2007) and zebrafish (Ng et al., 2004), the development of blood and endothelium was not studied. Loss of function studies in mouse ES cells, and *in vitro* differentiation demonstrated an early requirement in the formation of ectodermal, mesodermal and haematopoietic lineages. Additionally, in chimeric animals, *bcor* null cells showed reduced contribution to B-, T-, and erythroid lineages (Wamstad et al., 2008). We knocked down expression of *bcor* in zebrafish using a published morpholino (Ng et al., 2004). Analysis of cDNA from injected embryos revealed the presence of two additional bands, although the band corresponding to wildtype *bcor* was still present (Figure 4.8A). The larger band likely represents inclusion of an intron, and the small band skipping of an exon, although we did not confirm this. As has been observed previously, *bcor* morphants showed defects in the formation of the lens of the eye (Figure 4.8B) (Ng et al., 2004). Expression of *runx1*, *cmyb* and *ikaros*, which mark the HSC population, were reduced at 30 and 48 hpf in the AGM region (Figure 4.8 D-O), suggesting fewer HSCs were produced. However markers of HSC derivatives in the thymus and CHT were not reduced at 4 dpf (Figure 4.8 P-U), indicating that HSCs that are produced may expand to fully occupy the various niches as activity of the morpholino wears off with time. Alternatively, *bcor* may be necessary for the specification, but not maintenance and expansion, of the HSC pool.

Expression in tissues that precede development of the HSC are unaffected, including specification of endothelial and arterial populations, although expression of *msr* in the cardinal vein, but not PBI, was reduced (Figure 4.9 A-J). The PLM is also unaffected in *bcor* morphants (Anjali Verma and Phil Ingham, *unpublished*). Numbers of primitive erythrocytes at 33 hpf, as marked by *gata1* and *alas2*, are reduced in *bcor* morphants (Figure 4.9 K-N), but then recover by 3 dpf (Figure 4.8C). This may reflect loss of activity of the morpholino together with compensation from HSC-derived erythrocytes (Jin et al., 2009). Expression of *pu1*, marking the primitive myeloid population, is increased (Figure 4.9 O-P). As Gata1 and Pu1 are known to cross antagonise to affect the erythroid vs myeloid output, this may reflect a role of Bcor in modulating this balance, as has been demonstrated for Tif-1γ, however this was not investigated further (Monteiro et al., 2011). Taken together, we have identified a novel role for *bcor* in the expression of genes involved in programming the HSC, however it has not been formally demonstrated that HSC numbers are reduced. In agreement with the mouse

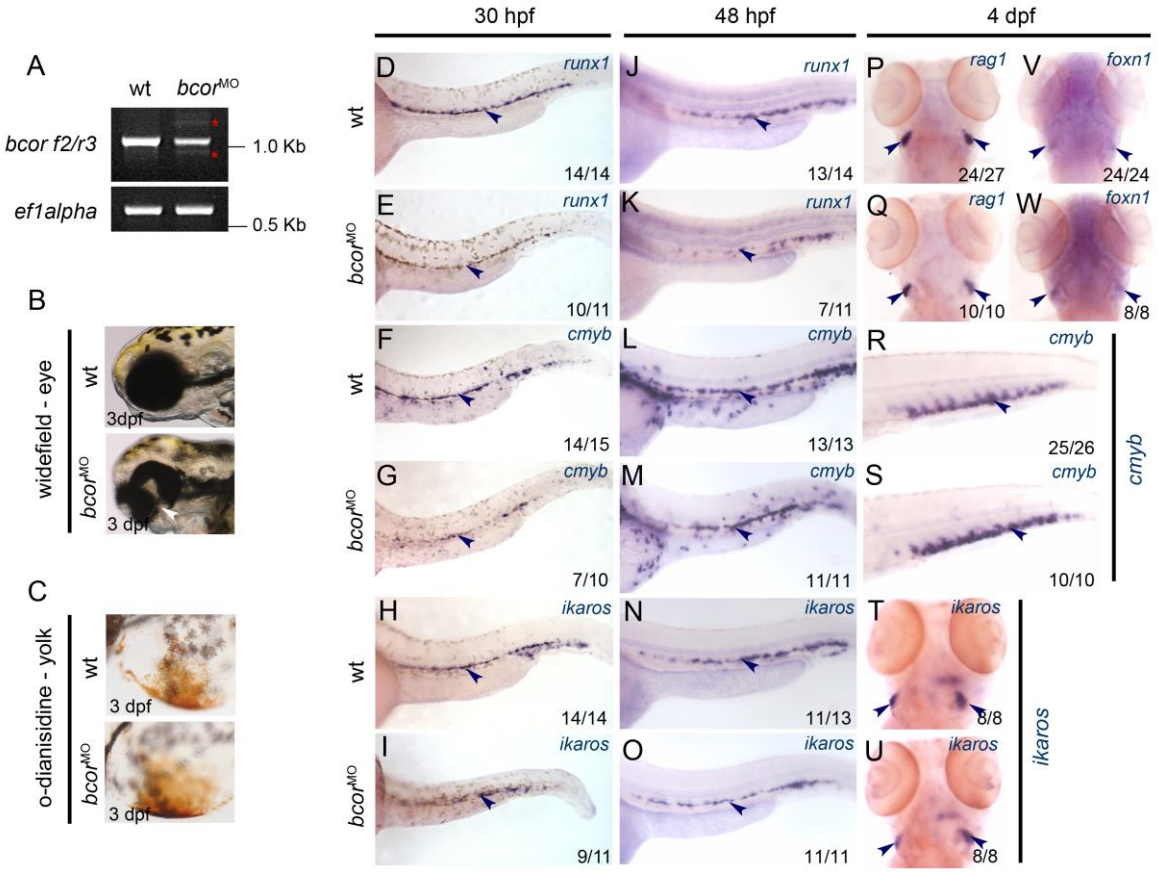

Figure 4.8 Knockdown of *bcor* results in reduced numbers of haematopoietic stem cells

(A) Analysis of cDNA from *bcor* morphants showed the presence of two additional bands. (B) The published ocular defect seen in *bcor* morphants could be reproduced (Ng et al., 2004). (C) Maintenance of primitive erythrocytes was unaffected in *bcor* morphants. (D – O) Expression of the HSC markers *runx1*, *cmyb*, and *ikaros*, around the dorsal aorta, were reduced in *bcor* morphants. (P – Q, T - U) T-cells derived from HSCs, development of thymic epithelium (V – W), and development of HSCs and their derivatives in the caudal haematopoietic tissue (R – S) were not reduced in *bcor* morphants.

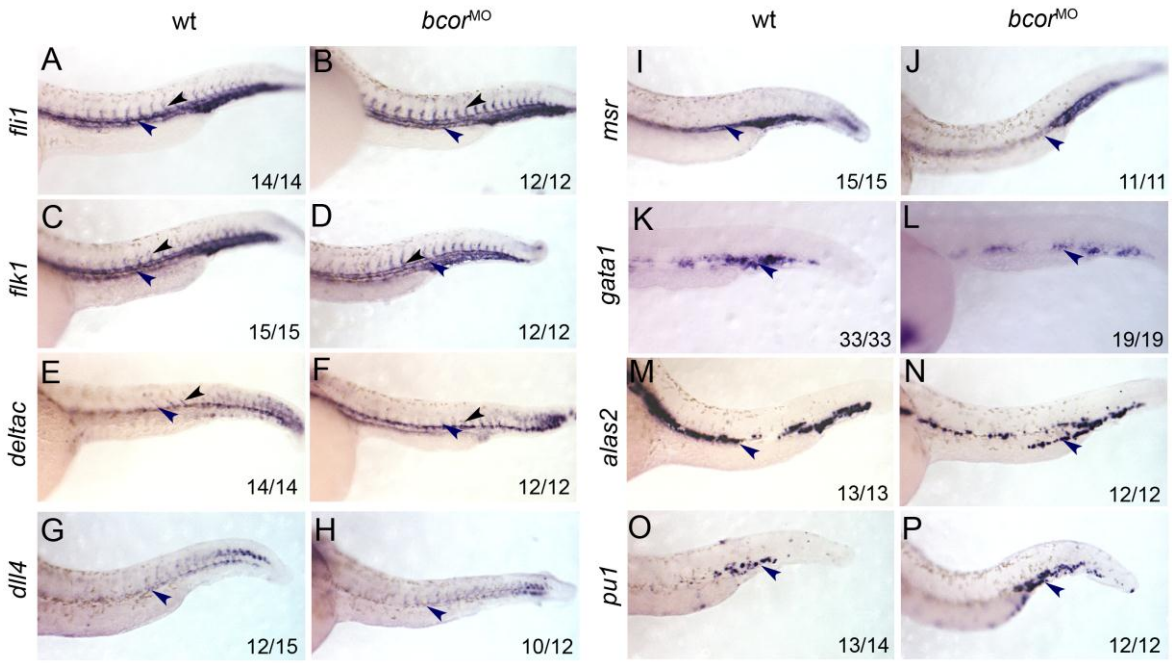

Figure 4.9 Precursor states of the haematopoietic stem cell are unaffected in *bcor* morphants

Expression of markers of the endothelium (A - D) and arterial fates (E – H) are not reduced in *bcor* morphants, blue arrowheads. Black arrowheads, intersegmental vessels. (I – J) *bcor* morphants have reduced *msr* expression in the vein. (K – P) Primitive blood, in circulation, is reduced in *bcor* morphants. Embryos imaged laterally at 33 hpf.

knockout, primitive erythroid blood is reduced. However, in contrast to the mouse, T-cells appear normal at 4 dpf. This may reflect a varying requirement between the two species, or loss of activity of the morpholino compared with the sustained genetic knockout achieved in the mouse.

4.5.3 Knockdown of *ncor* results in a loss of HSCs

Like Bcor, the nuclear corepressor protein (Ncor) has also been shown to interact with the POZ domain of the Bcl-6 corepressor, and its interaction is mutually exclusive with that of Bcor and Bcl-6 (Huynh et al., 2000). It has been shown that Ncor is required for many processes, including development, and is directly or indirectly involved in the progression of a number of neoplasms (Oberoi et al., 2011). In acute promyelocytic leukemia, it has been reported that retinoic acid receptor-α fusion products are impaired in their release of corepressors, including Ncor, upon activation, and this may contribute to their dominant-negative and oncogenic activity (Mengeling et al., 2011). In acute myeloid leukaemia, the Runx1-Eto fusion has been associated with disease progression; but additional mutagenic events are required for leukaemic progression, such as the loss of its interaction with Ncor (Yan et al., 2004). In oestrogen-dependent breast cancer, it has been shown that an artificial fusion between the oestrogen receptor and Ncor inhibits growth, suggesting that Ncor may provide a novel therapeutic target (Chien et al., 1999). Additionally, displacement of an Ncor-containing repressive complex from the *γ-globin* promoter is required for its expression. It has been suggested that disrupting this interaction may allow therapeutic induction of *γ-globin* expression as a therapy for β-haemoglobinopathies (Mankidy et al., 2006).

Homozygous knockdown of *ncor* in mice results in lethality around E15.5 due to defects in neural cell and definitive erythrocyte differentiation (Jepsen et al., 2000). Using K-562 cells, it has been shown that the erythroid defect may be in part due to failure in haemoglobin biosynthesis (Zhang et al., 2007). We designed two splice morpholinos to knockdown *ncor* in the zebrafish. Embryos injected with increasing amounts of morpholino 1 had reduced levels of *ncor* transcript, which upon sequencing, contained a deletion of exon 10 leading to a frame shift mutation and a premature stop codon (Figure 4.10 A-B). Analysis of cDNA from embryos injected with an increasing dose of morpholino 2

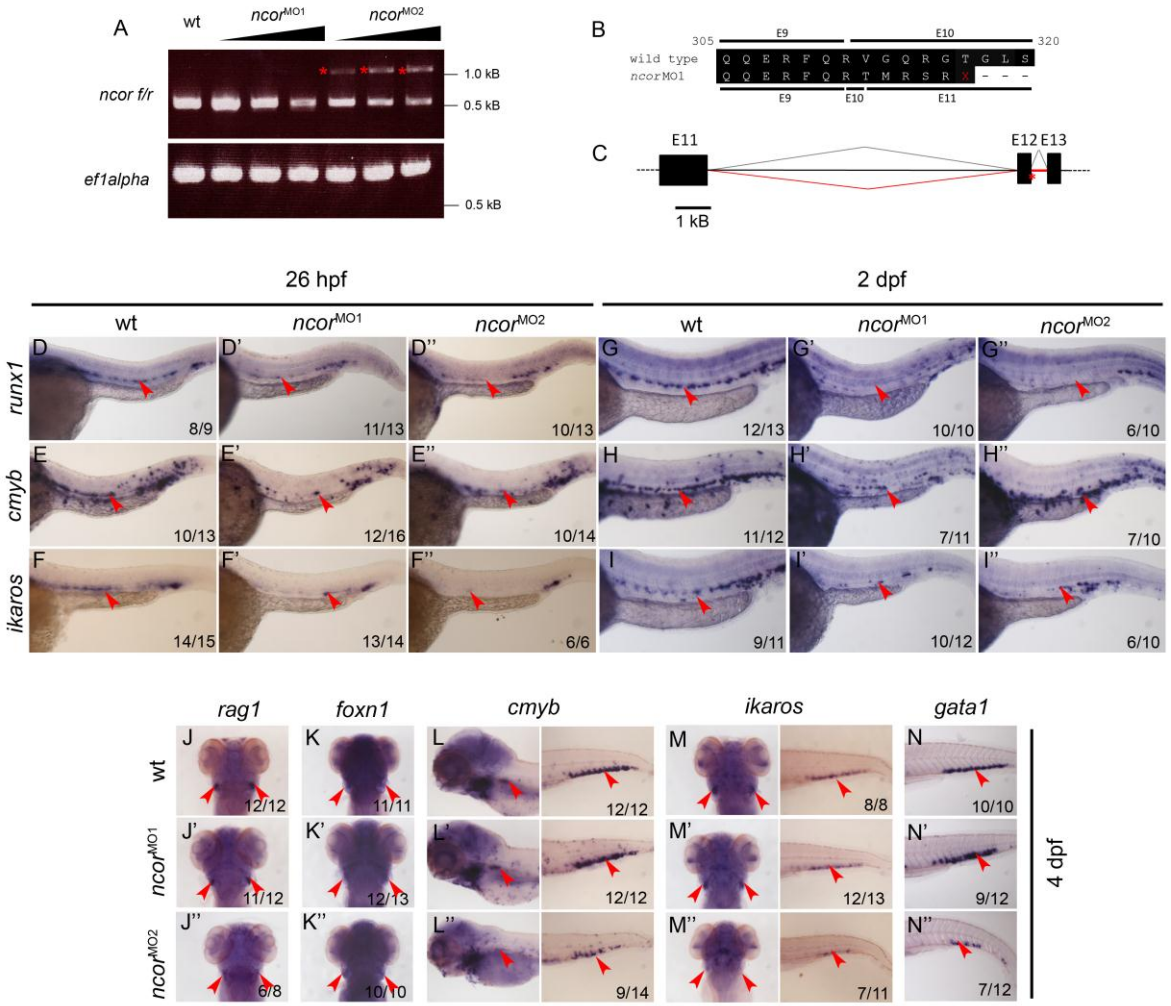

Figure 4.10 Knockdown of *ncor* results in a loss of the haematopoietic stem cell

Two splice morpholinos targeting *ncor* were injected and cDNA isolated. (A) Analysis of cDNA with gene specific primers as indicated. PCR fragments were cloned. Additional bands are indicated by a red asterisk. (B) Morpholino 1 causes a frame shift mutation resulting in a premature stop codon (X). (C) Morpholino 2 causes inclusion of intron 12. (D – I") *ncor* morphants lack markers of the HSC (red arrowheads). (J – N") *ncor*^{MO2}, but not *ncor*^{MO1}, lack HSC derived *rag1* and *ikaros* positive T-cells in the thymus (J – J", M – M"), *cmyb, ikaros* and *gata1* positive HSCs and their derivatives in the caudal haematopoietic tissue (L – N"), and *cmyb* positive HSCs and derivatives in the embryonic kidney (L – L"). Development of the thymic epithelium is unaffected (K – K"). Thymus imaged from the dorsal aspect; all other tissue imaged laterally.

indicated retention of intron 12 in a dose-dependent manner, causing a shift in the open reading frame (Figure 4.10 A and C). In contrast to the mouse knockout, we saw a defect in development of the HSC. We observed a loss of HSC markers in the AGM region at 26 hpf and 2 dpf with both morpholinos (Figure 4.10 D-I"). However, at 4 dpf, only morpholino 2 resulted in a loss of HSCs and their derivatives in the thymus, CHT and embryonic kidney (Figure 4.10 J-N"). This likely reflects degradation of *ncor* morpholino 1, or later redundancy. Markers for tissues from which the HSC has its developmental origin are not reduced, including endothelial and arterial markers (Figure 4.11 A-E"). Specification of primitive blood and the pronephric duct were also unaffected (Figure 4.11 H-J"). However, expression of *msr*, but not *mrc1*, in the cardinal vein was reduced (Figure 4.11 F-G").

In agreement with the mouse knockout, in which definitive, but not primitive, erythropoiesis is defective (Jepsen et al., 2000), we observe no defects in primitive erythropoiesis. However, in contrast, we see failure in HSC programming. This may reflect a differential requirement for Ncor in the mouse and zebrafish. Alternatively, as HSC emergence from the mouse AGM at around E10.5 was not investigated, it is possible that failure of definitive erythropoiesis at E15.5 was in part secondary to a reduction of HSC numbers. Due to the failure of HSC development in the zebrafish, and lack of a conditional *ncor* knockdown strategy, we did not look at definitive erythropoiesis in *ncor* morphants. Very recently, it has been shown that stabilisation of Ncor can promote the invasion of oesophageal cancer, a process that requires an epithelial to mesenchymal transition (EMT) (Yoo et al., 2012). As EMT and EHT are similar processes and may require a similar genetic events (Karima Kissa, *personal communication*), this raises the possibility that in addition to controlling *runx1* in the dorsal aorta, *ncor* directly regulates the EHT, although we have not yet demonstrated this.

4.5.4 Knockdown of *myef2* results in a loss of HSCs

The myelin gene expression factor-2 (*myef2*) was first identified as a protein that bound single-stranded DNA in mouse brain extracts, and repressed transcription of the myelin basic protein gene (Haas et al., 1995). Recently, it has been shown that Myef2 is bound to Runx1 in undifferentiated MEL cells, and that binding is lost upon induction, suggesting Runx1 and Myef2 may form a complex

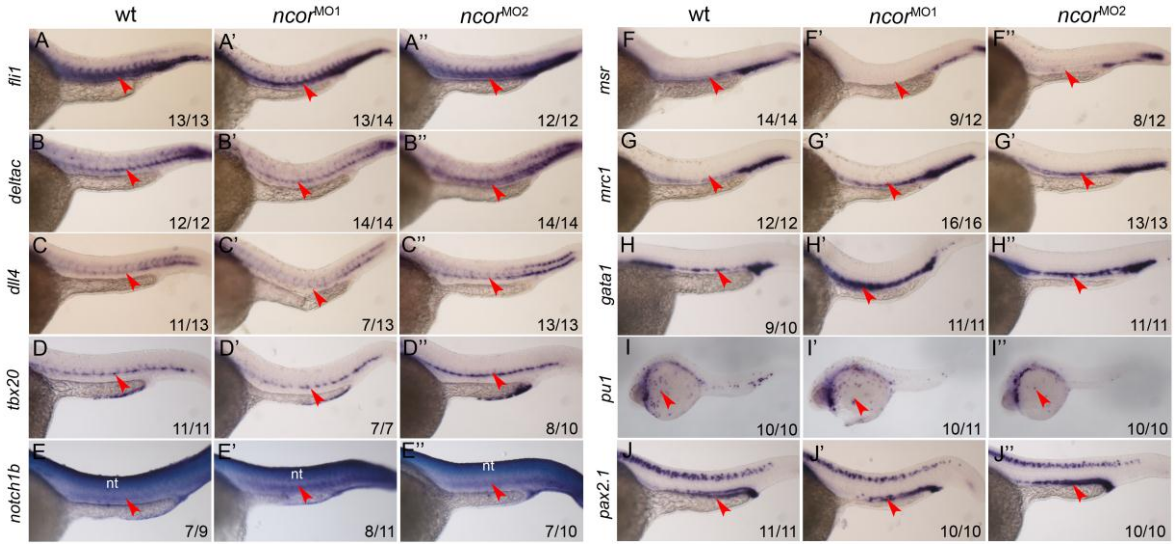

Figure 4.11 Precursor states of the haematopoietic stem cell are unaffected in *ncor* morphants

Expression of markers of the endothelium (A – A") and arterial fates (B – E") are not reduced in *ncor* morphants; nt, neural tube. (F – G") *ncor* morphants have reduced *msr*, but not *mrc1* expression in the vein. (H – I") Primitive blood programming is unaffected in *bcor* morphants. (J – J") The pronephric duct is unaffected in *ncor* morphants. Embryos imaged laterally at 26 hpf.

that prevents terminal commitment of definitive erythroid progenitors (van Riel et al., 2012). It may also bind Lmo4, although this has not been confirmed (Charlotte Andrieu-Soler, *personal communication*), and could therefore act as a bridging protein between the putative Lmo4 complex and Runx1. As *myef2* has not previously been depleted in any system, we designed two splice morpholinos to knockdown *myef2*. PCR analysis of cDNA isolated from *myef2*^{MO1} demonstrated inclusion of intron 2 and results in a frame shift. By contrast, *myef2*^{MO2} induced skipping of exon 3 (Figure 4.12 A-B). Markers of the HSC and their derivatives in the AGM, CHT and thymus were reduced in *myef2*^{MO2} embryos, but not *myef2*^{MO1} embryos (Figure 4.12 H-S). Expression of markers of tissues that precede development of the HSC are unaffected, including specification of endothelial and arterial populations. However, expression of *msr* was reduced in the cardinal vein, but not PBI (Figure 4.13 A-E"). The PLM is also unaffected in *myef2* morphants (Anjali Verma and Phil Ingham, *unpublished*). Expression of *eto2* in the somites, *pu1* in the primitive myeloid population and *pax2.1* in the pronephric duct was not affected in morphants, although expression of *gata1* in the ICM was reduced at 22 hpf (Figure 4.13 F-I"). In *myef2*^{MO2}, erythrocytes were reduced at 2 dpf, before the contribution of HSC derived red blood, and at 3.5 dpf, just before the first HSC derived definitive erythrocytes begin to entire circulation (Jin et al., 2009) (Figure 4.12 C-G). Thus, in addition to preventing the terminal differentiation of definitive erythrocytes, *myef2* is also required for primitive erythropoiesis in the zebrafish. We did not however investigate a role for *myef2* in definitive erythropoiesis, as without a conditional strategy, any interpretation would be confounded by the loss of HSCs.

While *myef2*^{MO2} animals showed a decrease in HSC markers and in primitive blood, *myef2*^{MO1} animals did not. This is likely because the wild type transcript predominated and very little mis-spliced product was present in *myef2*^{MO1} embryos. Therefore the level of knockdown was likely not sufficient to affect HSC programming (Figure 4.12A). However, as both morpholinos resulted in loss of *msr* expression in the vein, the venous programme may be more sensitive to the dose of *myef2*.

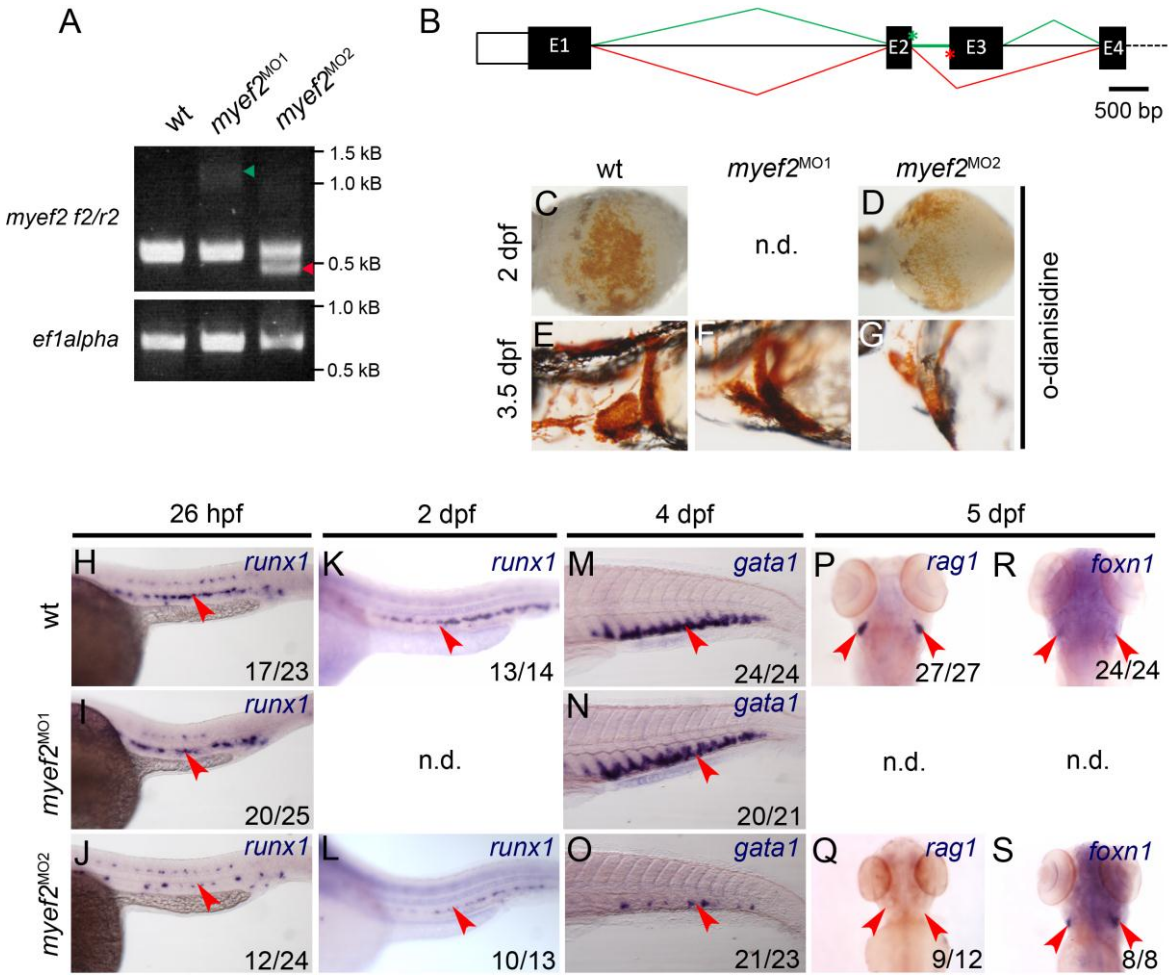

Figure 4.12 Knockdown of *myef2* results in a loss of the haematopoietic stem cell

Two splice morpholinos targeting *myef2* were injected and cDNA isolated. (A) Analysis of cDNA with gene specific primers as indicated. Additional PCR fragments (green and red arrowheads) were cloned. (B) Morpholino 1 caused the inclusion of intron 2, whereas morpholino 2 caused skipping of exon 3. Targets of morpholino 1 and 2 are shown by the green and red asterisks respectively. (C – G) Morpholino 2, but not morpholino 1, results in a reduction in circulating primitive erythrocytes. (H – L) Morpholino 2, but not morpholino 1, results in a loss of the HSC marker *runx1* in the dorsal aorta. (M – O) Morpholino 2, but not morpholino 1, results in a loss of *cmyb* positive HSCs and their derivatives in the caudal haematopoietic tissue. (P – S) *myef2* morpholino 2 causes a loss of *rag1* positive T-cells; *foxn1* positive thymic epithelium remains unaffected. Thymuses imaged from the dorsal aspect; (C – D) imaged ventrally; all other tissues imaged laterally.

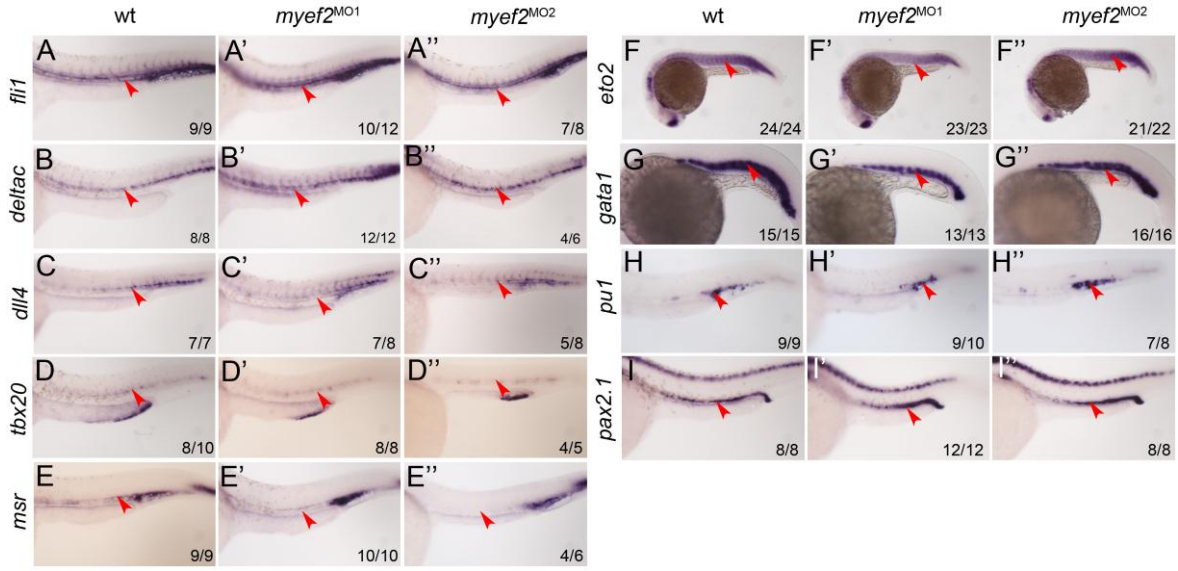

Figure 4.13 Precursor states of the haematopoietic stem cell are unaffected in *myef2* morphants

Expression of markers of the endothelium (A – A") and arterial fates (B – D") are not reduced in *myef2* morphants. (E – E") Expression of *msr* in the artery was reduced in *myef2* morphants. (F – F") *eto2* expression in the somites was unaffected in morphants at 23 hpf. (G – G") *gata1* expression in developing primitive erythrocytes at 22 hpf was reduced in morphants. (H – I") *pu1* primitive myeloid cells in circulation and the *pax2.1* positive pronephric duct were unaffected in *myef2* morphants. Embryos imaged laterally at 26 hpf, unless otherwise stated.

4.5.5 Knockdown of *ep400* results in a loss of HSCs

The E1A-associated p400 protein (Ep400 or mDomino), from here on in Ep400, is a SWI2/SNF2-type ATP dependent helicase originally identified through a yeast two-hybrid screen, and shown to interact with, and modulate the activity of, the myeloid zinc finger protein 2A (Ogawa et al., 2003). Ep400 has also been implicated in the p53/p21 pathway, preventing premature senescence (Chan et al., 2005), and has been shown to epigenetically modulate gene expression by directing localisation of the histone variant H2A.Z at multiple promoters (Gevry et al., 2007). Mice harbouring an engineered deletion in the N-terminal domain of Ep400 died at E11.5 due to anaemia, and also exhibit mild neural tube defects. Globin gene expression was reduced in E8.5 yolk sacs, and *in vitro* haematopoietic activity was blocked, suggesting impairment in primitive haematopoiesis (Ueda et al., 2007). A conditional Mx1-Cre-mediated deletion of *ep400* in adult mouse bone marrow caused a loss of HSPCs, and committed myeloid and erythroid cells. The authors went on to show that in cultured embryonic fibroblasts, Ep400 plays a role in proliferation by controlling a subset of cell-cycle genes (Fujii et al., 2010).

We designed two splice morpholinos to knockdown *ep400* in the zebrafish. Morpholino 1 caused a progressive loss of wildtype *ep400* and gain of a longer transcript, whereas morpholino 2 resulted in a smaller transcript (Figure 4.14). This likely respectively reflects inclusion of intron 7 and a resultant fameshift, or use of a cryptic splice donor or acceptor site, although we did not confirm this. At 26 hpf, expression of *ikaros* was reduced in both *ep400* morphants, however *runx1* was only reduced in *ep400*^{MO1} animals (Figure 4.14 C-D"). By 2 dpf, expression of all HSC markers used were reduced in both morphants (Figure 4.14 E-G"). Markers of HSC and their derivatives at 4 dpf were reduced in *ep400*^{MO1} animals, but not *ep400*^{MO2} animals. The requirement for *runx1* up to and during EHT, but not thereafter (Chen et al., 2009), together with normal *runx1* expression at 26 hpf, may explain the normal expression of markers of blood at 4 dpf in *ep400*^{MO2} animals. Alternatively, this may reflect loss of activity of morpoholino 2.

Expression of markers of precursor tissues of the HSC are unaffected in *ep400* morphants, including specification of endothelial and arterial populations, although expression of *msr* in the

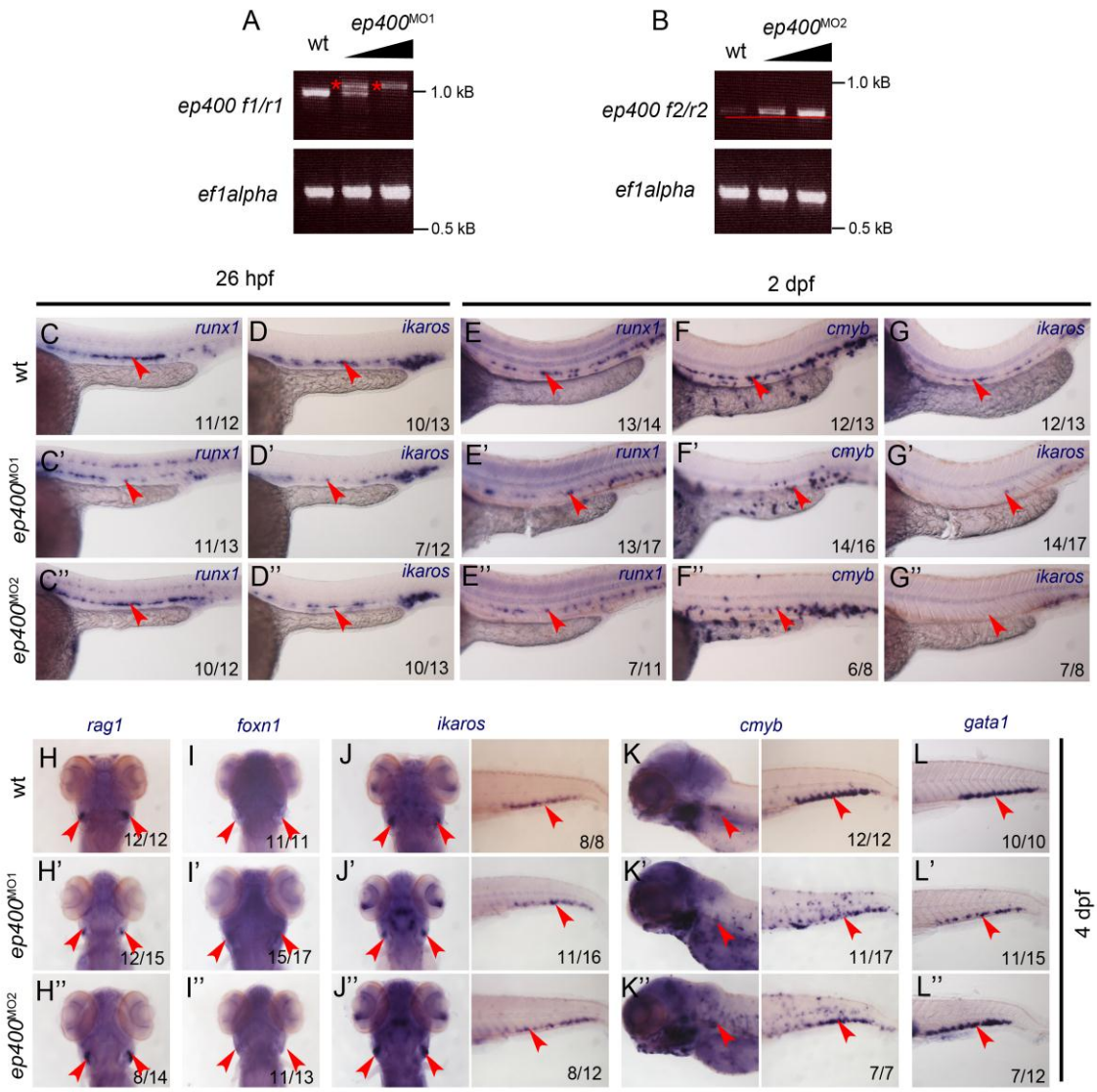

Figure 4.14 Knockdown of *ep400* results in a loss of the haematopoietic stem cell

Two splice morpholinos targeting *ep400* were injected and cDNA isolated with gene specific primers. (A) An additional band with reduced electrophoretic mobility was observed in *ep400*^{MO1} injected embryos (red asterisk). (B) Analysis of cDNA from *ep400*^{MO2} injected embryos revealed a band with increased electrophoretic mobility. (C – G") Markers of the HSC were reduced in *ep400* morphants. Morpholino 1, but not morpholino 2, resulted in a loss of T-cells (H –H", J – J") but did not affect development of the thymus (I – I"). Morpholino 1, but not morpholino 2, resulted in a reduction in HSCs and their derivatives in the caudal haematopoietic tissue (J – J", K – K" and L – L"). HSCs and their derivatives in the embryonic kidney were also reduced upon injection of morpholino 1, but not morpholino 2 (K – K"). Thymuses imaged from the dorsal aspect; all other tissues imaged laterally.

cardinal vein, but not PBI, is reduced (Figure 4.15 A-C" and E-F"). Additionally, ISVs do not form normally in *ep400*^{MO2} animals. This probably reflects the reduction of *tbx20* expression in the roof of the aorta (Figure 4.15 D-D"), as *tbx20* expression has been previously linked with ISV formation (Szeto et al., 2002). Expression of *pax2.1* in the pronephric duct is not affected, however primitive erythrocytes and myeloid cells, marked by *gata1* and *pu1* respectively, are reduced (Figure 4.15 G-I"). The defect in primitive haematopoiesis we see is also seen in a mouse mutant lacking the N-terminal region of *ep400* (Ueda et al., 2007). In contrast to this mouse model, we did not observe any early embryonic defects. This may reflect the level of knockdown achieved, as morpholinos were titrated to a level where gross morphological defects were not observed. Taken together, we have shown that *ep400* is required for the generation of HSCs from the AGM region. This complements the phenotype of the conditional mouse knockout, which shows defects in HSPC production in adult bone marrow, although the generation of HSCs in E10.5 AGMs has not been investigated in this model (Fujii et al., 2010).

4.5.6 Knockdown of *hdac7* results in a loss of HSCs

Eukaryotic transcriptional repressors nucleate large co-regulatory complexes, and target histone deacetylase enzymes (Hdacs) to promoters and enhancers to alter the chromatin state (Oberoi et al., 2011). One such enzyme is Hdac7, a class IIA Hdac that has been shown to interact with both Bcor and Ncor (Bertos et al., 2001; Pagan et al., 2007) and like Ep400, can inhibit cellular senescence (Zhu et al., 2011a). Upon induction of haematopoietic stress in a nonhuman primate model transfused with retrovirally labelled CD34 positive blood, it was found that a clone overexpressing *hdac7* due to insertional activation was able to outcompete other clones, suggesting *hdac7* may confer a survival advantage in this context (Xie et al., 2010). Overexpression of *hdac7* in bone marrow from children with acute lymphoblastic leukaemia has been associated with a poor prognosis and may represent a novel therapeutic target (Moreno et al., 2010). In the mouse, *hdac7* is expressed in CD4/CD8 double positive thymocytes where it is localised to the nucleus and acts as a transcriptional repressor. Upon successful challenge and activation of the T-cell receptor, it becomes phosphorylated and is exported

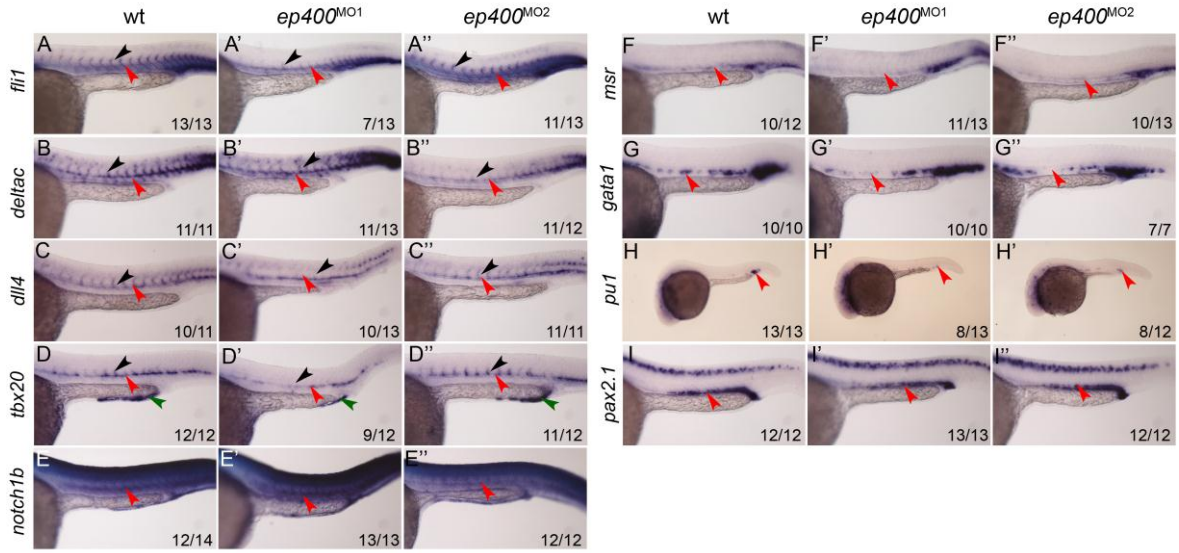

Figure 4.15 Precursor states of the haematopoietic stem cell are unaffected in *ep400* morphants

Expression of markers of the endothelium (A – A") and arterial fates (B – E") are not reduced in *ep400* morphants. (F – F") Expression of *msr* in the artery was reduced in *ep400* morphants. (G – H") Primitive blood development was reduced in *ep400* morphants. (I – I") Development of the pronephric duct was unaffected in the morphants. Embryos imaged laterally at 26 hpf; black arrowheads, intersegmental vessels; green arrowheads, *bmp* dependent *tbx20* expression.

to the cytoplasm, resulting in de-repression of target genes (Parra et al., 2007). Additionally, inhibition of Hdac7 has been shown to block angiogenesis *in vivo* and *in vitro* (Chang et al., 2006; Ha et al., 2008). Recently, it has been shown that this is in part by epigenetically controlling *akap12*, a negative regulator of angiogenesis (Turtoi et al., 2012).

We designed two splice morpholinos to knockdown *hdac7* in the zebrafish. PCR analysis showed that increasing doses of morpholino 1 result in a progressive reduction in wild type transcript and the appearance of two larger fragments. Treatment with morpholino 2 caused a progressive loss of the wild type transcript and gain of a smaller band (Figure 4.16A). Although we did not clone and sequence the additional products, they likely arise from intronic inclusion or deletion of coding sequence resulting from use of a cryptic splice site. At 26 hpf, *hdac7*^{MO1} animals, but not *hdac7*^{MO2} animals, have reduced expression of the HSC markers *runx1, cmyb* and *ikaros* (Figure 4.16 B-D"). By 2 dpf, both morpholinos caused a reduction in HSC markers, and at 4 dpf, markers of HSCs and their derivatives in the thymus, embryonic kidney and CHT were reduced or absent (Figure 4.16 E-K"). The PLM, which precedes development of HSCs, is largely unaffected, except for a slight reduction in *scl* expression in *hdac7*^{MO1}, but not *hdac7*^{MO1} embryos (Figure 4.17 A-B"). Markers of precursor states of the HSC downstream from the PLM, including the endothelial and arterial programmes were not reduced in either *hdac7* morphants (Figure 4.17 C-G"). Additionally, we did not see defects in markers of the pronephric duct, vein or primitive blood (Figure 4.17 H-K").

Knockout of *hdac7* in the mouse results in embryonic lethality at E10.5 due to loss of vascular integrity, haemorrhaging and defects in angiogenesis (Chang et al., 2006; Ha et al., 2008). We did not see these phenotypes in our morphants. This may reflect the level of knockdown, or a differential requirement for *hdac7*, between the two species. We did however uncover a novel requirement for *hdac7* in programming the first HSCs, which may have been overlooked in the mouse knockout due to the vascular defects.

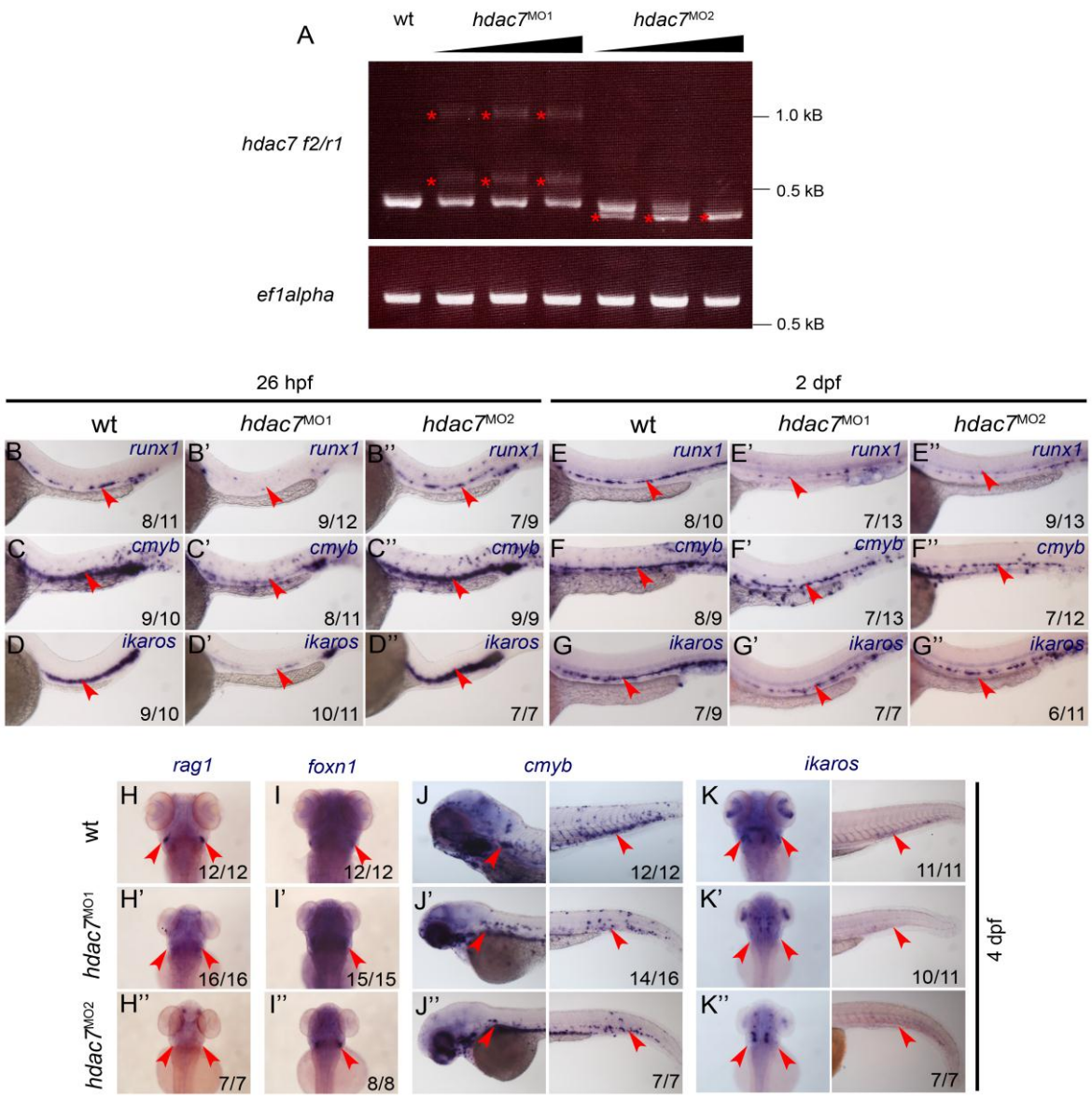

Figure 4.16 Knockdown of *hdac7* results in a loss of the haematopoietic stem cell

(A) Two splice morpholinos targeting *hdac7* were injected and cDNA isolated with gene specific primers. (A) Additional bands with reduced electrophoretic mobility were observed in *hdac7*^{MO1} injected embryos. In *hdac7*^{MO2} injected embryos, a band with increased mobility was observed. Red asterisks indicate non wild type bands. (B - D") HSC markers were reduced at 26 hpf in *hdac7*^{MO1}, but not *hdac7*^{MO2} embryos. By 2 dpf, all HSC markers looked at were reduced in both *hdac7* morphants (E – G"). Thymic T-cells were absent in *hdac7* morphants (H – H" and K – K"). Thymic development was unaffected (I – I"). HSCs and their derivatives in the embryonic kidney were reduced in *hdac7* morphants (J – J"). HSCs and their derivatives in the caudal haematopoietic tissue were also reduced (J – K"). Thymuses imaged from the dorsal aspect; all other tissues imaged laterally.

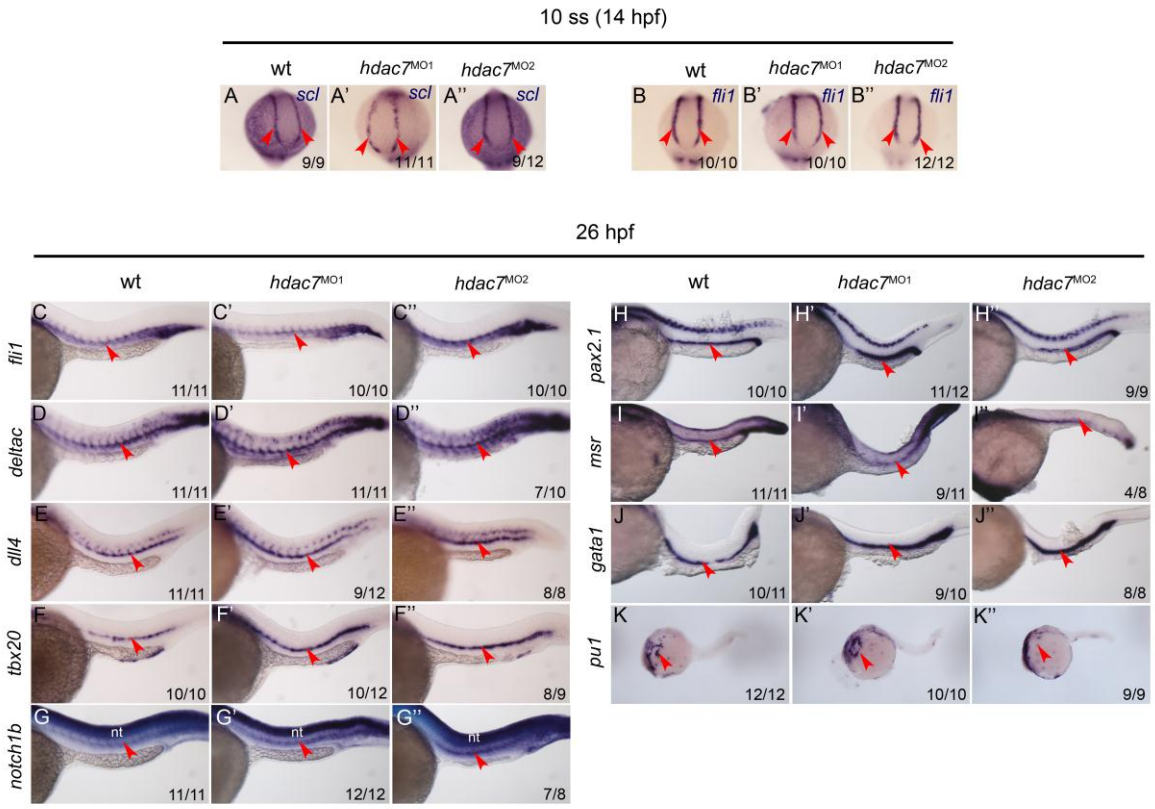

Figure 4.17 Precursor states of the haematopoietic stem cell are unaffected in *hdac7* morphants

(A – A") Expression of *scl* in the posterior lateral plate is reduced in *hdac7*^{MO1}, but not *hdac7*^{MO2}. (B – B") Expression of *fli1* is unaffected. Expression of markers of the endothelium (C – C") and arterial fates (D – G") are not reduced in *hdac7* morphants. (H - H") Development of the pronephric duct was unaffected in the morphants. (I – I") Expression of *msr* in the vein was reduced in *ep400* morphants. (J – K") Primitive blood development was unaffected in *hdac7* morphants. Embryos at the 10 somite stage (ss) were imaged dorsally, embryos at 26 hpf were imaged laterally.

4.6 Dose-dependent rescue of *lmo4a* morphants

Morpholinos can lead to off-target effects, confounding the analysis of potential phenotypes, and therefore controlling for this possibility is important (Eisen and Smith, 2008). One such control is the ability to reproduce the observed phenotype with two distinct morpholinos, as we have demonstrated for loss of HSCs in *lmo4a* morphants (Figure 4.3 D-O). Another important control is the ability to rescue the phenotype by specifically re-expressing the targeted gene. In the case of *lmo4a* morphants, we attempted to do this by overexpressing, in various vectors, both zebrafish *lmo4a* and mouse *lmo4* mRNA (Table 2.4). However, we were never able to rescue *lmo4a* morphant zebrafish, possibly because protein synthesised from the exogenous RNA could not be detected beyond 16 hpf (*data not shown*). We therefore generated transient transgenic animals, taking advantage of Tol2 mediated transgenesis (Kawakami et al., 1998; Kawakami et al., 2000). The desired cDNA sequence driven by the constitutive *ef1a* promoter, flanked by Tol2 arms, was co-injected with RNA coding for the *tol2-transposase* into embryos, and the F_0 population analysed.

A *gfp* control injection demonstrated that the transposase was active, resulting in *gfp* expression throughout the embryo, most notably in the muscle fibres of the trunk. The level of expression between individual embryos was variable, likely representing variability inherent to microinjections, as well as different integration sites in embryos (Figure 4.18 A-C'). As described previously, *lmo4a* 5'UTR morphants had reduced expression of *runx1* and lacked ISVs (Figure 4.18 E-F'). The loss of *runx1* could be partially rescued when the amount of tol2-flanked DNA was titrated down to 2 pg, but not when 10 or 25 pg of DNA was used. The loss of ISVs was never rescued (Figure 4.18 G-L'). Thus, we confirmed the specificity of the observed HSC defect. The low degree of rescue (50%) was likely due to the variability in the level of overexpression associated with transient transgenesis (Philip Pinheiro, *personal communication*). Of note, a proportion of embryos injected with 25 pg of DNA and the transposase, but not *lmo4*$^{MO(5'UTR)}$, had reduced *runx1* expression and lacked ISVs (Figure 4.18 G-G'). Additionally, these embryos had shorter trunks and tails, and these morphological defects were rescued upon depletion of *lmo4a* (Figure 4.18 G-H'), suggesting that overexpression of *lmo4a* causes defects in

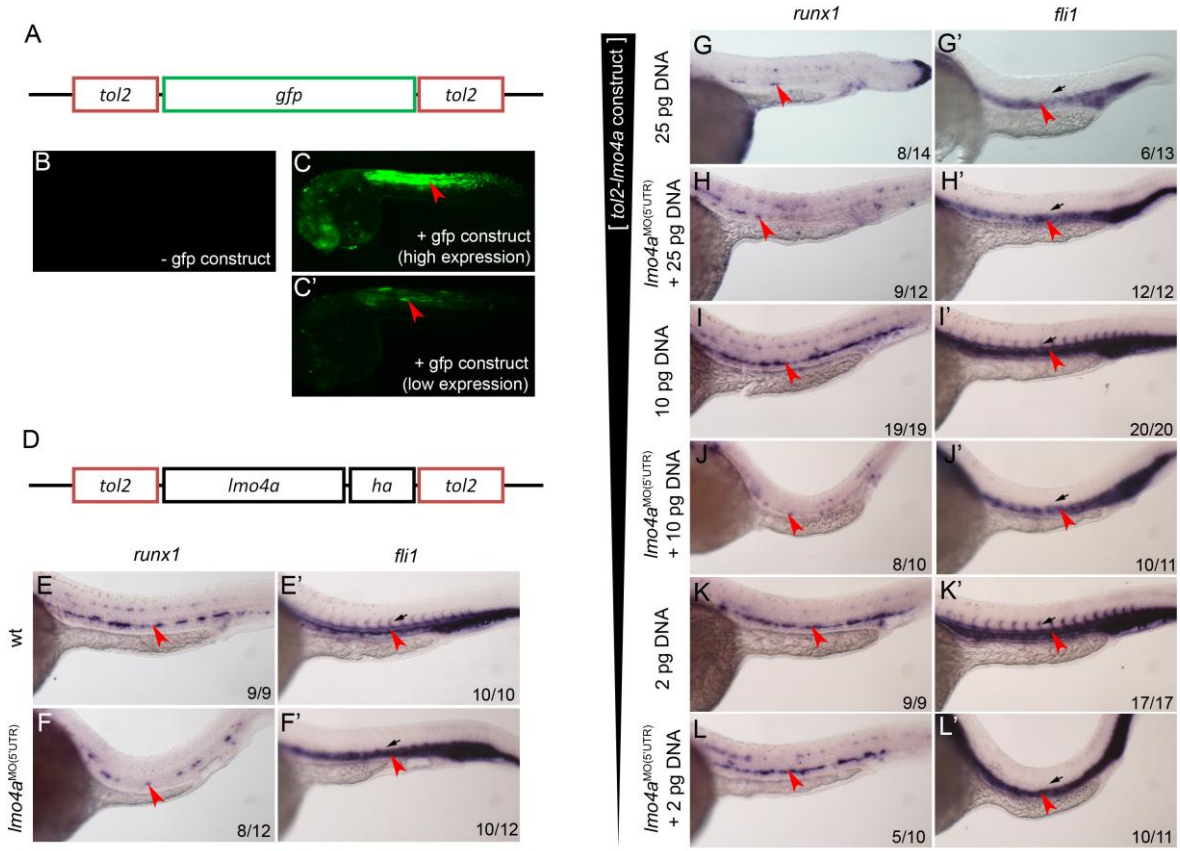

Figure 4.18 Dose-dependent DNA rescue of *lmo4a* morphants

Indicated amounts of *tol2* flanked constructs were injected as circular DNA along with 30 pg of *tol2* transposase. (A – C') Microinjection of 25 pg of *tol2* flanked gfp results in ubiquitous expression of *gfp* in the trunk of the embryo. The maximum and minimum from the range of *gfp* expressing embryos is indicated (C-C'). (D) *tol2*-flanked *lmo4a* construct. (E – F') *lmo4a* morphants have reduced *runx1* expression in the dorsal aorta and lack intersegmental vessels. (G – H') Injection of 25 pg of the *lmo4a-tol2* construct causes a phenotype similar to *lmo4a* morphants, and does not rescue *lmo4a* morphants. (I – J') Injection of 10 pg of the *lmo4a-tol2* construct does not rescue *lmo4a* morphants. (K – L') Injection of 2 pg of the *lmo4a-tol2* construct can rescue *lmo4a* morphants. All embryos viewed laterally at 30 hpf; red arrowhead, dorsal aorta; black arrows, intersegmental vessels.

anterior-posterior patterning, similar to the mild anterior-posterior defects seen when *lmo4* is mis-expressed in the mouse (Hahm et al., 2004).

4.7 HSCs fail to emerge from the dorsal aorta in *lmo4a* morphants

Depletion of *runx1* in the zebrafish results in abortive EHT events (Kissa and Herbomel, 2010). Having confirmed the specificity of the loss of HSCs in *lmo4a* 5'UTR morphants, and given that *runx1* is reduced in *lmo4a* morphants, we were interested in whether EHT stalled in a similar fashion as in *runx1* morphant animals. We imaged a 2.5 somite region of the dorsal aorta in Tg(*kdrl*:EGFP) animals, in which EGFP expression is driven strongly in the dorsal aorta. In uninjected siblings, we observed EHT events from around 33 hpf to 65 hpf (Figure 4.19 A-F). This was characterised by cells in the floor of the dorsal aorta contracting and undergoing an abluminal bending, remaining in this configuration for about 3 hours (Figure 4.19 B-C, green arrowhead). Endothelial cells positioned on either lateral side of the bent cell connect, maintaining vascular integrity (Kissa and Herbomel, 2010). The cell undergoing EHT rounds up, but remains connected to the dorsal aorta by anterior and lateral attachments, before releasing these contacts and entering circulation through the cardinal vein (Figure 4.19 D-F, green cell). In *lmo4a* 5'UTR morphants, EHT initiates around 33 hpf. Cells in the floor of the dorsal aorta expressing the *kdrl*:EGFP transgene contract and begin to bend (Figure 4.19 H and K). However, like in *runx1* morphants, they then burst as they begin to round up, failing to enter circulation (Figure 4.19 I and L, red cells). Quantitation of the number of EHT events revealed that they emerged at a frequency of 0.21 ± 0.05 cells per somite region per hour in uninjected siblings, corresponding to about 19 events in total (Figure 4.19M). This is in excellent agreement with previously published estimates in the zebrafish (Kissa and Herbomel, 2010; Kissa et al., 2008). However this is lower than estimates in the mouse AGM, where EHT also occurs during a shorter window of developmental time (Boisset et al., 2010). This may represent an artefact of the embryo free

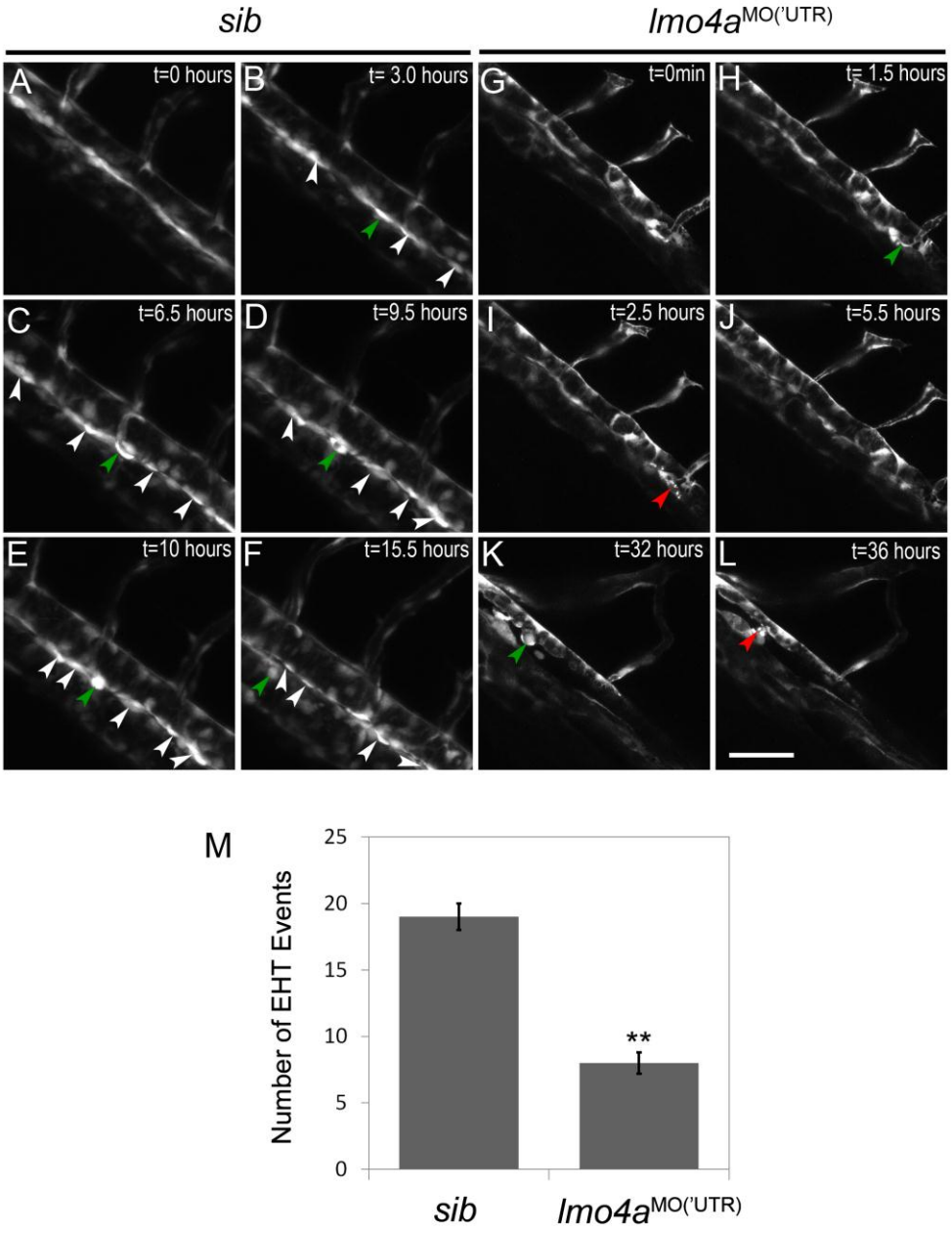

Figure 4.19 Live confocal imaging of haematopoietic stem cell emergence

A three somite region of the dorsal aorta was imaged laterally in Tg(*kdrl*:EGFP) siblings, or *lmo4a* morphant Tg(*kdrl*:EGFP). (A – F) White arrowheads, cells in the floor of the dorsal aorta about that undergo the endothelial to haematopoietic transition (EHT); green arrowheads, tracking a single cell undergoing EHT and entering the circulation through the underlying vein (F). (G – L) Green arrowhead, cells undergoing EHT; red arrowheads, cells aborting the EHT process; t_0 corresponds to fish at approximately 33 hpf; scale bar is 50 μm. (M) Quantitation of total EHT events observed. Error bars are representative of standard error from movies of at least three embryos; ** $p<0.01$.

culture system, or because the first HSCs in mouse undergo a more robust expansion than the first zebrafish HSCs (Ivanovs et al., 2011).

In *lmo4a* morphants, EHT events initiated at a frequency of 0.09 ± 0.02 cells per somite region per hour, corresponding to about 8 events in total (Figure 4.19 G-M). This represents about 2.5-fold fewer initiation events in morphant embryos. As most of the EHT events in *lmo4a* morphants abort by a process that seems to involve cytoplasmic blebbing, and blebbing is known to occur during apoptosis (Vermeulen et al., 2005), we investigated the possibility that cells in the floor of the dorsal aorta were undergoing apoptosis by fluorescent immunostaining using an antibody against activated caspase-3, a marker of apoptosis (Kratz et al., 2006). In wild type embryos, apoptosis was detected in the posterior pronephric duct (Figure 4.20 B-D), as previously reported (Monteiro et al., 2011). In both *lmo4a* morphants, apoptosis was not increased in the dorsal aorta, although in the 5'UTR morphant, additional apoptotic cells were observed in circulation and at somite boundaries in the tail (Figure 4.20 E-J). Therefore, apoptosis does not seem to contribute to abortive EHT events. It is possible that these cells do not remain viable due to defective cytoskeletal architecture (Karima Kissa, *personal communication*).

4.8 *lmo4a* does not lie upstream of Bmp4 or downstream of Notch signalling in the AGM

Along with the action of *runx1*, Bmp4 signalling is one of the few known drivers of HSC production in the floor of the dorsal aorta (Wilkinson et al., 2009). We therefore wanted to test if *bmp4* expression was affected in *lmo4a* morphants. At the 10 ss, prior to migration of cells in the PLM to the midline, and at 26 hpf in the floor and mesenchyme underlying the dorsal aorta, expression of *bmp4* was unaffected (Figure 4.21 D-E, J-K). However, at the 10 ss, expression of *tbx20*, which is under the transcriptional control of *bmp4* in this tissue, is reduced (Figure 4.21 A-C). One role of *tbx20* at this point in development is to restrict the posterior most expression of *gata1* (Pyati et al., 2006). Therefore, upon reduction of *tbx20*, *gata1* is expanded into the posterior most region of the PLM

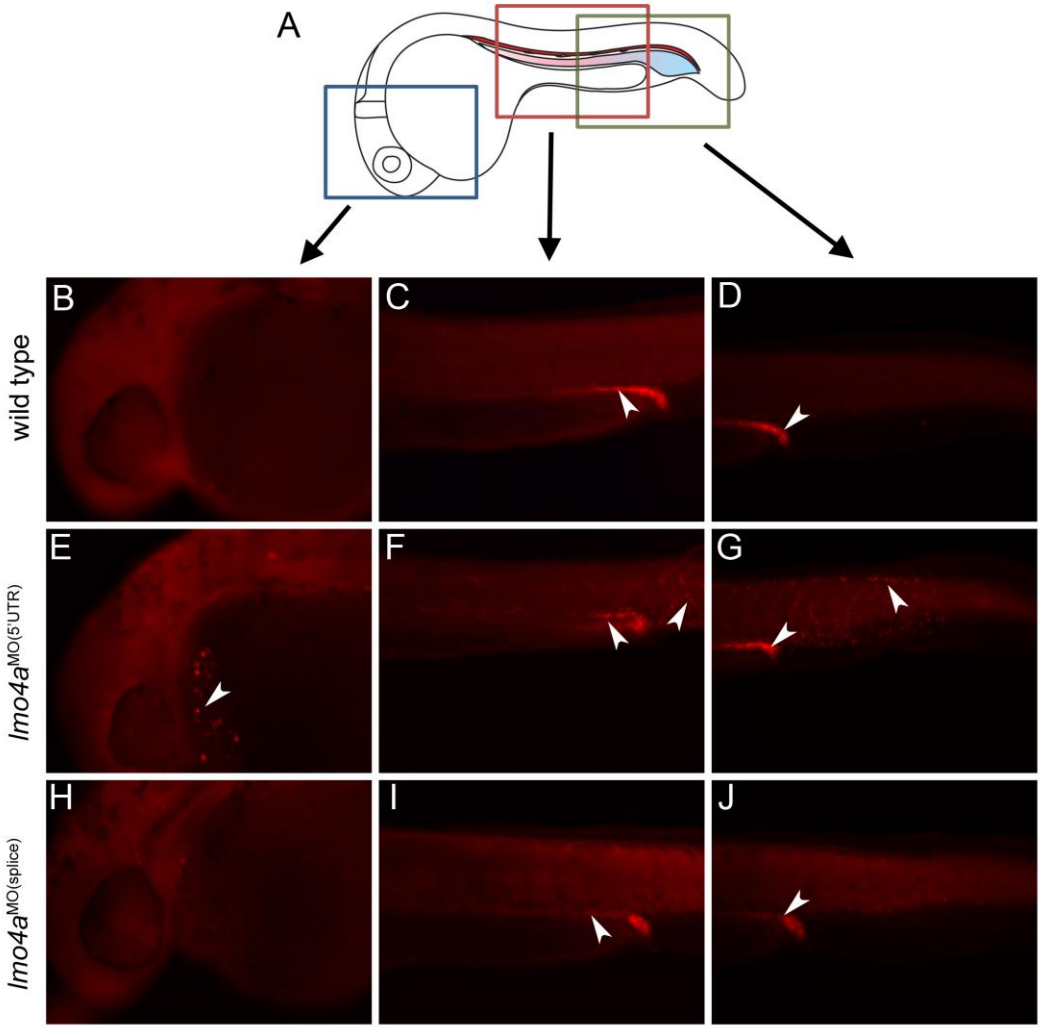

Figure 4.20 Apoptosis in the dorsal aorta is not detected in *lmo4a* morphants

(A) Zebrafish were fixed at 35 hpf and stained for activated caspase-3, a marker of apoptosis. Approximate areas imaged are indicated. (B – D) Tissue specific apoptosis is not observed in the head region. In the trunk and tail, apoptotic cells are observed in the pronephric duct, which lies bilaterally and ventrally to the dorsal aorta. (E – G) In *lmo4a* 5'UTR morphants, circulating apoptotic primitive blood cells are observed in the yolk, pronephric duct and somite borders. (H – J) Increased apoptosis is not detected in *lmo4a* splice morphants. White arrowhead; apoptotic cells; zebrafish were fixed at 35 hpf and imaged laterally.

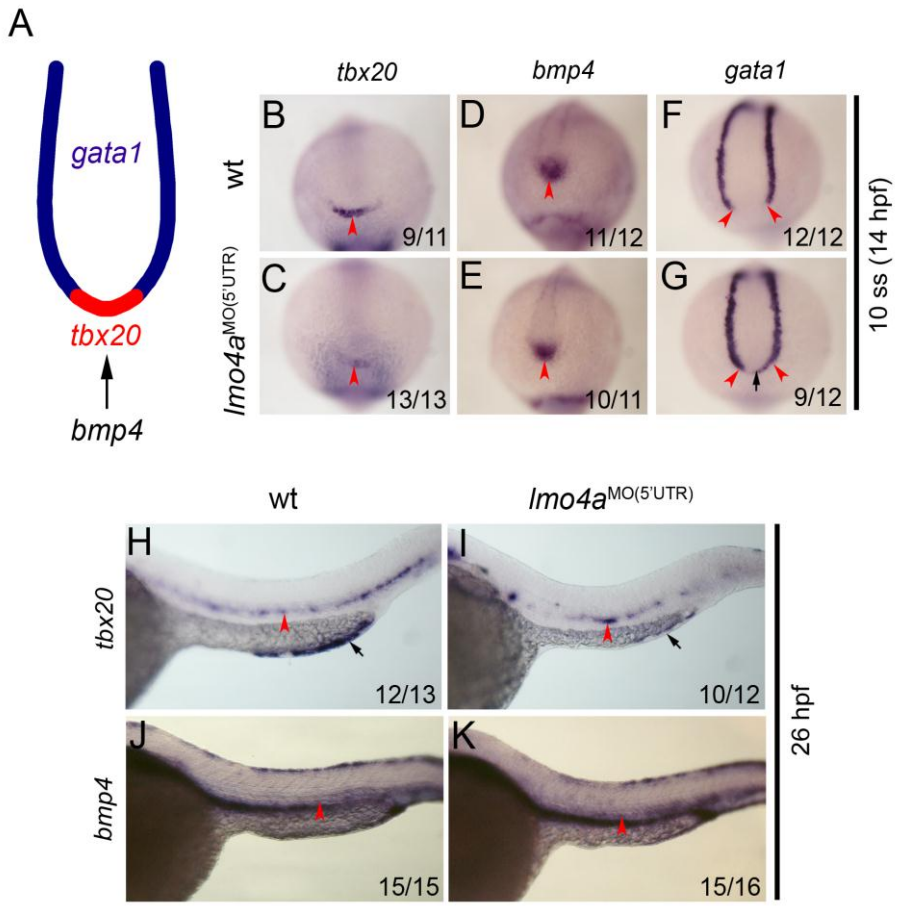

Figure 4.21 ***lmo4a*** **is required for** ***tbx20*** **expression**

(A) Schematic of gene expression in the posterior lateral plate (PLM) at the 10 somite stage (ss). Expression of *bmp4* controls expression of *tbx20* in the posterior most PLM, which restricts expression of *gata1*. (B – G) *lmo4a* morphants display no change in *bmp4* expression, but have a reduction in *tbx20* expression and ectopic *gata1*expression. Red arrowheads, normal expression; black arrows, ectopic expression; embryos imaged dorsally. (H –I) *lmo4a* morphants have reduced *tbx20* expression in the dorsal aorta (red arrowheads) and yolk extension (black arrows). (J – K) *bmp4* expression is unaffected at 26 hpf in *lmo4a* morphants. (H – K) Embryos imaged laterally.

(Figure 4.21 F-G). This result is unlikely to contribute to the ISV and HSC defects observed later in development, as the posterior PLM does not contribute to these populations. At 26 hpf, *tbx20* is expressed in the roof of the dorsal aorta (Wilkinson et al., 2009), and is reduced in *lmo4a* morphants. Additionally, Bmp dependent expression of *tbx20* expression under the yolk extension is reduced in *lmo4a* morphants (Figure 4.21 H-I). Therefore, *lmo4a* controls *tbx20* expression in distinct developmental contexts, and may mediate Bmp signalling.

Like Bmp signalling, notch signalling is important in programming the first HSCs, as well as in setting up the arterial programme (Burns et al., 2005; Gering and Patient, 2005). Although expression of notch receptors and ligands, is not affected in *lmo4a* morphants (Figure 4.4 I-I" and K-K"), it is possible that the HSC programme requires a higher level of notch signalling than the formation of dorsal aorta (Martin Gering, *personal communication*). We were therefore interested in whether inhibiting notch signalling with the potent γ-secretase inhibitor DAPM would affect expression of *lmo4a* (Figure 4.22 A-B). While expression of *ephrinb2a*, *dll4*, and *runx1* in the dorsal aorta was lost in DAPM-treated embryos, serving as a positive control for the chemical treatment (Figure 4.22 C-H). There was no change in the expression of *lmo4a* in DAPM treated embryos (Figure 4.22 I-J), suggesting that in this context transcriptional regulation of *lmo4a* is independent of notch signalling.

4.9 Survival of primitive erythrocytes is compromised in *lmo4a* morphants

We have previously shown that cells in the PLM, that migrate medially to form the ICM, are unaffected in *lmo4a* morphants (Figure 4.4 A-F'). We were however interested in whether formation of the ICM and primitive erythropoiesis was affected in *lmo4a* morphants. Expression of *gata1* in primitive erythrocytes in the ICM, prior to them entering circulation, was unaffected in *lmo4a* morphants (Figure 4.23 A-C). This is consistent with previous studies looking at expression of *zE1b-globin* in *lmo4a* morphants (Meier et al., 2006). Additionally, expression of *pu1* in the ALM and EMP-derived myeloid cells, was unaffected in *lmo4a* morphants (Figure 4.23 D-F). In zebrafish, primitive blood cells enter

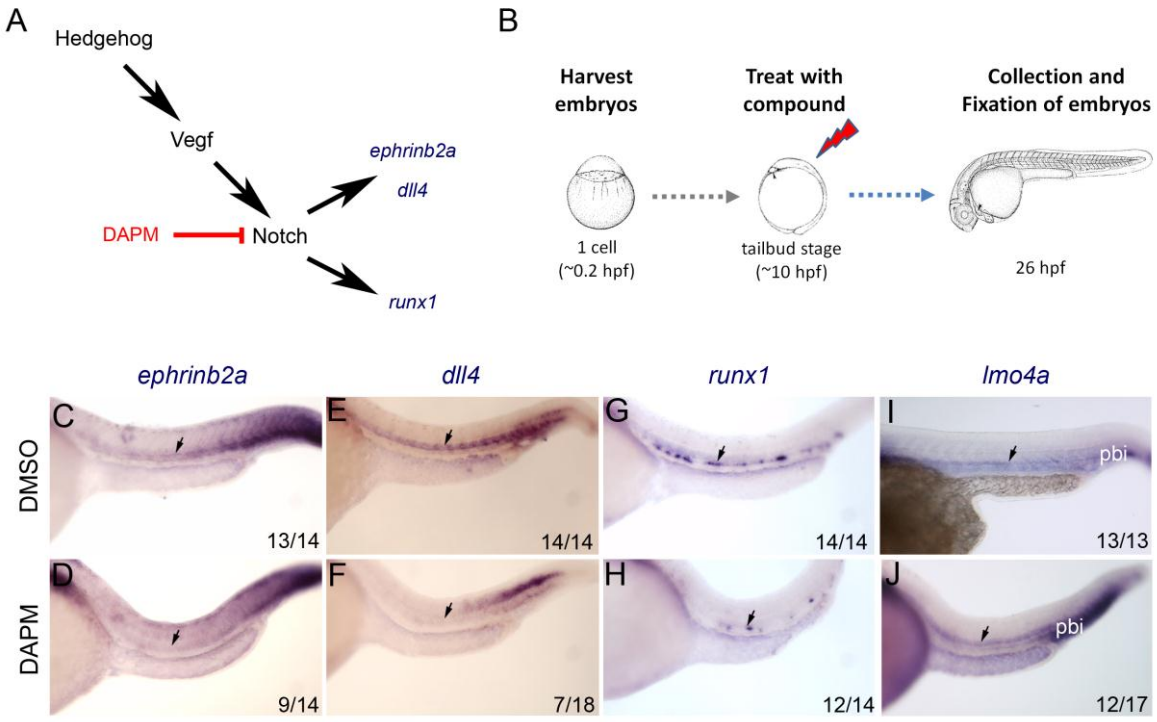

Figure 4.22 Inhibition of notch signalling does not affect *lmo4a* expression

(A) Schematic of the genetic cascade required for the arterial and HSC programme, adapted from (Gering and Patient, 2005). DAPM is a potent inhibitor of notch signalling and was applied to embryos from the tailbud stage. (B) Schematic of the treatment regime. (C – J) *lmo4a* expression was unaffected in DAPM treated embryos, however, markers of the arterial programme (*ephrinb2a* and *dll4*) and HSC (*runx1*) were reduced. Embryos fixed at 28 hpf and imaged from their lateral aspect.

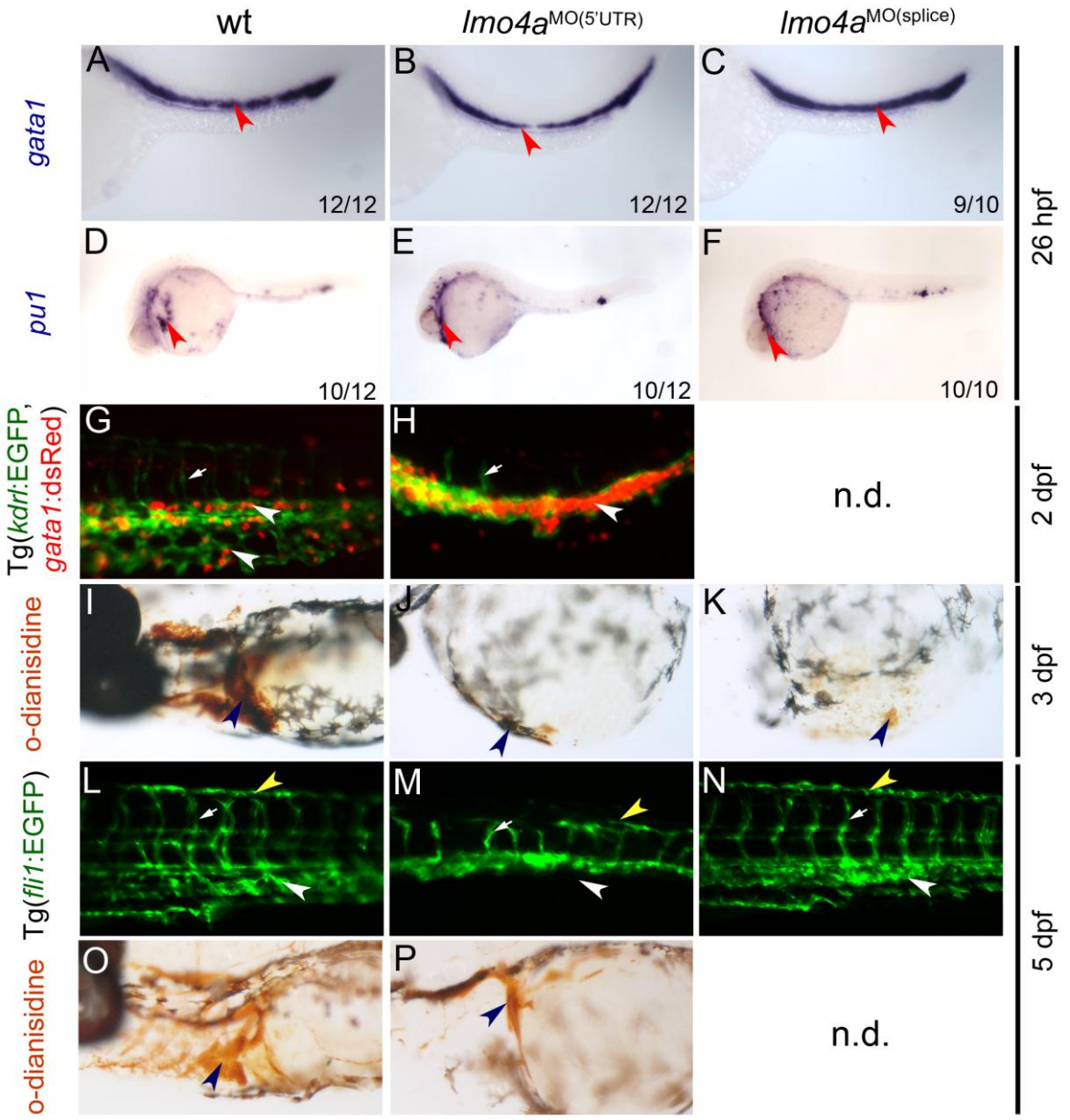

Figure 4.23 Development of primitive blood and the CHT in *lmo4a* morphants

(A – F) Specification of primitive blood is unaffected in *lmo4* morphants (red arrowheads). (G – H) Aggregation of primitive erythrocytes in the posterior dorsal aorta in Tg(*kdrl*:EGFP, *gata1*:dsred) double transgenic animals injected with *lmo4a* morpholino (white arrowheads). (I – K) Primitive erythrocytes are not maintained in *lmo4a* morphants. (L – N) The CHT fails to vascularise in *lmo4a* 5'UTR morphants (white arrowheads). (O – P) As definitive erythrocytes enter circulation, total erythrocytes remain reduced in *lmo4a* morphants. All embryos viewed laterally; white arrows, intersegmental vessels; yellow arrowheads, dorsolateral anastomotic vessel; blue arrowheads, o-dianisidine stained globinised cells.

circulation just after 26 hpf (Schier and Talbot, 2005). In *lmo4a* morphants, entry of cells into circulation is delayed by approximately 2 hours. Nevertheless a functional circulatory loop forms and is maintained. We however noticed that circulating blood cells had a tendency to pool in the tail region of *lmo4a* 5'UTR morphants, but not splice morphants. We confirmed that this was the case in *kdrl*:EGFP-*gata1*:dsred double transgenic embryos, marking vasculature and red blood respectively. In uninjected siblings, red blood can be seen circulating through the dorsal aorta and the CHT at 2 dpf. However, in *lmo4a* 5'UTR morphants, circulation of red blood was stalled in the tail, and the CHT failed to vascularise (Figure 4.23 G-H and L-N). Prior to 3 dpf, circulating cells represent the output of primitive haematopoiesis, however from 3.5 dpf, erythroid cells derived from HSCs begin to enter the circulation, eventually replacing all primitive blood (Jin et al., 2009). At both 3 and 5 dpf, numbers of circulating erythrocytes stained with o-dianisidine are reduced (Figure 4.23 I-K and O-P). This represents a failure to maintain erythrocytes that have been specified, possibly due to apoptosis (Figure 4.20E). Indeed, it was shown that depletion of *lmo4* resulted in an increase in apoptosis in breast cancer cell lines (Tian et al., 2010). By 5 dpf, reduction in numbers of circulating erythrocytes in *lmo4a* morphants is reflective of a reduction in definitive erythroid output due to fewer HSCs. Thus, Lmo4a is required for the survival of primitive blood, and this could be through an interaction with the known erythroid transcription factor Scl, which is required for development of red blood (Joshi et al., 2009; Robb et al., 1995).

4.10 Lmo4a may be required for sprouting angiogenesis

Primary ISVs sprout from the roof of the dorsal aorta from about 20 hpf, and represent the first sprouting angiogenic events in the fish (Blum et al., 2008). We have shown that ISVs do not develop in *lmo4a* 5'UTR morphants (Figure 4.4 H-H' and 4.24 A-B). To investigate this further, we followed angiogenic sprouting in a transgenic line expressing YFP under the control of the *vegfr1* (*flt1*) promoter, which drives transgene expression mainly in the dorsal aorta and primary ISVs (Hogan et al., 2009). In uninjected siblings, sprouting from the dorsal aorta is clearly visible along with the initial formation of the DLAV, and filopodial extensions can be seen extending and retracting,

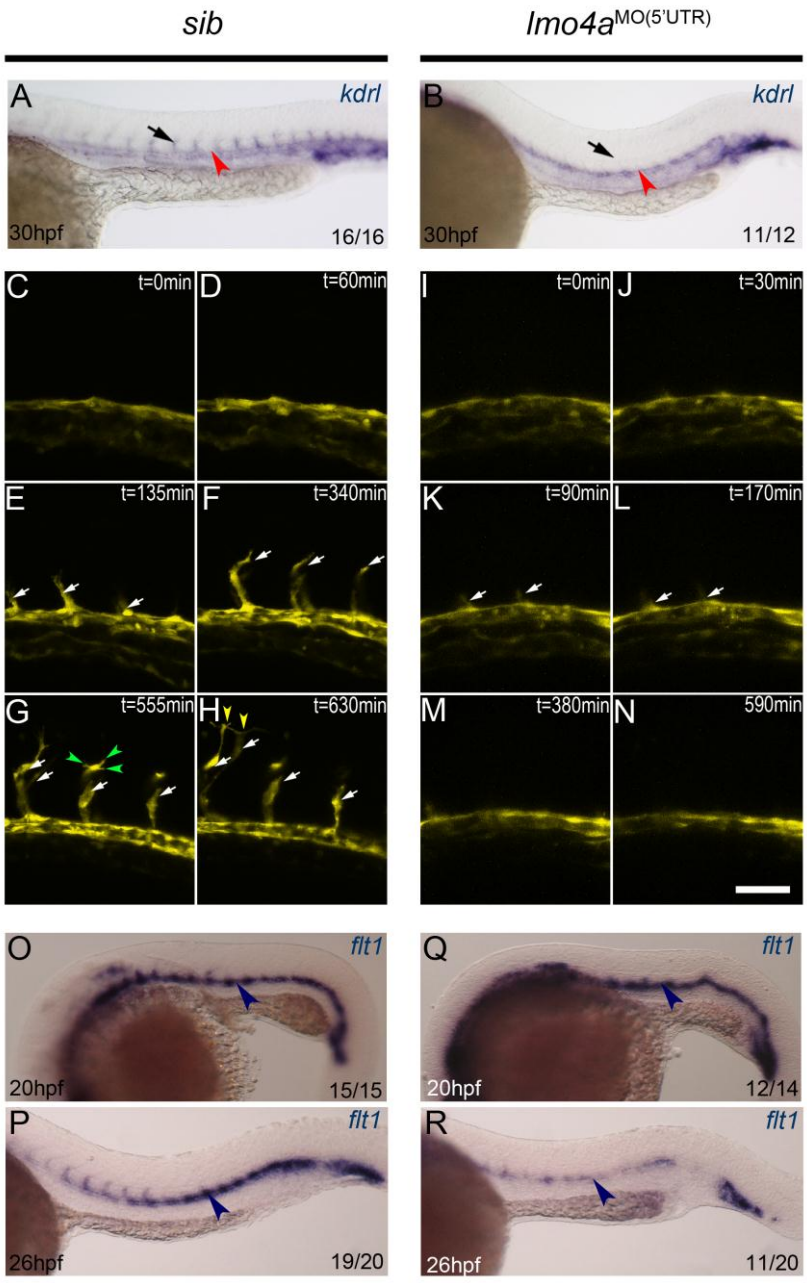

Figure 4.24 ***lmo4a*** **5'UTR morphants lack intersegmental vessels (ISVs)**

(A – B) The *lmo4a* 5'UTR morpholino causes a loss of primary ISVs (black arrows), but not of the dorsal aorta (red arrowheads). (C – H) Sprouting of ISVs in uninjected embryos in Tg(*flt1*:YFP) animals (white arrows). Filopodial extensions can be seen extending and retracting (green arrowheads). The beginning of the formation of the dorsolateral anastomotic vessel can also be seen (yellow arrowheads). (I – N) In *lmo4a* morphants, sprouting initiates (white arrows) but then regresses back into the dorsal aorta. t_0 corresponds to fish at approximately 20 hpf. Scale bar is 50 µm. (O – R) Expression of *flt1* is reduced in *lmo4a* morphants from 26 hpf. All embryos imaged from their lateral aspect.

presumably sampling the local signalling environment (Figure 4.24 C-H). Embryos injected with the *lmo4a* 5'UTR morpholino initiate sprouting, but then these sprouts appear to regress (Figure 4.24 I-N). Additionally, expression of the *flt1* driven transgene increases in the dorsal aorta of uninjected fish, however it is reduced in *lmo4a* morphant animals (Figure C-N). Nascent *flt1* transcripts are expressed at similar levels in wild type and *lmo4a* 5'UTR morphants at 20 hpf (Figure 4.24 O and Q), but by 26 hpf, *flt1* expression is reduced in the morphants (Figure 4.24 P and R). In this study, we do not distinguish between soluble and membrane-bound *flt1* expression which are both expressed in the zebrafish dorsal aorta and ISVs (Krueger et al., 2011). By 2 dpf, ISVs have started to sprout in *lmo4a* 5'UTR morphants, and by 5 dpf, a DLAV has formed, however the angiogenic sprouts are disorganised and rarely form a perfused circulatory network. This delay in sprouting may reflect either loss of activity of the morpholino or a reduced requirement for *lmo4a* with time. Development of the CHT also involves angiogenesis, and we have previously shown that this also fails to occur in *lmo4a* 5'UTR morphants (Figure 4.23 L-N). Bmp is required for angiogenesis in this tissue (Wiley et al., 2011), however we have not investigated whether signalling is affected in the CHT. As both the defect in the CHT and ISV were only observed with one morpholino, and we were never able to rescue the ISV defect by overexpressing *lmo4a* (Figure 4.18), this phenotype may represent an off-target effect of the 5'UTR morpholino.

4.11 Discussion

4.11.1 Overview

The adult-definitive haematopoietic tree initiates from the HSC, a pluripotent cell that emerges *de novo* from the floor of the dorsal aorta during embryonic development (Bertrand et al., 2010a; Boisset et al., 2010; Kissa and Herbomel, 2010). Much recent effort has focused on how this cell is first programmed during development, and whether the HSC pool can by artificially expanded. For example, taking advantage of the zebrafish, it has been shown that prostaglandin E2, interleukin 1, and even extracts of *Zingiber officinale* (common ginger) can promote haematopoiesis (Ferri-Lagneau et al.,

2012; North et al., 2007). However a complete landscape describing the generation of HSCs is still lacking. Previous work in the zebrafish uncovered a potential role for the scaffold protein *lmo4a* in the generation of the HSC (Meier et al., 2006). Using a variety of readouts, we have confirmed that this is the case. Lmo proteins do not directly bind DNA. Rather, they regulate gene expression indirectly by nucleating complexes containing transcription factors, chromatin remodelling factors, and transcriptional cofactors (Bach, 2000). In MEL cells, a novel Lmo4-containing complex has been identified, containing these known classes of proteins (Charlotte Andrieu-Soler, *unpublished*). We therefore hypothesised that these interactions with Lmo4 represent a novel transcriptional complex, and have gone on to investigate the roles of elements of this complex in generating zebrafish blood cells. Here we show that many of the Lmo4 partners play a role in the development of HSCs, and possibly also angiogenesis. It generally does not explore the mechanisms by which these proteins function. However, we have excluded a role for some known players in HSC formation, either upstream or downstream of *lmo4a*.

4.11.2 *lmo4* is required for HSC emergence

We show that the first detectable blood-related defect associated with depletion of *lmo4a* is reduction, but not total loss, of HSC markers in the AGM region. As markers of HSC derivatives in the CHT and thymus were also reduced, the reduction of HSC markers in the AGM likely corresponds to a *bona fide* reduction in numbers of HSCs, although we did not confirm this functionally by isolating and transplanting into irradiated recipients. Reduction in HSC-derived populations is unlikely to reflect an HSC homing defect, as we see fewer EHT events initiating in *lmo4a* morphants, and rarely see these cells enter circulation. Due to a gene duplication that occurred early in the evolution of ray-finned fish (Taylor et al., 2003), a second orthologue of the *lmo4* gene is present. This version, *lmo4b*, is closer in sequence and synteny to human *lmo4*. When depleted in the zebrafish, it causes loss of mesodermal and ectodermal markers, including those of the arterial programme, precluding an assessment of a potential role in the programming of HSCs. As *lmo4a* is expressed within the dorsal aorta, it is likely to be acting cell autonomously in generating HSCs. In contrast, *lmo4b* is not expressed in the dorsal aorta,

but in the somites, mirroring *lmo4* expression in the mouse and frog (Hahm et al., 2004) (Aldo Ciau-Uitz, *unpublished*). However we cannot rule out that *lmo4b* influences HSC development through cell non-autonomous mechanisms, distinct from its role in maintaining mesodermal and ectodermal tissues. For example, *lmo4b* could be required for paracrine signalling from the somites to the dorsal aorta, which has been shown to play a role in programming HSCs (Ciau-Uitz et al., 2010; Gering and Patient, 2005).

In the mouse and *Xenopus laevis*, *lmo2* is expressed within the dorsal aorta (Landry et al., 2009) (Aldo Ciau-Uitz, *unpublished*). Zebrafish *lmo4a*, but not mouse or frog orthologues, is expressed in the dorsal aorta (Hahm et al., 2004) (Aldo Ciau-Uitz, *unpublished*). It is therefore possible that in higher vertebrates, the role of *lmo4a* in the zebrafish dorsal aorta has been replaced by *lmo2*. Consistent with this, no blood defects were observed in the *lmo4* knockout mouse (Hahm et al., 2004). In contrast, *lmo2* null mice lack primitive erythrocytes like *lmo4a* zebrafish morphants, and may have defective HSC production (Warren et al., 1994). Additionally, *lmo2* null ES cells fail to contribute to haematopoietic populations (Yamada et al., 1998). Thus, Lmo2 and Lmo4 proteins may have a degree of functional overlap, acting redundantly and dynamically competing with each other for the formation of protein complexes. This would predict that an *lmo4a* morphant phenotype would be restricted to regions lacking *lmo2* and *lmo4b*. As discussed, this is true in the dorsal aorta. Additionally, *lmo4a* is expressed weakly throughout the PLM at the 10 ss, whereas *lmo4b* is not expressed. While *lmo2* is strongly expressed in this tissue, it does not extend into the posterior most region at the 10 ss (Patterson et al., 2005; Xiong et al., 2008). Consistent with this, in *lmo4a* morphants, we do not observe a loss of PLM markers, except in the posterior most region. However, knockdown of *lmo2* results in loss of markers of PLM (Patterson et al., 2007); perhaps as the weak levels of *lmo4a* cannot compensate for loss of *lmo2*.

As *lmo4b* is genetically and functionally closer to its vertebrate homologues, and Lmo proteins are structurally similar (Bach, 2000; Deane et al., 2004; El Omari et al., 2011), the duplication of the *lmo4* gene in zebrafish may have allowed *lmo4a* to evolve a new role in the dorsal aorta. Therefore *lmo4b* would represent an ancestral function of the gene, and *lmo4a* a novel function. Alternatively, an ancient

lmo4 gene, prior to duplication, may have had a functional output equivalent to the sum of the outputs of *lmo4a* and *lmo4b*. Post duplication, *lmo4a* retained its role in the dorsal aorta and lost other earlier functions, whereas *lmo4b* lost its role in the dorsal aorta, while retaining its earlier functions (Caetano-Anollés, 2010). This second scenario provides a natural conditional context within which to study the role of *lmo4* in the dorsal aorta. In a similar manner, Drosophila has a single Hedgehog gene, and through duplication events, mice and zebrafish have evolved respectively three and five hedgehog orthologues, which have evolved different expression and functions (Avaron et al., 2006; Ingham and McMahon, 2001; Ingham et al., 2011; Shimeld, 1999).

The transcription factor Scl is required for the specification, but not maintenance, of the HSC (Mikkola et al., 2003; Porcher et al., 1996; Robb et al., 1996), and Lmo4 has been shown to interact with Scl in transfected HEK cells (Joshi et al., 2009). It is therefore possible that Lmo4 and Scl work together in the zebrafish AGM, in a similar manner to Lmo2 and Scl (Chapter 3), and may form a similar basal complex bridging Gata and E-box sites, as has been suggested for the formation of inhibitory v2b-interneurons (Joshi et al., 2009). Of note, the deleted region in *lmo4a* splice morphants contains an arginine, the equivalent of the R86 residue in Lmo2, and lies in a structurally similar region (Deane et al., 2004). We have previously shown that this residue is required for the interaction of Lmo2 with Scl (Figure 3.4). Thus, if stable protein were made, its potentially important interaction with Scl is likely to be abolished.

In human breast cancer patients and cell lines, elevated *lmo4* has been shown to play a role in cell cycle progression, and has been associated with cell invasion and poor clinical prognosis (Montanez-Wiscovich et al., 2009; Sum et al., 2005; Visvader et al., 2001; Wang et al., 2007). Invasion of solid tumors requires an EMT (Yoo et al., 2012), a process which shares similarities with the EHT (Karima Kissa, *personal communication*), and Lmo4 may play direct and indirect roles in both these processes. Additionally, it has been demonstrated that a haemodynamic force, associated with blood flow, acting on the endothelial walls of the aorta is required for maintenance of HSC markers after initiation of their expression, and hence emergence of HSCs (Adamo et al., 2009; North et al., 2009; Wang et al., 2011). Furthermore, *lmo4* is a mechanosensitive gene, whose expression is increased in the

absence of circulation in mouse carotid arteries (Ni et al., 2010). As will be seen in the next chapter, overexpression of *lmo4a* may also result in the generation of fewer HSCs, suggesting that *lmo4a* may be partly responsible for coupling blood flow with HSC production, although we are yet to demonstrate this.

4.11.3 Presumptive partners of Lmo4 are required for HSC production

Novel protein partners of Lmo4 in MEL cells have been previously identified (Charlotte Andrieu-Soler, *unpublished*). We have knocked down the zebrafish orthologues of the corresponding genes and find that all the partners we look at are, like *lmo4a*, required for production of HSCs. However, we have not formally shown that the Lmo4 complex assembles in the floor of the dorsal aorta. Nevertheless, the fact that all the components are expressed within this tissue and give the same phenotype with respect to the HSC when knocked down, suggests that these components of the erythroid complexes also have a role in programming the HSC. This is similar to the reuse of Lmo2-Scl containing complexes in various developmental contexts, albeit with varying requirements for Scl DNA binding (Kassouf et al., 2008; Patterson et al., 2007; Schlaeger et al., 2004). It is unsurprising that complexes are reused because, of all the possible permutations for interactions within the proteome, only a subset would be functional, and these are likely to be selected and refined during evolution. The pull-down experiments, by which the complex was identified, represent a sum of all the interactions for a given cellular context. Therefore, while all the proteins may be contained within the same complex, it is also possible that various distinct Lmo4 complexes form, with overlapping and distinct roles.

Lmo proteins often act as a molecular scaffold together with Ldb proteins (Bach, 2000) (Chapter 3). Although, Lmo4 can bind with high affinity to both Ldb1 and Ldb2 (Agulnick et al., 1996; Jurata et al., 1996; Sugihara et al., 1998), only *ldb2* is expressed in the zebrafish dorsal aorta (Wenchao Gu and Rui Monteiro, *unpublished*). This is in contrast to MEL cells, where *ldb1*, but not *ldb2*, is expressed (Charlotte Andrieu-Soler, *unpublished*). Interestingly therefore, *ldb2*, but not *ldb1*, morphant zebrafish also fail to produce HSCs. Furthermore, like *lmo4a* morphants, *ldb2* morphants also lack ISVs

(Wenchao Gu and Rui Monteiro, *unpublished*). Taken together, this suggests that Lmo4 acts together with Ldb2 in the zebrafish dorsal aorta to nucleate protein complexes.

While Lmo4 and its partners are all required for HSC programming, our data also uncovers a differential requirement for various components of the complex elsewhere. For example, Hdac7 morphants have normal expression of *msr* in the vein, whereas morphants for *lmo4a* and its other partners have reduced *msr* expression, although the vein still forms part of a competent circulatory loop in all cases. Additionally, in *lmo4a* and *hdac7* morphants, the yolk cell failed to elongate between 2 dpf and 5 dpf, suggesting a possible role for these genes in this developmental process. Additionally, as expression of many of the genes studied in this chapter fade in the dorsal aorta from around 24 hpf, it is possible that some components of the putative complex are required to set up EHT, but are not required thereafter, as has been reported for *runx1* (Chen et al., 2009).

Thus our data, taken together with the pull downs carried out in MEL cells, suggests that, at least in the floor of the zebrafish dorsal aorta, Lmo4a is likely to form obligate interactions with Bcor, Ep400, Hdac7 and Ncor. However, we cannot formally exclude the possibility that they function independently of each of other within the same tissue, and have not yet attempted to disrupt the presumed interactions in the zebrafish. It is unlikely that these proteins are obligate functional partners of Lmo4b prior to HSC emergence, as their knockdown phenotype does not result in the loss of mesodermal and ectodermal markers associated with *lmo4b* morphants. However it is possible that their interactions become necessary later, given the similarity between the expression domains of *lmo4b* and the Lmo4 partners. We however have not investigated this due to the confounding earlier *lmo4b* morphant phenotype.

4.11.4 *Lmo4* and some of its partners may be required for angiogenesis

The *de novo* HSC generation by EHT, and the generation of primary ISVs, involve similar initial events. Both processes initiate from the dorsal aorta, albeit in a polarised fashion, and involve ablumenal bending of endothelial cells. EHT events are observed in the floor and ISV sprouts from the roof of the dorsal aorta. Indeed, the protease activated receptor Par1 has been shown to be

important in both processes (Hirano, 2007; Yue et al., 2012). Furthermore, some of the signals that set up a transiently polarised dorsal aorta have been identified. The domain of Hedgehog signalling from overlying midline structures extends only into the roof of the dorsal aorta, whereas Bmp signalling from the mesenchyme underlying the dorsal aorta does not extend beyond its floor (Wilkinson et al., 2009). It has previously been observed that endothelial cells in the dorsal aorta are dynamic; for example, individual cells can migrate between dorsal, lateral and ventral aspects of the vessel (Kissa and Herbomel, 2010). This raises the intriguing possibility that prior to polarisation, cells of the dorsal aorta are already biased to become endothelial tip and stalk cells, HSCs, or to remain as endothelial cells, but must actively position themselves correctly along the graded axes of cell-extrinsic factors for that fate to be realised.

We have shown that some *lmo4a* and *ep400* morphants fail to develop primary ISVs, suggesting that they are independently, or cooperatively required for angiogenesis. To date, we have not confirmed that these phenotypes are specifically associated with the morpholinos, as we were unable to reproduce them with a second morpholino, and in the case of *lmo4a* morphants, unable to rescue the defect. Nevertheless, given the possibility that EHT and ISV sprouting from the dorsal aorta are mechanistically linked, and that Lmo4a and Ep400 act together in both processes, we further investigated the loss of ISVs in *lmo4a* morphants. We show that tip cells begin to form sprouts, but that these fail to mature, and that the vascular plexus in the CHT fails to fully form. Mice lacking *lmo4* have not been reported to show angiogenic defects (Hahm et al., 2004; Tse et al., 2004). However, *lmo2* null mice display defects in angiogenesis (Yamada et al., 2000), therefore it is possible that during evolution, *lmo2* has replaced the angiogenic role of *lmo4*, as we proposed may be the case for the EHT. Alternatively, *lmo4a* may have acquired an angiogenic function in the zebrafish.

The initiation of ISV sprouting but failure to resolve to mature sprouts, that we see in *lmo4a* 5'UTR morphants, is a hallmark of *vegfa* zebrafish morphants (Isogai et al., 2003). Tip cells respond to guidance cues from vegf, and stalk cells proliferate in response to vegf (Krueger et al., 2011). Although we do not see a transcriptional effect on *vegfa* expression, it is possible that *lmo4a* is involved in transducing vegf signalling, or is transcriptionally downstream of it, although we have not tested this.

We also noted that the expression of the vegf receptor *flk1* was reduced in *lmo4a* morphants, although this is unlikely to be a cause of the sprouting defects, given that we detect reduced expression several hours after we first detect failure in ISV sprouting. Additionally, *flt1* has been reported to act negatively on the formation of tip cells and angiogenic branches in both the zebrafish and mouse, possibly by acting as a decoy receptor for vegfa, reducing its extracellular availability (Fong et al., 1995; Gerhardt et al., 2003; Krueger et al., 2011; Roberts et al., 2004). Previous work has demonstrated a role for *tbx20* in the roof of the dorsal aorta in generating ISV sprouts (Szeto et al., 2002), and its reduced expression in both *lmo4a* and *ep400* morphants may therefore also explain the absence of ISVs.

Chapter 5

Regulation of *gata2* is critical for specification of the first HSCs

5.1 Introduction

In the previous chapter, we have shown that there is a failure of HSC production in *lmo4a* morphants. In this chapter, we propose a genetic model to describe how *lmo4a* is functioning in the zebrafish dorsal aorta to specify HSCs. The model involves inputs from both Bmp signaling and *lmo4a* into *gata2a*, whose level in turn regulates expression of the master HSC regulator *runx1*.

The Gata family consists of a group of six transcription factors, each with tandem zinc fingers. They modulate gene expression in multiple tissues by binding the six nucleotide cognate consensus sequence WGATAR (Orkin, 2000). Expression of *gata1, 2* and *3* is restricted mainly to haematopoietic tissues, and both knockout and overexpression studies have revealed distinct and overlapping roles for these genes at multiple locations and stages of haematopoiesis (Orkin, 2000). In the mouse, *gata2* is expressed in developing and adult HSPCs, progenitors of the myeloid lineage and mast cells (Rodrigues et al., 2008; Rodrigues et al., 2005; Tsai et al., 1994). Its specific expression within the HSPC compartment is directed by a set of cis-acting elements. A 2.8 kb region lying upstream of the transcription initiation site confers HSPC activity, whereas a second region 1.8 kb upstream represses *gata2* during development of erythrocytes, partly through the increasing expression of *gata1*. Additionally, the *gata2* cis-elements contain consensus Gata sites, which allow for both auto- and Gata1-regulation (Snow et al., 2010; Snow et al., 2011). Furthermore, somatic mutations in *gata2*, causing premature termination of translation, or disrupting interactions between the *gata2* zinc fingers and DNA or protein, have been implicated in human disease (Adamo et al., 2009; Dickinson et al., 2011; Hahn et al., 2011; Hsu et al., 2011; Ostergaard et al., 2011; Rodrigues et al., 2012; Zhang et al., 2008).

gata2-null mice die at E10-11 due to severe anaemia (Tsai et al., 1994). In gata2 null/wild type chimeras, *gata2* null cells failed to generate a myeloid or erythroid output *in vivo*, and cultured *gata2* null ES cells had reduced responsiveness to cytokines, such as stem-cell factor (Tsai et al., 1994; Tsai and Orkin, 1997). These data suggested a role for *gata2* in the HSC, which was confirmed by analyzing *gata2*$^{+/-}$ mice, which show defects in the generation, self-renewal and expansion of the first HSCs in the AGM region, yolk sac and bone marrow (Ling et al., 2004). In adult mice, it has been demonstrated

that disruption of *gata2* results in HSCs that are both qualitatively and quantitatively compromised. HSCs in *gata2*$^{+/-}$ mouse bone marrow show increased apoptosis and increased quiescence, but self-renewal and lineage potential were not affected (Rodrigues et al., 2005). By contrast, two-fold upregulation of *gata2* expression in adult HSCs causes a 40-fold reduction in their numbers and loss of differentiation potential upon transplantation (Persons et al., 1999). Furthermore, enforced expression of *gata2* in human cord blood blocks the repopulation ability of HSCs and leads to increased G_0 residency (Tipping et al., 2009).

Bmp signaling has previously been shown to feed into *gata2* expression. In the ventral blood island (VBI) of the frog *Xenopus laevis*, a tissue which generates primitive blood, expression of *gata2*, but not the endothelial marker *fli1*, is dependent upon Bmp signaling. In the DLP, the lateral mesoderm precursor to the HSCs in Xenopus, Bmp is required to confer haematopoietic characteristics, and here both *gata2* and *fli1* are dependent on Bmp (Walmsley et al., 2002). However it is possible that the Bmp effect in the DLP is in fact due to an earlier requirement, rather than a direct effect in this tissue. Additionally, it has been shown in the zebrafish that Bmp signaling is required for the expression of *gata2* in the PLM, the single tissue that represents the equivalent of VBI and DLP (Liu et al., 2008). Ectopic Bmp is capable of inducing blood, and expression of the dominant negative BMP receptor has the opposite effect (Dale et al., 1992; Graff et al., 1994; Jones et al., 1992; Maeno et al., 1994; Robin and Durand, 2010). In both the zebrafish and mouse, *bmp4* is expressed just ventrally to the dorsal aorta, and is one of the few signals that has been shown to drive the generation, and possibly expansion, of the HSC from this tissue (Durand et al., 2007; Wilkinson et al., 2009). Additionally, it has been suggested that *bmp4* is required to maintain HSCs in adult murine bone marrow (Goldman et al., 2009). Recent data however suggest that Bmp signaling may not represent a necessary event for HSC programming in the chick and frog (Thierry Jaffredo and Stuart Meiklejohn, *personal communications*). Nevertheless, here we provide the first evidence that Bmp signaling regulates *gata2* expression in the dorsal aorta to control the production of HSCs in the zebrafish, and suggest that this relationship is modulated by the activity of *lmo4a*.

5.2 Knockdown of *lmo4a* causes an increase in *gata2a* expression

In the zebrafish, presumably as a result of an ancient duplication of the genome (Taylor et al., 2003), there are two orthologues of mammalian *gata2*, *gata2a* and *gata2b* (Zv9 Genome Build, Ensembl). To date, the role of *gata2b* has not been investigated. At the protein level, Gata2a shares 71% identity with human and mouse Gata2, whereas Gata2b shares around 54% identity with its human and mouse orthologues (Figure 5.1A). Therefore Gata2a is more closely related to its mammalian orthologues than Gata2b. In the zebrafish, *gata2a* is expressed maternally and then ubiquitously up to the tailbud stage (Figure 5.1 B-D). By the 10 ss, *gata2a* expression becomes restricted to the ALM and PLM, with expression in the PLM overlapping with that of *gata1* (Figure 5.1 F-F' and Figure 4.21F). Subsequently, *gata2a* becomes restricted to the ICM, dorsal aorta and PBI, haematovascular tissues derived from the PLM. It is also expressed in the developing spinal cord, lateral line and head region (Figure 5.1 G-I), consistent with previously reported roles for *gata2* in neural development in the mouse (Kala et al., 2009; Zhou et al., 2000). Within the dorsal aorta, *gata2a* is expressed throughout the vessel. Expression of *gata2a* in the ICM and dorsal aorta, respectively the initiating sites of primitive and definitive haematopoiesis in the zebrafish, is consistent with the known role of Gata2 in both primitive and definitive blood development in the mouse (Fujiwara et al., 2004; Ling et al., 2004; Rodrigues et al., 2012; Tsai et al., 1994).

In contrast to *gata2a*, *gata2b* is not expressed maternally, with expression turning on between the 1000-cell stage and 30% epiboly, and remaining ubiquitously throughout the embryo up to the 15ss (Figure 5.1 J-O). From 24 hpf, stronger expression is also observed in the dorsal aorta (Figure 5.1 P-Q). In the mouse, *gata2* is expressed in the lateral mesoderm, P-Sp, AGM region, including rounded cells in the dorsal aorta, and in neural tissues (Minegishi et al., 1999). In *Xenopus* laevis, *gata2* is expressed maternally and then in the VBI, the site of primitive blood development, the DLP, which is partially equivalent to the PLM in the fish and is the precursor to the dorsal aorta where *gata2* is also expressed, the head region, developing spinal cord and lateral line nerve (Partington et al., 1997) (Aldo Ciau-Uitz, *unpublished data*). Thus, the expression profile of *gata2a* absolutely overlaps with expression

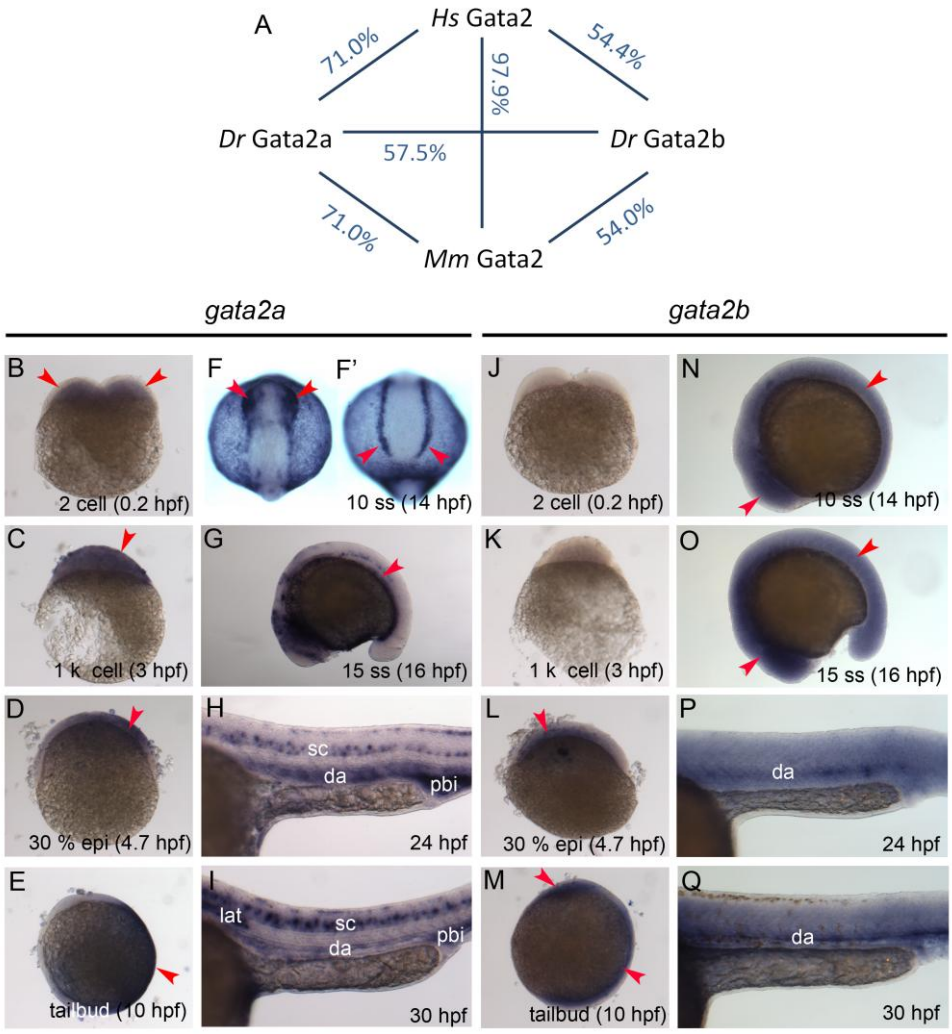

Figure 5.1 Expression of *gata2a* and *gata2b* in the zebrafish

(A) Amino acid pairwise identity between Human (*Hs*) ENSP00000345681, mouse (*Mm*) ENSMUSP00000015197, and zebrafish (*Dr*) ENSDARP00000076860 and ENSDARP00000120165 Gata2 orthologues. (B – E) *gata2a* is expressed maternally and at the tailbud stage, followed by expression in the anterior and posterior lateral plate mesoderm (F – F') and intermediate cell mass (G). (H – I) *gata2a* is expressed in the spinal cord (sc), dorsal aorta (da), posterior blood island (pbi) and lateral line (lat). (J – K) *gata2b* is not expressed maternally; expression starts between the 1 k cell stage and 30% epiboly. (L – Q) *gata2b* is expressed ubiquitously throughout the embryo, with stronger specific expression in the dorsal aorta. (F – F') Anterior and posterior lateral plate is imaged dorsally; all other embryos are imaged laterally.

of *gata2* orthologues in both the mouse and frog, whereas *gata2b* only overlaps with the dorsal aorta expression.

We have previously shown that knockdown of *lmo4a* results in defective HSC emergence, and that *lmo4a* does not lie transcriptionally up- or down-stream of Notch signalling, or upstream of *bmp4*, both signals having been shown to be important in HSC development. However, we noted that expression of *gata2a*, whose orthologue in mouse is known to be required for HSC production, was increased in *lmo4a* morphants, most notably at 31 hpf (Figure 5.2 A-F). Expression of *gata2a* was increased in the dorsal aorta, as well as the neural tissue and the PBI. We went on to quantitate this effect. We dissected the trunk and tail of Tg(*kdrl*:EGFP) animals, generated a single cell suspension, and sorted gfp positive cells, thus enriching for vascular cells. These constituted about 2.5% of the total cell population (Figure 5.3 A-F). Quantitative RT-PCR analysis revealed a 2.5 fold increase in *gata2a* expression in *lmo4a* morphants (Figure 5.3G). This was surprising, as siRNA mediated knockdown of *lmo4* in MEL cells results in decreased *gata2* expression (Charlotte Andrieu-Soler, *unpublished*). It is likely that the transcriptional input from *lmo4a* to *gata2a* is direct, as in ChiP-seq experiments in MEL cells using the same tagged Lmo4 construct used to identify a novel erythroid complex (Chapter 4) binding of Lmo4 in the vicinity of the *gata2* locus was revealed (Figure 5.2M) (Charlotte Andrieu-Soler, *unpublished data*). Several peaks, representing Lmo4 binding in MEL cells, are present in the region lying 4.0 to 9.5 kb upstream of the translation start site, and probably represent the promoter region. Additionally, there is strong binding 0.25 to 1.25 kb downstream of exon 4, likely representing an intronic enhancer (Figure 5.2M). However, we have not confirmed that direct binding occurs in the cells isolated from the zebrafish trunk and tail. In contrast to expression of *gata2a*, we do not observe an increase in *gata2b* expression in the *lmo4a* morphants, but rather a moderate decrease (Figure 5.2 G-I), which is consistent with the siRNA knockdown experiments in MEL cells (Charlotte Andrieu-Soler, *unpublished*). Expression of *runx1* was reduced in all *lmo4a* morphants, serving as a positive control (Figure 5.2 J-L).

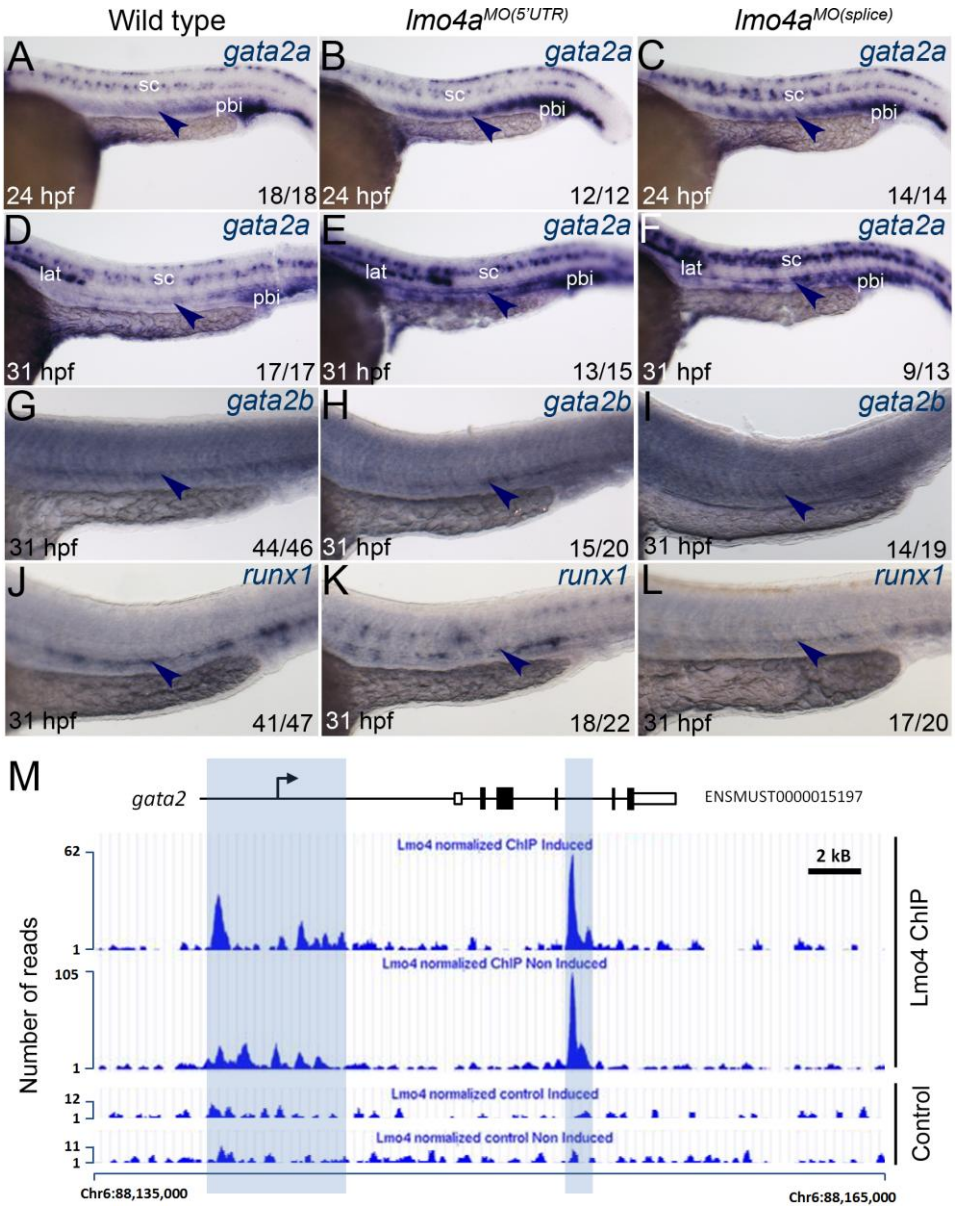

Figure 5.2 Knockdown of *lmo4a* causes an increase in *gata2a* expression

(A – F) *lmo4a* morphants have increased expression of *gata2a* in the trunk and tail; sc, spinal cord; pbi, posterior blood island; lat, lateral line nerve. (G – I) Expression of *gata2b* is not increased in *lmo4a* morphants. (J – K) *runx1* expression is reduced in *lmo4* morphants. All embryos viewed laterally; blue arrowhead, dorsal aorta. (M) ChIP-seq data from mouse erythroleukaemic cells. Biotin tagged Lmo4 directly binds the *gata2* promoter region, and a region in intron 4 of the *gata2* locus in induced (top track) and non-induced (lower track) mouse erythroleukaemic cells. Control tracks represent ChIP from BirA expressing MEL cells (C Andrieu-Soler, *unpublished data*).

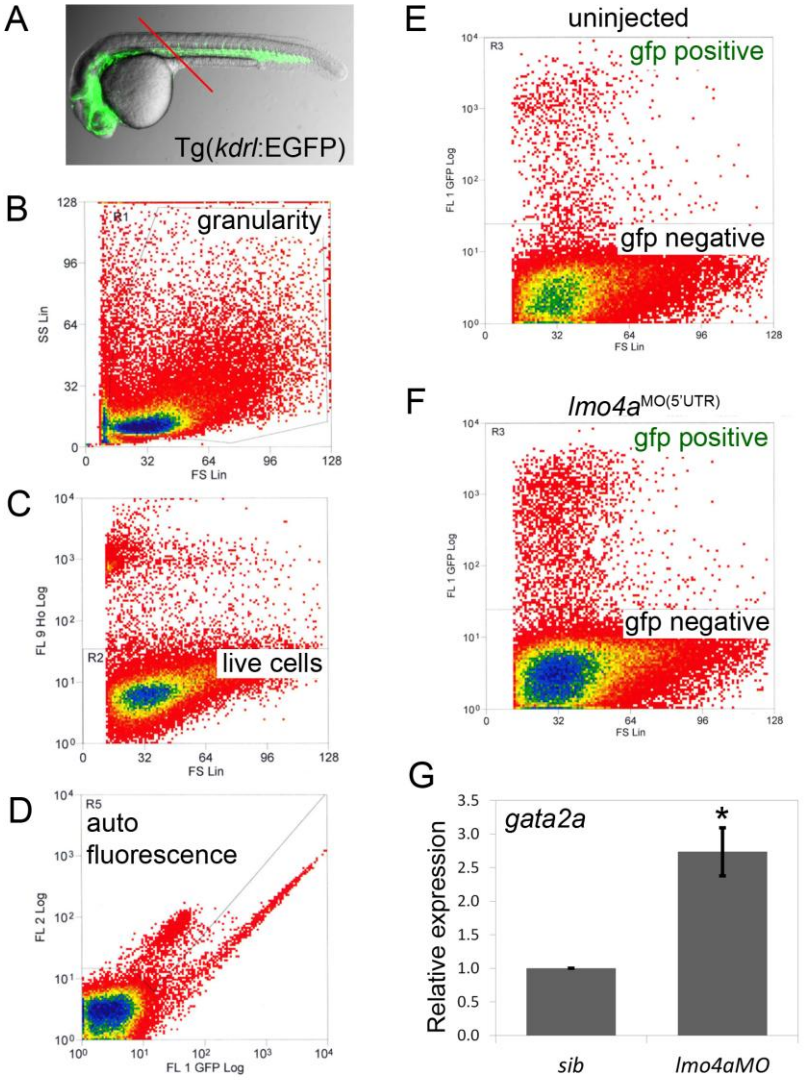

Figure 5.3 Expression of *gata2a* is increased in sorted vascular cells in *lmo4a* morphants

(A) The trunks and tails were dissected from Tg(*kdrl*:EGFP) animals, in which *gfp* expression is directed to the vasculature. Approximate location of the cut is indicated by the red line. (B – D) Single cell suspensions from excised trunks and tails were gated on their granularity and live hoechst negative cells. Auto fluorescent cells were excluded. From the resultant population, GFP positive cells were isolated (E – F). Representative plots are shown. (G) Levels of *gata2a* in the isolated GFP positive populations were assessed by RT-qPCR. Error bars are representative of the standard error from three biological replicates; * $p<0.05$.

5.3 Overexpression of *gata2* results in fewer HSCs

Overexpression of the transcription factor *gata2* in adult HSCs has been shown to have a negative impact on their quantity and quality (Heyworth et al., 1999; Persons et al., 1999; Tipping et al., 2009). As HSCs are not produced in *lmo4a* morphants, and show increased *gata2a* expression, we hypothesised that overexpression of *gata2* may also have a negative impact on the emergence of HSCs in the AGM region. As Gata2 is required for early development, for example in the induction of haematopoietic mesoderm (Maeno et al., 1996), we took advantage of a conditional strategy to overexpress *gata2* in a time-dependent manner, such that our interpretation was not confounded by events occurring earlier in development. The *Xenopus laevis* orthologue of *gata2* was fused to the glucocorticoid receptor, which sequesters Gata2 in the cytoplasm. Upon addition of the hormone dexamethasone, the *gata2* fusion protein will translocate to the nucleus to affect gene expression (Aldo Ciau-Uitz, *unpublished data*). The *gata2* fusion was introduced as RNA into embryos and activated from the 15-16ss by dexamethasone treatment (Figure 5.4A). The conditional overexpression of *gata2* resulted in specific loss of *runx1* expression in the dorsal aorta when compared to embryos where the *gata2* fusion was not activated (Figure 5.4 B-G). This recapitulates the phenotype seen in *lmo4a* morphants, and it is therefore likely that the RNA is stable and dexamethasone is penetrating the embryos. The effect on *runx1* was seen at 26 hpf, but was most robustly observed at 30 and 35 hpf, as cells in the floor of the dorsal aorta begin to undergo EHT, likely reflecting the reduction in the variation of *runx1* expression that we see over this period of time. Expression of *runx1* in the head was never affected (Figure 5.4 B-G). Additionally, dexamethasone-treated embryos showed loss HSC-derived T-cell progenitors in the thymus at 4 dpf, while development of the thymic epithelium was unaffected (Figure 5.4 H-K). We therefore conclude that, like in *lmo4a* morphants, overexpression of *gata2* results in a loss of HSCs.

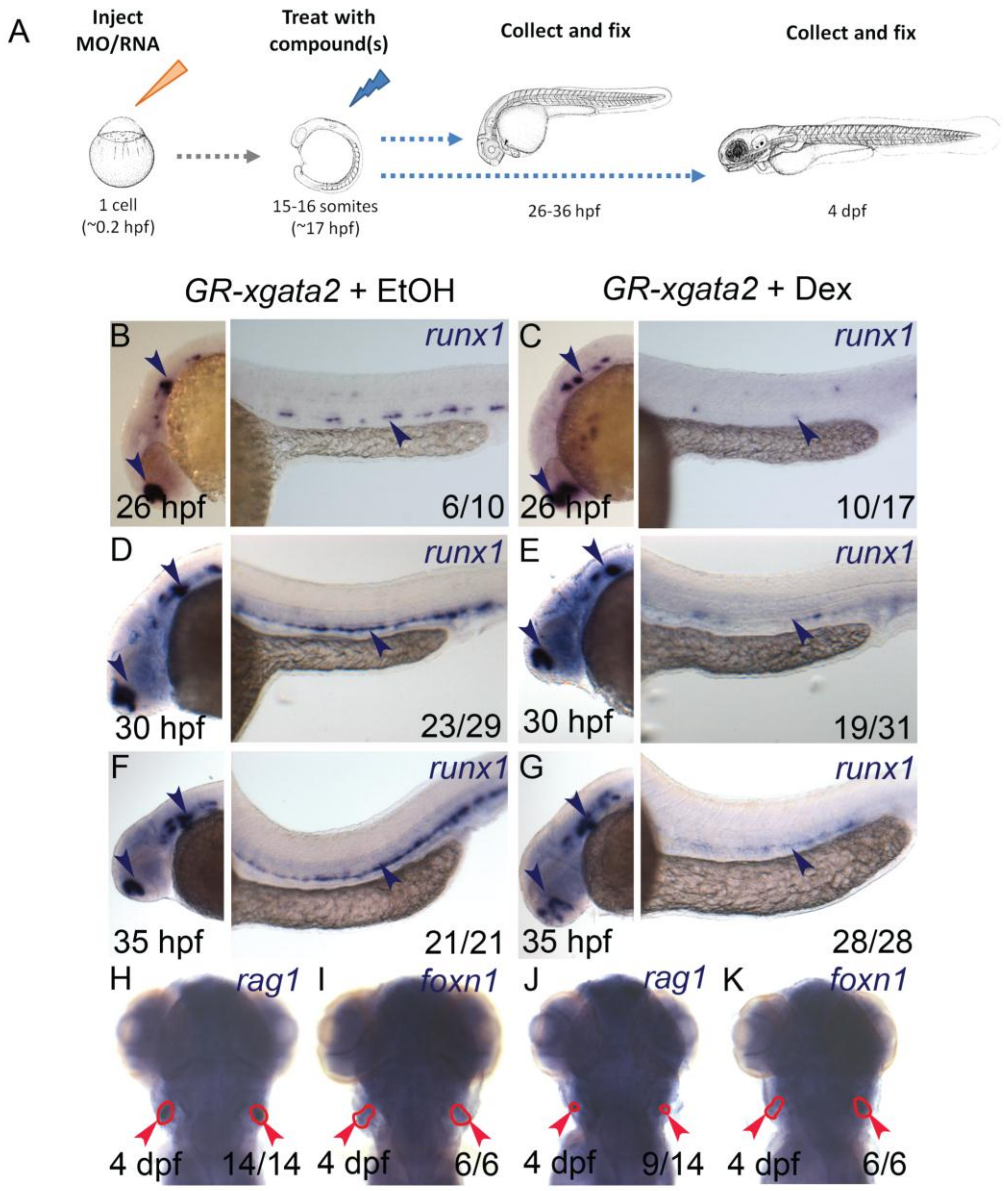

Figure 5.4 Conditional overexpression of *gata2* causes a reduction in haematopoietic stem cells

(A) Embryos were injected with 100 pg of *GR-xgata2* RNA and grown in media containing dexamethasone (Dex) or ethanol (EtOH) from the 15 – 16 somite stage. Ethanol was used as a control for the solvent used to dissolve dexamethasone. (B – G) Expression of the HSC marker *runx1* is specifically reduced in the dorsal aorta upon induction of *gata2*. Embryos imaged laterally. (H – K) *rag1* positive T-cells derived from HSCs are reduced upon induction of *gata2*, but *foxn1* positive thymic tissue is unaffected. Embryos imaged dorsally.

5.4 *gata2a* morphants have a similar phenotype to *lmo4b* morphants

Having shown that *lmo4a* morphants have increased expression of *gata2a* and fail to produce HSCs, and artificial overexpression of Xenopus *gata2* results in the same HSC defect, we reasoned that it should be possible to rescue *lmo4a* morphants by knocking down *gata2a* in *lmo4a* morphants. Given that we would only want to knock *gata2a* down to wild type levels, as *gata2* is required for production of HSCs in the mouse AGM (Ling et al., 2004; Nottingham et al., 2007), we investigated the possibility of using antisense morpholinos targeting *gata2a*, as they can be titrated to yield varying degrees of knockdown, although we were conscious of the lack of temporal control over the knockdown (Eisen and Smith, 2008; Summerton and Weller, 1997). We took advantage of a previously published *gata2a* splice morpholino (Galloway et al., 2005), and designed a novel translation-blocking morpholino. We showed that the splice morpholino resulted in the accumulation of mis-spliced transcript lacking exon 4 (Figure 5.5 A-B). As *gata2* is important in programming ventral mesoderm early in development (Maeno et al., 1996), we were not surprised that expression of the blood and endothelial genes *fli1, scl, gata1* and *pu1* in the PLM, but not the cardiac marker *nkx2.5*, were reduced, most notably in *gata2a* splice morphants (Figure 5.5 C-Q). This effect correlates with the *gata2a* domain of expression at this stage (Figure 5.1 F-F"). We were however surprised that the *gata2a* morphant phenotype was mild at this stage. This may reflect compensation from *gata2b*, although we did not investigate this potential input further.

At 20 hpf, we noted a slight reduction of *gata1* expression in the ICM of *gata2a* morphants, as previously reported (Figure 5.6 A-A") (Galloway et al., 2005). Expression of the HSC markers *runx1* and *ikaros* were reduced in the dorsal aorta of *gata2a* splice and ATG morphants from 24 to 28 hpf. However between 28 and 48 hpf, expression recovered in the *gata2a* ATG morphants (Figure 5.6 B-H"). The recovery of the HSC markers *runx1* and *ikaros* likely reflects loss of activity of the ATG morpholino, and suggests that *gata2a* is required not only for the initiation of HSC marker expression in the dorsal aorta, but also its maintenance. Consistent with this observation, at 4 dpf, *rag1, gata1, ikaros* and *cmyb*, markers for HSCs and their derivatives in the thymus and CHT, are reduced in *gata2a*

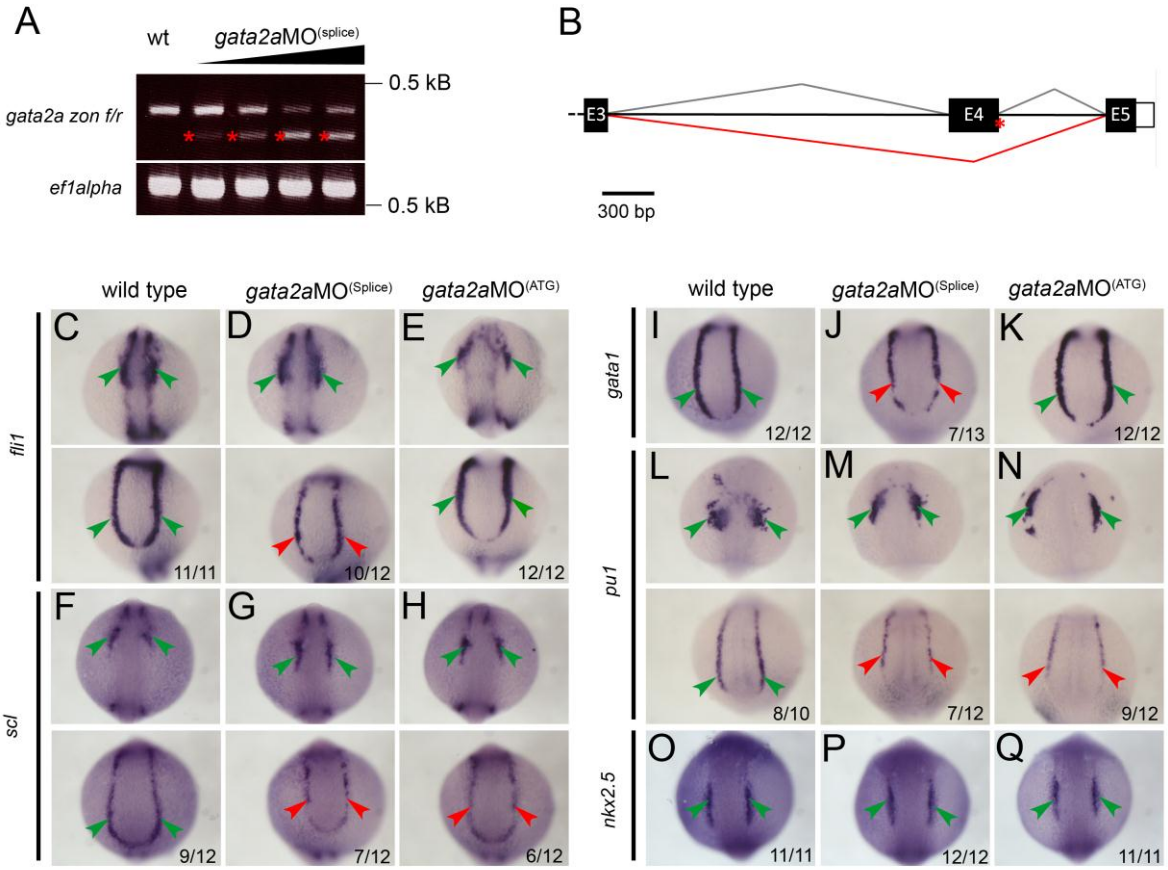

Figure 5.5 Knockdown of *gata2a* results in a reduction in posterior lateral plate markers

(A) Aanalysis of cDNA from embryos injected with 2, 4, 8 and 16 ng of *gata2a* splice morpholino. The new band is indicated by the red asterisk. (B) Cloning of the new band revealed that exon 4 was skipped in *gata2a* splice morphants. (C – N) Expression of markers of cells in the anterior and posterior lateral plate mesoderm. All embryos imaged from the dorsal aspect. (C – H and L – N) Anterior, top panel; posterior bottom panel; (I – K) Posterior mesoderm; (O – Q) Anterior cardiogenic mesoderm. Green arrowheads, wild type expression; red arrowheads, reduced expression.

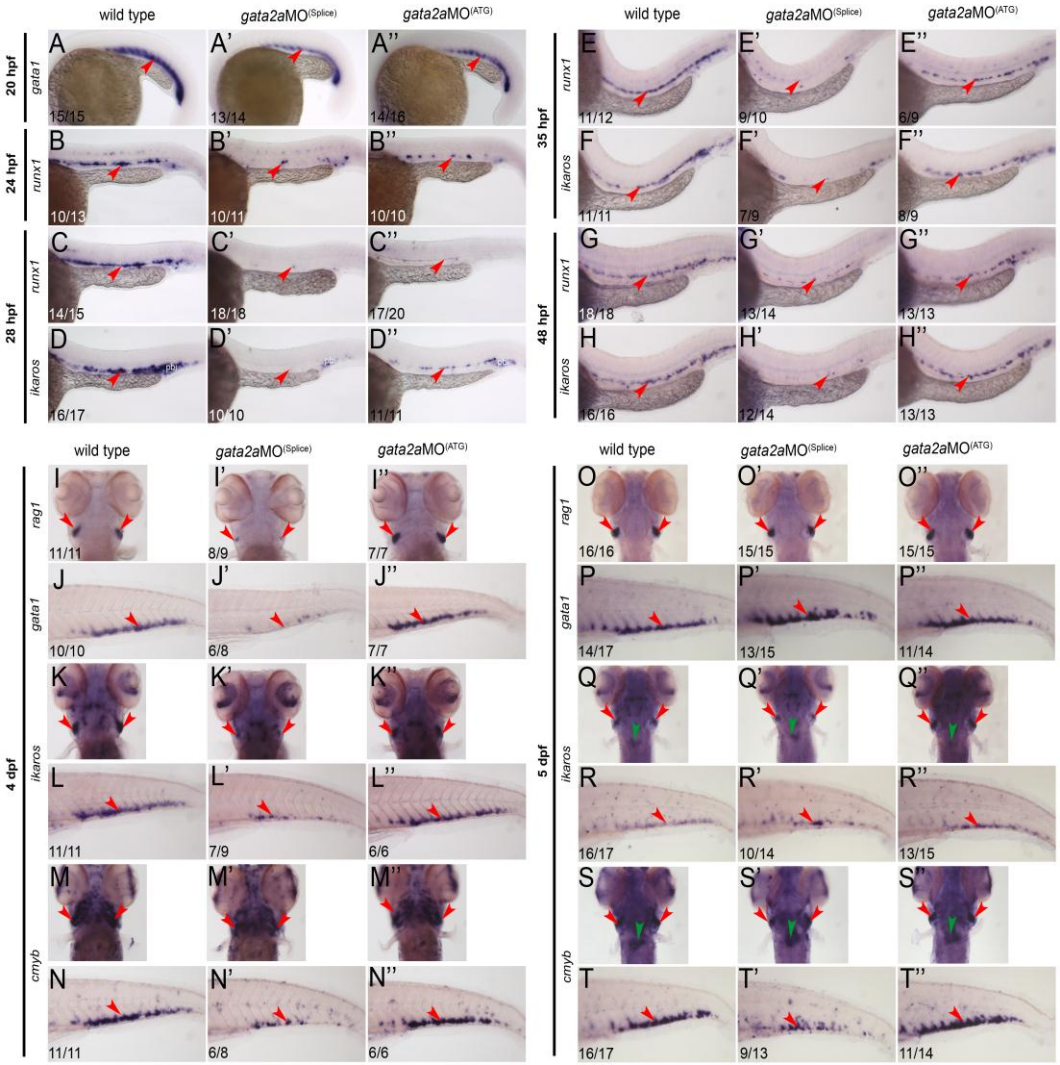

Figure 5.6 ***gata2a*** **morphants have fewer haematopoietic stem cells**

(A – A") Knockdown of *gata2a* results in a reduction in *gata1* expression. (B – H") Knockdown of *gata2a* results in a loss of HSC markers (red arrowheads). By 48 h, *gata2a* ATG morphants have recovered. (I – N") At 4 dpf, *gata2a* splice morphants, but not ATG morphants, have reduced expression of *rag1* and *ikaros* in developing T-cells, and *gata1, ikaros* and *cmyb* in the caudal haematopoietic tissue. (O – S") By 5 dpf, markers of HSCs and their derivatives in *gata2a* morphants are no longer reduced, including cells in the kidney (green arrowhead). (T – T") Expression of *cmyb* in the caudal haematopoietic tissue in *gata2a* slice morphants remains reduced.

splice morphants, but not *gata2a* ATG morphants (Figure 5.6 I-N"). By 5 dpf, expression of these markers, except *cmyb* in the CHT, recovered to wild type levels. This may represent loss of activity of the morpholino, or loss of the requirement for *gata2a*. These two possibilities are not mutually exclusive, however both possibilities would suggest that the remaining HSPCs expand to fully occupy the various niches.

We went on to look at markers for developmental stages that lie between the PLM and HSC. At 26 hpf, we observed a striking loss of markers of ectodermal and mesodermal derivatives, including the endothelial, arterial, venous, neural, pronephric fates, and primitive blood (Figure 5.7 A-I"). It has previously been reported through co-culture experiments in *Xenopus laevis*, that Gata2 functions in both mesoderm and ectoderm to direct globin gene expression. We did not look at any markers of populations derived from endoderm. Interestingly, the *gata2a* morphants mirror the *lmo4b* morphants (Figure 4.6), raising the possibility that *lmo4b* and *gata2a* function together, as has been demonstrated for the orthologues in human endothelial kidney cells (Joshi et al., 2009). Expression of *eto2* in the somites is unaffected in *gata2a* morphants, in contrast to *lmo4a* morphants, and *lmo4a* expression is not affected in *gata2a* morphants (Figure 4.6 B-B" and Figure 5.7 J-K"). It is thus more likely that *lmo4b* is epistatically upstream of *gata2a*. Thus, somitic gene expression is dependent only on *lmo4b*, whereas expression of markers of medial tissues are dependent on both *lmo4b* and *gata2a*. Additionally, expression of *gata2a* was increased in *gata2a* morphants (Figure 5.7 L-L"). While this suggests that *gata2a* may negatively autoregulate its expression in a similar manner to that of *gata1* in the CHT (Monteiro et al., 2011), we cannot exclude the possibility that this represents increased *gata2a* mRNA stability caused by the morpholino. Taken together, our data suggests that, like the mouse orthologue, *gata2a* may be required for HSC development in the zebrafish, however the data presented so far does not allow us to uncouple the potential HSC specific defects from earlier defects in the vasculature and somites.

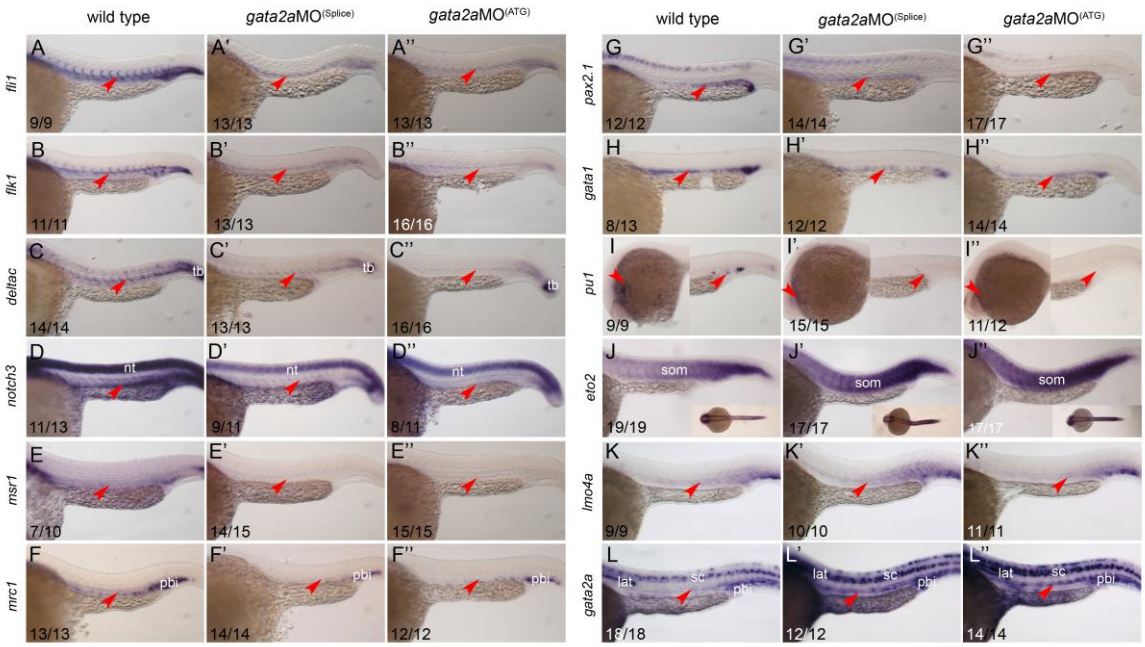

Figure 5.7 Ectodermal and mesodermal derivatives are lost at 26 hpf in *gata2a* morphants

Markers of the endothelium (A – B"), arterial programme (C – D"), venous programme (E – F"), pronephric duct (G – G"), and primitive blood (H – I") are reduced in the anterior, trunk and tail regions of *gata2a* morphants. (J – K") Expression of *eto2* and *lmo4a* is not reduced in *gata2a* morphants. (L – L") *gata2a* message is increased in *gata2a* morphants. Main panels viewed laterally; inserts viewed dorsally; nt, neural tube; tb, tailbud; som, somites; lat, lateral line; sc, spinal cord; pbi, posterior blood island.

5.5 Dose-dependent rescue of *lmo4a* morphants with a Gata antagonist

To overcome the pre-HSC defects seen in *gata2a* morphants, we made use of K-11706, a pharmacological inhibitor of Gata DNA binding activity, which has been shown to inhibit Gata2 activity (Nakano et al., 2004). This provided a degree of temporal control that we could not achieve with standard morpholinos. It has recently been reported that a zinc-finger nuclease induced truncation of zebrafish *gata2a* gene, lacking both zinc fingers may result in minor defects in vasculogenesis (Zhu et al., 2011b). Although the mechanism was not addressed, including the possibility that this was due to a dominant negative effect, the temporal control would allow us to bypass potential confounding influences on the HSC from defective vasculogenesis.

We treated embryos from the 15-16 ss. Therefore, although we did not investigate the pharmacodynamics and kinetics of K-11706 in the zebrafish, it is likely the compound would have penetrated the embryo as the HSC precursors reached the midline. Unsurprisingly, given the role of *gata2* in generating HSCs (Ling et al., 2004; Nottingham et al., 2007), we found that increasing the dose of Gata antagonist resulted in a progressive loss of *runx1* expression in the dorsal aorta, and a corresponding reduction in *rag1* expression in thymic T-cell progenitors (Figure 5.8 A-D and Figure 5.9 A-E). By titrating down the concentration of the compound, we were able to rescue the absence of *runx1* in *lmo4a* morphants (Figure 5.8 E-H). Using 10 μM of K-11706, we found that *runx1* expression was lost in the dorsal aorta, treatment with 2 μM of compound resulted in reduced *runx1* expression, and wild type *runx1* expression was observed in 78% of *lmo4a* morphants treated with 0.4 μM of compound (Figure 5.8 A-H). This suggested that the dose of Gata2 activity in the dorsal aorta was critical for the production of HSCs: both increased and reduced expression of *gata2* in the dorsal aorta results in loss of HSCs (Figure 5.8I). Consistent with this hypothesis, we were able to rescue the loss of *runx1* expression associated with specific overexpression of *gata2*, in a dose-dependent manner (Figure 5.9 F-J). It is thus unlikely that the rescues we see are due to other members of the Gata family, or off-target effects associated with the Gata inhibitor. However, as we are introducing *Xenopus gata2*, and frogs only have one *gata2* orthologue, by this approach we cannot differentiate between effects

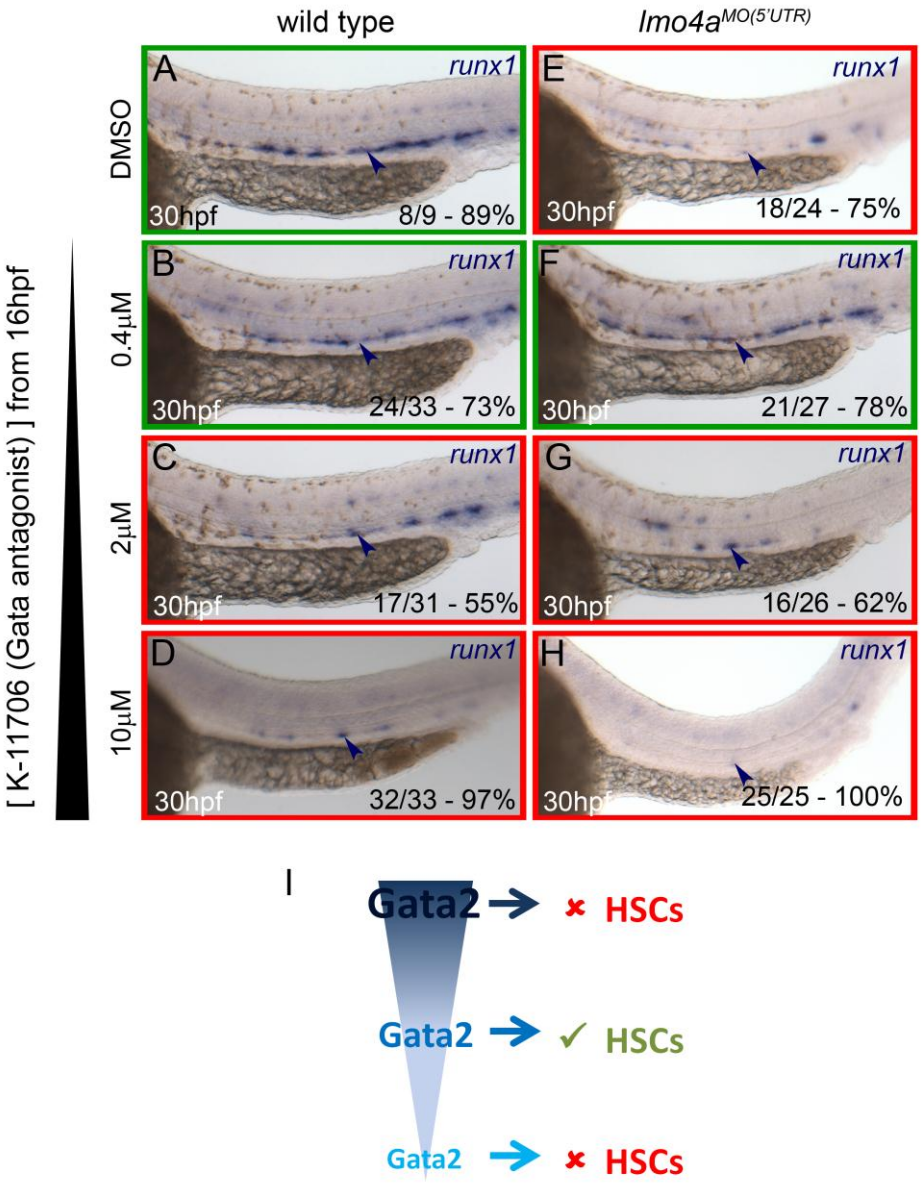

Figure 5.8 Dose-dependent inhibition of Gata activity rescues *lmo4a* morphants

(A – D) An increasing dose of the Gata antagonist K-11706 causes progressive loss of *runx1* expression. (B – H) Treatment with 0.4 µM of antagonist rescues *runx1* expression in *lmo4a* morphants, however at higher doses, expression of *runx1* is not rescued. Embryos imaged laterally; red boxes, reduced *runx1* expression; green boxes, normal *runx1* expression. (I) Model of Gata2 requirement in the HSC compartment.

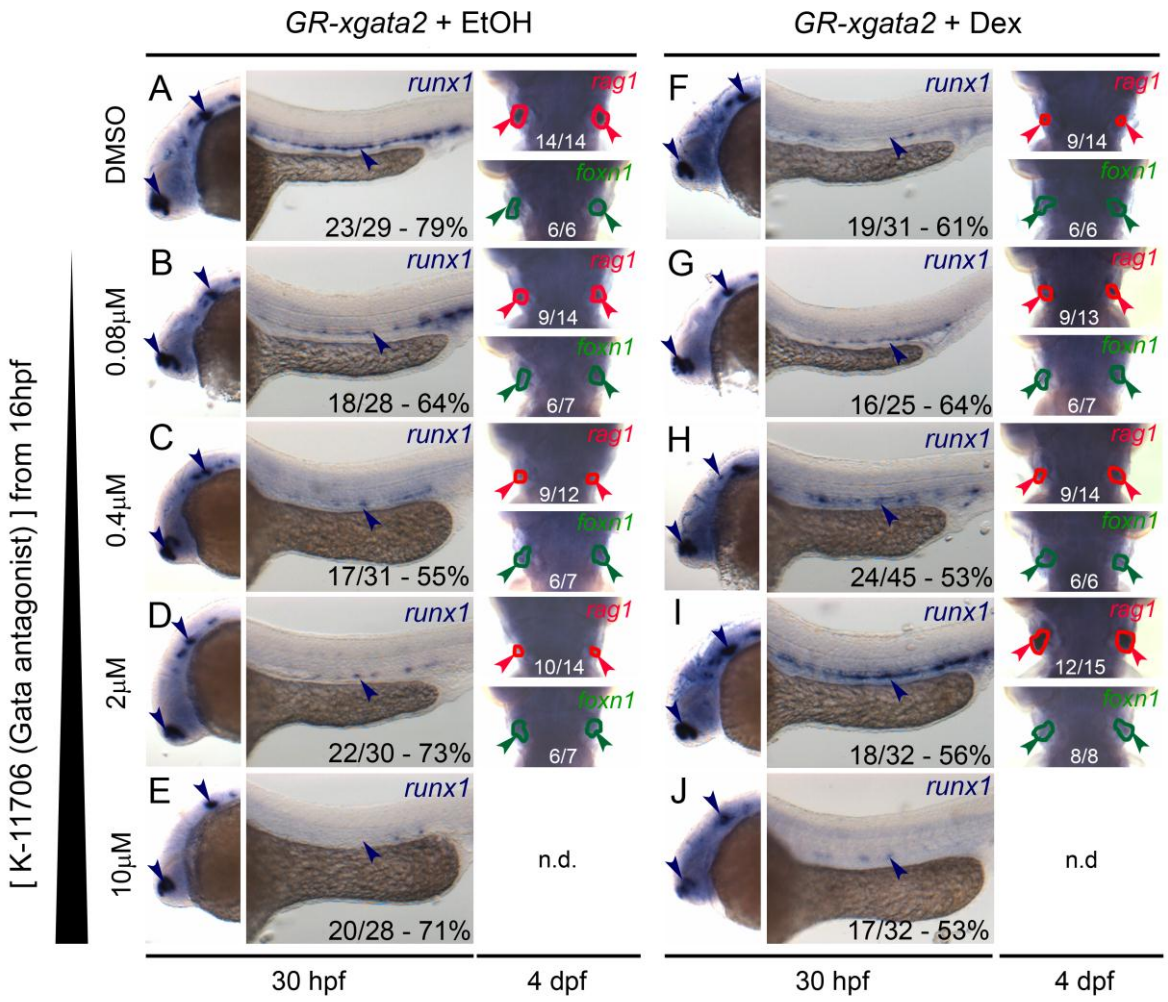

Figure 5.9 Inhibition of Gata activity rescues HSC production in embryos overexpressing *gata2*

(A – E) An increasing dose of the Gata antagonist K-11706 causes progressive loss of *runx1* expression in the dorsal aorta, but not the head. (F – J) Expression of *runx1* can be rescued by treatment with 2 µM of antagonist, but not higher or lower concentrations. *rag1* marks HSC derived T-cells in the thymus, whose level mirrors the expression of *runx1* in the AGM. Thymic epithelium remains unaffected, marked by *foxn1*; n.d., not done as embryos treated at this dose did not survive to 4 dpf.

mediated by *gata2a* and *gata2b*. The concentration of K-11706 at which we were able to rescue *runx1* expression varied between our *lmo4a* morphant and *gata2* overexpression experimental conditions. This is unsurprising and likely represents the variability in *gata2* levels between the two experiments. However, we were surprised that *gata2* overexpressing embryos rescued with 2 μM of compound showed an increase in *runx1* in the dorsal aorta. We think that this represents a *bona fide* increase in HSC production under these conditions, as we also see a corresponding increase in *rag1* in the thymus (compare Figure 5.9A and Figure 5.9I).

5.6 Bmp inhibition reveals multiple inputs into *gata2a* and can rescue *lmo4a* morphants

Bmp has previously been shown to control *gata2* expression at earlier stages of development (Liu et al., 2008; Maeno et al., 1996; Walmsley et al., 2002) and there is evidence that in the developing murine sensory cristae, *lmo4* lies epistatically downstream of Bmp4 (Chang et al., 2008b). We were therefore interested in investigating whether *bmp*, *lmo4*, and *gata2* form a regulatory triad in the dorsal aorta, that controls HSC emergence. Bmp, like Gata2, has been shown to have a critical early developmental role in the induction of haematopoietic mesoderm (Maeno et al., 1996) and Bmp has been shown be a potent ventralising factor (Dale et al., 1992; Kishimoto et al., 1997). We also used a pharmacological strategy to inhibit Bmp, which afforded a degree of temporal control. The Bmp antagonist dorsomorphin has previously been used to inhibit Bmp, but it has off-target effects on the Vegf receptor Flk1/Kdr (Hao et al., 2010). We therefore employed DMH-1, a dorsomorphin derivative that inhibits the phosphorylation of Bmp R-Smads by the type 1 Bmp receptors, but has no effect on Vegf signalling (Hao et al., 2010).

Treatment of wild type embryos from the 16ss with increasing doses of DMH-1 resulted in a progressive loss of *lmo4a* expression in the dorsal aorta (Figure 5.10 A-E). The degree to which somitic expression of *lmo4b* extended anteriorly varied between embryos in the same treatment groups, however, the average level of expression was unaffected (Figure 5.10 F-H). Strikingly, expression of

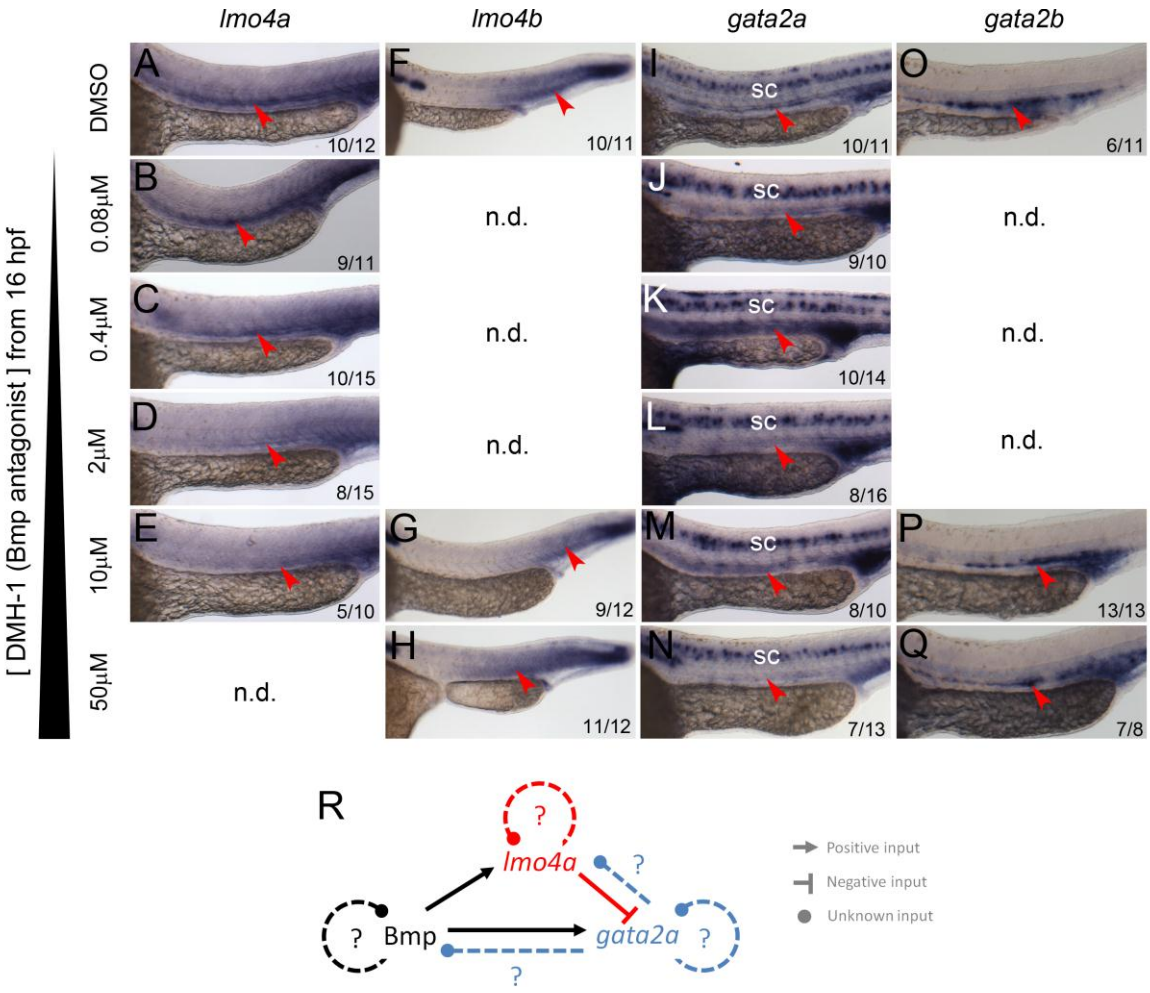

Figure 5.10 Inhibition of Bmp reveals multiple inputs into *gata2a*

(A – H) Increased inhibition of Bmp signalling results in a loss of *lmo4a*, but not *lmo4b* expression. (I – N) Increasing inhibition of Bmp results in oscillating levels of expression of *gata2a* in the dorsal aorta. (O – Q) *gata2b* expression is not affected by Bmp inhibition. Red arrowheads, dorsal aorta; n.d. not done; sc, spinal cord; embryos fixed at 33 hpf and imaged laterally. (R) Possible interactions between Bmp, *lmo4a* and *gata2a*. Solid lines have been demonstrated in this thesis, dotted lines remain to be tested.

gata2a in the dorsal aorta appeared to oscillate, although expression of *gata2a* in the spinal cord was largely unaffected. At 0.08 μM DMH-1, *gata2a* expression in the dorsal aorta was reduced, at 0.40 μM increased, at 2 μM it was reduced, at 10 μM it was increased and at 50 μM it was reduced (Figure 5.10 I-N). By contrast, expression of *gata2b* in the dorsal aorta was not affected by Bmp inhibition (Figure 5.10 O-Q). Thus, we propose that in the zebrafish dorsal aorta, Bmp drives expression of *lmo4a* and may drive expression of *gata2a*. However, many of the potential feedback and autoregulatory inputs for this kernel have yet to be defined (Figure 5.10R). Consistent with our proposed regulatory relationship, a single canonical Smad binding element is present in a potential upstream regulatory region of the *lmo4a* gene, but not of the *lmo4b* gene (Appendix II). Additionally, three Smad binding elements are present in the 10 kb region lying upstream of the first exon of *gata2a*. We are however yet to formally show that these elements are bound by Bmp Smads under the relevant conditions.

Taken together with our previous data demonstrating a dose-dependent requirement of *gata2a* for *runx1* expression, the regulatory triad we propose predicts that we should rescue *runx1* expression in *lmo4a* morphants by modulating Bmp signalling in such a way that *gata2a* is expressed at wild type levels. Titrating up the concentration of DMH-1 resulted in an oscillatory expression of *runx1* in the dorsal aorta (Figure 5.11 A-F). At 0.08 μM expression was reduced, at 0.40 μM it was at near wild type levels, at 2 and 10 μM it was reduced, and at 50 μM it was at wild type levels. Consistent with our proposed model for *gata2a* function in the dorsal aorta, expression of *gata2a* was either increased or decreased whenever *runx1* was reduced (Figure 5.11 G-L). Significantly, we were able to rescue *runx1* expression in *lmo4a* 5'UTR morphants by treating with 10 and 2 μM of DMH-1. However we did not achieve a rescue at lower concentrations (Figure 5.11 M-Q). Furthermore, at concentrations of DMH-1 where we observed a rescue, expression of *gata2a* in the dorsal aorta tended to mirror wild type expression (Figure 5.11 R-V). Taken together, it appears that in response to increasing concentrations of DMH-1, *runx1* in the dorsal aorta oscillates between wild type and reduced expression, and expression of *gata2a* in the dorsal aorta oscillates from increased to reduced expression (Figure 5.11W). Over the range of Bmp inhibition studied, the profiles of *runx1* and *gata2a* expression may be described by two sinusoidal waves that start out of phase. The wave representing *runx1* expression cycles at

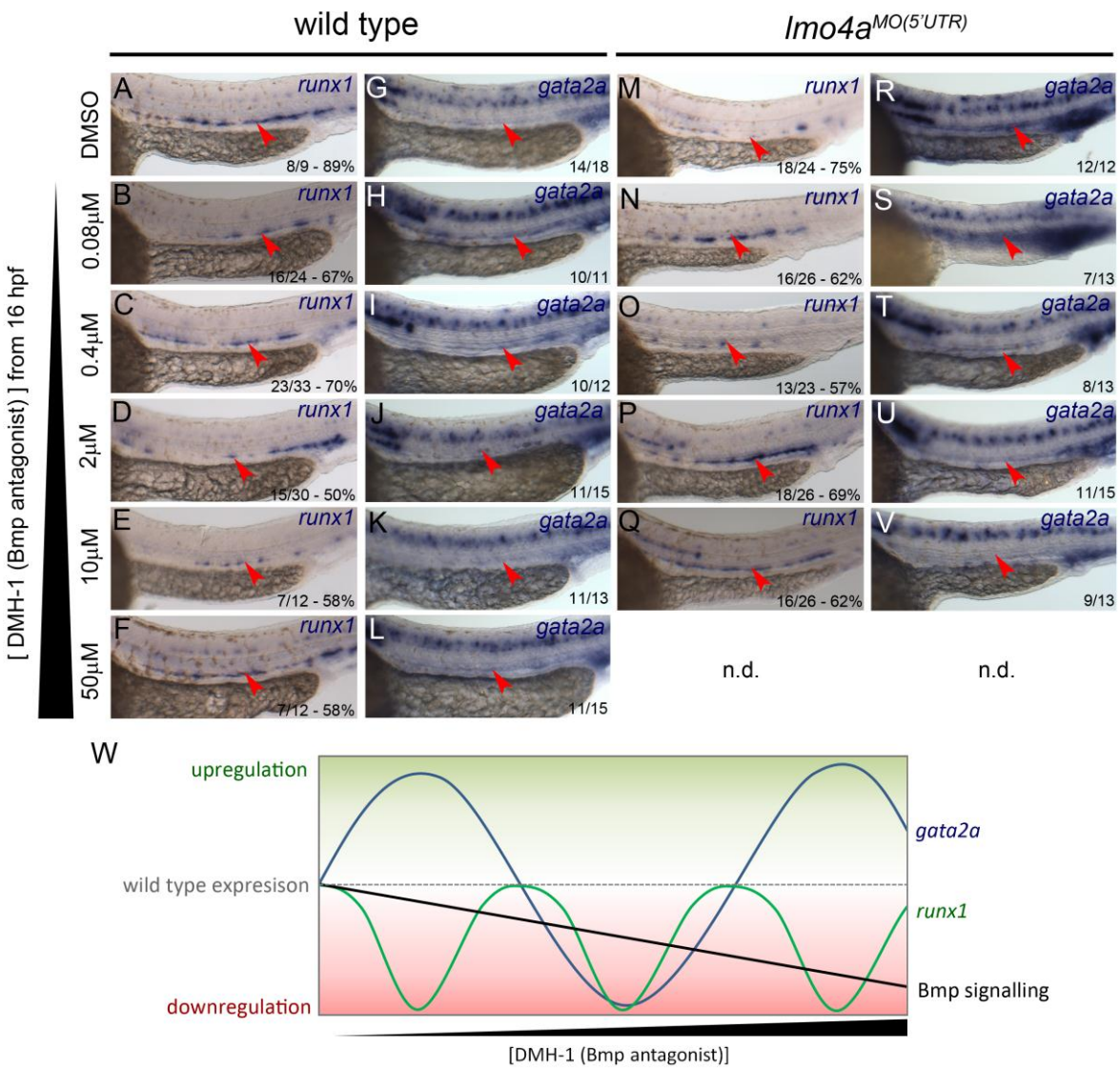

Figure 5.11 Dose-dependent inhibition of Bmp activity rescues *lmo4a* morphants

(A – F) An increasing dose of the Bmp antagonist DMH-1 causes cyclic loss of *runx1* expression. (G – L) *gata2a* expression is either increased or decreased in the dorsal aorta whenever *runx1* expression is reduced. (M – Q) Titration of DMH-1 dose lead to cyclic expression of *runx1*expression in *lmo4a* morphants, and can rescue *lmo4a* morphants. (R – V) *gata2a* expression is increased in *lmo4a* morphants and returns to wild type levels when *runx1* is rescued. (W) Schematic representation of the variation of *gata2a* and *runx* gene expression levels with respect to varying levels of Bmp activity. All embryos imaged laterally; n.d., not done.

double the frequency of the wave corresponding to *gata2a* expression. Whenever *gata2a* expression deviates from wild type levels, this results in reduced *runx1* expression (Figure 5.11I).

We were able to rescue expression of *runx1* in *lmo4a* 5'UTR morphants by inhibiting the activity of either Bmp or Gata (Figure 5.8, 5.9 and 5.11). However, we were never able to rescue the loss of ISVs seen in *lmo4a* 5'UTR morphants by inhibiting Bmp or Gata activity (Figure 5.12). Together with our previous data (Figure 4.18), this suggests that the ISV defect observed in *lmo4a* 5'UTR morphants may be the result of an off-target effect of the *lmo4a* 5'UTR morpholino. When embryos were treated with higher doses of the Gata antagonist, we noted that angiogenic sprouting was reduced (Figure 5.12 E-F). This likely reflects the modulated DNA binding activity of the bHLH transcription factor HIF-1, which has been associated with the use of the compound at higher concentrations, as HIF-1 plays a well-documented role in regulating angiogenesis (Harada et al., 2007; Nakano et al., 2004).

5.7 Discussion

5.7.1 Overview

Inputs from Gata2, Runx1 and Bmp signalling are required to correctly programme the first HSCs (Durand et al., 2007; Kissa and Herbomel, 2010; Ling et al., 2004; Wang et al., 1996; Wilkinson et al., 2009). In the previous chapter, we identified novel *lmo4a* partners and showed they are required for HSCs. In this chapter, we begin to mechanistically investigate the role of *lmo4a*, concluding that it forms a transcriptional regulatory triad with *gata2a* and Bmp signalling, which is required to control expression of the master HSC transcription factor *runx1*. Thus, we have begun to uncover regulatory relationships between both known and novel molecules within the zebrafish dorsal aorta. We also described a second zebrafish orthologue of *gata2*, *gata2b*, which is not regulated by Bmp. However, its role in development remains to be investigated.

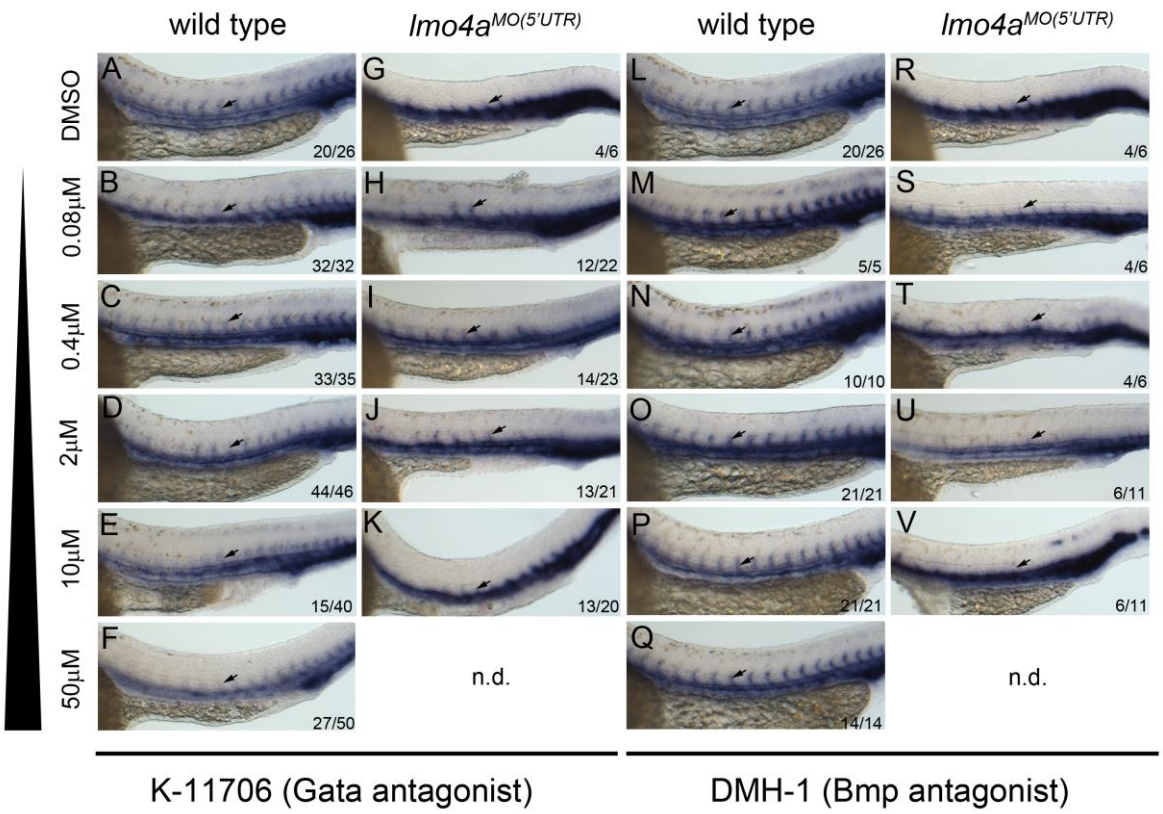

Figure 5.12 Gata or Bmp inhibition does not rescue ISV *fli1* expression *lmo4a* 5'UTR morphants

(A – F) The Gata antagonist causes a reduction in *fli1* expression at the highest two doses. (G – K) Loss of intersegmental vessels (ISVs) in *lmo4a* 5'UTR morphants was not rescued by inhibition of Gata activity. (L – Q) The Bmp antagonist does not affect *fli1* expression. (R – V) Loss of ISVs in *lmo4a* 5'UTR morphants is not rescued by inhibition of Bmp activity. Embryos fixed at 33 hpf and imaged laterally; black arrows, ISVs; n.d., not done.

5.7.2 *lmo4a* negatively regulates *gata2a* expression

In MEL cells, it has been shown by ChIP-seq that Lmo4 binds directly to the likely enhancers at the *gata2* locus. Additionally, siRNA mediated knockdown followed by expression profiling in MEL cells, suggested that *lmo4* positively regulates expression of *gata2* (Charlotte Andrieu-Soler, *unpublished data*). In contrast, we see an increase in *gata2a* expression in the zebrafish dorsal aorta in response to depletion of *lmo4a*. However this is consistent with the idea that Lmo proteins can act both positively and negatively in a context-dependent manner, where its functional output is modulated by changes in its interactions with the proteome (Matthews and Visvader, 2003). Also, although *lmo4a* and its partners are expressed in tissues where we see expansion of *gata2a*, we cannot formally exclude the possibility that the increase in *gata2a* is a result of an earlier activity that we detect from 1 dpf. As the partners of Lmo4 identified in MEL cells consist of co-repressors and histone deacetylases (Chapter 4), it is possible that they act together to form a repressive complex in the zebrafish dorsal aorta, that down regulates expression of *gata2a*, although we have not looked at *gata2a* expression in morphants for the Lmo4 partners. Consistent with direct control of *gata2* by Lmo4 and its partners, it has been demonstrated that an Lmo4-containing complex directly binds a Gata2 enhancer in chick V2 interneurones (Joshi et al., 2009).

Given that Lmo4 is acting positively on *gata2* in MEL cells, it is puzzling why it associates with a negative complex in this context. However, only Lmo4, rather than the entire repressive complex, was shown to bind DNA, and specifically to the *gata2* locus. It is therefore possible that in contrast to the zebrafish, Lmo4 may act independently of the complex to activate *gata2* expression in MEL cells, while members of the complex sequester Lmo4 away from active chromatin. Indeed it has been shown that Hdac7 and Ncor, two of the Lmo4 partners in MEL cells, can sequester proteins to specific subcellular regions (Furuya et al., 2007; Jensen et al., 2008). Intriguingly, Ncor was only identified as an Lmo4 partner in differentiated MEL cells, and may therefore, through this mechanism, fine-tune *gata2* expression, thus contributing to the Gata2 to Gata1 developmental switch that drives erythroid development (Bresnick et al., 2010).

As an alternative to direct inhibition of *gata2a* expression in the zebrafish, it is possible that *lmo4a* acts indirectly. It has been shown in the zebrafish that Lmo4a interacts with Ldb1 and Ldb2 (Ji, 2005), and Ldb2 transcriptionally regulates expression of the inhibitory Smads, *smad6* and *smad7* (Wenchao Gu, *unpublished*), which are both expressed around the zebrafish dorsal aorta (Robert Wilkinson, *unpublished*). Additionally, very recently it was shown that *smad6* can repress *gata2* expression in cord blood HSCs (Kang et al., 2012). It is therefore possible that *lmo4a* inhibits *gata2a* expression in the zebrafish by regulating, or cooperating, with *smad6*, although we have not investigated this. Consistent with this, *ldb2* morphants also lack HSCs (Wenchao Gu, *unpublished*).

5.7.3 A critical dose of *gata2a* in the dorsal aorta is required for HSC production

Enforced expression of *gata2* in bone marrow or cord blood HSCs detrimentally affects their numbers and repopulating ability (Heyworth et al., 1999; Tipping et al., 2009). Additionally, elevated levels of *gata2* correlate with a poor prognosis in acute myeloid leukaemia (Luesink et al., 2012; Vicente et al., 2012), which may reflect a role in promoting the treatment-resistance and propagating activity of an HSPC-like cancer stem cell. To date, *gata2* has never been conditionally overexpressed around the time of *de novo* HSC generation. As in the adult HSC compartment, our data showed that overexpression of *gata2* in the dorsal aorta resulted in fewer HSCs, suggesting that the increase in *gata2a* observed in *lmo4a* morphants was responsible for the loss of HSCs. Consistent with this, pharmacological inhibition of Gata binding activity with a small molecule antagonist, could rescue the HSC defects in *lmo4a* morphants and importantly, in embryos overexpressing *gata2*. Higher or lower doses of the Gata antagonist resulted in loss of HSCs. This likely represents a requirement for a particular concentration of *gata2a* in the dorsal aorta, where only an optimal dose results in production of HSCs (Figure 5.8I). A similar dose response to *gata2* has been described in CD45 positive haematopoietic cells in the murine yolk sac, where this population progressively increased in response to decreasing doses of *gata2* (Minegishi et al., 2003).

As *gata2* has been shown to directly regulate expression of *runx1*, for example by binding to the +23 enhancer that confers haematopoietic expression of *runx1* (Nottingham et al., 2007; Wilson et al., 2010), it is likely that reduction of *gata2a* levels leads to reduced *runx1* expression in the zebrafish dorsal aorta. Consistent with this, the Gata antagonist used in this study has been shown to inhibit DNA binding activity (Nakano et al., 2004), and lead to progressive loss of *runx1* expression. Additionally, both over- and under-expression of Gata2 may shift binding equilibria with protein partners away from functional interactions, resulting in the build-up of non-functional complexes that are unable to effect gene expression (Babu et al., 2011). As Lmo4 can bind repressive chromatin modifiers (Chapter 4), it is also possible that high levels of unbound Lmo4 could alter gene expression by titrating its protein partners away from chromatin, as has been postulated for the Bmp7 promoter in mammary epithelial cells (Wang et al., 2007). Mesodermal *brachyury* expression is dependent on an intermediate dose of Tgf-β signalling (Green et al., 1992; Green et al., 1994). In a similar fashion, *lmo4a* and *gata2a* may control *runx1* expression by modulating cell signalling. Indeed, Lmo4 can interact with Smads to modulate Tgf-β signalling (Lu et al., 2006), and Tgf-β is necessary for *runx1* expression in the zebrafish (Rui Monteiro, *unpublished*). We have not yet excluded or confirmed any of these possibilities in the relevant cell types, therefore these ideas may not be mutually exclusive. However, they potentially explain why a marginal knockdown of some of the *lmo4a* MEL cell partners results in loss of HSCs (Chapter 4). Additionally, although *runx1* or *gata2* heterozygous mice do not exhibit a strong phenotype, compound heterozygotes are not viable, and E12.5 foetal livers from these animials display severe defects in their clonogenic progenitor potential (Cai et al., 2000; Ling et al., 2004; Wilson et al., 2010). Thus, it is likely that *runx1* and *gata2* have a synthetically lethal relationship; the two genes are able to buffer for each other's depletion and therefore function in a common pathway.

It was also intriguing to observe an apparent enhancement in the production of *runx1* positive cells when embryos overexpressing *gata2* were treated with 2 μM of the Gata antagonist. We have not investigated whether known stimulators of HSC development were affected, such as levels of prostaglandin E2 (North et al., 2007). Nevertheless, within the dorsal aorta, the output of *gata2* based on the tuneable rheostat of expression, which we propose here, is not complete, as this model does not allow for increased HSC production. In the bone marrow of adult *gata2*$^{+/-}$ mice, *in vitro* and *in vivo*

assessment of the granulocyte-macrophage progenitors revealed a reduction in the size and functionality of this compartment, which may reflect defects in lineage commitment (Rodrigues et al., 2008). Consistent with this idea, it has been proposed that *gata2* inhibits the differentiation of progenitors in the murine yolk sac, thus preventing depletion of this population (Minegishi et al., 2003). It is therefore possible that in the zebrafish dorsal aorta, *gata2a* has an analogous role, limiting the number of cells that undergo the EHT. This may involve modulations in Notch signalling, which is required for *runx1*expression in the dorsal aorta (Burns et al., 2005; Gering and Patient, 2005), given that Gata2 has been placed both up- and down-stream of this signalling event in various haematopoietic and non-haematopoietic contexts (Da'as et al., 2012; Joshi et al., 2009; Kumano et al., 2001; Robert-Moreno et al., 2008; Rodrigues et al., 2008). However, this hypothesis remains to be investigated.

Although we employ a pan-Gata antagonist in our rescue experiments, it is likely that the effect we see is specific to Gata2, as no other Gata factor is expressed in the dorsal aorta at this time. Expression of *gata1* is restricted to primitive erythrocytes in the ICM underlying the dorsal aorta (Monteiro et al., 2011), *gata3* is restricted to neural and pronephric populations (Neave et al., 1995), and *gata4*, *gata5*, and *gata6* are restricted to the heart and gut (Peterkin et al., 2005). However, as there are two zebrafish *gata2* orthologues expressed in the dorsal aorta, *gata2a* and *gata2b*, we cannot exclude that *gata2b* also plays a role in HSC emergence as the Gata antagonist likely inhibits the DNA binding activity of both orthologues. Additionally in our overexpression experiments, we used the Xenopus *gata2* orthologue, of which there is only one. Therefore, it is possible that the combined levels of *gata2a* and *gata2b* programme the HSC, or equally that *gata2b* does not play a role in programming the HSC. Nevertheless, to our knowledge, this is the first time that the dose of *gata2* has been demonstrated to be critical in specifying the first HSCs in the dorsal aorta.

5.7.4 An incoherent feed forward loop may control *gata2a* expression in the dorsal aorta

Previous work from our laboratory, together with that of others, has shown that Bmp signalling can control *gata2* expression in various haematopoietic tissues (Ferri-Lagneau et al., 2012; Liu et al., 2008; Maeno et al., 1996; Walmsley et al., 2002; Xu et al., 1999). We therefore tested whether this relationship was also true in the dorsal aorta of the zebrafish, around the time when this tissue has haemogenic activity. Additionally, given that we show that *lmo4a* negatively controls *gata2a* expression in this tissue, and *lmo4* has been reported to be under the control of Bmp signalling where it instructs ventral patterning in the frog and development of the murine vestibular apparatus (Chang et al., 2008b; de la Calle-Mustienes et al., 2003), we also investigated if the *lmo4a* input into *gata2a* was Bmp dependent. Using increasing doses of a specific Bmp antagonist, we demonstrated that expression of *lmo4a*, but not *lmo4b*, is under the control of Bmp signalling. Consistent with this, a putative *lmo4a*, but not *lmo4b* regulatory region contains a canonical Smad binding motif. However we have not directly demonstrated that the Bmp Smads transduce signalling through this motif. As Lmo4 has been shown to physically interact with the Bmp Smads in mammary epithelial cells in culture (Lu et al., 2006), it is also possible that an Lmo4a containing complex directs activated Smad molecules to the *gata2a* locus. Furthermore, as R-Smads have been shown to directly interact with Runx transcription factors (Hanai et al., 1999; Ito and Miyazono, 2003), it is possible that a complex containing Lmo4, R-Smads and Runx directs various cellular outputs in the dorsal aorta region. These possibilities remain to be investigated in the context of HSC emergence in the dorsal aorta.

Expression of *gata2a*, but not *gata2b*, is under the control of Bmp signalling. However, this relationship is not as straightforward as what we observe between Bmp and *lmo4a*: in response to increasing Bmp inhibition, the level of *gata2a* in the dorsal aorta oscillates around the wild type expression levels. Strikingly, expression of *runx1* behaved in a similar oscillatory fashion in response to Bmp inhibition. This is likely a result of the dual and antagonist inputs to *gata2a* from Bmp and *lmo4a* and reflects which input onto *gata2a* predominates in response to a particular dose of Bmp signalling. We however cannot exclude the possibility that Bmp signalling also directly controls *runx1* expression,

as has been reported for *runx2* in a mesenchymal cell line (Lee et al., 2000). Consistent with our model where only an intermediate dose of *gata2a* in the dorsal aorta results in HSCs, whenever *runx1* expression was reduced, *gata2a* levels were either elevated or decreased, and we were able to rescue *runx1* expression in *lmo4a* morphants by using doses of Bmp antagonist that resulted in wild type expression of *gata2a* (Figure 5.11). Of note, in *lmo4a* morphants, the oscillatory behaviour of *gata2a* in response to increasing Bmp inhibition is not so apparent, with *gata2a* responding to Bmp inhibition in a similar manner to *lmo4a*. This may reflect the loss of opposing inputs into *gata2a* in the context of *lmo4a* inhibition, however further work is required to quantify and characterise this effect.

The Bmp antagonist employed here does not allow us to distinguish between Bmp ligands, receptors and R-Smads transducing signals in the dorsal aorta. However, in the zebrafish dorsal aorta, of the possible Bmp ligands, only *bmp4* is expressed, and has previously been implicated in HSC emergence; of the possible receptors, *bmpr2a* and *bmpr2b* (Monteiro et al., 2008), *alk1* and *alk3* are expressed; and out of possible R-Smads, only *smad5* is expressed (Wilkinson et al., 2009) (Robert Wilkinson's Thesis, *unpublished*). It is therefore likely that it is a combination of these factors that transduce Bmp signalling in the dorsal aorta.

Gene regulatory networks are central to generating and maintaining forward momentum for developmental processes, and the topology of such systems can be represented diagrammatically (Bolouri and Davidson, 2002). We can integrate the relationships that we have defined into such a regulatory network (Figure 5.13A). This results in a network where "Gene A" turns on "Gene B" and "Gene C", with "Gene B" also turning off "Gene C". This relationship is classed as a type 1 incoherent feed-forward loop (Mangan and Alon, 2003). A role for such a motif has been described in settings as diverse as the tuning of the response time of the *E.coli gal* system, or the generation of a temporal pulse of gene expression in the chick ear (Mangan et al., 2006; Neves et al., 2012). In addition to generating a pulse of expression, such a motif can also dampen the steady state expression of *gata2a* (Figure 5.13C), depending on the strength, timing and functional thresholds of the individual interactions (Alon, 2007). Our data suggests that it is unlikely that a strict "AND" genetic logic gate integrates the Bmp and *lmo4a* input onto *gata2a*, as we still detect *gata2a* transcripts when we inhibit

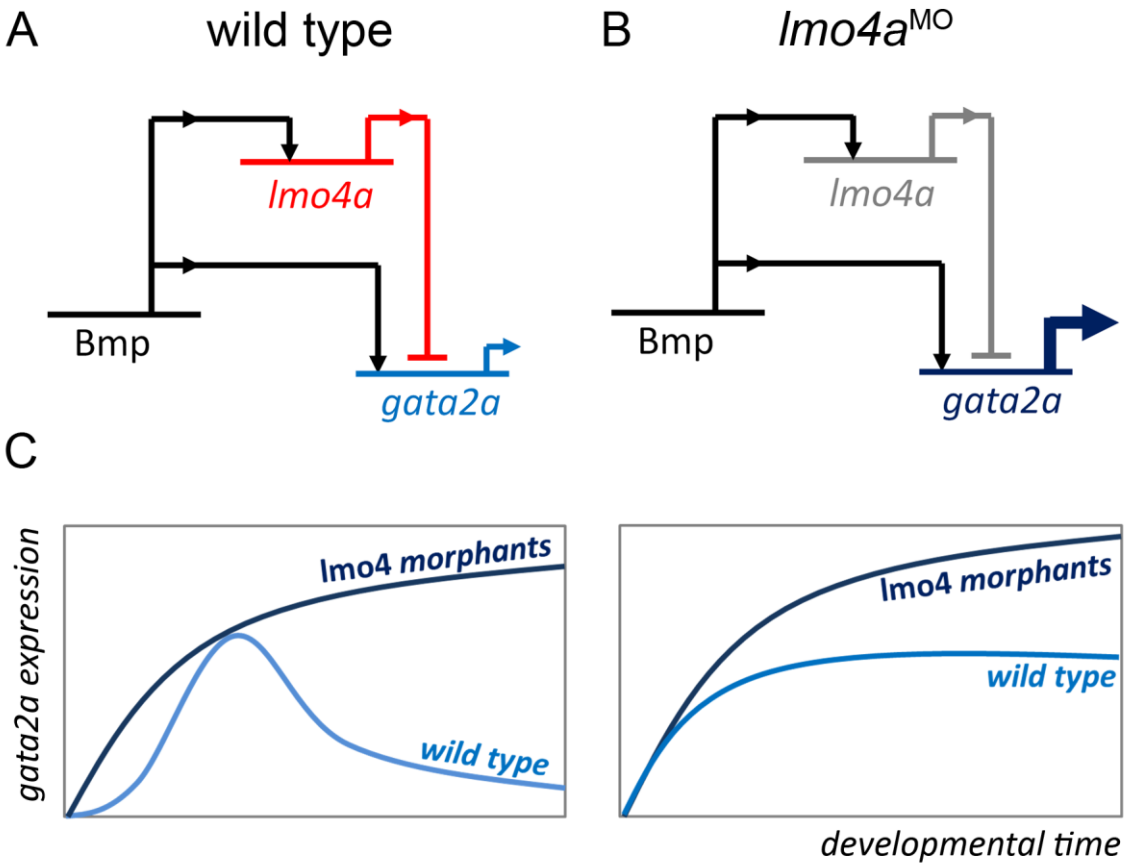

Figure 5.13 An incoherent feed forward loop limits *gata2a* expression

(A) Bmp drives *gata2a* expression, and expression of *lmo4a*, a repressor of *gata2a*. This network architecture is classed as an incoherent feed forward loop. (B) Depletion of *lmo4a* results in increased *gata2a* expression. (C) Two possible graphs describing expression of *gata2a* with time.

either input. Indeed it is likely there are additional inputs into *gata2*. However, as we have not looked at DNA binding of the Bmp Smads or *lmo4a*, we cannot exclude the possibility that binding is mutually exclusive, and therefore steric competition exists between the two opposing regulatory arms at the *gata2a* locus.

We initially observe little difference in *gata2a* expression in *lmo4a* morphants at 24 hpf. However within a few hours, this resolves to a striking increase (Figure 5.2 A-F). This presumably reflects an *lmo4a* independent window, during which *gata2a* expression is solely dependent on Bmp signalling, followed by increasing influence of the negative regulation by *lmo4a*. While either of the predicted profiles could reflect these observations (Figure 5.13 B-C), further experimental data tracking *gata2a* levels over time, in the relevant cells, is required to determine which, if any, of the proposed graphs are correct. We have not determined all the possible regulatory relationships that exist between gene nodes in the triad (Figure 5.10R). It is likely that our proposed network is incomplete as we do not know what initially turns on Bmp expression, and negative feedback may be required to generate the oscillatory gene expression that we observe in response to varying doses of Bmp signaling. In various theoretical and biological systems, it has been shown that negative feedback is a minimum requirement to generate a temporal oscillator, and also to stabilise gene regulatory networks (Novak and Tyson, 2008; Tigges et al., 2009). Indeed, it has been demonstrated through stochastic and deterministic models of genetic networks that delayed negative feedback can result in a transient increase in gene expression variability, which resolves with time to stable expression (Maithreye et al., 2008). This may account for the variability in *runx1* expression we see in 24 hpf zebrafish, but not post 26 hpf fish.

Chapter 6

Conclusions

The haematopoietic system has provided an accessible system to study stem cell biology, including normal and abnormal lineage commitment. Indeed, the HSC remains to date the best characterised tissue stem cell (Orkin and Zon, 2008). In this thesis, we have identified functionally important residues on the surface of a key regulator of blood and endothelial development. A subset of these cells generate the first adult HSCs, which during ontogeny emerge from the floor of the transiently polarised embryonic dorsal aorta. We have gone on to explore links between some of the genetic signals controlling this process.

The transcription factors, Lmo2 and Scl, are together master regulators of the haemangioblast programme (Patterson et al., 2007). We have utilised this activity, together with recent structural work, to identify functionally important residues on the Lmo2 molecule. We demonstrate that conformational flexibility in Lmo2 is necessary for its role in the haemangioblast and go on to identify residues on the Lmo2 molecule that are necessary for its interaction with Scl and Gata1. Although we studied the functionality of these residues in the zebrafish haemangioblast, it is likely that at least some of these interactions are also important in generating functional complexes in other contexts, such as during erythroid development. In contrast to Lmo2, we show that the related protein, Lmo4a, is not active in development of the haemangioblast. However it is essential for HSC development, mediating Bmp induction of the HSC programme by tightly regulating the levels of the transcription factor *gata2a* in the dorsal aorta, and may play a role in angiogenesis. Furthermore, we have shown that at least some of the protein partners of Lmo4 identified in MEL cells are also required for HSC development in the zebrafish. We therefore conclude that Lmo proteins assemble critical complexes at multiple stages of blood and endothelial development.

We focus on the role of Lmo2 and Lmo4 in the distinct tissues of the haemangioblast and haemogenic endothelium, respectively. However, due to the earlier requirement for Lmo2 in the haemangioblast, we cannot exclude the possibility that Lmo2 is also required for endothelial or HSC development. The recent ability to turn genes both on and off in a time-dependent manner with photo-morpholinos would allow such questions to be addressed (Tallafuss et al., 2012). Given the sequence and structural homology between Lmo2 and Lmo4 (Deane et al., 2004; El Omari et al.,

2011), it is likely that many of the residues that we have shown to be required for Lmo2, are also required for the normal and pathological activity of Lmo4. Indeed, Lmo2 and Lmo4 are often overexpressed in prostate and breast carcinomas, respectively: cancers that have similar developmental progressions (Ma et al., 2007; Montanez-Wiscovich et al., 2009; Struewing et al., 1997; Sum et al., 2005). While Lmo2 and Lmo4 may have overlapping functions, they also have distinct roles, for example it has been shown that in contrast to Lmo2, Lmo4 does not bind the N-finger of Gata1 *in vitro* (Wilkinson-White et al., 2011). Understanding these differences will be essential in order to develop therapeutic reagents that selectively target a particular Lmo protein. Towards this goal, it has been demonstrated that Lmo2 interacts more extensively with the Ldb1-LID domain when compared to Lmo4, and that the region in Lmo2-LIM2 that interacts with the Gata1 N-finger is absent in Lmo4-LIM2 (Deane et al., 2004; El Omari et al., 2011).

We have shown that Lmo4a, together with many of its protein partners, is required for HSC production. However, we currently lack the technology to functionally assess HSC output (de Jong and Zon, 2012). Additionally, we have not studied whether Lmo4 or it partners play a role in adult HSPCs or their commitment. The ability to analyse distinct blood lineages from total blood by FACS, along with the impending availability of mutant lines (Wittamer et al., 2011) (Zebrafish Mutation Project) would facilitate these studies and also allow us to confirm our interpretation of the morphant phenotypes, particularly those relating to the partners of Lmo4. In this thesis, we have taken advantage of biochemical analysis of Lmo4 DNA and protein binding carried out in MEL cells. In contrast to cells in culture, the embryo consists of a heterogeneous population of cells. As interactions are not uniform across tissues, the ability to isolate sufficient numbers of cells of interest, for example from the dorsal aorta, in quantities sufficient to allow for biochemical analysis, will be important for future studies.

In exploring the genetic mechanisms controlling HSC production, we show that Bmp signalling controls expression of both *gata2a* and *lmo4a*, and *lmo4a* also negatively controls *gata2a* expression. We propose that this generates an incoherent feed forward loop that limits *gata2a* expression in the dorsal aorta and may result in oscillatory gene expression in response to decreasing

Bmp activity, although we have not looked at the response to increased Bmp activity. It will also be interesting to investigate whether *gata2a* expression naturally oscillates during HSC production, as may be the case in the mouse (Elaine Dzierzak, *personal communication*). While these are all attractive ideas, further investigation is required. For example, careful quantitation of the effects and the generation of tools that would allow real-time *in vivo* tracking of gene expression, as has been used to study the oscillatory waves of gene expression in the developing somites (Masamizu et al., 2006), will be necessary. Additionally, as we have not defined parameters for all the possible variables, it is not possible to generate a deterministic model for the proposed regulatory triad. However stochastic modelling, utilising ordinary differential equations, may allow non-intuitive predictions to be made and tested. Due to the oscillatory behaviour of *gata2a* in response to Bmp inhibition, the precise nature of this input is still not clear. However, in whole kidney marrow from adult zebrafish, it has been demonstrated that a positive input from Bmp to *gata2a* exists (Trompouki et al., 2011).

An underlying theme of this thesis is the re-use of transcriptional complex components at different stages of development, and in distinct tissues. While we have begun to investigate the role of Lmo2- and Lmo4-containing protein complexes during haematopoiesis, a complete description of complex assembly would necessitate an understanding of various kinetic parameters. These include the association and dissociation constants describing protein:protein and DNA:protein interactions, along with the concentrations of the various components. This would be particularly relevant in disease states, where the outcome of competitive binding events can be modulated resulting in the loss of normal function, or gain of pathological functions. Significantly, in this thesis we show for the first time that the dose of *gata2a* in the dorsal aorta is critical for HSC production, and specifically that increase in *gata2a* levels has a detrimental effect on programming the first HSCs. The consensus between different experimental systems, each with their own technical limitations, along with differences, can be informative. It would therefore be interesting to establish whether the dose of *gata2* is also critical during HSC generation in other systems, such as the mouse. Currently, this is being investigated in at least one laboratory (J Doug Engle, *personal communication*). Taken together, the data presented in this study expands our understanding of haematopoiesis, and is likely to inform on-going efforts to produce and expand clinical-grade HSCs *ex vivo*.

Appendices

Appendix I – Expression of *aspp* transcripts in zebrafish

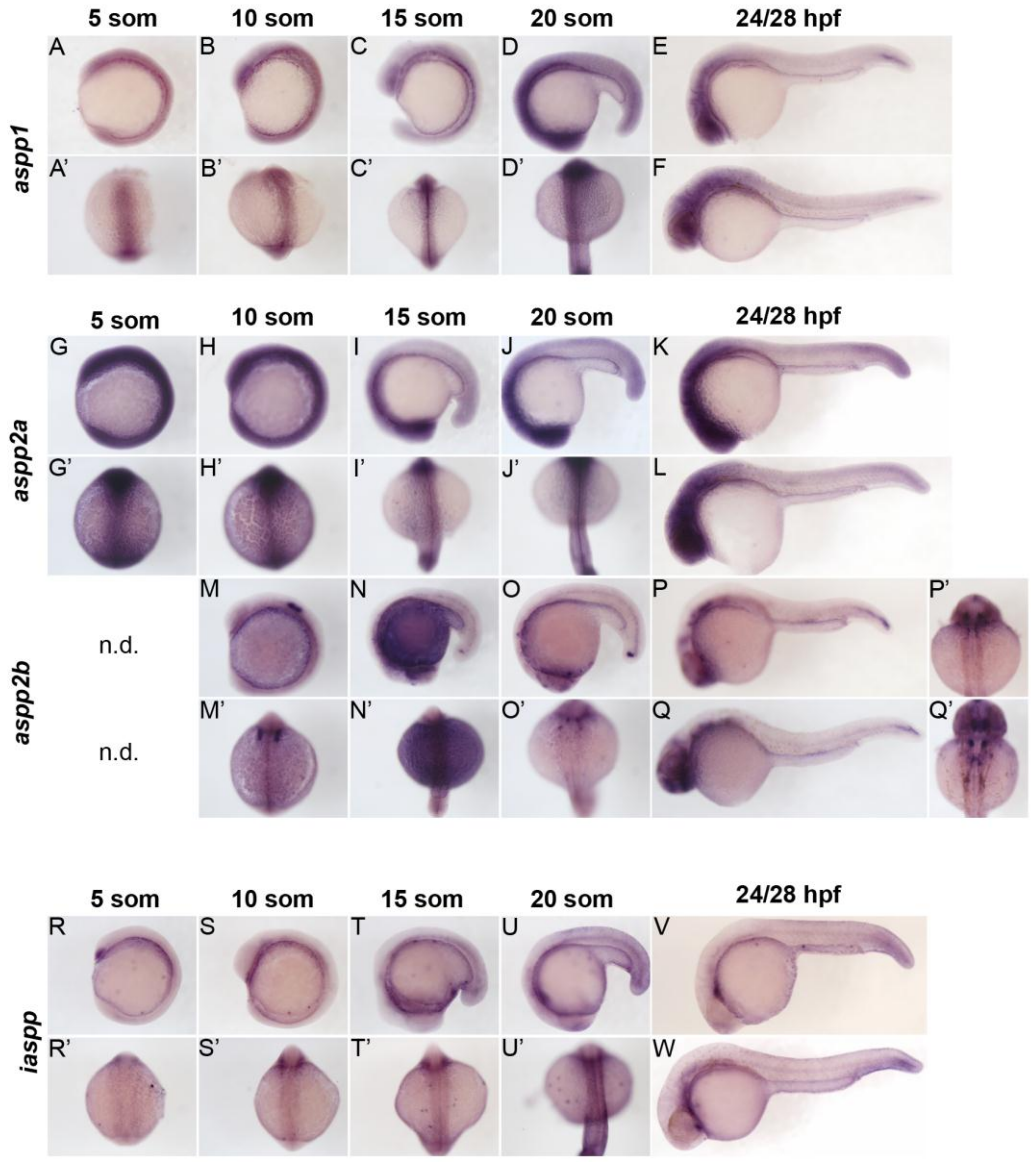

Figure S1 Expression of *aspp* transcripts in zebrafish

The ASPP proteins represent a recently identified family of ankyrin-repeat-containing, SH3-domain-containing, and proline-rich-region-containing proteins that bind the tumour suppressor p53, and may therefore represent novel targets for cancer therapeutics. They are conserved from worm to human (Bergamaschi et al., 2003; Samuels-Lev et al., 2001). ASPP1 and 2 transactivate p53, whereas iASPP competes at the binding site and inhibits activity of p53. Consistent with these observations, it has been reported that ASPP1 and 2 are often downregulated in human cancers, whereas iASPP is often unregulated (Liu et al., 2005). In the mouse, ASPP1 is expressed in the vascular and lymphatic endothelium, and mice lacking *aspp1* display delayed lymphatic vessel

formation and mispatterned collecting lymphatic vessels (Hirashima et al., 2008). (A – F) The zebrafish *aspp1* orthologue (NM_001044824) is not expressed in vasculature and was therefore not studied further. Mice lacking *aspp2* display leaky vessels peri- and post-natally and defects in tight junctions and cell polarity. Furthermore, ASPP2 may directly regulate Notch sinalling (Xin Lu, *personal communication*). (G – Q') In the zebrafish, *aspp2a* (NM_214814) and *aspp2b* (NM_001045153) are not expressed in the vasculature, and so were not studied further. The most ancient member of the family is iASPP. *iaspp* knockout mice die of cardiac defects. However 4-hydroxytamoxifen mediated deletion of *iaspp* revealed a role in stratification of epithelium and endothelium; vascular smooth muscle collapsed in knockout mice and the vascular diameter was reduced (Notari et al., 2011). (R – W) As *iaspp1* (NM_001014320) is not expressed in the vasculature in zebrafish, it was not studied further. Of note, *aspp2a* and *iaspp* in the zebrafish are expressed in neural cells, partially mirroring the murine expression. Furthermore, the expression of *aspp1* and *aspp2a* in the zebrafish is similar to expression of its target *p53* in the head region of zebrafish (Zfin.org). In contrast, in *Xenopus*, the ASPP family are expressed in the dorsal aorta (Ado Ciau-Uitz, *personal communication*).

Appendix II – Analysis of un-methlyated regions around the *lmo4* locus

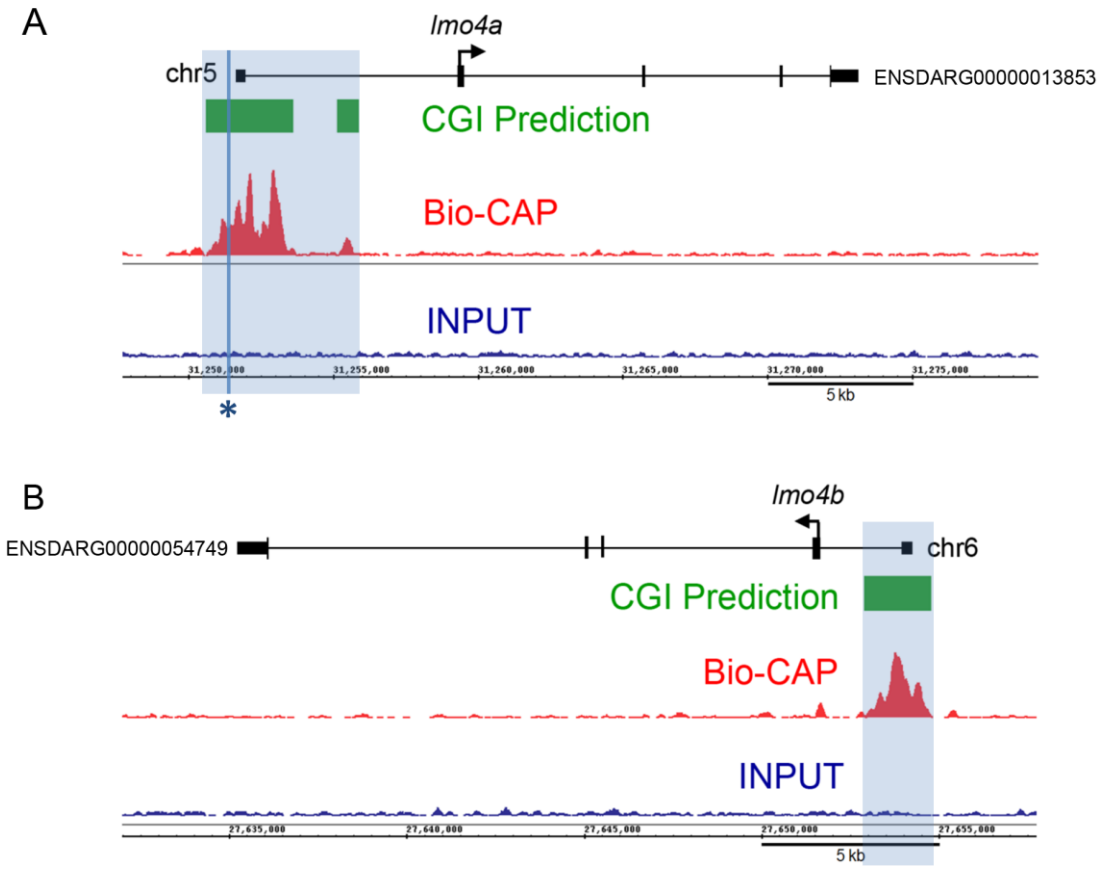

Figure S2 Analysis of un-methlyated regions around the *lmo4* locus

CpG dinucleotide are underrepresented in mammalian genomes, likely reflecting an evolutionary desire to reduce the mutational burden caused by spontaneous deamination of methylated cytosines to thymidine. However CpG islands, regions containing runs of CpGs tend to be un-methylated, and are often associated with genes, in particular with transcriptional start sites (TSS) (Saxonov et al., 2006). An algorithm predicting CpG islands (CGIs) in zebrafish predicts many sites that are not associated with genes (Gardiner-Garden and Frommer, 1987). Using a novel technique to isolate and analyse un-methylated DNA (Blackledge et al., 2012) (Bio-CAP), a genome wide map of un-methylated regions of several species has been generated (Neil Blackledge, Hannah Long, Rob Klose, *in submission*). (A - B) Zooming into the two zebrafish *lmo4* loci reveals good overlap between the CGI prediction and Bio-CAP at both sites. The presence of peaks corresponding to un-methylated regions around the transcription start sites suggests that these regions represent the major regulatory elements for the gene. This may have implications for future efforts to generate transgenic animals. Additionally, a motif search for the canonical Smad DNA binding site TCTAGA in the regions shaded in blue (Stopa et al., 2000), revealed a single candidate Smad site in the *lmo4a* TSS (blue asterisk), but not in the *lmo4b* TSS. Figure adapted from (Hannah Long, *unpublished*).

Appendix III – Activity of Nodal and Bmp in *lmo4* morphants

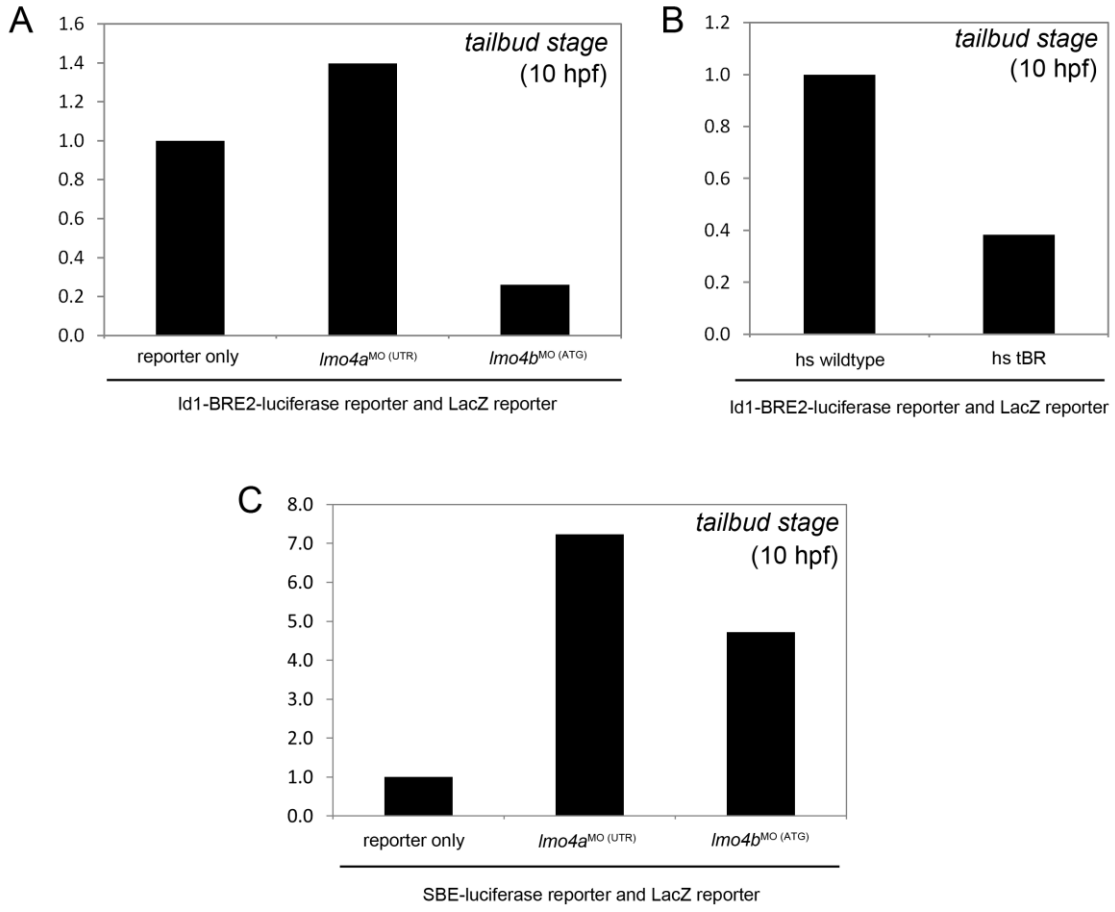

Figure S3 Activity of Nodal and Bmp in *lmo4* morphants

(A) The Bmp Response Element (BRE) was coupled to luciferase to specifically report on Bmp signalling (Monteiro et al., 2008). At tailbud stage, *lmo4a* morphants showed elevated Bmp signalling whereas *lmo4b* morphants showed decreased Bmp signalling. (B) Activation of the dominant negative Bmp receptor by heat shock (hs) in hsp70l:dnBmpr-GFP transgenic animals results in a reduction in Bmp signalling. This acts as a positive control for the BRE-luciferase construct. (C) The Smad Binding Element (SBE) was coupled to luciferase to report on Tgf-β family signalling (Jonk et al., 1998). At the tailbud stage, both *lmo4a* and *4b* morphants show elevated Tgf-β family signalling. Taken together with the Bmp reporter activity, this suggests that signalling through other non-Bmp Tgf-β family members is increased, however it is not clear which specific pathways are affected. Constructs were injected as circular DNA in one cell stage embryos. Embryos were heat shocked at 42 °C for 30 minutes between 8- and 32- cell stages. Embryos were collected for the luciferase assay at the tailbud stage (10 hpf). Graphs are representative of two independent biological experiments and results normalised to a LacZ reporter. Experiments carried out in collaboration with Wenchao Gu.

Appendix IV – *lmo2/4a* do not cooperate in the PLM and *lmo2* cannot rescue *lmo4a* morphants

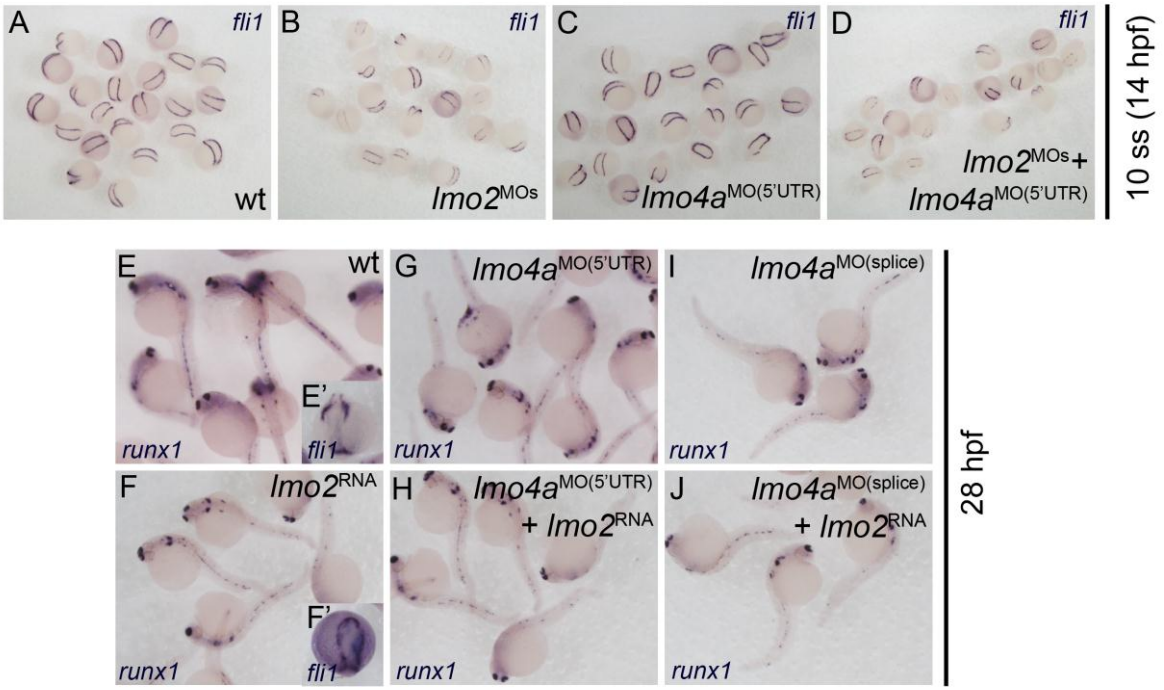

Figure S4 ***lmo2/4a*** **do not act cooperatively, and** ***lmo2*** **cannot rescue** ***lmo4a*** **morphants**

(A –D) Using a dual morpholino strategy (Patterson et al., 2007), knockdown of *lmo2* results in a reduction of *fli1* expression in the posterior lateral plate mesoderm (PLM). This effect is not enhanced by co-knockdown of *lmo4a*. (E – J) *lmo2* RNA may cause a reduction in *runx1* expression in the AGM region, and cannot rescue *lmo4a* morphants. Inserts; wild type anterior *fli1* expression (E') is expanded when the *lmo2* RNA construct was co-injected with *scl*, demonstrating that *lmo2* RNA is functional.

Appendix V – *irf2bp2b* is expressed ubiquitously and is required for the HSC

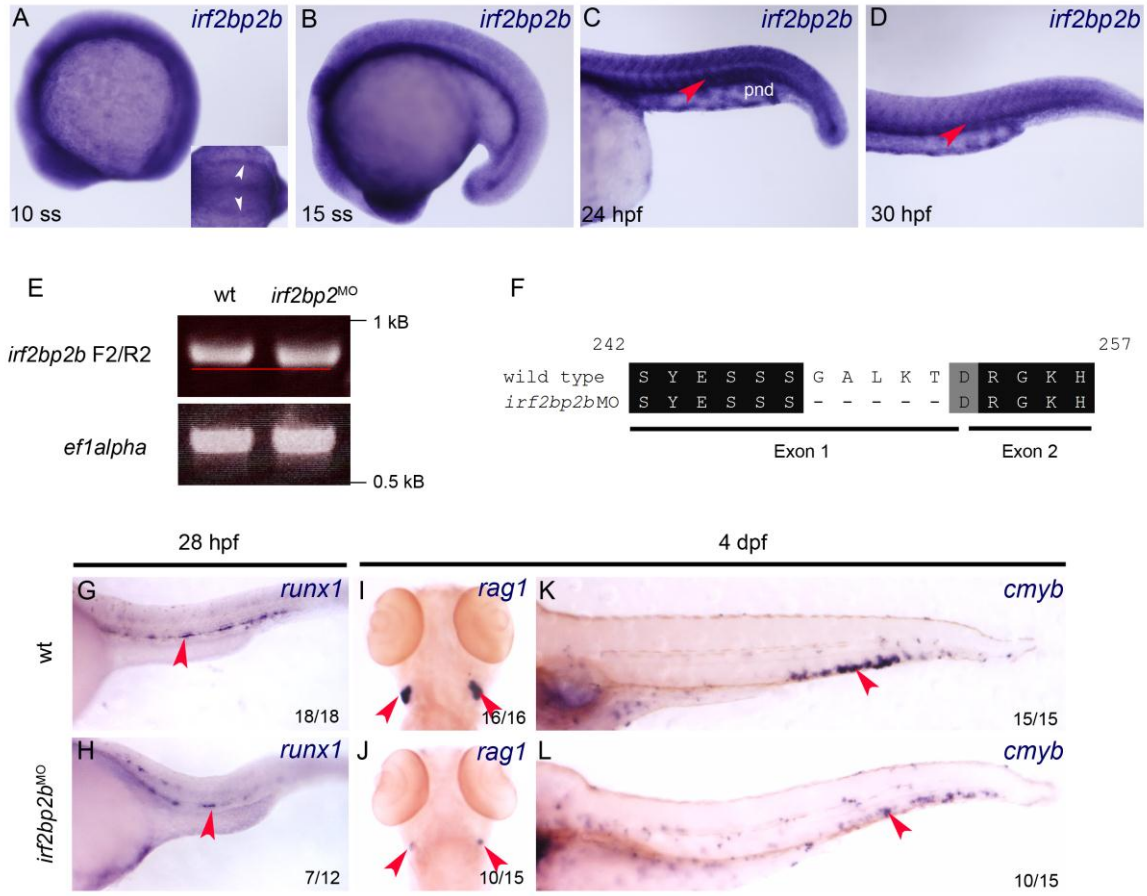

Figure S5 Expression of *irf2bp2b*

Irf2bp2 was originally identified as a co-repressor Interferon Regulatory Factor-2 (Childs and Goodbourn, 2003), and has since been identified as a p53 target gene (Koeppel et al., 2009). It is enriched in skeletal and cardiac tissue, where it activates expression of *vegfa* (Teng et al., 2010). Recent work has suggested that it binds the co-repressor Eto-2 in MEL cells, which itself is a partner of Ldb1 (Eric Soler, *unpublished*). As depletion of Eto-2 has previously been shown to result in loss of the HSC marker *runx1* in zebrafish (Meier et al., 2006), we were interested if Ifr2bp2 also had a role in haematopoiesis. (A – D) Expression of *irf2bp2b* is ubiquitous, with weak specific expression in the PLM (white arrowheads), and later on in the dorsal aorta (red arrowhead) and pronephric duct (pnd) (Rui Monteiro, *unpublished*). (E – F) The *irf2bp2b* morpholino causes a five amino acid deletion at the end of exon 1. This is due to utilisation of a cryptic splice donor site in exon 1. In *irf2bp2b* morphants, the HSC marker *runx1* is reduced (G – H), along with T-cell progenitors in the thymus (I – J), and HSCs and their derivatives in the caudal haematopoietic tissue (K – L).

Appendix VI – Precursor states of the HSC are unaffected in *irf2bp2b* morphants

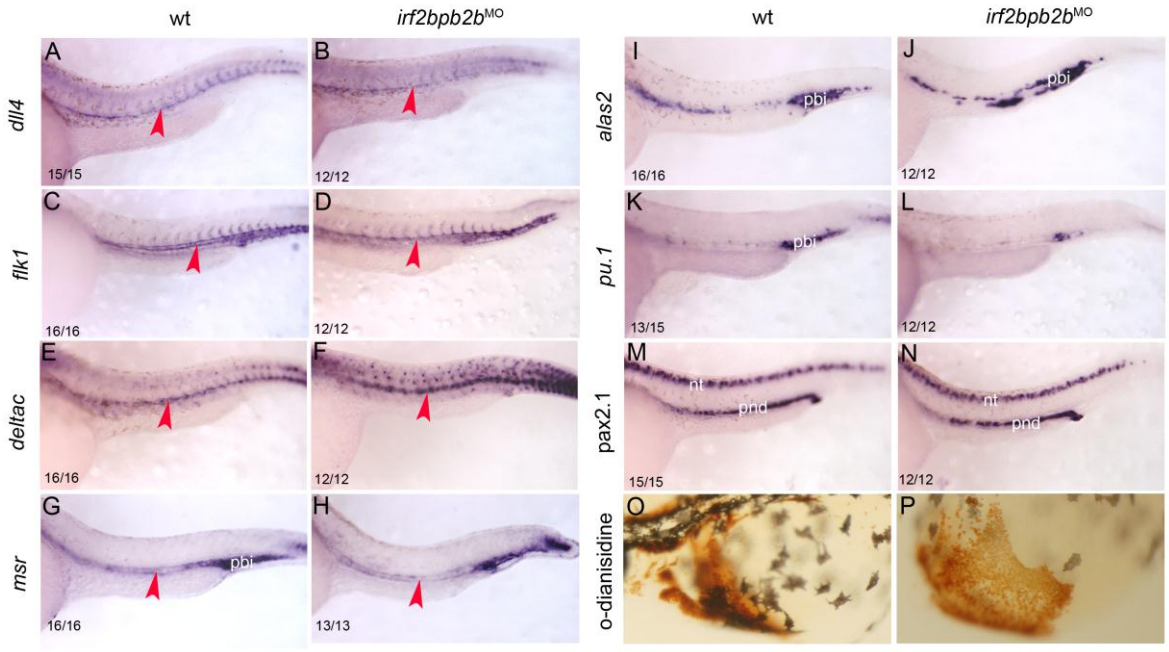

Figure S6 Precursor states of the haematopoietic stem cell are unaffected in *irf2bp2b* morphants

Endothelial (C – D) and arterial (A – B and E – F) markers were not reduced in *irf2bp2b* morphants. Specification of primitive blood (I – L) and maintenance of primitive erythrocytes was unaffected (O – P). Development of the pronephric duct (pnd) was unaffected in morphants (M – N). However, *msr* expression in the vein was reduced (G – H). The PLM is also unaffected in *irf2bp2b* morphants (Anjali Verma and Phil Ingham, *unpublished*). (A – N) *In situs* were performed at 33 hpf; (O – P) o-dianisidine staining was performed and embryos imaged at 3 dpf; nt, neural tube; pbi, posterior blood island.

References

Adamo, L., O. Naveiras, P.L. Wenzel, S. McKinney-Freeman, P.J. Mack, J. Gracia-Sancho, A. Suchy-Dicey, M. Yoshimoto, M.W. Lensch, M.C. Yoder, G. Garcia-Cardena, and G.Q. Daley. 2009. Biomechanical forces promote embryonic haematopoiesis. *Nature* 459:1131-U1120.

Adolfsson, J., O.J. Borge, D. Bryder, K. Theilgaard-Monch, I. Astrand-Grundstrom, E. Sitnicka, Y. Sasaki, and S.E. Jacobsen. 2001. Upregulation of Flt3 expression within the bone marrow Lin(-)Sca1(+)c-kit(+) stem cell compartment is accompanied by loss of self-renewal capacity. *Immunity* 15:659-669.

Adolfsson, J., R. Mansson, N. Buza-Vidas, A. Hultquist, K. Liuba, C.T. Jensen, D. Bryder, L. Yang, O.J. Borge, L.A. Thoren, K. Anderson, E. Sitnicka, Y. Sasaki, M. Sigvardsson, and S.E. Jacobsen. 2005. Identification of Flt3+ lympho-myeloid stem cells lacking erythro-megakaryocytic potential a revised road map for adult blood lineage commitment. *Cell* 121:295-306.

Agulnick, A.D., M. Taira, J.J. Breen, T. Tanaka, I.B. Dawid, and H. Westphal. 1996. Interactions of the LIM-domain-binding factor Ldb1 with LIM homeodomain proteins. *Nature* 384:270-272.

Akashi, K., D. Traver, T. Miyamoto, and I.L. Weissman. 2000. A clonogenic common myeloid progenitor that gives rise to all myeloid lineages. *Nature* 404:193-197.

Alon, U. 2007. Network motifs: theory and experimental approaches. *Nat Rev Genet* 8:450-461.

Altschul, S.F., W. Gish, W. Miller, E.W. Myers, and D.J. Lipman. 1990. Basic Local Alignment Search Tool. *J Mol Biol* 215:403-410.

Alvarez-Silva, M., P. Belo-Diabangouaya, J. Salaun, and F. Dieterlen-Lievre. 2003. Mouse placenta is a major hematopoietic organ. *Development (Cambridge, England)* 130:5437-5444.

Anguita, E., J. Hughes, C. Heyworth, G.A. Blobel, W.G. Wood, and D.R. Higgs. 2004. Globin gene activation during haemopoiesis is driven by protein complexes nucleated by GATA-1 and GATA-2. *Embo Journal* 23:2841-2852.

Aoyama, M., T. Ozaki, H. Inuzuka, D. Tomotsune, J. Hirato, Y. Okamoto, H. Tokita, M. Ohira, and A. Nakagawara. 2005. LMO3 interacts with neuronal transcription factor, HEN2, and acts as an oncogene in neuroblastoma. *Cancer Res* 65:4587-4597.

Appert, A., C.H. Nam, N. Lobato, E. Priego, R.N. Miguel, T. Blundell, L. Drynan, H. Sewell, T. Tanaka, and T. Rabbitts. 2009. Targeting LMO2 with a Peptide Aptamer Establishes a Necessary Function in Overt T-Cell Neoplasia. *Cancer Res* 69:4784-4790.

Arnold, K., L. Bordoli, J. Kopp, and T. Schwede. 2006. The SWISS-MODEL workspace: a web-based environment for protein structure homology modelling. *Bioinformatics* 22:195-201.

Artus, J., P. Douvaras, A. Piliszek, J. Isern, M.H. Baron, and A.K. Hadjantonakis. 2012. BMP4 signaling directs primitive endoderm-derived XEN cells to an extraembryonic visceral endoderm identity. *Dev Biol* 361:245-262.

Asahara, T., T. Murohara, A. Sullivan, M. Silver, R. vanderZee, T. Li, B. Witzenbichler, G. Schatteman, and J.M. Isner. 1997. Isolation of putative progenitor endothelial cells for angiogenesis. *Science* 275:964-967.

Avaron, F., L. Hoffman, D. Guay, and M.A. Akimenko. 2006. Characterization of two new zebrafish members of the hedgehog family: Atypical expression of a zebrafish indian hedgehog gene in skeletal elements of both endochondral and dermal origins. *Dev Dynam* 235:478-489.

Babu, M.M., R. van der Lee, N.S. de Groot, and J. Gsponer. 2011. Intrinsically disordered proteins: regulation and disease. *Curr Opin Struct Biol* 21:432-440.

Bach, I. 2000. The LIM domain: regulation by association. *Mech Develop* 91:5-17.

Bailey, A.S., S.G. Jiang, M. Afentoulis, C.I. Baumann, D.A. Schroeder, S.B. Olson, M.H. Wong, and W.H. Fleming. 2004. Transplanted adult hematopoietic stems cells differentiate into functional endothelial cells. *Blood* 103:13-19.

Baron, M. 2001. Induction of embryonic hematopoietic and endothelial stem/progenitor cells by hedgehog-mediated signals. *Differentiation* 68:175-185.

Baron, M.H. 2003. Embryonic origins of mammalian hematopoiesis. *Exp Hematol* 31:1160-1169.

Baron, M.H. 2005. Early patterning of the mouse embryo: implications for hematopoietic commitment and differentiation. *Exp Hematol* 33:1015-1020.

Baron, M.H., J. Isern, and S.T. Fraser. 2012. The embryonic origins of erythropoiesis in mammals. *Blood* 119:4828-4837.

Baum, C.M., I.L. Weissman, A.S. Tsukamoto, A.M. Buckle, and B. Peault. 1992. Isolation of a Candidate Human Hematopoietic Stem-Cell Population. *P Natl Acad Sci USA* 89:2804-2808.

Becker, A.J., C.E. Mc, and J.E. Till. 1963. Cytological demonstration of the clonal nature of spleen colonies derived from transplanted mouse marrow cells. *Nature* 197:452-454.

Begley, C.G., and A.R. Green. 1999. The SCL gene: from case report to critical hematopoietic regulator. *Blood* 93:2760-2770.

Belaoussoff, M., S.M. Farrington, and M.H. Baron. 1998. Hematopoietic induction and respecification of A-P identity by visceral endoderm signaling in the mouse embryo. *Development* 125:5009-5018.

Ben-Zvi, D., B.Z. Shilo, A. Fainsod, and N. Barkai. 2008. Scaling of the BMP activation gradient in Xenopus embryos. *Nature* 453:1205-1211.

Bergamaschi, D., Y. Samuels, N.J. O'Neil, G. Trigiante, T. Crook, J.K. Hsieh, D.J. O'Connor, S. Zhong, I. Campargue, M.L. Tomlinson, P.E. Kuwabara, and X. Lu. 2003. iASPP oncoprotein is a key inhibitor of p53 conserved from worm to human. *Nat Genet* 33:162-167.

Bertos, N.R., A.H. Wang, and X.J. Yang. 2001. Class II histone deacetylases: structure, function, and regulation. *Biochem Cell Biol* 79:243-252.

Bertrand, J.Y., N.C. Chi, B. Santoso, S.T. Teng, D.Y.R. Stainier, and D. Traver. 2010a. Haematopoietic stem cells derive directly from aortic endothelium during development. *Nature* 464:108-U120.

Bertrand, J.Y., J.L. Cisson, D.L. Stachura, and D. Traver. 2010b. Notch signaling distinguishes 2 waves of definitive hematopoiesis in the zebrafish embryo. *Blood* 115:2777-2783.

Bertrand, J.Y., S. Giroux, R. Golub, M. Klaine, A. Jalil, L. Boucontet, I. Godin, and A. Cumano. 2005. Characterization of purified intraembryonic hematopoietic stem cells as a tool to define their site of origin. *P Natl Acad Sci USA* 102:134-139.

Bertrand, J.Y., A.D. Kim, E.P. Violette, D.L. Stachura, J.L. Cisson, and D. Traver. 2007. Definitive hematopoiesis initiates through a committed erythromyeloid progenitor in the zebrafish embryo. *Development* 134:4147-4156.

Blackledge, N.P., H.K. Long, J.C. Zhou, S. Kriaucionis, R. Patient, and R.J. Klose. 2012. Bio-CAP: a versatile and highly sensitive technique to purify and characterise regions of non-methylated DNA. *Nucleic Acids Res* 40:e32.

Blum, Y., H.G. Belting, E. Ellertsdottir, L. Herwig, F. Luders, and M. Affolter. 2008. Complex cell rearrangements during intersegmental vessel sprouting and vessel fusion in the zebrafish embryo. *Dev Biol* 316:312-322.

Boehm, T., L. Foroni, Y. Kaneko, M.F. Perutz, and T.H. Rabbitts. 1991. The rhombotin family of cysteine-rich LIM-domain oncogenes: distinct members are involved in T-cell translocations to human chromosomes 11p15 and 11p13. *P Natl Acad Sci USA* 88:4367-4371.

Boisset, J.C., W. van Cappellen, C. Andrieu-Soler, N. Galjart, E. Dzierzak, and C. Robin. 2010. In vivo imaging of haematopoietic cells emerging from the mouse aortic endothelium. *Nature* 464:116-U131.

Bolouri, H., and E.H. Davidson. 2002. Modeling DNA sequence-based cis-regulatory gene networks. *Dev Biol* 246:2-13.

Bourgeas, R., M.J. Basse, X. Morelli, and P. Roche. 2010. Atomic Analysis of Protein-Protein Interfaces with Known Inhibitors: The 2P2I Database. *PLoS One* 5:

Bresnick, E.H., H.Y. Lee, T. Fujiwara, K.D. Johnson, and S. Keles. 2010. GATA switches as developmental drivers. *J Biol Chem* 285:31087-31093.

Brown, L.A., A.R.F. Rodaway, T.F. Schilling, T. Jowett, P.W. Ingham, R.K. Patient, and A.D. Sharrocks. 2000. Insights into early vasculogenesis revealed by expression of the ETS-domain transcription factor Fli-1 in wild-type and mutant zebrafish embryos. *Mech Develop* 90:237-252.

Burns, C.E., D. Traver, E. Mayhall, J.L. Shepard, and L.I. Zon. 2005. Hematopoietic stem cell fate is established by the Notch-Runx pathway. *Genes Dev* 19:2331-2342.

Bussmann, J., J. Bakkers, and S. Schulte-Merker. 2007. Early endocardial morphogenesis requires Scl/Tal1. *Plos Genet* 3:1425-1437.

Bussmann, J., F.L. Bos, A. Urasaki, K. Kawakami, H.J. Duckers, and S. Schulte-Merker. 2010. Arteries provide essential guidance cues for lymphatic endothelial cells in the zebrafish trunk. *Development* 137:2653-2657.

Caetano-Anollés, G. 2010. Evolutionary genomics and systems biology. Wiley-Blackwell, Hoboken, N.J. xix, 465 p., 440 p. of plates pp.

Cai, Z., M. de Bruijn, X. Ma, B. Dortland, T. Luteijn, R.J. Downing, and E. Dzierzak. 2000. Haploinsufficiency of AML1 affects the temporal and spatial generation of hematopoietic stem cells in the mouse embryo. *Immunity* 13:423-431.

Caprioli, A., K. Minko, C. Drevon, A. Eichmann, F. Dieterlen-Lievre, and T. Jaffredo. 2001. Hemangioblast commitment in the avian allantois: cellular and molecular aspects. *Dev Biol* 238:64-78.

Carmeliet, P., V. Ferreira, G. Breier, S. Pollefeyt, L. Kieckens, M. Gertsenstein, M. Fahrig, A. Vandenhoeck, K. Harpal, C. Eberhardt, C. Declercq, J. Pawling, L. Moons, D. Collen, W. Risau, and A. Nagy. 1996.

Abnormal blood vessel development and lethality in embryos lacking a single VEGF allele. *Nature* 380:435-439.

Chan, H.M., M. Narita, S.W. Lowe, and D.M. Livingston. 2005. The p400 E1A-associated protein is a novel component of the p53 --> p21 senescence pathway. *Genes Dev* 19:196-201.

Chang, H.H., M. Hemberg, M. Barahona, D.E. Ingber, and S. Huang. 2008a. Transcriptome-wide noise controls lineage choice in mammalian progenitor cells. *Nature* 453:544-547.

Chang, S., B.D. Young, S. Li, X. Qi, J.A. Richardson, and E.N. Olson. 2006. Histone deacetylase 7 maintains vascular integrity by repressing matrix metalloproteinase 10. *Cell* 126:321-334.

Chang, W.I., Z.S. Lin, H. Kulessa, J. Hebert, B.L.M. Hogan, and D.K. Wu. 2008b. Bmp4 is essential for the formation of the vestibular apparatus that detects angular head movements. *Plos Genet* 4:

Chen, A.T., and L.I. Zon. 2009. Zebrafish Blood Stem Cells. *J Cell Biochem* 108:35-42.

Chen, J.N., and M.C. Fishman. 1996. Zebrafish tinman homolog demarcates the heart field and initiates myocardial differentiation. *Development* 122:3809-3816.

Chen, M.J., Y. Li, M.E. De Obaldia, Q. Yang, A.D. Yzaguirre, T. Yamada-Inagawa, C.S. Vink, A. Bhandoola, E. Dzierzak, and N.A. Speck. 2011. Erythroid/Myeloid Progenitors and Hematopoietic Stem Cells Originate from Distinct Populations of Endothelial Cells. *Cell Stem Cell* 9:541-552.

Chen, M.J., T. Yokomizo, B.M. Zeigler, E. Dzierzak, and N.A. Speck. 2009. Runx1 is required for the endothelial to haematopoietic cell transition but not thereafter. *Nature* 457:887-891.

Chien, P.Y., M. Ito, Y. Park, T. Tagami, B.D. Gehm, and J.L. Jameson. 1999. A fusion protein of the estrogen receptor (ER) and nuclear receptor corepressor (NCoR) strongly inhibits estrogen-dependent responses in breast cancer cells. *Mol Endocrinol* 13:2122-2136.

Childs, K.S., and S. Goodbourn. 2003. Identification of novel co-repressor molecules for Interferon Regulatory Factor-2. *Nucleic Acids Res* 31:3016-3026.

Chocron, S., M.C. Verhoeven, F. Rentzsch, M. Hammerschmidt, and J. Bakkers. 2007. Zebrafish Bmp4 regulates left-right asymmetry at two distinct developmental time points. *Dev Biol* 305:577-588.

Choi, K., M. Kennedy, A. Kazarov, J.C. Papadimitriou, and G. Keller. 1998. A common precursor for hematopoietic and endothelial cells. *Development* 125:725-732.

Ciau-Uitz, A., P. Pinheiro, R. Gupta, T. Enver, and R. Patient. 2010. Tel1/ETV6 specifies blood stem cells through the agency of VEGF signaling. *Dev Cell* 18:569-578.

Ciau-Uitz, A., M. Walmsley, and R. Patient. 2000. Distinct origins of adult and embryonic blood in Xenopus. *Cell* 102:787-796.

Cleaver, O., and P.A. Krieg. 1998. VEGF mediates angioblast migration during development of the dorsal aorta in Xenopus. *Development* 125:3905-3914.

Clements, W.K., A.D. Kim, K.G. Ong, J.C. Moore, N.D. Lawson, and D. Traver. 2011. A somitic Wnt16/Notch pathway specifies haematopoietic stem cells. *Nature* 474:220-224.

Corbel, C., J. Salaun, P. Belo-Diabangouaya, and F. Dieterlen-Lievre. 2007. Hematopoietic potential of the pre-fusion allantois. *Dev Biol* 301:478-488.

Cormier, F., and F. Dieterlenlievre. 1988. The Wall of the Chick-Embryo Aorta Harbors M-Cfc, G-Cfc, Gm-Cfc and Bfu-E. *Development* 102:279-&.

Costa, G., V. Kouskoff, and G. Lacaud. 2012. Origin of blood cells and HSC production in the embryo. *Trends Immunol* 33:215-223.

Coultas, L., K. Chawengsaksophak, and J. Rossant. 2005. Endothelial cells and VEGF in vascular development. *Nature* 438:937-945.

Cox, C.M., and T.J. Poole. 2000. Angioblast differentiation is influenced by the local environment: FGF-2 induces angioblasts and patterns vessel formation in the quail embryo. *Dev Dynam* 218:371-382.

Cumano, A., F. Dieterlen-Lievre, and I. Godin. 1996. Lymphoid potential, probed before circulation in mouse, is restricted to caudal intraembryonic splanchnopleura. *Cell* 86:907-916.

Cumano, A., J.C. Ferraz, M. Klaine, J.P. Di Santo, and I. Godin. 2001. Intraembryonic, but not yolk sac hematopoietic precursors, isolated before circulation, provide long-term multilineage reconstitution. *Immunity* 15:477-485.

Cumano, A., C. Furlonger, and C.J. Paige. 1993. Differentiation and Characterization of B-Cell Precursors Detected in the Yolk-Sac and Embryo Body of Embryos Beginning at the 10-Somite to 12-Somite Stage. *P Natl Acad Sci USA* 90:6429-6433.

Cumano, A., and I. Godin. 2007. Ontogeny of the hematopoietic system. *Annu Rev Immunol* 25:745-785.

Curry, J.L., and J.J. Trentin. 1967. Hemopoietic spleen colony studies. I. Growth and differentiation. *Dev Biol* 15:395-413.

D'Souza, S.L., A.G. Elefanty, and G. Keller. 2005. SCL/Tal-1 is essential for hematopoietic commitment of the hemangioblast but not for its development. *Blood* 105:3862-3870.

Da'as, S.I., A.J. Coombs, T.B. Balci, C.A. Grondin, A.A. Ferrando, and J.N. Berman. 2012. The zebrafish reveals dependence of the mast cell lineage on Notch signaling in vivo. *Blood* 119:3585-3594.

Dahm, R., and R. Geisler. 2006. Learning from small fry: The zebrafish as a genetic model organism for aquaculture fish species. *Mar Biotechnol* 8:329-345.

Dale, L., G. Howes, B.M. Price, and J.C. Smith. 1992. Bone morphogenetic protein 4: a ventralizing factor in early Xenopus development. *Development* 115:573-585.

de Boer, E., P. Rodriguez, E. Bonte, J. Krijgsveld, E. Katsantoni, A. Heck, F. Grosveld, and J. Strouboulis. 2003. Efficient biotinylation and single-step purification of tagged transcription factors in mammalian cells and transgenic mice. *P Natl Acad Sci USA* 100:7480-7485.

de Bruijn, M.F.T.R., X.Q. Ma, C. Robin, K. Ottersbach, M.J. Sanchez, and E. Dzierzak. 2002. Hematopoietic stem cells localize to the endothelial cell layer in the midgestation mouse aorta. *Immunity* 16:673-683.

de Jong, J.L., and L.I. Zon. 2012. Histocompatibility and hematopoietic transplantation in the zebrafish. *Adv Hematol* 2012:282318.

de la Calle-Mustienes, E., Z. Lu, M. Cortes, B. Andersen, J. Modolell, and J.L. Gomez-Skarmeta. 2003. Xenopus Xlmo4 is a GATA cofactor during ventral mesoderm formation and regulates Ldb1 availability at the dorsal mesoderm and the neural plate. *Dev Biol* 264:564-581.

de Vries, S.J., A.D. van Dijk, and A.M. Bonvin. 2006. WHISCY: what information does surface conservation yield? Application to data-driven docking. *Proteins* 63:479-489.

Deane, J.E., D.P. Ryan, M. Sunde, M.J. Maher, J.M. Guss, J.E. Visvader, and J.M. Matthews. 2004. Tandem LIM domains provide synergistic binding in the LMO4 : Ldb1 complex. *Embo Journal* 23:3589-3598.

Deane, J.E., E. Sum, J.P. Mackay, G.J. Lindeman, J.E. Visvader, and J.M. Matthews. 2001. Design, production and characterization of FLIN2 and FLIN4: the engineering of intramolecular ldb1 : LMO complexes. *Protein Eng* 14:493-499.

Detrich, H.W., M.W. Kieran, F.Y. Chan, L.M. Barone, K. Yee, J.A. Rundstadler, S. Pratt, D. Ransom, and L.I. Zon. 1995. Intraembryonic Hematopoietic-Cell Migration during Vertebrate Development. *P Natl Acad Sci USA* 92:10713-10717.

Dickinson, R.E., H. Griffin, V. Bigley, L.N. Reynard, R. Hussain, M. Haniffa, J.H. Lakey, T. Rahman, X.-N. Wang, N. McGovern, S. Pagan, S. Cookson, D. McDonald, I. Chua, J. Wallis, A. Cant, M. Wright, B. Keavney, P.F. Chinnery, J. Loughlin, S. Hambleton, M. Santibanez-Koref, and M. Collin. 2011. Exome sequencing identifies GATA-2 mutation as the cause of dendritic cell, monocyte, B and NK lymphoid deficiency. *Blood* 118:2656-2658.

Dieterlen-Lievre, F. 1975. On the origin of haemopoietic stem cells in the avian embryo: an experimental approach. *J Embryol Exp Morphol* 33:607-619.

Dieterlen-Lievre, F., and C. Martin. 1981. Diffuse intraembryonic hemopoiesis in normal and chimeric avian development. *Dev Biol* 88:180-191.

Dieterlen-Lievre, F., C. Pouget, K. Bollerot, and T. Jaffredo. 2006. Are intra-aortic hemopoietic cells derived from endothelial cells during ontogeny? *Trends Cardiovasc Med* 16:128-139.

Doulatov, S., F. Notta, E. Laurenti, and J.E. Dick. 2012. Hematopoiesis: A Human Perspective. *Cell Stem Cell* 10:120-136.

Durand, C., C. Robin, K. Bollerot, M.H. Baron, K. Ottersbach, and E. Dzierzak. 2007. Embryonic stromal clones reveal developmental regulators of definitive hematopoietic stem cells. *P Natl Acad Sci USA* 104:20838-20843.

Dussault, A.A., and M. Pouliot. 2006. Rapid and simple comparison of messenger RNA levels using real-time PCR. *Biol Proced Online* 8:1-10.

Dyer, M.A., S.M. Farrington, D. Mohn, J.R. Munday, and M.H. Baron. 2001. Indian hedgehog activates hematopoiesis and vasculogenesis and can respecify prospective neurectodermal cell fate in the mouse embryo. *Development* 128:1717-1730.

Dzierzak, E., and N.A. Speck. 2008. Of lineage and legacy: the development of mammalian hematopoietic stem cells. *Nat Immunol* 9:129-136.

Eichmann, A., C. Marcelle, C. Breant, and N.M. Le Douarin. 1993. Two molecules related to the VEGF receptor are expressed in early endothelial cells during avian embryonic development. *Mech Develop* 42:33-48.

Eichmann, A., L. Yuan, D. Moyon, F. Lenoble, L. Pardanaud, and C. Breant. 2005. Vascular development: from precursor cells to branched arterial and venous networks. *Int J Dev Biol* 49:259-267.

Eilken, H.M., S. Nishikawa, and T. Schroeder. 2009. Continuous single-cell imaging of blood generation from haemogenic endothelium. *Nature* 457:896-900.

Eisen, J.S., and J.C. Smith. 2008. Controlling morpholino experiments: don't stop making antisense. *Development* 135:1735-1743.

El Omari, K., S.J. Hoosdally, K. Tuladhar, D. Karia, P. Vyas, R. Patient, C. Porcher, and E.J. Mancini. 2011. Structure of the leukemia oncogene LMO2: implications for the assembly of a hematopoietic transcription factor complex. *Blood* 117:2146-2156.

Elefanty, A.G., C.G. Begley, L. Hartley, B. Papaevangeliou, and L. Robb. 1999. SCL expression in the mouse embryo detected with a targeted lacZ reporter gene demonstrates its localization to hematopoietic, vascular, and neural tissues. *Blood* 94:3754-3763.

Ellertsdottir, E., A. Lenard, Y. Blum, A. Krudewig, L. Herwig, M. Affolter, and H.G. Belting. 2010. Vascular morphogenesis in the zebrafish embryo. *Dev Biol* 341:56-65.

Ema, M., P. Faloon, W.J. Zhang, M. Hirashima, T. Reid, W.L. Stanford, S. Orkin, K. Choi, and J. Rossant. 2003. Combinatorial effects of Flk1 and Tal1 on vascular and hematopoietic development in the mouse. *Genes Dev* 17:380-393.

Emekli, U., D. Schneidman-Duhovny, H.J. Wolfson, R. Nussinov, and T. Haliloglu. 2008. HingeProt: Automated prediction of hinges in protein structures. *Proteins-Structure Function and Bioinformatics* 70:1219-1227.

Emmel, V.E. 1916. The cell clusters in the dorsal aorta of mammalian embryos. *American Journal of Anatomy* 19:401-421.

Endoh, M., M. Ogawa, S. Orkin, and S. Nishikawa. 2002. SCL/tal-1-dependent process determines a competence to select the definitive hematopoietic lineage prior to endothelial differentiation. *Embo J* 21:6700-6708.

Faloon, P., E. Arentson, A. Kazarov, C.X. Deng, C. Porcher, S. Orkin, and K. Choi. 2000. Basic fibroblast growth factor positively regulates hematopoietic development. *Development* 127:1931-1941.

Fan, Z.P., T. Yamaza, J.S. Lee, J.H. Yu, S.L. Wang, G.P. Fan, S.T. Shi, and C.Y. Wang. 2009. BCOR regulates mesenchymal stem cell function by epigenetic mechanisms. *Nat Cell Biol* 11:1002-U1215.

Ferrando, A.A., S. Herblot, T. Palomero, M. Hansen, T. Hoang, E.A. Fox, and A.T. Look. 2004. Biallelic transcriptional activation of oncogenic transcription factors in T-cell acute lymphoblastic leukemia. *Blood* 103:1909-1911.

Ferrando, A.A., D.S. Neuberg, J. Staunton, M.L. Loh, C. Huard, S.C. Raimondi, F.G. Behm, C.H. Pui, J.R. Downing, D.G. Gilliland, E.S. Lander, T.R. Golub, and A.T. Look. 2002. Gene expression signatures define novel oncogenic pathways in T cell acute lymphoblastic leukemia. *Cancer Cell* 1:75-87.

Ferrara, N., K. Carver-Moore, H. Chen, M. Dowd, L. Lu, K.S. O'Shea, L. Powell-Braxton, K.J. Hillan, and M.W. Moore. 1996. Heterozygous embryonic lethality induced by targeted inactivation of the VEGF gene. *Nature* 380:439-442.

Ferri-Lagneau, K.F., K.S. Moshal, M. Grimes, B. Zahora, L. Lv, S. Sang, and T. Leung. 2012. Ginger Stimulates Hematopoiesis via Bmp Pathway in Zebrafish. *PLoS One* 7:e39327.

Fisch, P., T. Boehm, I. Lavenir, T. Larson, J. Arno, A. Forster, and T.H. Rabbitts. 1992. T-Cell Acute Lymphoblastic Lymphoma Induced in Transgenic Mice by the Rbtn1 and Rbtn2 Lim-Domain Genes. *Oncogene* 7:2389-2397.

Flicek, P., M.R. Amode, D. Barrell, K. Beal, S. Brent, D. Carvalho-Silva, P. Clapham, G. Coates, S. Fairley, S. Fitzgerald, L. Gil, L. Gordon, M. Hendrix, T. Hourlier, N. Johnson, A.K. Kahari, D. Keefe, S. Keenan, R. Kinsella, M. Komorowska, G. Koscielny, E. Kulesha, P. Larsson, I. Longden, W. McLaren, M. Muffato, B. Overduin, M. Pignatelli, B. Pritchard, H.S. Riat, G.R.S. Ritchie, M. Ruffier, M. Schuster, D. Sobral, Y.A. Tang, K. Taylor, S. Trevanion, J. Vandrovcova, S. White, M. Wilson, S.P. Wilder, B.L. Aken, E. Birney, F. Cunningham, I. Dunham, R. Durbin, X.M. Fernandez-Suarez, J. Harrow, J. Herrero, T.J.P. Hubbard, A. Parker, G. Proctor, G. Spudich, J. Vogel, A. Yates, A. Zadissa, and S.M.J. Searle. 2012. Ensembl 2012. *Nucleic Acids Res* 40:D84-D90.

Folkman, J. 1971. Tumor angiogenesis: therapeutic implications. *N Engl J Med* 285:1182-1186.

Fong, G.H., J. Rossant, M. Gertsenstein, and M.L. Breitman. 1995. Role of the Flt-1 receptor tyrosine kinase in regulating the assembly of vascular endothelium. *Nature* 376:66-70.

Fong, G.H., L. Zhang, D.M. Bryce, and J. Peng. 1999. Increased hemangioblast commitment, not vascular disorganization, is the primary defect in flt-1 knock-out mice. *Development* 126:3015-3025.

Fontaineperus, J.C., F.M. Calman, C. Kaplan, and N.M. Ledouarin. 1981. Seeding of the 10-Day Mouse Embryo Thymic Rudiment by Lymphocyte Precursors Invitro. *J Immunol* 126:2310-2316.

Fouquet, B., B.M. Weinstein, F.C. Serluca, and M.C. Fishman. 1997. Vessel patterning in the embryo of the zebrafish: guidance by notochord. *Dev Biol* 183:37-48.

Frazer, K.A., L. Pachter, A. Poliakov, E.M. Rubin, and I. Dubchak. 2004. VISTA: computational tools for comparative genomics. *Nucleic Acids Res* 32:W273-W279.

Fujii, T., T. Ueda, S. Nagata, and R. Fukunaga. 2010. Essential role of p400/mDomino chromatin-remodeling ATPase in bone marrow hematopoiesis and cell-cycle progression. *The Journal of biological chemistry* 285:30214-30223.

Fujiwara, Y., A.N. Chang, A.M. Williams, and S.H. Orkin. 2004. Functional overlap of GATA-1 and GATA-2 in primitive hematopoietic development. *Blood* 103:583-585.

Furuya, F., C.J. Guigon, L. Zhao, C. Lu, J.A. Hanover, and S.Y. Cheng. 2007. Nuclear receptor corepressor is a novel regulator of phosphatidylinositol 3-kinase signaling. *Mol Cell Biol* 27:6116-6126.

Galloway, J.L., R.A. Wingert, C. Thisse, B. Thisse, and L.I. Zon. 2005. Loss of gata1 but not gata2 converts erythropoiesis to myelopoiesis in zebrafish embryos. *Dev Cell* 8:109-116.

Garcia-Porrero, J.A., I.E. Godin, and F. Dieterlen-Lievre. 1995. Potential intraembryonic hemogenic sites at pre-liver stages in the mouse. *Anat Embryol (Berl)* 192:425-435.

Gardiner-Garden, M., and M. Frommer. 1987. CpG islands in vertebrate genomes. *J Mol Biol* 196:261-282.

Gearhart, M.D., C.M. Corcoran, J.A. Wamstad, and V.J. Bardwell. 2006. Polycomb group and SCF ubiquitin ligases are found in a novel BCOR complex that is recruited to BCL6 targets. *Mol Cell Biol* 26:6880-6889.

Gekas, C., F. Dieterlen-Lievre, S.H. Orkin, and H.K.A. Mikkola. 2005. The placenta is a niche for hematopoietic stem cells. *Dev Cell* 8:365-375.

Gerhardt, H., M. Golding, M. Fruttiger, C. Ruhrberg, A. Lundkvist, A. Abramsson, M. Jeltsch, C. Mitchell, K. Alitalo, D. Shima, and C. Betsholtz. 2003. VEGF guides angiogenic sprouting utilizing endothelial tip cell filopodia. *J Cell Biol* 161:1163-1177.

Gering, M., and R. Patient. 2005. Hedgehog signaling is required for adult blood stem cell formation in zebrafish embryos. *Dev Cell* 8:389-400.

Gering, M., A.R. Rodaway, B. Gottgens, R.K. Patient, and A.R. Green. 1998. The SCL gene specifies haemangioblast development from early mesoderm. *Embo J* 17:4029-4045.

Gering, M., Y. Yamada, T.H. Rabbitts, and R.K. Patient. 2003. Lmo2 and Scl/Tal1 convert non-axial mesoderm into haemangioblasts which differentiate into endothelial cells in the absence of Gata1. *Development* 130:6187-6199.

Gevry, N., H.M. Chan, L. Laflamme, D.M. Livingston, and L. Gaudreau. 2007. p21 transcription is regulated by differential localization of histone H2A.Z. *Genes Dev* 21:1869-1881.

Ghetu, A.F., C.M. Corcoran, L. Cerchietti, V.J. Bardwell, A. Melnick, and G.G. Prive. 2008. Structure of a BCOR corepressor peptide in complex with the BCL6 BTB domain dimer. *Mol Cell* 29:384-391.

Godin, I., and A. Cumano. 2002. The hare and the tortoise: an embryonic haematopoietic race. *Nat Rev Immunol* 2:593-604.

Godin, I., J.A. Garcia-Porrero, F. Dieterlen-Lievre, and A. Cumano. 1999. Stem cell emergence and hemopoietic activity are incompatible in mouse intraembryonic sites. *J Exp Med* 190:43-52.

Godin, I.E., J.A. Garcia-Porrero, A. Coutinho, F. Dieterlen-Lievre, and M.A. Marcos. 1993. Para-aortic splanchnopleura from early mouse embryos contains B1a cell progenitors. *Nature* 364:67-70.

Goldman, D.C., A.S. Bailey, D.L. Pfaffle, A. Al Masri, J.L. Christian, and W.H. Fleming. 2009. BMP4 regulates the hematopoietic stem cell niche. *Blood* 114:4393-4401.

Gore, A.V., K. Monzo, Y.R. Cha, W. Pan, and B.M. Weinstein. 2012. Vascular development in the zebrafish. *Cold Spring Harb Perspect Med* 2:a006684.

Gottgens, B., A. Nastos, S. Kinston, S. Piltz, E.C. Delabesse, M. Stanley, M.J. Sanchez, A. Ciau-Uitz, R. Patient, and A.R. Green. 2002. Establishing the transcriptional programme for blood: the SCL stem cell enhancer is regulated by a multiprotein complex containing Ets and GATA factors. *Embo J* 21:3039-3050.

Graff, J.M., R.S. Thies, J.J. Song, A.J. Celeste, and D.A. Melton. 1994. Studies with a Xenopus BMP receptor suggest that ventral mesoderm-inducing signals override dorsal signals in vivo. *Cell* 79:169-179.

Grant, M.B., W.S. May, S. Caballero, G.A. Brown, S.M. Guthrie, R.N. Mames, B.J. Byrne, T. Vaught, P.E. Spoerri, A.B. Peck, and E.W. Scott. 2002. Adult hematopoietic stem cells provide functional hemangioblast activity during retinal neovascularization. *Nat Med* 8:607-612.

Greaves, M., J. Robinson, D. Delia, R. Sutherland, R. Newman, and C. Sieff. 1981. Mapping cell surface antigen expression of haemopoietic progenitor cells using monoclonal antibodies. *Ciba Found Symp* 84:109-129.

Green, J.B., H.V. New, and J.C. Smith. 1992. Responses of embryonic Xenopus cells to activin and FGF are separated by multiple dose thresholds and correspond to distinct axes of the mesoderm. *Cell* 71:731-739.

Green, J.B., J.C. Smith, and J.C. Gerhart. 1994. Slow emergence of a multithreshold response to activin requires cell-contact-dependent sharpening but not prepattern. *Development* 120:2271-2278.

Griffin, K.J.P., J. Stoller, M. Gibson, S. Chen, D. Yelon, D.Y.R. Stainier, and D. Kimelman. 2000. A conserved role for H15-related T-box transcription factors in zebrafish and Drosophila heart formation. *Dev Biol* 218:235-247.

Grossmann, V., E. Tiacci, A.B. Holmes, A. Kohlmann, M.P. Martelli, W. Kern, A. Spanhol-Rosseto, H.U. Klein, M. Dugas, S. Schindela, V. Trifonov, S. Schnittger, C. Haferlach, R. Bassan, V.A. Wells, O. Spinelli, J. Chan, R. Rossi, S. Baldoni, L. De Carolis, K. Goetze, H. Serve, R. Peceny, K.A. Kreuzer, D. Oruzio, G. Specchia, F. Di Raimondo, F. Fabbiano, M. Sborgia, A. Liso, L. Farinelli, A. Rambaldi, L. Pasqualucci, R. Rabadan, T. Haferlach, and B. Falini. 2011. Whole-exome sequencing identifies somatic mutations of BCOR in acute myeloid leukemia with normal karyotype. *Blood* 118:6153-6163.

Grosveld, F., P. Rodriguez, N. Meier, S. Krpic, F. Pourfarzad, P. Papadopoulos, K. Kolodziej, G.P. Patrinos, A. Hostert, and J. Strouboulis. 2005. Isolation and characterization of hematopoietic transcription factor complexes by in vivo biotinylation tagging and mass spectrometry. *Ann Ny Acad Sci* 1054:55-67.

Grutz, G., A. Forster, and T.H. Rabbitts. 1998. Identification of the LMO4 gene encoding an interaction partner of the LIM-binding protein LDB1/NLI1: a candidate for displacement by LMO proteins in T cell acute leukaemia. *Oncogene* 17:2799-2803.

Gunsilius, E., H.C. Duba, A.L. Petzer, C.M. Kahler, K. Grunewald, G. Stockhammer, C. Gabl, S. Dirnhofer, J. Clausen, and G. Gastl. 2000. Evidence from a leukaemia model for maintenance of vascular endothelium by bone-marrow-derived endothelial cells. *Lancet* 355:1688-1691.

Ha, C.H., B.S. Jhun, H.Y. Kao, and Z.G. Jin. 2008. VEGF stimulates HDAC7 phosphorylation and cytoplasmic accumulation modulating matrix metalloproteinase expression and angiogenesis. *Arterioscler Thromb Vasc Biol* 28:1782-1788.

Haas, S., A. Steplewski, L.D. Siracusa, S. Amini, and K. Khalili. 1995. Identification of a sequence-specific single-stranded DNA binding protein that suppresses transcription of the mouse myelin basic protein gene. *The Journal of biological chemistry* 270:12503-12510.

Hacein-Bey-Abina, S., C. Von Kalle, M. Schmidt, M.P. McCormack, N. Wulffraat, P. Leboulch, A. Lim, C.S. Osborne, R. Pawliuk, E. Morillon, R. Sorensen, A. Forster, P. Fraser, J.I. Cohen, G. de Saint Basile, I. Alexander, U. Wintergerst, T. Frebourg, A. Aurias, D. Stoppa-Lyonnet, S. Romana, I. Radford-Weiss, F. Gross, F. Valensi, E. Delabesse, E. Macintyre, F. Sigaux, J. Soulier, L.E. Leiva, M. Wissler, C. Prinz, T.H. Rabbitts, F. Le Deist, A. Fischer, and M. Cavazzana-Calvo. 2003. LMO2-associated clonal T cell proliferation in two patients after gene therapy for SCID-X1. *Science* 302:415-419.

Hahm, K.M., E.Y.M. Sum, Y. Fujiwara, G.J. Lindeman, J.E. Visvader, and S.H. Orkin. 2004. Defective neural tube closure and anteroposterior patterning in mice lacking the LIM protein LMO4 or its interacting partner deaf-1. *Mol Cell Biol* 24:2074-2082.

Hahn, C.N., C.-E. Chong, C.L. Carmichael, E.J. Wilkins, P.J. Brautigan, X.-C. Li, M. Babic, M. Lin, A. Carmagnac, Y.K. Lee, C.H. Kok, L. Gagliardi, K.L. Friend, P.G. Ekert, C.M. Butcher, A.L. Brown, I.D. Lewis, L.B. To, A.E. Timms, J. Storek, S. Moore, M. Altree, R. Escher, P.G. Bardy, G.K. Suthers, R.J. D'Andrea, M.S. Horwitz, and H.S. Scott. 2011. Heritable GATA2 mutations associated with familial myelodysplastic syndrome and acute myeloid leukemia. *Nat Genet* 43:1012-1017.

Hale, G., and H. Waldmann. 1994. Control of graft-versus-host disease and graft rejection by T cell depletion of donor and recipient with Campath-1 antibodies. Results of matched sibling transplants for malignant diseases. *Bone Marrow Transplant* 13:597-611.

Hanai, J., L.F. Chen, T. Kanno, N. Ohtani-Fujita, W.Y. Kim, W.H. Guo, T. Imamura, Y. Ishidou, M. Fukuchi, M.J. Shi, J. Stavnezer, M. Kawabata, K. Miyazono, and Y. Ito. 1999. Interaction and functional cooperation of PEBP2/CBF with Smads - Synergistic induction of the immunoglobulin germline C alpha promoter. *J Biol Chem* 274:31577-31582.

Hao, J., J.N. Ho, J.A. Lewis, K.A. Karim, R.N. Daniels, P.R. Gentry, C.R. Hopkins, C.W. Lindsley, and C.C. Hong. 2010. In vivo structure-activity relationship study of dorsomorphin analogues identifies selective VEGF and BMP inhibitors. *ACS Chem Biol* 5:245-253.

Harada, H., S. Kizaka-Kondoh, G. Li, S. Itasaka, K. Shibuya, M. Inoue, and M. Hiraoka. 2007. Significance of HIF-1-active cells in angiogenesis and radioresistance. *Oncogene* 26:7508-7516.

Harland, R., and J. Gerhart. 1997. Formation and function of Spemann's organizer. *Annu Rev Cell Dev Bi* 13:611-667.

Herbomel, P., B. Thisse, and C. Thisse. 1999. Ontogeny and behaviour of early macrophages in the zebrafish embryo. *Development* 126:3735-3745.

Herbomel, P., B. Thisse, and C. Thisse. 2001. Zebrafish early macrophages colonize cephalic mesenchyme and developing brain, retina, and epidermis through a M-CSF receptor-dependent invasive process. *Dev Biol* 238:274-288.

Heyworth, C., K. Gale, M. Dexter, G. May, and T. Enver. 1999. A GATA-2/estrogen receptor chimera functions as a ligand-dependent negative regulator of self-renewal. *Genes Dev* 13:1847-1860.

Hilton, E.N., F.D.C. Manson, J.E. Urquhart, J.J. Johnston, A.M. Slavotinek, P. Hedera, E.L. Stattin, A. Nordgren, L.G. Biesecker, and G.C.M. Black. 2007. Left-sided embryonic expression of the BCL-6 corepressor, BCOR, is required for vertebrate laterality determination. *Hum Mol Genet* 16:1773-1782.

Hirano, K. 2007. The roles of proteinase-activated receptors in the vascular physiology and pathophysiology. *Arterioscler Thromb Vasc Biol* 27:27-36.

Hirashima, M., K. Sano, T. Morisada, K. Murakami, J. Rossant, and T. Suda. 2008. Lymphatic vessel assembly is impaired in Aspp1-deficient mouse embryos. *Dev Biol* 316:149-159.

His, W. 1900. Lecithoblast und Angioblast der Wirbelthiere: Histogenetische Studien. Teubner,

Hodgson, G.S., and T.R. Bradley. 1979. Properties of haematopoietic stem cells surviving 5-fluorouracil treatment: evidence for a pre-CFU-S cell? *Nature* 281:381-382.

Hogan, B.M., F.L. Bos, J. Bussmann, M. Witte, N.C. Chi, H.J. Duckers, and S. Schulte-Merker. 2009. ccbe1 is required for embryonic lymphangiogenesis and venous sprouting. *Nat Genet* 41:396-398.

Hong, C.C., Q.P. Peterson, J.Y. Hong, and R.T. Peterson. 2006. Artery/vein specification is governed by opposing phosphatidylinositol-3 kinase and MAP kinase/ERK signaling. *Curr Biol* 16:1366-1372.

Hoogenkamp, M., M. Lichtinger, H. Krysinska, C. Lancrin, D. Clarke, A. Williamson, L. Mazzarella, R. Ingram, H. Jorgensen, A. Fisher, D.G. Tenen, V. Kouskoff, G. Lacaud, and C. Bonifer. 2009. Early chromatin

unfolding by RUNX1: a molecular explanation for differential requirements during specification versus maintenance of the hematopoietic gene expression program. *Blood* 114:299-309.

Hsu, A.P., E.P. Sampaio, J. Khan, K.R. Calvo, J.E. Lemieux, S.Y. Patel, D.M. Frucht, D.C. Vinh, R.D. Auth, A.F. Freeman, K.N. Olivier, G. Uzel, C.S. Zerbe, C. Spalding, S. Pittaluga, M. Raffeld, D.B. Kuhns, L. Ding, M.L. Paulson, B.E. Marciano, J.C. Gea-Banacloche, J.S. Orange, J. Cuellar-Rodriguez, D.D. Hickstein, and S.M. Holland. 2011. Mutations in GATA2 are associated with the autosomal dominant and sporadic monocytopenia and mycobacterial infection (MonoMAC) syndrome. *Blood* 118:2653-2655.

Hsu, Y.C., and E. Fuchs. 2012. A family business: stem cell progeny join the niche to regulate homeostasis. *Nat Rev Mol Cell Bio* 13:103-114.

Huang, G., P. Zhang, H. Hirai, S. Elf, X.M. Yan, Z. Chen, S. Koschmieder, Y. Okuno, T. Dayaram, J.D. Growney, R.A. Shivdasani, D.G. Gilliland, N.A. Speck, S.D. Nimer, and D.G. Tenen. 2008. PU.1 is a major downstream target of AML1 (RUNX1) in adult mouse hematopoiesis (vol 40, pg 51, 2008). *Nat Genet* 40:255-255.

Huber, T.L., V. Kouskoff, H.J. Fehling, J. Palis, and G. Keller. 2004. Haemangioblast commitment is initiated in the primitive streak of the mouse embryo. *Nature* 432:625-630.

Huppert, S.S., A. Le, E.H. Schroeter, J.S. Mumm, M.T. Saxena, L.A. Milner, and R. Kopan. 2000. Embryonic lethality in mice homozygous for a processing-deficient allele of Notch1. *Nature* 405:966-970.

Huynh, K.D., W. Fischle, E. Verdin, and V.J. Bardwell. 2000. BCoR, a novel corepressor involved in BCL-6 repression. *Genes Dev* 14:1810-1823.

Iacovino, M., D. Chong, I. Szatmari, L. Hartweck, D. Rux, A. Caprioli, O. Cleaver, and M. Kyba. 2011. HoxA3 is an apical regulator of haemogenic endothelium. *Nat Cell Biol* 13:72-U165.

Iida, A., K. Sakaguchi, K. Sato, H. Sakurai, D. Nishimura, A. Iwaki, M. Takeuchi, M. Kobayashi, K. Misaki, S. Yonemura, A. Kawahara, and A. Sehara-Fujisawa. 2010. Metalloprotease-dependent onset of blood circulation in zebrafish. *Current biology : CB* 20:1110-1116.

Ingham, P.W., and A.P. McMahon. 2001. Hedgehog signaling in animal development: paradigms and principles. *Genes Dev* 15:3059-3087.

Ingham, P.W., Y. Nakano, and C. Seger. 2011. Mechanisms and functions of Hedgehog signalling across the metazoa. *Nat Rev Genet* 12:393-406.

Isogai, S., N.D. Lawson, S. Torrealday, M. Horiguchi, and B.M. Weinstein. 2003. Angiogenic network formation in the developing vertebrate trunk. *Development* 130:5281-5290.

Ito, Y., and K. Miyazono. 2003. RUNX transcription factors as key targets of TGF-beta superfamily signaling. *Curr Opin Genet Dev* 13:43-47.

Iuchi, I., and M. Yamamoto. 1983. Erythropoiesis in the developing rainbow trout, Salmo gairdneri irideus: histochemical and immunochemical detection of erythropoietic organs. *J Exp Zool* 226:409-417.

Ivanovs, A., S. Rybtsov, L. Welch, R.A. Anderson, M.L. Turner, and A. Medvinsky. 2011. Highly potent human hematopoietic stem cells first emerge in the intraembryonic aorta-gonad-mesonephros region. *The Journal of experimental medicine* 208:2417-2427.

Jaffredo, T., K. Bollerot, D. Sugiyama, R. Gautier, and C. Drevon. 2005. Tracing the hemangioblast during embryogenesis: developmental relationships between endothelial and hematopoietic cells. *International Journal of Developmental Biology* 49:269-277.

Jaffredo, T., R. Gautier, A. Eichmann, and F. Dieterlen-Lievre. 1998. Intraaortic hemopoietic cells are derived from endothelial cells during ontogeny. *Development* 125:4575-4583.

Jensen, E.D., T.M. Schroeder, J. Bailey, R. Gopalakrishnan, and J.J. Westendorf. 2008. Histone deacetylase 7 associates with Runx2 and represses its activity during osteoblast maturation in a deacetylation-independent manner. *J Bone Miner Res* 23:361-372.

Jepsen, K., O. Hermanson, T.M. Onami, A.S. Gleiberman, V. Lunyak, R.J. McEvilly, R. Kurokawa, V. Kumar, F. Liu, E. Seto, S.M. Hedrick, G. Mandel, C.K. Glass, D.W. Rose, and M.G. Rosenfeld. 2000. Combinatorial roles of the nuclear receptor corepressor in transcription and development. *Cell* 102:753-763.

Ji, D. 2005. Elucidating the mechanism of action of Lmo4 in vertebrate eye development. In.

Jiang, S., A.S. Bailey, D.C. Goldman, J.R. Swain, M.H. Wong, P.R. Streeter, and W.H. Fleming. 2008. Hematopoietic stem cells contribute to lymphatic endothelium. *PLoS One* 3:e3812.

Jin, H., R. Sood, J. Xu, F. Zhen, M.A. English, P.P. Liu, and Z. Wen. 2009. Definitive hematopoietic stem/progenitor cells manifest distinct differentiation output in the zebrafish VDA and PBI. *Development* 136:647-654.

Jin, S.W., D. Beis, T. Mitchell, J.N. Chen, and D.Y. Stainier. 2005. Cellular and molecular analyses of vascular tube and lumen formation in zebrafish. *Development* 132:5199-5209.

Jing, L.L., and L.I. Zon. 2011. Zebrafish as a model for normal and malignant hematopoiesis. *Dis Model Mech* 4:433-438.

Johansson, B.M., and M.V. Wiles. 1995. Evidence for involvement of activin A and bone morphogenetic protein 4 in mammalian mesoderm and hematopoietic development. *Mol Cell Biol* 15:141-151.

Jones, C.M., K.M. Lyons, P.M. Lapan, C.V. Wright, and B.L. Hogan. 1992. DVR-4 (bone morphogenetic protein-4) as a posterior-ventralizing factor in Xenopus mesoderm induction. *Development* 115:639-647.

Jonk, L.J.C., S. Itoh, C.H. Heldin, P. ten Dijke, and W. Kruijer. 1998. Identification and functional characterization of a Smad binding element (SBE) in the JunB promoter that acts as a transforming growth factor-beta, activin, and bone morphogenetic protein-inducible enhancer. *J Biol Chem* 273:21145-21152.

Jordan, C.T., and I.R. Lemischka. 1990. Clonal and systemic analysis of long-term hematopoiesis in the mouse. *Genes Dev* 4:220-232.

Jordan, C.T., J.P. McKearn, and I.R. Lemischka. 1990. Cellular and developmental properties of fetal hematopoietic stem cells. *Cell* 61:953-963.

Joshi, K., S. Lee, B. Lee, J.W. Lee, and S.-K. Lee. 2009. LMO4 controls the balance between excitatory and inhibitory spinal V2 interneurons. *Neuron* 61:839-851.

Jurata, L.W., D.A. Kenny, and G.N. Gill. 1996. Nuclear LIM interactor, a rhombotin and LIM homeodomain interacting protein, is expressed early in neuronal development. *P Natl Acad Sci USA* 93:11693-11698.

Kadrmas, J.L., and M.C. Beckerle. 2004. The LIM domain: from the cytoskeleton to the nucleus. *Nat Rev Mol Cell Biol* 5:920-931.

Kala, K., M. Haugas, K. Lillevali, J. Guimera, W. Wurst, M. Salminen, and J. Partanen. 2009. Gata2 is a tissue-specific post-mitotic selector gene for midbrain GABAergic neurons. *Development (Cambridge, England)* 136:253-262.

Kalev-Zylinska, M.L., J.A. Horsfield, M.V.C. Flores, J.H. Postlethwait, M.R. Vitas, A.M. Baas, P.S. Crosier, and K.E. Crosier. 2002. Runx1 is required for zebrafish blood and vessel development and expression of a human RUNX1-CBF2T1 transgene advances a model for studies of leukemogenesis. *Development* 129:2015-2030.

Kallianpur, A.R., J.E. Jordan, and S.J. Brandt. 1994. The Scl/Tal-1 Gene Is Expressed in Progenitors of Both the Hematopoietic and Vascular Systems during Embryogenesis. *Blood* 83:1200-1208.

Kamei, M., W.B. Saunders, K.J. Bayless, L. Dye, G.E. Davis, and B.M. Weinstein. 2006. Endothelial tubes assemble from intracellular vacuoles in vivo. *Nature* 442:453-456.

Kanatsu, M., and S.I. Nishikawa. 1996. In vitro analysis of epiblast tissue potency for hematopoietic cell differentiation. *Development* 122:823-830.

Kane, D.A., and C.B. Kimmel. 1993. The zebrafish midblastula transition. *Development* 119:447-456.

Kang, Y.J., J.W. Shin, J.H. Yoon, I.H. Oh, S.P. Lee, S.Y. Kim, S.H. Park, and M. Mamura. 2012. Inhibition of erythropoiesis by Smad6 in human cord blood hematopoietic stem cells. *Biochem Bioph Res Co* 423:750-756.

Karamysheva, A.F. 2008. Mechanisms of angiogenesis. *Biochemistry (Mosc)* 73:751-762.

Kassouf, M.T., H. Chagraoui, P. Vyas, and C. Porcher. 2008. Differential use of SCL/TAL-1 DNA-binding domain in developmental hematopoiesis. *Blood* 112:1056-1067.

Kassouf, M.T., J.R. Hughes, S. Taylor, S.J. McGowan, S. Soneji, A.L. Green, P. Vyas, and C. Porcher. 2010. Genome-wide identification of TAL1's functional targets: Insights into its mechanisms of action in primary erythroid cells. *Genome Res* 20:1064-1083.

Kawakami, K., A. Koga, H. Hori, and A. Shima. 1998. Excision of the tol2 transposable element of the medaka fish, Oryzias latipes, in zebrafish, Danio rerio. *Gene* 225:17-22.

Kawakami, K., A. Shima, and N. Kawakami. 2000. Identification of a functional transposase of the Tol2 element, an Ac-like element from the Japanese medaka fish, and its transposition in the zebrafish germ lineage. *P Natl Acad Sci USA* 97:11403-11408.

Kawakami, K., H. Takeda, N. Kawakami, M. Kobayashi, N. Matsuda, and M. Mishina. 2004. A transposon-mediated gene trap approach identifies developmentally regulated genes in zebrafish. *Dev Cell* 7:133-144.

Kawasaki, T., T. Kitsukawa, Y. Bekku, Y. Matsuda, M. Sanbo, T. Yagi, and H. Fujisawa. 1999. A requirement for neuropilin-1 in embryonic vessel formation. *Development* 126:4895-4902.

Keller, G., and R. Snodgrass. 1990. Life span of multipotential hematopoietic stem cells in vivo. *The Journal of experimental medicine* 171:1407-1418.

Kenny, D.A., L.W. Jurata, Y. Saga, and G.N. Gill. 1998. Identification and characterization of LMO4, an LMO gene with a novel pattern of expression during embryogenesis. *P Natl Acad Sci USA* 95:11257-11262.

Kimmel, C.B., W.W. Ballard, S.R. Kimmel, B. Ullmann, and T.F. Schilling. 1995. Stages of embryonic development of the zebrafish. *Dev Dyn* 203:253-310.

Kimmel, C.B., and R.D. Law. 1985. Cell lineage of zebrafish blastomeres. II. Formation of the yolk syncytial layer. *Dev Biol* 108:86-93.

Kimmel, C.B., R.M. Warga, and T.F. Schilling. 1990. Origin and organization of the zebrafish fate map. *Development* 108:581-594.

Kishimoto, Y., K.H. Lee, L. Zon, M. Hammerschmidt, and S. Schulte-Merker. 1997. The molecular nature of zebrafish swirl: BMP2 function is essential during early dorsoventral patterning. *Development* 124:4457-4466.

Kissa, K., and P. Herbomel. 2010. Blood stem cells emerge from aortic endothelium by a novel type of cell transition. *Nature* 464:112-U125.

Kissa, K., E. Murayama, A. Zapata, A. Cortes, E. Perret, C. Machu, and P. Herbomel. 2008. Live imaging of emerging hematopoietic stem cells and early thymus colonization. *Blood* 111:1147-1156.

Koeppel, M., S.J. van Heeringen, L. Smeenk, A.C. Navis, E.M. Janssen-Megens, and M. Lohrum. 2009. The novel p53 target gene IRF2BP2 participates in cell survival during the p53 stress response. *Nucleic Acids Res* 37:322-335.

Kondo, M., I.L. Weissman, and K. Akashi. 1997. Identification of clonogenic common lymphoid progenitors in mouse bone marrow. *Cell* 91:661-672.

Kratz, E., P.M. Eimon, K. Mukhyala, H. Stern, J. Zha, A. Strasser, R. Hart, and A. Ashkenazi. 2006. Functional characterization of the Bcl-2 gene family in the zebrafish. *Cell Death Differ* 13:1631-1640.

Krauss, S., J.P. Concordet, and P.W. Ingham. 1993. A functionally conserved homolog of the Drosophila segment polarity gene hh is expressed in tissues with polarizing activity in zebrafish embryos. *Cell* 75:1431-1444.

Krueger, J., D. Liu, K. Scholz, A. Zimmer, Y. Shi, C. Klein, A. Siekmann, S. Schulte-Merker, M. Cudmore, A. Ahmed, and F. le Noble. 2011. Flt1 acts as a negative regulator of tip cell formation and branching morphogenesis in the zebrafish embryo. *Development (Cambridge, England)* 138:2111-2120.

Kumano, K., S. Chiba, A. Kunisato, M. Sata, T. Saito, E. Nakagami-Yamaguchi, T. Yamaguchi, S. Masuda, K. Shimizu, T. Takahashi, S. Ogawa, Y. Hamada, and H. Hirai. 2003. Notch1 but not Notch2 is essential for generating hematopoietic stem cells from endothelial cells. *Immunity* 18:699-711.

Kumano, K., S. Chiba, K. Shimizu, T. Yamagata, N. Hosoya, T. Saito, T. Takahashi, Y. Hamada, and H. Hirai. 2001. Notch1 inhibits differentiation of hematopoietic cells by sustaining GATA-2 expression. *Blood* 98:3283-3289.

Kumaravelu, P., L. Hook, A.M. Morrison, J. Ure, S.L. Zhao, S. Zuyev, J. Ansell, and A. Medvinsky. 2002. Quantitative developmental anatomy of definitive haematopoietic stem cells long-term repopulating units (HSC/RUs): role of the aorta-gonad-mesonephros (AGM) region and the yolk sac in colonisation of the mouse embryonic liver. *Development* 129:4891-4899.

Lacaud, G., L. Gore, M. Kennedy, V. Kouskoff, P. Kingsley, C. Hogan, L. Carlsson, N. Speck, J. Palis, and G. Keller. 2002. Runx1 is essential for hematopoietic commitment at the hemangioblast stage of development in vitro. *Blood* 100:458-466.

Lancrin, C., P. Sroczynska, C. Stephenson, T. Allen, V. Kouskoff, and G. Lacaud. 2009. The haemangioblast generates haematopoietic cells through a haemogenic endothelium stage. *Nature* 457:892-895.

Landry, J.-R., N. Bonadies, S. Kinston, K. Knezevic, N.K. Wilson, S.H. Oram, M. Janes, S. Piltz, M. Hammett, J. Carter, T. Hamilton, I.J. Donaldson, G. Lacaud, J. Frampton, G. Follows, V. Kouskoff, and B. Gottgens. 2009. Expression of the leukemia oncogene Lmo2 is controlled by an array of tissue-specific elements dispersed over 100 kb and bound by Tal1/Lmo2, Ets, and Gata factors. *Blood* 113:5783-5792.

Landry, J.R., S. Kinston, K. Knezevic, M.F. de Bruijn, N. Wilson, W.T. Nottingham, M. Peitz, F. Edenhofer, J.E. Pimanda, K. Ottersbach, and B. Gottgens. 2008. Runx genes are direct targets of Scl/Tal1 in the yolk sac and fetal liver. *Blood* 111:3005-3014.

Larrivee, B., C. Freitas, S. Suchting, I. Brunet, and A. Eichmann. 2009. Guidance of vascular development: lessons from the nervous system. *Circ Res* 104:428-441.

Larson, R.C., I. Lavenir, T.A. Larson, R. Baer, A.J. Warren, I. Wadman, K. Nottage, and T.H. Rabbitts. 1996. Protein dimerization between Lmo2 (Rbtn2) and Tal1 alters thymocyte development and potentiates T cell tumorigenesis in transgenic mice. *Embo Journal* 15:1021-1027.

Lawson, N.D., N. Scheer, V.N. Pham, C.H. Kim, A.B. Chitnis, J.A. Campos-Ortega, and B.M. Weinstein. 2001. Notch signaling is required for arterial-venous differentiation during embryonic vascular development. *Development* 128:3675-3683.

Lawson, N.D., A.M. Vogel, and B.M. Weinstein. 2002. sonic hedgehog and vascular endothelial growth factor act upstream of the notch pathway during arterial endothelial differentiation. *Dev Cell* 3:127-136.

Lawson, N.D., and B.M. Weinstein. 2002. In vivo imaging of embryonic vascular development using transgenic zebrafish. *Dev Biol* 248:307-318.

Le Blanc, K., F. Frassoni, L. Ball, F. Locatelli, H. Roelofs, I. Lewis, E. Lanino, B. Sundberg, M.E. Bernardo, M. Remberger, G. Dini, R.M. Egeler, A. Bacigalupo, W. Fibbe, and O. Ringden. 2008. Mesenchymal stem cells for treatment of steroid-resistant, severe, acute graft-versus-host disease: a phase II study. *Lancet* 371:1579-1586.

Le Guyader, D., M.J. Redd, E. Colucci-Guyon, E. Murayama, K. Kissa, V. Briolat, E. Mordelet, A. Zapata, H. Shinomiya, and P. Herbomel. 2008. Origins and unconventional behavior of neutrophils in developing zebrafish. *Blood* 111:132-141.

Lecuyer, E., and T. Hoang. 2004. SCL: from the origin of hematopoiesis to stem cells and leukemia. *Exp Hematol* 32:11-24.

Lecuyer, E., S. Lariviere, M.C. Sincennes, A. Haman, R. Lahlil, M. Todorova, M. Tremblay, B.C. Wilkes, and T. Hoang. 2007. Protein stability and transcription factor complex assembly determined by the SCL-LMO2 interaction. *J Biol Chem* 282:

Lee, K.S., H.J. Kim, Q.L. Li, X.Z. Chi, C. Ueta, T. Komori, J.M. Wozney, E.G. Kim, J.Y. Choi, H.M. Ryoo, and S.C. Bae. 2000. Runx2 is a common target of transforming growth factor beta 1 and bone morphogenetic protein 2, and cooperation between Runx2 and Smad5 induces osteoblast-specific gene expression in the pluripotent mesenchymal precursor cell line C2C12. *Mol Cell Biol* 20:8783-8792.

Lee, S.-K., L.W. Jurata, R. Nowak, K. Lettieri, D.A. Kenny, S.L. Pfaff, and G.N. Gill. 2005. The LIM domain-only protein LMO4 is required for neural tube closure. *Mol Cell Neurosci* 28:205-214.

Lemischka, I.R. 1991. Clonal, in vivo behavior of the totipotent hematopoietic stem cell. *Semin Immunol* 3:349-355.

Lensch, M.W., and G.Q. Daley. 2004. Origins of mammalian hematopoiesis: in vivo paradigms and in vitro models. *Curr Top Dev Biol* 60:127-196.

Lieschke, G.J., A.C. Oates, B.H. Paw, M.A. Thompson, N.E. Hall, A.C. Ward, R.K. Ho, L.I. Zon, and J.E. Layton. 2002. Zebrafish SPI-1 (PU.1) marks a site of myeloid development independent of primitive erythropoiesis: implications for axial patterning. *Dev Biol* 246:274-295.

Liew, C.K., R.J.Y. Simpson, A.H.Y. Kwan, L.A. Crofts, F.E. Loughlin, J.M. Matthews, M. Crossley, and J.P. Mackay. 2005. Zinc fingers as protein recognition motifs: Structural basis for the GATA-1/Friend of GATA interaction. *P Natl Acad Sci USA* 102:583-588.

Lim, K.-C., Brandt, W., Ku, C-J, Hosoya-Ohmura, S., Camper, S., Yamamoto, M., Hosoya, T. and J.D. Engel. 2012. A Gata2 vascular endothelial enhancer is required for the generation of hematopoietic stem cells. *J. Clinical Investigation (in press)*

Lin, F.J., M.J. Tsai, and S.Y. Tsai. 2007. Artery and vein formation: a tug of war between different forces. *Embo Rep* 8:920-924.

Ling, K.W., K. Ottersbach, J.P. van Hamburg, A. Oziemlak, F.Y. Tsai, S.H. Orkin, R. Ploemacher, R.W. Hendricks, and E. Dzierzak. 2004. GATA-2 plays two functionally distinct roles during the ontogeny of hematopoietic stem cells. *J Exp Med* 200:871-882.

Link, V., A. Shevchenko, and C.P. Heisenberg. 2006. Proteomics of early zebrafish embryos. *Bmc Dev Biol* 6:

Liu, F., M. Walmsley, A. Rodaway, and R. Patient. 2008. Fli1 acts at the top of the transcriptional network driving blood and endothelial development. *Curr Biol* 18:1234-1240.

Liu, Z.J., X. Lu, and S. Zhong. 2005. ASPP - Apoptotic specific regulator of p53. *Bba-Rev Cancer* 1756:77-80.

Longo, A., G.P. Guanga, and R.B. Rose. 2008. Crystal structure of E47 neuroD1/Beta2 bHLH domain DNA complex: Heterodimer selectivity and DNA recognition. *Biochemistry-Us* 47:218-229.

Lowery, L.A., and H. Sive. 2004. Strategies of vertebrate neurulation and a re-evaluation of teleost neural tube formation. *Mech Develop* 121:1189-1197.

Lu, R., N.F. Neff, S.R. Quake, and I.L. Weissman. 2011. Tracking single hematopoietic stem cells in vivo using high-throughput sequencing in conjunction with viral genetic barcoding. *Nat Biotechnol* 29:928-U229.

Lu, Z., K.S. Lam, N. Wang, X. Xu, M. Cortes, and B. Andersen. 2006. LMO4 can interact with Smad proteins and modulate transforming growth factor-beta signaling in epithelial cells. *Oncogene* 25:2920-2930.

Luc, S., T.C. Luis, H. Boukarabila, I.C. Macaulay, N. Buza-Vidas, T. Bouriez-Jones, M. Lutteropp, P.S. Won, S.J. Loughran, A.J. Mead, A. Hultquist, J. Brown, T. Mizukami, S. Matsuoka, H. Ferry, K. Anderson, S. Duarte, D. Atkinson, S. Soneji, A. Domanski, A. Farley, A. Sanjuan-Pla, C. Carella, R. Patient, M. de Bruijn, T. Enver, C. Nerlov, C. Blackburn, I. Godin, and S.E.W. Jacobsen. 2012. The earliest thymic T cell progenitors sustain B cell and myeloid lineage potential. *Nat Immunol* 13:412-419.

Luesink, M., I.H. Hollink, V.H. van der Velden, R.H. Knops, J.B. Boezeman, V. de Haas, J. Trka, A. Baruchel, D. Reinhardt, B.A. van der Reijden, M.M. van den Heuvel-Eibrink, C.M. Zwaan, and J.H. Jansen. 2012. High GATA2 expression is a poor prognostic marker in pediatric acute myeloid leukemia. *Blood* 120:2064-2075.

Lux, C.T., M. Yoshimoto, K. McGrath, S.J. Conway, J. Palis, and M.C. Yoder. 2008. All primitive and definitive hematopoietic progenitor cells emerging before E10 in the mouse embryo are products of the yolk sac. *Blood* 111:3435-3438.

Lyons, M.S., B. Bell, D. Stainier, and K.G. Peters. 1998. Isolation of the zebrafish homologues for the tie-1 and tie-2 endothelium-specific receptor tyrosine kinases. *Dev Dynam* 212:133-140.

Ma, S., X.Y. Guan, P.S.L. Beh, K.Y. Wong, Y.P. Chan, H.F. Yuen, J. Vielkind, and K.W. Chan. 2007. The significance of LMO2 expression in the progression of prostate cancer. *J Pathol* 211:278-285.

Maeno, M., P.E. Mead, C. Kelley, R.H. Xu, H.F. Kung, A. Suzuki, N. Ueno, and L.I. Zon. 1996. The role of BMP-4 and GATA-2 in the induction and differentiation of hematopoietic mesoderm in Xenopus laevis. *Blood* 88:1965-1972.

Maeno, M., R.C. Ong, Y. Xue, S. Nishimatsu, N. Ueno, and H.F. Kung. 1994. Regulation of primary erythropoiesis in the ventral mesoderm of Xenopus gastrula embryo: evidence for the expression of a stimulatory factor(s) in animal pole tissue. *Dev Biol* 161:522-529.

Maeno, M., S. Tochinai, and C. Katagiri. 1985. Differential participation of ventral and dorsolateral mesoderms in the hemopoiesis of Xenopus, as revealed in diploid-triploid or interspecific chimeras. *Dev Biol* 110:503-508.

Magli, M.C., N.N. Iscove, and N. Odartchenko. 1982. Transient nature of early haematopoietic spleen colonies. *Nature* 295:527-529.

Maithreye, R., R.R. Sarkar, V.K. Parnaik, and S. Sinha. 2008. Delay-Induced Transient Increase and Heterogeneity in Gene Expression in Negatively Auto-Regulated Gene Circuits. *PLoS One* 3:

Mandal, L., U. Banerjee, and V. Hartenstein. 2004. Evidence for a fruit fly hemangioblast and similarities between lymph-gland hematopoiesis in fruit fly and mammal aorta-gonadal-mesonephros mesoderm. *Nat Genet* 36:1019-1023.

Mangan, S., and U. Alon. 2003. Structure and function of the feed-forward loop network motif. *P Natl Acad Sci USA* 100:11980-11985.

Mangan, S., S. Itzkovitz, A. Zaslaver, and U. Alon. 2006. The incoherent feed-forward loop accelerates the response-time of the gal system of Escherichia coli. *J Mol Biol* 356:1073-1081.

Mankidy, R., D.V. Faller, R. Mabaera, C.H. Lowrey, M.S. Boosalis, G.L. White, S.A. Castaneda, and S.P. Perrine. 2006. Short-chain fatty acids induce gamma-globin gene expression by displacement of a HDAC3-NCoR repressor complex. *Blood* 108:3179-3186.

Marshall, C.J., C. Kinnon, and A.J. Thrasher. 2000. Polarized expression of bone morphogenetic protein-4 in the human aorta-gonad-mesonephros region. *Blood* 96:1591-1593.

Masamizu, Y., T. Ohtsuka, Y. Takashima, H. Nagahara, Y. Takenaka, K. Yoshikawa, H. Okamura, and R. Kageyama. 2006. Real-time imaging of the somite segmentation clock: Revelation of unstable oscillators in the individual presomitic mesoderm cells. *P Natl Acad Sci USA* 103:1313-1318.

Mathieu, J., K. Griffin, P. Herbomel, T. Dickmeis, U. Strahle, D. Kimelman, F.M. Rosa, and N. Peyrieras. 2004. Nodal and Fgf pathways interact through a positive regulatory loop and synergize to maintain mesodermal cell populations. *Development* 131:629-641.

Matsuzaki, Y., K. Kinjo, R.C. Mulligan, and H. Okano. 2004. Unexpectedly efficient homing capacity of purified murine hematopoietic stem cells. *Immunity* 20:87-93.

Matthews, J.M., and J.E. Visvader. 2003. LIM-domain-binding protein 1: a multifunctional cofactor that interacts with diverse proteins. *Embo Rep* 4:1132-1137.

McCollum, C.W., S.R. Amin, P. Pauerstein, and M.E. Lane. 2007. A zebrafish LMO4 ortholog limits the size of the forebrain and eyes through negative regulation of six3b and rx3. *Dev Biol* 309:373-385.

McCormack, M.P., L.F. Young, S. Vasudevan, C.A. de Graaf, R. Codrington, T.H. Rabbitts, S.M. Jane, and D.J. Curtis. 2010. The Lmo2 oncogene initiates leukemia in mice by inducing thymocyte self-renewal. *Science* 327:879-883.

McKercher, S.R., B.E. Torbett, K.L. Anderson, G.W. Henkel, D.J. Vestal, H. Baribault, M. Klemsz, A.J. Feeney, G.E. Wu, C.J. Paige, and R.A. Maki. 1996. Targeted disruption of the PU.1 gene results in multiple hematopoietic abnormalities. *Embo Journal* 15:5647-5658.

Mead, P.E., A.E. Deconinck, T.L. Huber, S.H. Orkin, and L.I. Zon. 2001. Primitive erythropoiesis in the Xenopus embryo: the synergistic role of LMO-2, SCL and GATA-binding proteins. *Development* 128:2301-2308.

Medvinsky, A., and E. Dzierzak. 1996. Definitive hematopoiesis is autonomously initiated by the AGM region. *Cell* 86:897-906.

Medvinsky, A.L., N.L. Samoylina, A.M. Muller, and E.A. Dzierzak. 1993. An early pre-liver intraembryonic source of CFU-S in the developing mouse. *Nature* 364:64-67.

Megason, S.G., and S.E. Fraser. 2003. Digitizing life at the level of the cell: high-performance laser-scanning microscopy and image analysis for in toto imaging of development. *Mech Develop* 120:1407-1420.

Meier, N., S. Krpic, P. Rodriguez, J. Strouboulis, M. Monti, J. Krijgsveld, M. Gering, R. Patient, A. Hostert, and F. Grosveld. 2006. Novel binding partners of Ldb1 are required for haematopoietic development. *Development* 133:4913-4924.

Mengeling, B.J., T.Q. Phan, M.L. Goodson, and M.L. Privalsky. 2011. Aberrant corepressor interactions implicated in PML-RAR(alpha) and PLZF-RAR(alpha) leukemogenesis reflect an altered recruitment and release of specific NCoR and SMRT splice variants. *The Journal of biological chemistry* 286:4236-4247.

Michell, A.C., J. Braganca, C. Broadbent, B. Joyce, A. Franklyn, J.E. Schneider, S. Bhattacharya, and S.D. Bamforth. 2010. A novel role for transcription factor Lmo4 in thymus development through genetic interaction with Cited2. *Dev Dyn* 239:1988-1994.

Mikkola, H.K., J. Klintman, H. Yang, H. Hock, T.M. Schlaeger, Y. Fujiwara, and S.H. Orkin. 2003. Haematopoietic stem cells retain long-term repopulating activity and multipotency in the absence of stem-cell leukaemia SCL/tal-1 gene. *Nature* 421:547-551.

Millauer, B., S. Wizigmannvoos, H. Schnurch, R. Martinez, N.P.H. Moller, W. Risau, and A. Ullrich. 1993. High-Affinity Vegf Binding and Developmental Expression Suggest Flk-1 as a Major Regulator of Vasculogenesis and Angiogenesis. *Cell* 72:835-846.

Minegishi, N., J. Ohta, H. Yamagiwa, N. Suzuki, S. Kawauchi, Y.H. Zhou, S. Takahashi, N. Hayashi, J.D. Engel, and M. Yamamoto. 1999. The mouse GATA-2 gene is expressed in the para-aortic splanchnopleura and aorta-gonads and mesonephros region. *Blood* 93:4196-4207.

Minegishi, N., N. Suzuki, T. Yokomizo, X. Pan, T. Fujimoto, S. Takahashi, T. Hara, A. Miyajima, S. Nishikawa, and M. Yamamoto. 2003. Expression and domain-specific function of GATA-2 during differentiation of the hematopoietic precursor cells in midgestation mouse embryos. *Blood* 102:896-905.

Miura, Y., and F.H. Wilt. 1969. Tissue interaction and the formation of the first erythroblasts of the chick embryo. *Dev Biol* 19:201-211.

Montanez-Wiscovich, M.E., D.D. Seachrist, M.D. Landis, J. Visvader, B. Andersen, and R.A. Keri. 2009. LMO4 is an essential mediator of ErbB2/HER2/Neu-induced breast cancer cell cycle progression. *Oncogene* 28:3608-3618.

Monteiro, R., C. Pouget, and R. Patient. 2011. The gata1/pu.1 lineage fate paradigm varies between blood populations and is modulated by tif1 gamma. *Embo Journal* 30:1093-1103.

Monteiro, R., M. van Dinther, J. Bakkers, R. Wilkinson, R. Patient, P. ten Dijke, and C. Mummery. 2008. Two novel type II receptors mediate BMP signalling and are required to establish left-right asymmetry in zebrafish. *Dev Biol* 315:55-71.

Moore, M.A., and D. Metcalf. 1970. Ontogeny of the haemopoietic system: yolk sac origin of in vivo and in vitro colony forming cells in the developing mouse embryo. *Br J Haematol* 18:279-296.

Moreno, D.A., C.A. Scrideli, M.A. Cortez, R. de Paula Queiroz, E.T. Valera, V. da Silva Silveira, J.A. Yunes, S.R. Brandalise, and L.G. Tone. 2010. Differential expression of HDAC3, HDAC7 and HDAC9 is associated with prognosis and survival in childhood acute lymphoblastic leukaemia. *Br J Haematol* 150:665-673.

Morita, Y., A. Iseki, S. Okamura, S. Suzuki, H. Nakauchi, and H. Ema. 2011. Functional characterization of hematopoietic stem cells in the spleen. *Exp Hematol* 39:351-359.

Morrison, S.J., and I.L. Weissman. 1994. The long-term repopulating subset of hematopoietic stem cells is deterministic and isolatable by phenotype. *Immunity* 1:661-673.

Mukhopadhyay, M., A. Teufel, T. Yamashita, A.D. Agulnick, L. Chen, K.M. Downs, A. Schindler, A. Grinberg, S.P. Huang, D. Dorward, and H. Westphal. 2003. Functional ablation of the mouse Ldb1 gene results in severe patterning defects during gastrulation. *Development* 130:495-505.

Mukouyama, Y.S., D. Shin, S. Britsch, M. Taniguchi, and D.J. Anderson. 2002. Sensory nerves determine the pattern of arterial differentiation and blood vessel branching in the skin. *Cell* 109:693-705.

Muller, A.M., A. Medvinsky, J. Strouboulis, F. Grosveld, and E. Dzierzak. 1994. Development of hematopoietic stem cell activity in the mouse embryo. *Immunity* 1:291-301.

Murayama, E., K. Kissa, A. Zapata, E. Mordelet, V. Briolat, H.F. Lin, R.I. Handin, and P. Herbomel. 2006. Tracing hematopoietic precursor migration to successive hematopoietic organs during zebrafish development. *Immunity* 25:963-975.

Murray, P.D.F. 1932. The Development in vitro of the Blood of the Early Chick Embryo. *Proceedings of the Royal Society of London. Series B, Containing Papers of a Biological Character* 111:497-521.

Naito, M., S. Umeda, T. Yamamoto, H. Moriyama, H. Umezu, G. Hasegawa, H. Usuda, L.D. Shultz, and K. Takahashi. 1996. Development, differentiation, and phenotypic heterogeneity of murine tissue macrophages. *J Leukoc Biol* 59:133-138.

Nakagawa, M., M. Ichikawa, K. Kumano, S. Goyama, M. Kawazu, T. Asai, S. Ogawa, M. Kurokawa, and S. Chiba. 2006. AML1/Runx1 rescues Notch1-null mutation-induced deficiency of para-aortic splanchnopleural hematopoiesis. *Blood* 108:3329-3334.

Nakano, Y., S. Imagawa, K. Matsumoto, C. Stockmann, N. Obara, N. Suzuki, T. Doi, T. Kodama, S. Takahashi, T. Nagasawa, and M. Yamamoto. 2004. Oral administration of K-11706 inhibits GATA binding activity, enhances hypoxia-inducible factor 1 binding activity, and restores indicators in an in vivo mouse model of anemia of chronic disease. *Blood* 104:4300-4307.

Neave, B., N. Holder, and R. Patient. 1997. A graded response to BMP-4 spatially coordinates patterning of the mesoderm and ectoderm in the zebrafish. *Mech Develop* 62:183-195.

Neave, B., A. Rodaway, S.W. Wilson, R. Patient, and N. Holder. 1995. Expression of zebrafish GATA 3 (gta3) during gastrulation and neurulation suggests a role in the specification of cell fate. *Mech Develop* 51:169-182.

Neves, J., M. Uchikawa, A. Bigas, and F. Giraldez. 2012. The Prosensory Function of Sox2 in the Chicken Inner Ear Relies on the Direct Regulation of Atoh1. *PLoS One* 7:

Ng, D., N. Thakker, C.M. Corcoran, D. Donnai, R. Perveen, A. Schneider, D.W. Hadley, C. Tifft, L. Zhang, A.O. Wilkie, J.J. van der Smagt, R.J. Gorlin, S.M. Burgess, V.J. Bardwell, G.C. Black, and L.G. Biesecker. 2004. Oculofaciocardiodental and Lenz microphthalmia syndromes result from distinct classes of mutations in BCOR. *Nat Genet* 36:411-416.

Ni, C.-W., H. Qiu, A. Rezvan, K. Kwon, D. Nam, D.J. Son, J.E. Visvader, and H. Jo. 2010. Discovery of novel mechanosensitive genes in vivo using mouse carotid artery endothelium exposed to disturbed flow. *Blood* 116:e66-73.

Nishikawa, S., S. Nishikawa, M. Hirashima, N. Matsuyoshi, and H. Kodama. 1998. Progressive lineage analysis by cell sorting and culture identifies FLK1(+)VE-cadherin(+) cells at a diverging point of endothelial and hemopoietic lineages. *Development* 125:1747-1757.

Nooren, I.M., and J.M. Thornton. 2003. Diversity of protein-protein interactions. *Embo J* 22:3486-3492.

North, T., T.L. Gu, T. Stacy, Q. Wang, L. Howard, M. Binder, M. Marin-Padilla, and N.A. Speck. 1999. Cbfa2 is required for the formation of intra-aortic hematopoietic clusters. *Development* 126:2563-2575.

North, T.E., M.F.T.R. de Bruijin, T. Stacy, L. Talebian, E. Lind, C. Robin, M. Binder, E. Dzierzak, and N.A. Speck. 2002. Runx1 expression marks long-term repopulating hematopoietic stem cells in the midgestation mouse embryo. *Immunity* 16:661-672.

North, T.E., W. Goessling, M. Peeters, P.L. Li, C. Ceol, A.M. Lord, G.J. Weber, J. Harris, C.C. Cutting, P. Huang, E. Dzierzak, and L.I. Zon. 2009. Hematopoietic Stem Cell Development Is Dependent on Blood Flow. *Cell* 137:736-748.

North, T.E., W. Goessling, C.R. Walkley, C. Lengerke, K.R. Kopani, A.M. Lord, G.J. Weber, T.V. Bowman, I.-H. Jang, T. Grosser, G.A. Fitzgerald, G.Q. Daley, S.H. Orkin, and L.I. Zon. 2007. Prostaglandin E2 regulates vertebrate haematopoietic stem cell homeostasis. *Nature* 447:1007-1011.

Notari, M., Y. Hu, S. Koch, M. Lu, I. Ratnayaka, S. Zhong, C. Baer, A. Pagotto, R. Goldin, V. Salter, E. Candi, G. Melino, and X. Lu. 2011. Inhibitor of apoptosis-stimulating protein of p53 (iASPP) prevents senescence and is required for epithelial stratification. *Proc Natl Acad Sci U S A* 108:16645-16650.

Notredame, C., D.G. Higgins, and J. Heringa. 2000. T-Coffee: A novel method for fast and accurate multiple sequence alignment. *J Mol Biol* 302:205-217.

Nottingham, W.T., A. Jarratt, M. Burgess, C.L. Speck, J.F. Cheng, S. Prabhakar, E.M. Rubin, P.S. Li, J. Sloane-Stanley, A.S.J. Kong, and M.F. de Bruijn. 2007. Runx1-mediated hematopoietic stem-cell emergence is controlled by a Gata/Ets/SCL-regulated enhancer. *Blood* 110:4188-4197.

Novak, B., and J.J. Tyson. 2008. Design principles of biochemical oscillators. *Nat Rev Mol Cell Bio* 9:981-991.

Oberoi, J., L. Fairall, P.J. Watson, J.C. Yang, Z. Czimmerer, T. Kampmann, B.T. Goult, J.A. Greenwood, J.T. Gooch, B.C. Kallenberger, L. Nagy, D. Neuhaus, and J.W. Schwabe. 2011. Structural basis for the assembly of the SMRT/NCoR core transcriptional repression machinery. *Nat Struct Mol Biol* 18:177-184.

Ochoa, S.D., S. Salvador, and C. LaBonne. 2012. The LIM adaptor protein LMO4 is an essential regulator of neural crest development. *Dev Biol* 361:313-325.

Ogawa, H., T. Ueda, T. Aoyama, A. Aronheim, S. Nagata, and R. Fukunaga. 2003. A SWI2/SNF2-type ATPase/helicase protein, mDomino, interacts with myeloid zinc finger protein 2A (MZF-2A) to regulate its transcriptional activity. *Genes Cells* 8:325-339.

Okada, H., T. Watanabe, M. Niki, H. Takano, N. Chiba, N. Yanai, K. Tani, H. Hibino, S. Asano, M.L. Mucenski, Y. Ito, T. Noda, and M. Satake. 1998. AML1(-/-) embryos do not express certain hematopoiesis-related gene transcripts including those of the PU.1 gene. *Oncogene* 17:2287-2293.

Okada, S., H. Nakauchi, K. Nagayoshi, S. Nishikawa, Y. Miura, and T. Suda. 1992. In vivo and in vitro stem cell function of c-kit- and Sca-1-positive murine hematopoietic cells. *Blood* 80:3044-3050.

Okuda, T., J. vanDeursen, S.W. Hiebert, G. Grosveld, and J.R. Downing. 1996. AML1, the target of multiple chromosomal translocations in human leukemia, is essential for normal fetal liver hematopoiesis. *Cell* 84:321-330.

Omichinski, J.G., G.M. Clore, O. Schaad, G. Felsenfeld, C. Trainor, E. Appella, S.J. Stahl, and A.M. Gronenborn. 1993. Nmr Structure of a Specific DNA Complex of Zn-Containing DNA-Binding Domain of Gata-1. *Science* 261:438-446.

Orkin, S.H. 2000. Diversification of haematopoietic stem cells to specific lineages. *Nature reviews. Genetics* 1:57-64.

Orkin, S.H., and L.I. Zon. 2008. Hematopoiesis: An evolving paradigm for stem cell biology. *Cell* 132:631-644.

Osada, H., G. Grutz, H. Axelson, A. Forster, and T.H. Rabbitts. 1995. Association of Erythroid Transcription Factors - Complexes Involving the Lim Protein Rbtn2 and the Zinc-Finger Protein Gata1. *P Natl Acad Sci USA* 92:9585-9589.

Osada, H., G.G. Grutz, H. Axelson, A. Forster, and T.H. Rabbitts. 1997. LIM-only protein Lmo2 forms a protein complex with erythroid transcription factor GATA-1. *Leukemia : official journal of the Leukemia Society of America, Leukemia Research Fund, U.K* 11 Suppl 3:307-312.

Osawa, M., K. Hanada, H. Hamada, and H. Nakauchi. 1996. Long-term lymphohematopoietic reconstitution by a single CD34-low/negative hematopoietic stem cell. *Science* 273:242-245.

Ostergaard, P., M.A. Simpson, F.C. Connell, C.G. Steward, G. Brice, W.J. Woollard, D. Dafou, T. Kilo, S. Smithson, P. Lunt, V.A. Murday, S. Hodgson, R. Keenan, D.T. Pilz, I. Martinez-Corral, T. Makinen, P.S. Mortimer, S. Jeffery, R.C. Trembath, and S. Mansour. 2011. Mutations in GATA2 cause primary lymphedema associated with a predisposition to acute myeloid leukemia (Emberger syndrome). *Nat Genet* 43:929-931.

Ottersbach, K., and E. Dzierzak. 2005. The murine placenta contains hematopoietic stem cells within the vascular labyrinth region. *Dev Cell* 8:377-387.

Pagan, J.K., J. Arnold, K.J. Hanchard, R. Kumar, T. Bruno, M.J.K. Jones, D.J. Richard, A. Forrest, A. Spurdle, E. Verdin, M. Crossley, M. Fanciulli, G. Chenevix-Trench, D.B. Young, and K.K. Khanna. 2007. A novel corepressor, BCoR-L1, represses transcription through an interaction with CtBP. *J Biol Chem* 282:15248-15257.

Palii, C.G., C. Perez-Iratxeta, Z.Z. Yao, Y. Cao, F.T. Dai, J. Davison, H. Atkins, D. Allan, F.J. Dilworth, R. Gentleman, S.J. Tapscott, and M. Brand. 2011. Differential genomic targeting of the transcription factor TAL1 in alternate haematopoietic lineages. *Embo Journal* 30:494-509.

Palis, J., J. Malik, K.E. McGrath, and P.D. Kingsley. 2010. Primitive erythropoiesis in the mammalian embryo. *Int J Dev Biol* 54:1011-1018.

Palis, J., S. Robertson, M. Kennedy, C. Wall, and G. Keller. 1999. Development of erythroid and myeloid progenitors in the yolk sac and embryo proper of the mouse. *Development* 126:5073-5084.

Pardanaud, L., and F. Dieterlen-Lievre. 1993. Emergence of endothelial and hemopoietic cells in the avian embryo. *Anat Embryol (Berl)* 187:107-114.

Pardanaud, L., and F. Dieterlen-Lievre. 1999. Manipulation of the angiopoietic/hemangiopoietic commitment in the avian embryo. *Development* 126:617-627.

Parra, M., T. Mahmoudi, and E. Verdin. 2007. Myosin phosphatase dephosphorylates HDAC7, controls its nucleocytoplasmic shuttling, and inhibits apoptosis in thymocytes. *Genes Dev* 21:638-643.

Partington, G.A., D. Bertwistle, R.H. Nicolas, W.J. Kee, J.A. Pizzey, and R.K. Patient. 1997. GATA-2 is a maternal transcription factor present in Xenopus oocytes as a nuclear complex which is maintained throughout early development. *Dev Biol* 181:144-155.

Patan, S. 2000. Vasculogenesis and angiogenesis as mechanisms of vascular network formation, growth and remodeling. *J Neuro-Oncol* 50:1-15.

Patel-Hett, S., and P.A. D'Amore. 2011. Signal transduction in vasculogenesis and developmental angiogenesis. *Int J Dev Biol* 55:353-363.

Patterson, L.J., M. Gering, C.E. Eckfeldt, A.R. Green, C.M. Verfaillie, S.C. Ekker, and R. Patient. 2007. The transcription factors Scl and Lmo2 act together during development of the hemangioblast in zebrafish. *Blood* 109:2389-2398.

Patterson, L.J., M. Gering, and R. Patient. 2005. Scl is required for dorsal aorta as well as blood formation in zebrafish embryos. *Blood* 105:3502-3511.

Pearson, S., P. Sroczynska, G. Lacaud, and V. Kouskoff. 2008. The stepwise specification of embryonic stem cells to hematopoietic fate is driven by sequential exposure to Bmp4, activin A, bFGF and VEGF. *Development* 135:1525-1535.

Pelosi, E., M. Valtieri, S. Coppola, R. Botta, M. Gabbianelli, V. Lulli, G. Marziali, B. Masella, R. Muller, C. Sgadari, U. Testa, G. Bonanno, and C. Peschle. 2002. Identification of the hemangioblast in postnatal life. *Blood* 100:3203-3208.

Persons, D.A., J.A. Allay, E.R. Allay, R.A. Ashmun, D. Orlic, S.M. Jane, J.M. Cunningham, and A.W. Nienhuis. 1999. Enforced expression of the GATA-2 transcription factor blocks normal hematopoiesis. *Blood* 93:488-499.

Peterkin, T., A. Gibson, M. Loose, and R. Patient. 2005. The roles of GATA-4, -5 and -6 in vertebrate heart development. *Semin Cell Dev Biol* 16:83-94.

Pfeffer, P.L., T. Gerster, K. Lun, M. Brand, and M. Busslinger. 1998. Characterization of three novel members of the zebrafish Pax2/5/8 family: dependency of Pax5 and Pax8 expression on the Pax2.1 (noi) function. *Development* 125:3063-3074.

Pierron, G., F. Tirode, C. Lucchesi, S. Reynaud, S. Ballet, S. Cohen-Gogo, V. Perrin, J.-M. Coindre, and O. Delattre. 2012. A new subtype of bone sarcoma defined by BCOR-CCNB3 gene fusion. *Nat Genet* 44:461-466.

Pina, C., C. Fugazza, A.J. Tipping, J. Brown, S. Soneji, J. Teles, C. Peterson, and T. Enver. 2012. Inferring rules of lineage commitment in haematopoiesis. *Nat Cell Biol* 14:287-294.

Pinheiro, P., M. Gering, and R. Patient. 2004. The basic helix-loop-helix transcription factor, Tal2, marks the lateral floor plate of the spinal cord in zebrafish. *Gene Expr Patterns* 4:85-92.

Porcher, C., E.C. Liao, Y. Fujiwara, L.I. Zon, and S.H. Orkin. 1999. Specification of hematopoietic and vascular development by the bHLH transcription factor SCL without direct DNA binding. *Development* 126:4603-4615.

Porcher, C., W. Swat, K. Rockwell, Y. Fujiwara, F.W. Alt, and S.H. Orkin. 1996. The T cell leukemia oncoprotein SCL/tal-1 is essential for development of all hematopoietic lineages. *Cell* 86:47-57.

Pouget, C., R. Gautier, M.A. Teillet, and T. Jaffredo. 2006. Somite-derived cells replace ventral aortic hemangioblasts and provide aortic smooth muscle cells of the trunk. *Development* 133:1013-1022.

Pugh, T.J., S.D. Weeraratne, T.C. Archer, D.A. Pomeranz Krummel, D. Auclair, J. Bochicchio, M.O. Carneiro, S.L. Carter, K. Cibulskis, R.L. Erlich, H. Greulich, M.S. Lawrence, N.J. Lennon, A. McKenna, J. Meldrim, A.H. Ramos, M.G. Ross, C. Russ, E. Shefler, A. Sivachenko, B. Sogoloff, P. Stojanov, P. Tamayo, J.P. Mesirov, V. Amani, N. Teider, S. Sengupta, J.P. Francois, P.A. Northcott, M.D. Taylor, F. Yu, G.R. Crabtree, A.G. Kautzman, S.B. Gabriel, G. Getz, N. Jager, D.T. Jones, P. Lichter, S.M. Pfister, T.M. Roberts, M. Meyerson, S.L. Pomeroy, and Y.J. Cho. 2012. Medulloblastoma exome sequencing uncovers subtype-specific somatic mutations. *Nature* 488:106-110.

Pyati, U.J., M.S. Cooper, A.J. Davidson, A. Nechiporuk, and D. Kimelman. 2006. Sustained Bmp signaling is essential for cloaca development in zebrafish. *Development* 133:2275-2284.

Pyati, U.J., A.E. Webb, and D. Kimelman. 2005. Transgenic zebrafish reveal stage-specific roles for Bmp signaling in ventral and posterior mesoderm development. *Development* 132:2333-2343.

Quinkertz, A., and J.A. Campos-Ortega. 1999. A new beta-globin gene from the zebrafish, beta(E1), and its pattern of transcription during embryogenesis. *Dev Genes Evol* 209:126-131.

Rampon, C., and P. Huber. 2003. Multilineage hematopoietic progenitor activity generated autonomously in the mouse yolk sac: analysis using angiogenesis-defective embryos. *Int J Dev Biol* 47:273-280.

Ransom, D.G., P. Haffter, J. Odenthal, A. Brownlie, E. Vogelsang, R.N. Kelsh, M. Brand, F.J.M. vanEeden, M. FurutaniSeiki, M. Granato, M. Hammerschmidt, C.P. Heisenberg, Y.J. Jiang, D.A. Kane, M.C. Mullins, and C. NussleinVolhard. 1996. Characterization of zebrafish mutants with defects in embryonic hematopoiesis. *Development* 123:311-319.

Reagan, F.P. 1915. Vascularization phenomena in fragments of embryonic bodies completely isolated from yolk-sac blastoderm. *Anat Rec* 9:329-341.

Renaud, O., P. Herbomel, and K. Kissa. 2011. Studying cell behavior in whole zebrafish embryos by confocal live imaging: application to hematopoietic stem cells. *Nat Protoc* 6:1897-1904.

Rhee, J.M., and P.M. Iannaccone. 2012. Mapping mouse hemangioblast maturation from headfold stages. *Dev Biol* 365:1-13.

Rhodes, K.E., C. Gekas, Y. Wang, C.T. Lux, C.S. Francis, D.N. Chan, S. Conway, S.H. Orkin, M.C. Yoder, and H.K.A. Mikkola. 2008. The emergence of hematopoietic stem cells is initiated in the placental vasculature in the absence of circulation. *Cell Stem Cell* 2:252-263.

Ribatti, D., B. Nico, and E. Crivellato. 2009. Morphological and molecular aspects of physiological vascular morphogenesis. *Angiogenesis* 12:101-111.

Risau, W. 1997. Mechanisms of angiogenesis. *Nature* 386:671-674.

Risau, W., and V. Lemmon. 1988. Changes in the vascular extracellular matrix during embryonic vasculogenesis and angiogenesis. *Dev Biol* 125:441-450.

Risau, W., H. Sariola, H.G. Zerwes, J. Sasse, P. Ekblom, R. Kemler, and T. Doetschman. 1988. Vasculogenesis and angiogenesis in embryonic-stem-cell-derived embryoid bodies. *Development* 102:471-478.

Robb, L., N.J. Elwood, A.G. Elefanty, F. Kontgen, R. Li, L.D. Barnett, and C.G. Begley. 1996. The scl gene product is required for the generation of all hematopoietic lineages in the adult mouse. *Embo J* 15:4123-4129.

Robb, L., I. Lyons, R.L. Li, L. Hartley, F. Kontgen, R.P. Harvey, D. Metcalf, and C.G. Begley. 1995. Absence of Yolk-Sac Hematopoiesis from Mice with a Targeted Disruption of the Scl Gene. *P Natl Acad Sci USA* 92:7075-7079.

Robert-Moreno, A., J. Guiu, C. Ruiz-Herguido, M.E. Lopez, J. Ingles-Esteve, L. Riera, A. Tipping, T. Enver, E. Dzierzak, T. Gridley, L. Espinosa, and A. Bigas. 2008. Impaired embryonic haematopoiesis yet normal arterial development in the absence of the Notch ligand Jagged1. *Embo J* 27:1886-1895.

Roberts, D.M., J.B. Kearney, J.H. Johnson, M.P. Rosenberg, R. Kumar, and V.L. Bautch. 2004. The vascular endothelial growth factor (VEGF) receptor Flt-1 (VEGFR-1) modulates Flk-1 (VEGFR-2) signaling during blood vessel formation. *Am J Pathol* 164:1531-1535.

Robin, C., and C. Durand. 2010. The roles of BMP and IL-3 signaling pathways in the control of hematopoietic stem cells in the mouse embryo. *International Journal of Developmental Biology* 54:1189-1200.

Robin, C., K. Ottersbach, C. Durand, M. Peeters, L. Vanes, V. Tybulewicz, and E. Dzierzak. 2006. An unexpected role for IL-3 in the embryonic development of hematopoietic stem cells. *Dev Cell* 11:171-180.

Rodrigues, N.P., A.S. Boyd, C. Fugazza, G.E. May, Y. Guo, A.J. Tipping, D.T. Scadden, P. Vyas, and T. Enver. 2008. GATA-2 regulates granulocyte-macrophage progenitor cell function. *Blood* 112:4862-4873.

Rodrigues, N.P., V. Janzen, R. Forkert, D.M. Dombkowski, A.S. Boyd, S.H. Orkin, T. Enver, P. Vyas, and D.T. Scadden. 2005. Haploinsufficiency of GATA-2 perturbs adult hematopoietic stem-cell homeostasis. *Blood* 106:477-484.

Rodrigues, N.P., A.J. Tipping, Z.K. Wang, and T. Enver. 2012. GATA-2 mediated regulation of normal hematopoietic stem/progenitor cell function, myelodysplasia and myeloid leukemia. *Int J Biochem Cell B* 44:457-460.

Rodriguez, P., E. Bonte, J. Krijgsveld, K.E. Kolodziej, B. Guyot, A.J.R. Heck, P. Vyas, E. de Boer, F. Grosveld, and J. Strouboulis. 2005. GATA-1 forms distinct activating and repressive complexes in erythroid cells. *Embo Journal* 24:2354-2366.

Rossant, J., and L. Howard. 2002. Signaling pathways in vascular development. *Annu Rev Cell Dev Bi* 18:541-573.

Royer-Pokora, B., U. Loos, and W.D. Ludwig. 1991. TTG-2, a new gene encoding a cysteine-rich protein with the LIM motif, is overexpressed in acute T-cell leukaemia with the t(11;14)(p13;q11). *Oncogene* 6:1887-1893.

Ryan, D.P., J.L. Duncan, C. Lee, P.W. Kuchel, and J.M. Matthews. 2008. Assembly of the oncogenic DNA-binding complex LMO2 center dot Ldb1 center dot TAL1 center dot E12. *Proteins-Structure Function and Bioinformatics* 70:1461-1474.

Rybtsov, S., M. Sobiesiak, S. Taoudi, C. Souilhol, J. Senserrich, A. Liakhovitskaia, A. Ivanovs, J. Frampton, S.L. Zhao, and A. Medvinsky. 2011. Hierarchical organization and early hematopoietic specification of the developing HSC lineage in the AGM region. *J Exp Med* 208:1305-1315.

Sabin, F.R. 1917. Classic report in hematotherapy - Preliminary note on the differentiation of angioblasts and the method by which they produce blood-vessels, blood-plasma and red blood-cells as seen in the living chick (Reprinted from The Anatomical Record, vol 13, pg 199-204, 1917). *J Hematoth Stem Cell* 11:5-7.

Sabin, F.R. 1920. Studies on the origin of blood-vessels and of red blood-corpuscles as seen in the living blastoderm of chicks during the second day of incubation.

Samokhvalov, I.M., N.I. Samokhvalova, and S. Nishikawa. 2007. Cell tracing shows the contribution of the yolk sac to adult haematopoiesis. *Nature* 446:1056-1061.

Samuels-Lev, Y., D.J. O'Connor, D. Bergamaschi, G. Trigiante, J.K. Hsieh, S. Zhong, I. Campargue, L. Naumovski, T. Crook, and X. Lu. 2001. ASPP proteins specifically stimulate the apoptotic function of p53. *Mol Cell* 8:781-794.

Sanchez, C., I. Sanchez, J.A.A. Demmers, P. Rodriguez, J. Strouboulis, and M. Vidal. 2007. Proteomics analysis of Ring1B/Rnf2 interactors identifies a novel complex with the Fbxl10/Jhdm1B histone demethylase and the Bcl6 interacting corepressor. *Mol Cell Proteomics* 6:820-834.

Saxonov, S., P. Berg, and D.L. Brutlag. 2006. A genome-wide analysis of CpG dinucleotides in the human genome distinguishes two distinct classes of promoters. *P Natl Acad Sci USA* 103:1412-1417.

Schier, A.F., and W.S. Talbot. 2005. Molecular genetics of axis formation in zebrafish. *Annu Rev Genet* 39:561-613.

Schlaeger, T.M., H.K. Mikkola, C. Gekas, H.B. Helgadottir, and S.H. Orkin. 2005. Tie2Cre-mediated gene ablation defines the stem-cell leukemia gene (SCL/tal1)-dependent window during hematopoietic stem-cell development. *Blood* 105:3871-3874.

Schlaeger, T.M., A. Schuh, S. Flitter, A. Fisher, H. Mikkola, S.H. Orkin, P. Vyas, and C. Porcher. 2004. Decoding hematopoietic specificity in the helix-loop-helix domain of the transcription factor SCL/Tal-1. *Mol Cell Biol* 24:7491-7502.

Schofield, R. 1978. The relationship between the spleen colony-forming cell and the haemopoietic stem cell. *Blood Cells* 4:7-25.

Seki, T., S. Yuasa, M. Oda, T. Egashira, K. Yae, D. Kusumoto, H. Nakata, S. Tohyama, H. Hashimoto, M. Kodaira, Y. Okada, H. Seimiya, N. Fusaki, M. Hasegawa, and K. Fukuda. 2010. Generation of induced pluripotent stem cells from human terminally differentiated circulating T cells. *Cell Stem Cell* 7:11-14.

Shalaby, F., J. Ho, W.L. Stanford, K.D. Fischer, A.C. Schuh, L. Schwartz, A. Bernstein, and J. Rossant. 1997. A requirement for Flk1 in primitive and definitive hematopoiesis and vasculogenesis. *Cell* 89:981-990.

Shalaby, F., J. Rossant, T.P. Yamaguchi, M. Gertsenstein, X.F. Wu, M.L. Breitman, and A.C. Schuh. 1995. Failure of blood-island formation and vasculogenesis in Flk-1-deficient mice. *Nature* 376:62-66.

Shimeld, S.M. 1999. The evolution of the hedgehog gene family in chordates: insights from amphioxus hedgehog. *Dev Genes Evol* 209:40-47.

Shivdasani, R.A., E.L. Mayer, and S.H. Orkin. 1995. Absence of Blood Formation in Mice Lacking the T-Cell Leukemia Oncoprotein Tal-1/Scl. *Nature* 373:432-434.

Siekmann, A.F., L. Covassin, and N.D. Lawson. 2008. Modulation of VEGF signalling output by the Notch pathway. *Bioessays* 30:303-313.

Silver, L., and J. Palis. 1997. Initiation of murine embryonic erythropoiesis: A spatial analysis. *Blood* 89:1154-1164.

Siminovitch, L., E.A. McCulloch, and J.E. Till. 1963. THE DISTRIBUTION OF COLONY-FORMING CELLS AMONG SPLEEN COLONIES. *J Cell Physiol* 62:327-336.

Simoes, F.C., T. Peterkin, and R. Patient. 2011. Fgf differentially controls cross-antagonism between cardiac and haemangioblast regulators. *Development* 138:3235-3245.

Sinha, A.U., and J. Meller. 2007. Cinteny: flexible analysis and visualization of synteny and genome rearrangements in multiple organisms. *Bmc Bioinformatics* 8:

Smith, R.A., and C.A. Glomski. 1977. Embryonic and fetal hemopoiesis in the Mongolian gerbil (Meriones unguiculatus). *Anat Rec* 189:499-517.

Snow, J.W., J.J. Trowbridge, T. Fujiwara, N.E. Emambokus, J.A. Grass, S.H. Orkin, and E.H. Bresnick. 2010. A single cis element maintains repression of the key developmental regulator Gata2. *Plos Genet* 6:

Snow, J.W., J.J. Trowbridge, K.D. Johnson, T. Fujiwara, N.E. Emambokus, J.A. Grass, S.H. Orkin, and E.H. Bresnick. 2011. Context-dependent function of "GATA switch" sites in vivo. *Blood* 117:4769-4772.

Spangrude, G.J., S. Heimfeld, and I.L. Weissman. 1988. Purification and characterization of mouse hematopoietic stem cells. *Science* 241:58-62.

Speck, N.A., and D.G. Gilliland. 2002. Core-binding factors in haematopoiesis and leukaemia. *Nat Rev Cancer* 2:502-513.

Srinivasan, R.S., A.C. de Erkenez, and C.S. Hemenway. 2003. The mixed lineage leukemia fusion partner AF9 binds specific isoforms of the BCL-6 corepressor. *Oncogene* 22:3395-3406.

Staal, F.J., C. Baum, C. Cowan, E. Dzierzak, S. Hacein-Bey-Abina, S. Karlsson, T. Lapidot, I. Lemischka, S. Mendez-Ferrer, H. Mikkers, K. Moore, E. Moreno, C.L. Mummery, C. Robin, T. Suda, M. Van Pel, G. Vanden Brink, J.J. Zwaginga, and W.E. Fibbe. 2011. Stem cell self-renewal: lessons from bone marrow, gut and iPS toward clinical applications. *Leukemia : official journal of the Leukemia Society of America, Leukemia Research Fund, U.K* 25:1095-1102.

Stadtfeld, M., and K. Hochedlinger. 2010. Induced pluripotency: history, mechanisms, and applications. *Genes Dev* 24:2239-2263.

Staerk, J., M.M. Dawlaty, Q. Gao, D. Maetzel, J. Hanna, C.A. Sommer, G. Mostoslavsky, and R. Jaenisch. 2010. Reprogramming of human peripheral blood cells to induced pluripotent stem cells. *Cell Stem Cell* 7:20-24.

Stainier, D.Y.R., B.M. Weinstein, H.W. Detrich, L.I. Zon, and M.C. Fishman. 1995. Cloche, an Early Acting Zebrafish Gene, Is Required by Both the Endothelial and Hematopoietic Lineages. *Development* 121:3141-3150.

Stern, C.D. 2004. Gastrulation : from cells to embryo. Cold Spring Harbor Laboratory Press, Cold Spring Harbor, N.Y. xvi, 731 p. pp.

Stopa, M., D. Anhuf, L. Terstegen, P. Gatsios, A.M. Gressner, and S. Dooley. 2000. Participation of Smad2, Smad3, and Smad4 in transforming growth factor beta (TGF-beta)-induced activation of Smad7. THE TGF-beta response element of the promoter requires functional Smad binding element and E-box sequences for transcriptional regulation. *The Journal of biological chemistry* 275:29308-29317.

Struewing, J.P., P. Hartge, S. Wacholder, S.M. Baker, M. Berlin, M. McAdams, M.M. Timmerman, L.C. Brody, and M.A. Tucker. 1997. The risk of cancer associated with specific mutations of BRCA1 and BRCA2 among Ashkenazi Jews. *New Engl J Med* 336:1401-1408.

Sturgeon, C.M., L. Chicha, A. Ditadi, Q. Zhou, K.E. McGrath, J. Palis, S.M. Hammond, S. Wang, E.N. Olson, and G. Keller. 2012. Primitive Erythropoiesis Is Regulated by miR-126 via Nonhematopoietic Vcam-1(+) Cells. *Dev Cell*

Sugihara, T.M., I. Bach, C. Kioussi, M.G. Rosenfeld, and B. Andersen. 1998. Mouse deformed epidermal autoregulatory factor 1 recruits a LIM domain factor, LMO-4, and CLIM coregulators. *P Natl Acad Sci USA* 95:15418-15423.

Sum, E.Y.M., D. Segara, B. Duscio, M.L. Bath, A.S. Field, R.L. Sutherland, G.J. Lindeman, and J.E. Visvader. 2005. Overexpression of LMO4 induces mammary hyperplasia, promotes cell invasion, and is a predictor of poor outcome in breast cancer. *P Natl Acad Sci USA* 102:7659-7664.

Summerton, J., and D. Weller. 1997. Morpholino antisense oligomers: design, preparation, and properties. *Antisense Nucleic Acid Drug Dev* 7:187-195.

Summerton, J.E. 2007. Morpholino, siRNA, and S-DNA compared: impact of structure and mechanism of action on off-target effects and sequence specificity. *Curr Top Med Chem* 7:651-660.

Sun, Z., Y. Zhang, K.R. Brunt, J. Wu, S.H. Li, S. Fazel, R.D. Weisel, A. Keating, and R.K. Li. 2010. An adult uterine hemangioblast: evidence for extramedullary self-renewal and clonal bilineage potential. *Blood* 116:2932-2941.

Szabo, E., S. Rampalli, R.M. Risueno, A. Schnerch, R. Mitchell, A. Fiebig-Comyn, M. Levadoux-Martin, and M. Bhatia. 2010. Direct conversion of human fibroblasts to multilineage blood progenitors. *Nature* 468:521-526.

Szeto, D.P., K.J.P. Griffin, and D. Kimelman. 2002. HrT is required for cardiovascular development in zebrafish. *Development (Cambridge, England)* 129:5093-5101.

Takahashi, K., K. Tanabe, M. Ohnuki, M. Narita, T. Ichisaka, K. Tomoda, and S. Yamanaka. 2007. Induction of pluripotent stem cells from adult human fibroblasts by defined factors. *Cell* 131:861-872.

Takahashi, K., and S. Yamanaka. 2006. Induction of pluripotent stem cells from mouse embryonic and adult fibroblast cultures by defined factors. *Cell* 126:663-676.

Takashina, T. 1987. Haemopoiesis in the human yolk sac. *J Anat* 151:125-135.

Tallafuss, A., D. Gibson, P. Morcos, Y.F. Li, S. Seredick, J. Eisen, and P. Washbourne. 2012. Turning gene function ON and OFF using sense and antisense photo-morpholinos in zebrafish. *Development* 139:1691-1699.

Taoudi, S., and A. Medvinsky. 2007. Functional identification of the hematopoietic stem cell niche in the ventral domain of the embryonic dorsal aorta. *P Natl Acad Sci USA* 104:9399-9403.

Tapscott, S.J. 2005. The circuitry of a master switch: Myod and the regulation of skeletal muscle gene transcription. *Development* 132:2685-2695.

Tavian, M., L. Coulombel, D. Luton, H. SanClemente, F. DieterlenLievre, and B. Peault. 1996. Aorta-associated CD34(+) hematopoietic cells in the early human embryo. *Blood* 87:67-72.

Tavian, M., M.F. Hallais, and B. Peault. 1999. Emergence of intraembryonic hematopoietic precursors in the pre-liver human embryo. *Development* 126:793-803.

Tavian, M., and B. Peault. 2005. The changing cellular environments of hematopoiesis in human development in utero. *Exp Hematol* 33:1062-1069.

Tavian, M., C. Robin, L. Coulombel, and B. Peault. 2001. The human embryo, but not its yolk sac, generates lympho-myeloid stem cells: mapping multipotent hematopoietic cell fate in intraembryonic mesoderm. *Immunity* 15:487-495.

Taylor, J.S., I. Braasch, T. Frickey, A. Meyer, and Y. Van de Peer. 2003. Genome duplication, a trait shared by 22000 species of ray-finned fish. *Genome Res* 13:382-390.

Teng, A.C.T., D. Kuraitis, S.A. Deeke, A. Ahmadi, S.G. Dugan, B.L.M. Cheng, M.G. Crowson, P.G. Burgon, E.J. Suuronen, H.H. Chen, and A.F.R. Stewart. 2010. IRF2BP2 is a skeletal and cardiac muscle-enriched ischemia-inducible activator of VEGFA expression. *Faseb J* 24:4825-4834.

Teranoa, T., Y. Zhong, S. Toyokuni, H. Hiai, and Y. Yamada. 2005. Transcriptional control of fetal liver hematopoiesis: dominant negative effect of the overexpression of the LIM domain mutants of LMO2. *Exp Hematol* 33:641-651.

Thompson, M.A., D.G. Ransom, S.J. Pratt, H. MacLennan, M.W. Kieran, H.W. Detrich, B. Vail, T.L. Huber, B. Paw, A.J. Brownlie, A.C. Oates, A. Fritz, M.A. Gates, A. Amores, N. Bahary, W.S. Talbot, H. Her, D.R. Beier, J.H. Postlethwait, and L.I. Zon. 1998. The cloche and spadetail genes differentially affect hematopoiesis and vasculogenesis. *Dev Biol* 197:248-269.

Thurston, G., and G.D. Yancopoulos. 2001. Gridlock in the blood. *Nature* 414:163-164.

Tian, Y., N. Wang, and Z. Lu. 2010. Repression of Lim only protein 4-activated transcription inhibits proliferation and induces apoptosis of normal mammary epithelial cells and breast cancer cells. *Clin Exp Metastasis* 27:455-463.

Tiedemann, K. 1977. On the yolk sac of the cat. II. Erythropoietic phases, ultrastructure of aging primitive erythroblasts, and blood vessels. *Cell Tissue Res* 183:71-89.

Tigges, M., T.T. Marquez-Lago, J. Stelling, and M. Fussenegger. 2009. A tunable synthetic mammalian oscillator. *Nature* 457:309-312.

Till, J.E., and E.A. McCulloch. 1961. A Direct Measurement of the Radiation Sensitivity of Normal Mouse Bone Marrow Cells. *Radiat Res* 14:213-212.

Tipping, A.J., C. Pina, A. Castor, D.L. Hong, N.P. Rodrigues, L. Lazzari, G.E. May, S.E.W. Jacobsen, and T. Enver. 2009. High GATA-2 expression inhibits human hematopoietic stem and progenitor cell function by effects on cell cycle. *Blood* 113:2661-2672.

Tongers, J., J.G. Roncalli, and D.W. Losordo. 2010. Role of endothelial progenitor cells during ischemia-induced vasculogenesis and collateral formation. *Microvasc Res* 79:200-206.

Tran, Y.H., Z. Xu, A. Kato, A.C. Mistry, Y. Goya, M. Taira, S.J. Brandt, and S. Hirose. 2006. Spliced isoforms of LIM-domain-binding protein (CLIM/NLI/Ldb) lacking the LIM-interaction domain. *J Biochem* 140:105-119.

Traver, D., B.H. Paw, K.D. Poss, W.T. Penberthy, S. Lin, and L.I. Zon. 2003. Transplantation and in vivo imaging of multilineage engraftment in zebrafish bloodless mutants. *Nat Immunol* 4:1238-1246.

Trompouki, E., T.V. Bowman, L.N. Lawton, Z.P. Fan, D.C. Wu, A. DiBiase, C.S. Martin, J.N. Cech, A.K. Sessa, J.L. Leblanc, P.L. Li, E.M. Durand, C. Mosimann, G.C. Heffner, G.Q. Daley, R.F. Paulson, R.A. Young, and L.I. Zon. 2011. Lineage Regulators Direct BMP and Wnt Pathways to Cell-Specific Programs during Differentiation and Regeneration. *Cell* 147:577-589.

Tsai, F.Y., G. Keller, F.C. Kuo, M. Weiss, J. Chen, M. Rosenblatt, F.W. Alt, and S.H. Orkin. 1994. An early haematopoietic defect in mice lacking the transcription factor GATA-2. *Nature* 371:221-226.

Tsai, F.Y., and S.H. Orkin. 1997. Transcription factor GATA-2 is required for proliferation/survival of early hematopoietic cells and mast cell formation, but not for erythroid and myeloid terminal differentiation. *Blood* 89:3636-3643.

Tse, E., A.J. Smith, S. Hunt, I. Lavenir, A. Forster, A.J. Warren, G. Grutz, L. Foroni, M.B. Carlton, W.H. Colledge, T. Boehm, and T.H. Rabbitts. 2004. Null mutation of the Lmo4 gene or a combined null

mutation of the Lmo1/Lmo3 genes causes perinatal lethality, and Lmo4 controls neural tube development in mice. *Mol Cell Biol* 24:2063-2073.

Turpen, J.B., C.M. Knudson, and P.S. Hoefen. 1981. The early ontogeny of hematopoietic cells studied by grafting cytogenetically labeled tissue anlagen: localization of a prospective stem cell compartment. *Dev Biol* 85:99-112.

Turtoi, A., D. Mottet, N. Matheus, B. Dumont, P. Peixoto, V. Hennequiere, C. Deroanne, A. Colige, E. De Pauw, A. Bellahcene, and V. Castronovo. 2012. The angiogenesis suppressor gene AKAP12 is under the epigenetic control of HDAC7 in endothelial cells. *Angiogenesis*

Ueda, T., R. Watanabe-Fukunaga, H. Ogawa, H. Fukuyama, Y. Higashi, S. Nagata, and R. Fukunaga. 2007. Critical role of the p400/mDomino chromatin-remodeling ATPase in embryonic hematopoiesis. *Genes Cells* 12:581-592.

Ueno, H., and I.L. Weissman. 2006. Clonal analysis of mouse development reveals a polyclonal origin for yolk sac blood islands. *Dev Cell* 11:519-533.

Valgearcher, V.E., H. Osada, A.J. Warren, A. Forster, J. Li, R. Baer, and T.H. Rabbitts. 1994. The Lim Protein Rbtn2 and the Basic Helix-Loop-Helix Protein Tal1 Are Present in a Complex in Erythroid-Cells. *P Natl Acad Sci USA* 91:8617-8621.

Van Handel, B., A. Montel-Hagen, R. Sasidharan, H. Nakano, R. Ferrari, C.J. Boogerd, J. Schredelseker, Y.L. Wang, S. Hunter, T. Org, J. Zhou, X.M. Li, M. Pellegrini, J.N. Chen, S.H. Orkin, S.K. Kurdistani, S.M. Evans, A. Nakano, and H.K.A. Mikkola. 2012. Scl Represses Cardiomyogenesis in Prospective Hemogenic Endothelium and Endocardium. *Cell* 150:590-605.

van Riel, B., T. Pakozdi, R. Brouwer, R. Monteiro, K. Tuladhar, V. Franke, J.C. Bryne, R. Jorna, E.-J. Rijkers, W. van Ijcken, C. Andrieu-Soler, J. Demmers, R. Patient, E. Soler, B. Lenhard, and F. Grosveld. 2012. A Novel Complex, RUNX1-MYEF2, Represses Hematopoietic Genes in Erythroid Cells. *Mol Cell Biol* 32:3814-3822.

Vermeulen, K., D.R. Van Bockstaele, and Z.N. Berneman. 2005. Apoptosis: mechanisms and relevance in cancer. *Ann Hematol* 84:627-639.

Vicente, C., I. Vazquez, A. Conchillo, M.A. Garcia-Sanchez, N. Marcotegui, O. Fuster, M. Gonzalez, M.J. Calasanz, I. Lahortiga, and M.D. Odero. 2012. Overexpression of GATA2 predicts an adverse prognosis for patients with acute myeloid leukemia and it is associated with distinct molecular abnormalities. *Leukemia* 26:550-554.

Villa, N., L. Walker, C.E. Lindsell, J. Gasson, M.L. Iruela-Arispe, and G. Weinmaster. 2001. Vascular expression of Notch pathway receptors and ligands is restricted to arterial vessels. *Mech Develop* 108:161-164.

Visvader, J.E., D. Venter, K. Hahm, M. Santamaria, E.Y. Sum, L. O'Reilly, D. White, R. Williams, J. Armes, and G.J. Lindeman. 2001. The LIM domain gene LMO4 inhibits differentiation of mammary epithelial cells in vitro and is overexpressed in breast cancer. *P Natl Acad Sci USA* 98:14452-14457.

Vogeli, K.M., S.W. Jin, G.R. Martin, and D.Y. Stainier. 2006. A common progenitor for haematopoietic and endothelial lineages in the zebrafish gastrula. *Nature* 443:337-339.

Vokes, S.A., and P.A. Krieg. 2002. Endoderm is required for vascular endothelial tube formation, but not for angioblast specification. *Development* 129:775-785.

Vokes, S.A., T.A. Yatskievych, R.L. Heimark, J. McMahon, A.P. McMahon, P.B. Antin, and P.A. Krieg. 2004. Hedgehog signaling is essential for endothelial tube formation during vasculogenesis. *Development* 131:4371-4380.

Waddington, C.H. 1957. The strategy of the genes : a discussion of some aspects of theoretical biology. Allen & Unwin, London. ix, 262 p. pp.

Wadman, I.A., H. Osada, G.G. Grutz, A.D. Agulnick, H. Westphal, A. Forster, and T.H. Rabbitts. 1997. The LIM-only protein Lmo2 is a bridging molecule assembling an erythroid, DNA-bindinq complex which includes the TAL1, E47, GATA-1 and Ldb1/NLI proteins. *Embo Journal* 16:3145-3157.

Walmsley, M., A. Ciau-Uitz, and R. Patient. 2002. Adult and embryonic blood and endothelium derive from distinct precursor populations which are differentially programmed by BMP in Xenopus. *Development* 129:5683-5695.

Walmsley, M., D. Cleaver, and R. Patient. 2008. Fibroblast growth factor controls the timing of Scl, Lmo2, and Runx1 expression during embryonic blood development. *Blood* 111:1157-1166.

Wamstad, J.A., and V.J. Bardwell. 2007. Characterization of Bcor expression in mouse development. *Gene expression patterns : GEP* 7:550-557.

Wamstad, J.A., C.M. Corcoran, A.M. Keating, and V.J. Bardwell. 2008. Role of the Transcriptional Corepressor Bcor in Embryonic Stem Cell Differentiation and Early Embryonic Development. *PLoS One* 3:

Wang, H.U., Z.F. Chen, and D.J. Anderson. 1998. Molecular distinction and angiogenic interaction between embryonic arteries and veins revealed by ephrin-B2 and its receptor Eph-B4. *Cell* 93:741-753.

Wang, L., P.P. Zhang, Y.L. Wei, Y. Gao, R. Patient, and F. Liu. 2011. A blood flow-dependent klf2a-NO signaling cascade is required for stabilization of hematopoietic stem cell programming in zebrafish embryos. *Blood* 118:4102-4110.

Wang, N., K.K. Lin, Z. Lu, K.S. Lam, R. Newton, X. Xu, Z. Yu, G.N. Gill, and B. Andersen. 2007. The LIM-only factor LMO4 regulates expression of the BMP7 gene through an HDAC2-dependent mechanism, and controls cell proliferation and apoptosis of mammary epithelial cells. *Oncogene* 26:6431-6441.

Wang, Q., T. Stacy, M. Binder, M. MarinPadilla, A.H. Sharpe, and N.A. Speck. 1996. Disruption of the Cbfa2 gene causes necrosis and hemorrhaging in the central nervous system and blocks definitive hematopoiesis. *P Natl Acad Sci USA* 93:3444-3449.

Warren, A.J., W.H. Colledge, M.B. Carlton, M.J. Evans, A.J. Smith, and T.H. Rabbitts. 1994. The oncogenic cysteine-rich LIM domain protein rbtn2 is essential for erythroid development. *Cell* 78:45-57.

Weinstein, B.M., A.F. Schier, S. Abdelilah, J. Malicki, L. SolnicaKrezel, D.L. Stemple, D.Y.R. Stainier, F. Zwartkruis, W. Driever, and M.C. Fishman. 1996. Hematopoietic mutations in the zebrafish. *Development* 123:303-309.

Wiley, D.M., J.D. Kim, J.J. Hao, C.C. Hong, V.L. Bautch, and S.W. Jin. 2011. Distinct signalling pathways regulate sprouting angiogenesis from the dorsal aorta and the axial vein. *Nat Cell Biol* 13:686-U138.

Wilkinson-White, L., R. Gamsjaeger, S. Dastmalchi, B. Wienert, P.H. Stokes, M. Crossley, J.P. Mackay, and J.M. Matthews. 2011. Structural basis of simultaneous recruitment of the transcriptional regulators LMO2 and FOG1/ZFPM1 by the transcription factor GATA1. *P Natl Acad Sci USA* 108:14443-14448.

Wilkinson, R.N., M.J. Koudijs, R.K. Patient, P.W. Ingham, S. Schulte-Merker, and F.J. van Eeden. 2012. Hedgehog signaling via a calcitonin receptor-like receptor can induce arterial differentiation independently of VEGF signaling in zebrafish. *Blood* 120:477-488.

Wilkinson, R.N., C. Pouget, M. Gering, A.J. Russell, S.G. Davies, D. Kimelman, and R. Patient. 2009. Hedgehog and Bmp Polarize Hematopoietic Stem Cell Emergence in the Zebrafish Dorsal Aorta. *Dev Cell* 16:909-916.

Willett, C.E., A. Cortes, A. Zuasti, and A.G. Zapata. 1999. Early hematopoiesis and developing lymphoid organs in the zebrafish. *Dev Dyn* 214:323-336.

Willett, C.E., H. Kawasaki, C.T. Amemiya, S. Lin, and L.A. Steiner. 2001. Ikaros expression as a marker for lymphoid progenitors during zebrafish development. *Dev Dynam* 222:694-698.

Wilson, N.K., S.D. Foster, X. Wang, K. Knezevic, J. Schutte, P. Kaimakis, P.M. Chilarska, S. Kinston, W.H. Ouwehand, E. Dzierzak, J.E. Pimanda, M.F. de Bruijn, and B. Gottgens. 2010. Combinatorial transcriptional control in blood stem/progenitor cells: genome-wide analysis of ten major transcriptional regulators. *Cell Stem Cell* 7:532-544.

Wilt, F.H. 1965. Erythropoiesis in the Chick Embryo: The Role of Endoderm. *Science* 147:1588-1590.

Winnier, G., M. Blessing, P.A. Labosky, and B.L.M. Hogan. 1995. Bone Morphogenetic Protein-4 Is Required for Mesoderm Formation and Patterning in the Mouse. *Genes Dev* 9:2105-2116.

Wise, L.M., T. Veikkola, A.A. Mercer, L.J. Savory, S.B. Fleming, C. Caesar, A. Vitali, T. Makinen, K. Alitalo, and S.A. Stacker. 1999. Vascular endothelial growth factor (VEGF)-like protein from orf virus NZ2 binds to VEGFR2 and neuropilin-1. *P Natl Acad Sci USA* 96:3071-3076.

Wittamer, V., J.Y. Bertrand, P.W. Gutschow, and D. Traver. 2011. Characterization of the mononuclear phagocyte system in zebrafish. *Blood* 117:7126-7135.

Wong, P.M., S.W. Chung, D.H. Chui, and C.J. Eaves. 1986. Properties of the earliest clonogenic hemopoietic precursors to appear in the developing murine yolk sac. *P Natl Acad Sci USA* 83:3851-3854.

Wu, A.M., J.E. Till, L. Siminovitch, and E.A. McCulloch. 1967. A cytological study of the capacity for differentiation of normal hemopoietic colony-forming cells. *J Cell Physiol* 69:177-184.

Xie, J., A. Larochelle, I. Maric, M. Faulhaber, R.E. Donahue, and C.E. Dunbar. 2010. Repetitive busulfan administration after hematopoietic stem cell gene therapy associated with a dominant HDAC7 clone in a nonhuman primate. *Hum Gene Ther* 21:695-703.

Xiong, J.-W., Q. Yu, J. Zhang, and J.D. Mably. 2008. An acyltransferase controls the generation of hematopoietic and endothelial lineages in zebrafish. *Circ Res* 102:1057-1064.

Xu, M.J., S. Matsuoka, F.C. Yang, Y. Ebihara, A. Manabe, R. Tanaka, M. Eguchi, S. Asano, T. Nakahata, and K. Tsuji. 2001. Evidence for the presence of murine primitive megakaryocytopoiesis in the early yolk sac. *Blood* 97:2016-2022.

Xu, R.H., K.T. Ault, J. Kim, M.J. Park, Y.S. Hwang, Y. Peng, D. Sredni, and H.F. Kung. 1999. Opposite effects of FGF and BMP-4 on embryonic blood formation: Roles of PV.1 and GATA-2. *Dev Biol* 208:352-361.

Yamada, Y., R. Pannell, A. Forster, and T.H. Rabbitts. 2000. The oncogenic LIM-only transcription factor Lmo2 regulates angiogenesis but not vasculogenesis in mice. *P Natl Acad Sci USA* 97:320-324.

Yamada, Y., R. Pannell, A. Forster, and T.H. Rabbitts. 2002. The LIM-domain protein Lmo2 is a key regulator of tumour angiogenesis: a new anti-angiogenesis drug target. *Oncogene* 21:1309-1315.

Yamada, Y., A.J. Warren, C. Dobson, A. Forster, R. Pannell, and T.H. Rabbitts. 1998. The T cell leukemia LIM protein Lmo2 is necessary for adult mouse hematopoiesis. *P Natl Acad Sci USA* 95:3890-3895.

Yamaguchi, T.P., D.J. Dumont, R.A. Conlon, M.L. Breitman, and J. Rossant. 1993. Flk-1, an Flt-Related Receptor Tyrosine Kinase Is an Early Marker for Endothelial-Cell Precursors. *Development* 118:489-498.

Yamamoto, Y., S. Tsuzuki, M. Tsuzuki, K. Handa, Y. Inaguma, and N. Emi. 2010. BCOR as a novel fusion partner of retinoic acid receptor alpha in a t(X;17)(p11;q12) variant of acute promyelocytic leukemia. *Blood* 116:4274-4283.

Yan, M., S.A. Burel, L.F. Peterson, E. Kanbe, H. Iwasaki, A. Boyapati, R. Hines, K. Akashi, and D.E. Zhang. 2004. Deletion of an AML1-ETO C-terminal NcoR/SMRT-interacting region strongly induces leukemia development. *P Natl Acad Sci USA* 101:17186-17191.

Yang, L., D. Bryder, J. Adolfsson, J. Nygren, R. Mansson, M. Sigvardsson, and S.E. Jacobsen. 2005. Identification of Lin(-)Sca1(+)kit(+)CD34(+)Flt3- short-term hematopoietic stem cells capable of rapidly reconstituting and rescuing myeloablated transplant recipients. *Blood* 105:2717-2723.

Yaniv, K., S. Isogai, D. Castranova, L. Dye, J. Hitomi, and B.M. Weinstein. 2006. Live imaging of lymphatic development in the zebrafish. *Nat Med* 12:711-716.

Yoder, M.C., K. Hiatt, P. Dutt, P. Mukherjee, D.M. Bodine, and D. Orlic. 1997. Characterization of definitive lymphohematopoietic stem cells in the day 9 murine yolk sac. *Immunity* 7:335-344.

Yokomizo, T., M. Ogawa, M. Osato, T. Kanno, H. Yoshida, T. Fujimoto, S. Fraser, S. Nishikawa, H. Okada, M. Satake, T. Noda, and Y. Ito. 2001. Requirement of Runx1/AML1/PEBP2alphaB for the generation of haematopoietic cells from endothelial cells. *Genes Cells* 6:13-23.

Yoo, J.Y., H.K. Choi, K.C. Choi, S.Y. Park, I. Ota, J.I. Yook, Y.H. Lee, K. Kim, and H.G. Yoon. 2012. Nuclear hormone receptor corepressor promotes esophageal cancer cell invasion by transcriptional repression of interferon-gamma-inducible protein 10 in a casein kinase 2-dependent manner. *Mol Biol Cell* 23:2943-2954.

Yoshimoto, M., E. Montecino-Rodriguez, M.J. Ferkowicz, P. Porayette, W.C. Shelley, S.J. Conway, K. Dorshkind, and M.C. Yoder. 2011. Embryonic day 9 yolk sac and intra-embryonic hemogenic endothelium independently generate a B-1 and marginal zone progenitor lacking B-2 potential. *P Natl Acad Sci USA* 108:1468-1473.

You, L.R., F.J. Lin, C.T. Lee, F.J. DeMayo, M.J. Tsai, and S.Y. Tsai. 2005. Suppression of Notch signalling by the COUP-TFII transcription factor regulates vein identity. *Nature* 435:98-104.

Yu, J., M.A. Vodyanik, K. Smuga-Otto, J. Antosiewicz-Bourget, J.L. Frane, S. Tian, J. Nie, G.A. Jonsdottir, V. Ruotti, R. Stewart, Slukvin, II, and J.A. Thomson. 2007. Induced pluripotent stem cell lines derived from human somatic cells. *Science* 318:1917-1920.

Yue, R., H. Li, H. Liu, Y. Li, B. Wei, G. Gao, Y. Jin, T. Liu, L. Wei, J. Du, and G. Pei. 2012. Thrombin receptor regulates hematopoiesis and endothelial-to-hematopoietic transition. *Dev Cell* 22:1092-1100.

Zambidis, E.T., T.S. Park, W. Yu, A. Tam, M. Levine, X. Yuan, M. Pryzhkova, and B. Peault. 2008. Expression of angiotensin-converting enzyme (CD143) identifies and regulates primitive hemangioblasts derived from human pluripotent stem cells. *Blood* 112:3601-3614.

Zeigler, B.M., D. Sugiyama, M. Chen, Y. Guo, K.M. Downs, and N.A. Speck. 2006. The allantois and chorion, when isolated before circulation or chorio-allantoic fusion, have hematopoietic potential. *Development (Cambridge, England)* 133:4183-4192.

Zhang, D., E. Cho, and J. Wong. 2007. A critical role for the co-repressor N-CoR in erythroid differentiation and heme synthesis. *Cell Res* 17:804-814.

Zhang, S.-J., L.-Y. Ma, Q.-H. Huang, G. Li, B.-W. Gu, X.-D. Gao, J.-Y. Shi, Y.-Y. Wang, L. Gao, X. Cai, R.-B. Ren, J. Zhu, Z. Chen, and S.-J. Chen. 2008. Gain-of-function mutation of GATA-2 in acute myeloid transformation of chronic myeloid leukemia. *P Natl Acad Sci USA* 105:2076-2081.

Zhang, X.Y., and A.R.F. Rodaway. 2007. SCL-GFP transgenic zebrafish: In vivo imaging of blood and endothelial development and identification of the initial site of definitive hematopoiesis. *Dev Biol* 307:179-194.

Zhang, Y., H. Jin, L. Li, F.X. Qin, and Z. Wen. 2011. cMyb regulates hematopoietic stem/progenitor cell mobilization during zebrafish hematopoiesis. *Blood* 118:4093-4101.

Zhong, T.P., S. Childs, J.P. Leu, and M.C. Fishman. 2001. Gridlock signalling pathway fashions the first embryonic artery. *Nature* 414:216-220.

Zhong, T.P., M. Rosenberg, M.A.P.K. Mohideen, B. Weinstein, and M.C. Fishman. 2000. gridlock, an HLH gene required for assembly of the aorta in zebrafish. *Science* 287:1820-1824.

Zhou, Y., M. Yamamoto, and J.D. Engel. 2000. GATA2 is required for the generation of V2 interneurons. *Development (Cambridge, England)* 127:3829-3838.

Zhu, C., Q. Chen, Z. Xie, J. Ai, L. Tong, J. Ding, and M. Geng. 2011a. The role of histone deacetylase 7 (HDAC7) in cancer cell proliferation: regulation on c-Myc. *J Mol Med (Berl)* 89:279-289.

Zhu, C., T. Smith, J. McNulty, A.L. Rayla, A. Lakshmanan, A.F. Siekmann, M. Buffardi, X.D. Meng, J. Shin, A. Padmanabhan, D. Cifuentes, A.J. Giraldez, A.T. Look, J.A. Epstein, N.D. Lawson, and S.A. Wolfe. 2011b. Evaluation and application of modularly assembled zinc-finger nucleases in zebrafish. *Development* 138:4555-4564.

Zovein, A.C., J.J. Hofmann, M. Lynch, W.J. French, K.A. Turlo, Y. Yang, M.S. Becker, L. Zanetta, E. Dejana, J.C. Gasson, M.D. Tallquist, and M.L. Iruela-Arispe. 2008. Fate Tracing Reveals the Endothelial Origin of Hematopoietic Stem Cells. *Cell Stem Cell* 3:625-636.